Mechano-electrical transduction in cochlear hair cells: channel blockers, an anomalous mechano-sensitive current and TRPC knockout mice

Submitted by Terri Desmonds for the degree of Ph.D.

University of Sussex

September 2015

DECLARATION

Whilst I have collected the majority of the data described in Chapters 4 and 5, a proportion of it was obtained by Dr. Nerissa Kirkwood and with her permission I have presented it here and included it in the averages I calculated. In Chapter 4, some cells from the following conditions and concentrations were obtained by Dr. Kirkwood: *MET current traces* - 300 nM apical D-TAT, 100 nM basal D-TAT, 300 nM basal D-TAT, 1 µM basal D-TAT, 30 nM basal D-JNKi1, 300 nM basal D-JNKi1; *Current- voltage curves and fractional block figures* - 100 nM apical D-TAT (5 cells), 300 nM apical D-TAT (all cells), 10 nM basal D-TAT (3 cells), 100 nM basal D-TAT (all cells), 300 nM basal D-TAT (all cells), 1 µM basal D-TAT (all cells), 300 nM apical D-JNKi1 (3 cells), 10 nM basal DJNki1 (3 cells), 30 nM basal D-JNKi1 (all cells), 100 nM basal D-JNKi1 (2 cells), 300 nM basal D-JNki1 (all cells), 1 µM basal D-JNKi1 (1 cell); *Chapter 5* - 30 nM basal D-JNKi1 (all cells), 100 nM basal D-JNKi1 (all cells).

I hereby declare that this thesis has not been and will not be, submitted in whole or in part to another university for the award of any other degree.

_____

Terri Desmonds

Lovingly dedicated to my mother, Karin Desmonds.

"Finding is losing something else.

I think about, perhaps even mourn,

what I lost to find this."

- Richard Brautigan

ACKNOWLEDGEMENTS

I would like to thank Prof. Corne Kros for being a very rare combination of intellectually brilliant, kind, compassionate, hilarious and fun. I really cannot thank him enough for shepherding me through the course of the last four years.

Prof. Guy Richardson for all his help and guidance; Dr. Nerissa Kirkwood for her help and letting me use some of her data in this thesis; Dr. Terri Roberts for teaching me how to patch clamp; Dr. Richard Goodyear for his help; Dr. Nicola Allen for being there with me the whole way.

My stoical, ardent and beloved mother and father Karin Desmonds and Terance Rack; Emily McCarthy for being my most enduring, excellent and dearest human; my second parentals Rachel McCarthy and Keith Bacon; Will Groves for being a lovely creature and doing all manner of nice things for me in order to ease my bouts of insanity; Dorian Lloyd for being like a brother; Ren Stewart for always being there even when she's far away; Emma Gatrill for being my sunshine; Chris Lucraft for living with me and always being brilliant; Anthony Chalmers for being so enthused by the prospect of 'Dr. Desmonds', always offering up some big tunes and being very supportive; Amit Jagdev, Jonathan Portlock, Claudia Cramer, Jenni Hamill, Andrew Wallis, Frances Donnelly, Dan Harding, Patrick Lawrence, Hannah Clark, Alex Chai, Alex Warburton, Jonny Wildey, Effie Love, Marcus Hamblett, James Ormondroyd, Tristram Bawtree, Neil Noon, Daire Cantillon and Matthew Butt for all being wonderful humans and inspiring me, not forgetting anyone else who has formed a salient portion of my life in the last four years.

ABSTRACT

Transforming sound vibrations into neural signals, the process of mechano-electrical transduction (MET), is achieved via the movement of rows of stereocilia located atop cochlear hair cells, activating non-selective MET channels. Recording MET currents using whole-cell patch clamp electrophysiology has allowed for various investigations centred on the MET channel.

There is a statistically significant difference in MET current amplitudes between mid-apical and mid-basal outer hair cells. The larger MET current, flowing through basal hair cells explains a key contributory element to their increased susceptibility to the ototoxic effects of aminoglycoside antibiotics, as they are thus able to enter these cells more readily, in greater abundance.

The cell penetrating peptides D-TAT and D-JNKi1 have been studied in cochlear hair cells. They are both high affinity, voltage dependent, permeant blockers of the MET channel in inner (IHCs) and outer hair cells (OHCs). Whilst ototoxic at higher concentrations, they may have therapeutic potential at lower concentrations, providing ototoprotection against aminoglycoside induced ototoxicity by competitively blocking the MET channel. There is an apical to basal gradient in the OHC MET channel block caused by D-TAT and D-JNKi1, the affinity of the block increasing from apex to base. Compellingly, the first evidence of a gradient in the MET channel properties of IHCs is presented here, a gradient in D-JNKi1 block.

Properties of an anomalous mechano-sensitive current, elicited by inverse stimuli relative to the MET current, have been elucidated via the use of the compounds dihydrostreptomycin (DHS) and FM1-43. When compared with the MET current, DHS block of the anomalous current is two orders of magnitude less strong and FM1-43 block has altered voltage dependence. TRPC3/6 knock-out mice, whilst previously thought to have a basal OHC specific MET deficit, have been shown to exhibit normal MET currents. In addition, so too have TRPC1/3/6 and TRPC1/3/5/6 knock-out mice.

TABLE OF CONTENTS

ABBREVIATIONS

4-HNE	4-Hydroxynonenal
ABR	Auditory Brainstem Response
AITC	Allyl Isothiocyanate
CDH23	Cadherin 23
CPP	Cell penetrating peptide
DHS	Dihydrostreptomycin
DKO	Double Knock-Out
D-JNKi1	D-JNK inhibitor 1
DPOAE	Distortion Product Otoacoustic Emissions
D-TAT	D-retro-inverso HIV-TAT
GTTR	Texas Red conjugated Gentamicin
IHC	Inner Hair Cell
K_D	Half Blocking Concentration
MET	Mechano-Electrical Transduction
MET Channel	Mechano-Electrical Transducer Channel
n_H	Hill Coefficient
OHC	Outer Hair Cell
PS	Phosphatidylserine
PCDH15	Protocadherin 15
QKO	Quadruple Knock-Out
ROS	Reactive Oxygen Species
TKO	Triple Knock-Out
TMC	Transmembrane Channel
TR D-JNKi1	Texas Red conjugated D-JNKi1
TR D-TAT	Texas Red conjugated D-TAT
TRPA1	Transient Receptor Potential A1
TRPC	Transient Receptor Potential Cation Channels

AIMS

The aims of this thesis were as follows:

- The overarching aim was to investigate the properties of the MET channel.

- To investigate the efficacy of the D-TAT and D-JNKi1 peptides as blockers of the MET channel in outer and inner cochlear hair cells.

- To further illuminate the apical to basal gradient in macroscopic MET current size by comparing recordings from a large number of OHCs in mid-apical and mid-basal cochlear regions, with a particular view to looking at the difference in the efficaciousness of the block by D-TAT and D-JNKi1 in these regions.

- To test the kinetics and concentration dependence of the channel block of dihydrostreptomycin and FM1-43 on the anomalous current in cochlear outer hair cells.

- To investigate the effects of knocking out TRPC 1/3/6, TRPC 1/3/5/6, and reviewing previous data on TRPC 3/6 mice, on mechano-electrical transduction in cochlear outer hair cells.

1 INTRODUCTION

1.1 Form and function of the cochlea

The processing of sound, which allows it to be interpreted by the brain, is a complex, intricate and finely tuned process. Sound vibrations, once amplified and funnelled through the ear canal, aided by the pinna, are then sent to the middle ear. Here the tympanic membrane (eardrum) and three bones of the middle ear: the malleus, incus and stapes, vibrate due to longitudinal pressure waves of sound (Pickles, 2008). Impedance matching from the relatively sizeable, low impedance tympanic membrane to the smaller, high impedance oval window is a very important function of the middle ear. Without it, the energy in the system would be lost, with only a tiny fraction being transmitted (Reichenbach and Hudspeth, 2014). The movement of the malleus, incus and finally the stapes, pushes this pressure through the oval window, generating a travelling wave in the fluid-filled middle cochlear chamber, the scala media. The three cochlear compartments are distinct from one another. The scala vestibuli sits at the top, the scala tympani at the bottom and the - organ of Corti containing - scala media in the middle. The scala media contains endolymph whilst the scala vestibuli and scala tympani contain perilymph (Pickles, 2008).

Sound evokes a full cycle of up and down basilar membrane motion. The stapes is pushed into and pulled out of the oval window, in a piston like fashion. Fluid motion of the perilymph in the scala vestibuli is generated by this motion and due to the elasticity of the cochlear membranes, the fluid moves not only forward but also downward, causing the elastic basilar membrane to move downward, displacing the endolymph in the scala media. This results in an increase in pressure in the scala tympani, pushing the round window outwards and then inwards again when the stapes moves back. The basilar membrane is then pushed upwards (Pickles, 2008).

The conversion of vibrations of high displacement but low pressure, into those appropriate for the cochlea - which cause low displacement but are higher in pressure - is achieved by conducting the vibrations from the larger tympanic membrane to the smaller footplate of the stapes, so they in effect become concentrated. Additionally, the longer armed malleus, pushing on the shorter armed incus increases force but decreases velocity before the vibrations are transmitted through the stapes (Pickles, 2008) (FIGURE 1-1).

The basilar membrane is tonotopically mapped, such that the distance which an incoming sound wave propagates along the length of the basilar membrane is frequency dependent; there are different regions of maximum basilar membrane deformation for different frequency waves. Higher frequencies cause greater movement in the stiff basal region, causing energy to dissipate more quickly, thus the wave propagates less far, whereas lower frequency waves will propagate further (Reichenbach and Hudspeth, 2014). Travelling waves for each frequency component of a given sound are generated in the basilar membrane, which increase in size whilst their wavelengths and propagation-velocities are reduced, thus the frequency of the waves stay the same, until the peak is reached at a particular region (Ren, 2002; Reichenbach and Hudspeth, 2014). This is because, basilar membrane thickness increases and rigidity decreases along its length from base to apex, as the elastic fibres from which it is formed are increasingly long but less densely packed (Pickles, 2008).

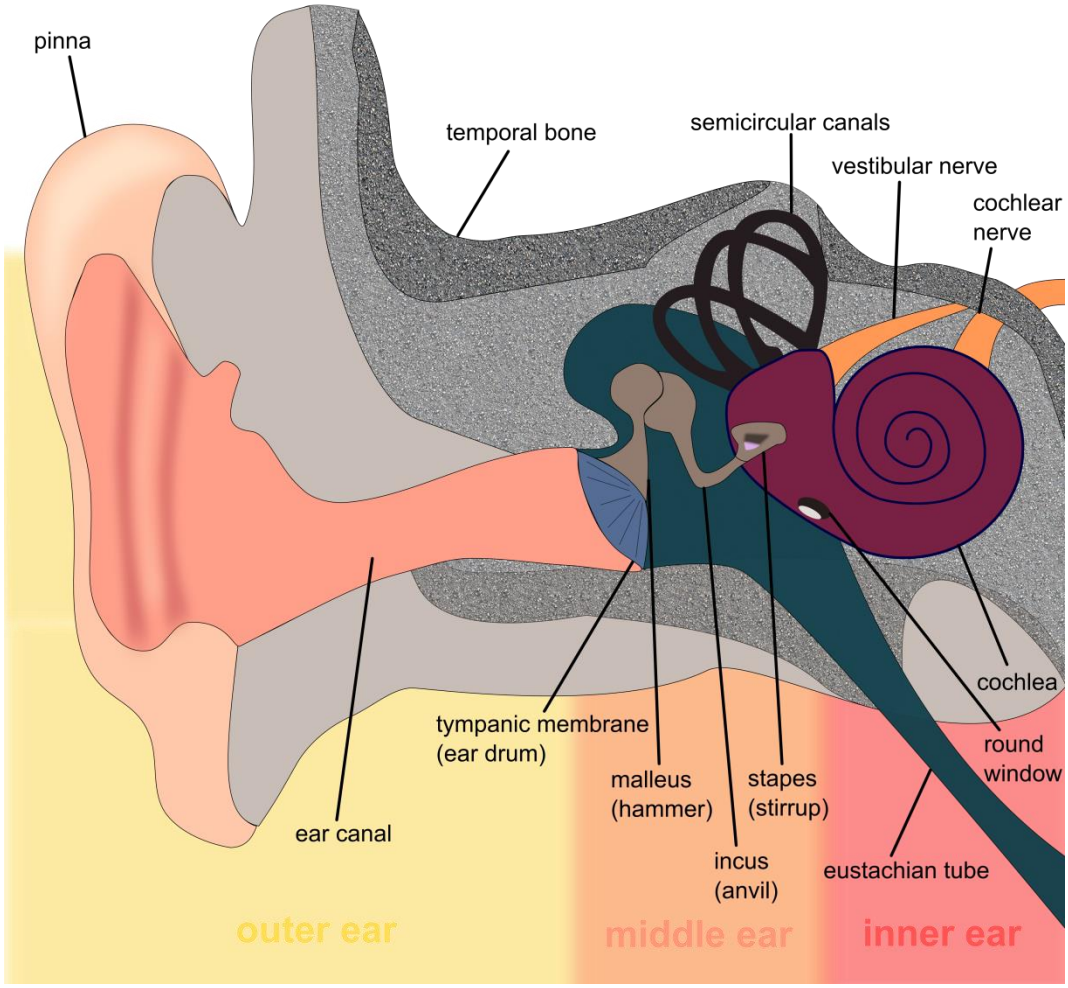

FIGURE 1-1 : Anatomy of the ear. Component parts of the outer, middle and inner ear illustrated.

1.1.1 Inner and outer cochlear hair cells

On top of the basilar membrane is where the highly specialised sensory hair cells reside. The placental mammalian complement consists of a single row of inner hair cells (IHCs) and three rows of outer hair cells (OHCs) (Pickles, 2008). In humans there are approximately 3,500 IHCs and 11,000 OHCs, compared with closer to 800 and 2,500, respectively, in a house mouse (Ehret and Frankenreiter, 1977). They are two distinct varieties of hair cell. Inner hair cells have many afferent auditory nerve fibre innervations and are thus the true sensory cells of the inner ear. Outer hair cells are primarily innervated by efferent nerve fibres with only a few afferent fibre innervations, important for their role in amplification (FIGURE 1-2).

On top of each hair cell is V-shaped hair bundle formed of rows of stereocilia which are ordered from tallest to shortest, although overall height varies with position along the length of the basilar membrane, decreasing from apex to base (Roth and Bruns, 1992). The OHCs are in contact within the gel-like tectorial membrane, which lies above them, and surrounded by supporting cells. Whilst the IHCs are also surrounded by supporting cells the stereocilia atop them are free-standing, not coming into contact with the tectorial membrane. Vibrations generated by sound stimuli generate tiny motions of the basilar membrane which displace the hair bundles. Whilst perilymph possesses the usual complement of ions expected of an extracellular fluid containing a high concentration of Na^+, endolymph contains a high concentration of K^+. Cochlear hair cells reside above the basilar membrane, with their basolateral surfaces immersed in perilympth. The apical surfaces of the cells, where the hair bundle forming stereocilia sit, are bathed in endolymph (FIGURE 1-2).

OHCs act as active mechanical amplifiers of the inputted auditory signals they receive, augmenting the movement of the basilar membrane, thereby crucially heightening the

frequency selectivity and sensitivity of the cochlea (Hudspeth, 2008). OHC somatic electromotility is thought to be generated by the motor protein prestin (Zheng et al., 2000), which is expressed in the basolateral membrane of OHCs. When the basilar membrane moves upward, stereocilia are deflected in the excitatory direction, towards the tallest stereocilia. This in turn causes the opening of the mechano-electrical transducer (MET) channels and subsequent depolarisation of the OHCs. Prestin then causes the OHCs to shorten, enhancing the motion of the basilar membrane and increasing tension on IHCs. When the OHCs are then hyperpolarised by the downward motion of the basilar membrane, prestin causes the OHCs to lengthen, decreasing tension on IHCs. This process is proposed to be driven by changes in membrane potential (Santos-Sacchi and Dilger, 1988). The high frequency encoding basal region of the cochlea is most reliant on amplification driven by somatic motility (Hudspeth, 2008).

A hair bundle motor component has also been proposed, involving the MET channel itself. Evidence for this is based on results which demonstrate reduced bundle motion after the MET channel is blocked with dihydrostreptomicin (DHS) by Kennedy et al. (2006). Somatic motility was also assessed here using salicylate, known to interfere with electromotility (Shehata et al., 1991). The MET-channel based motor component is proposed to interact with the somatic motility component due to the witnessed reductions in hair bundle motion, by inhibiting the two motors, adding up to a greater than 100% reduction when summated. They state that if these mechanisms were acting independently, their contributions should total 100% of motility, or less than this if there is yet another component (Kennedy et al., 2006).

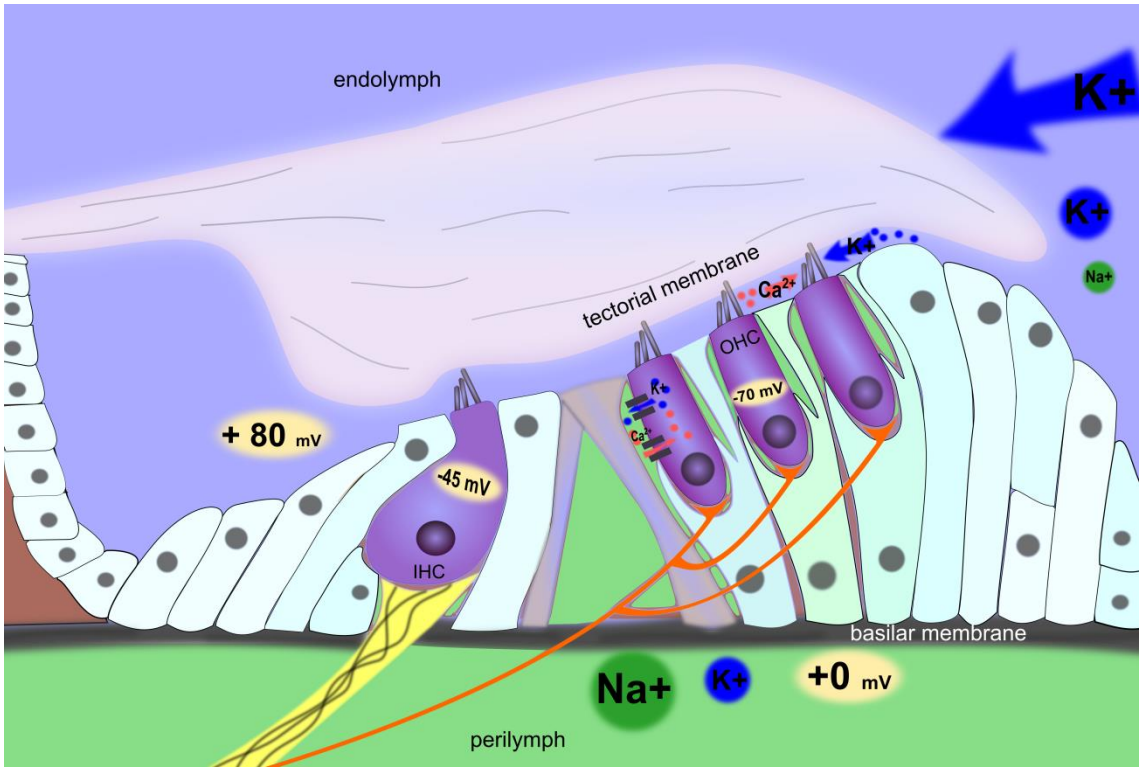

FIGURE 1-2 : Inner and outer hair cells in the organ of Corti. Illustration of a cross section of the organ of Corti with inner and outer hair cells.

1.1.2 The endocochlear potential

The endocochlear potential (EP) is the pivotal driving force for mechano-electrical transduction (MET) in the cochlea. It is established chiefly by the stria vasicularis as it contributes significantly to the high K^+ content of the endolymph (Tasaki and Spyropoulos, 1959). Homeostasis and the establishment and maintenance of the endocochlear potential are crucial. The ~ +80 mV transepithelial EP is generated by the abnormally highly concentrated K^+ in the endolymph which is contained within the endolymphatic space of the scala media. The source of the EP is the stria vasicularis (Tasaki and Spyropoulos, 1959), a two-layer epithelium, which resides on the lateral wall of the cochlea adjacent to the spiral ligament. Formed of a layer of marginal cells on the endolymphatic wall, followed by an intermediate region of capillaries and intermediate cells, with flat basal cells on the side where it is in contact with the spiral ligament, it transports and secretes K^+ ions. Both the separation of component cells and connections between the constituent compartments of the stria vasicularis are vital for the generation of the EP. Here, tight junctions and gap junctions are pivotal components in creating cohesion (Marcus et al., 2002).

The EP increases from apex to base along the length of the cochlea. This is the greatest transepithelial voltage generated within mammalian anatomy (Wangemann, 2006). This in turn contributes to generation of a large potential across the apical surface of cochlear hair cells of 140 mV, allowing the MET currents to flow across the MET channel. This large potential drives the MET process.

All the mice used in my experiments were 2 postnatal days old (P2) and grown in culture for 1 (P2 + 1) or 2 (P2 +2) days. This growth in culture effectively represented maturation to P3 and P4 developmental stages, respectively (Waguespack et al., 2007). The endocochlear potential during the first few postnatal days is however very small (Rybak et al., 1992).

1.1.3 The mouse as a model for hearing research

Mice can hear higher frequency sounds than us of some 2.3 – 85.5 kHz (at 60 dB SPL), often communicating at frequencies beyond the human range of perception. Human hearing lies in the range of 31 Hz – 17.6 kHz (at 60 dB SPL) (Heffner and Heffner, 2007). Nonetheless, the mouse genome and the anatomy of the inner ear are similar to those of humans. Their vulnerability to damage by noise makes them good candidates for assessing hearing loss. Moreover, the shortness of their lifespan makes them ideal for studying age related hearing loss. The creation of knock out and mutant mouse models by knocking out or mutating certain genes has allowed for the emulation and studying of conditions akin to those suffered by humans (Ohlemiller et al., 1999; Avraham, 2003).

1.1.4 Hair cell development and the P2 mouse

The cochlea undergoes morphological and functional changes as it develops. The V-shaped hair bundle arrangement atop the hair cells is the most distinctive morphological feature, forming during the first few days after birth (Waguespack et al., 2007). MET also begins to develop at this stage. The onset of hearing in mice is at around P12 but some properties, including the complete differentiation of inner and outer hair cells, will only be fully developed by the end of the third postnatal week (Pujol et al., 1998).

P2 is in many ways the optimal developmental stage at which to prepare and grow the mouse organ of Corti in culture. At this stage, an intact preparation of the coil is easiest to achieve due to the bones surrounding the cochlear and the cochlear capsule not yet being ossified, whilst being firm enough as not to bounce away when manipulated. Moreover, it has been demonstrated that P2 mice have 100% functionally mechanotransducing OHCs in basal cochlear regions and 80% in the apical regions (Lelli et al., 2009), with peak amplitudes being

reached and sustained between P2 and P4, apical hair cell maturity following that in the base (Lelli et al., 2009; Kim and Fettiplace, 2013). Additionally, hair cells mature in culture and thus are more like those from P3, P4 or P5 mice after 1, 2 or 3 days in culture, respectively. By having cultured them at the P2 stage, one also avoids the witnessed decline in the amount of functional OHCs seen after P2, thought to be caused by damage to the hair cells where bones are more ossified. It should also be noted that experimentation on OHCs is preferred compared to that on IHCs because they are far easier to access, more plentiful and can be stimulated with greater ease (Lelli et al., 2009).

1.2 The mechano-electrical transduction complex

In order for functional hearing to occur, the mechanical stimulation generated by the movement of fluid in the cochlea must be converted into electrical signals in the form of graded receptor potentials so that signals can be sent along the afferent auditory nerve fibres to the auditory brain regions (Pickles, 2008). This is achieved by the MET channels. Whilst the molecular identity of the MET channel remains elusive, several components of the MET machinery have been identified.

MET channels are opened when the stereocilia on hair cells are deflected in the excitatory direction (towards the tallest stereocilia) (Pickles, 2008). Recent research has suggested that there are two MET channels per stereocilium and whilst the location of the MET channel is still somewhat debated, they are widely thought to be located at the base of the tip links in the second and third stereociliary rows (Beurg et al., 2009).

There are many pieces of biological machinery which are involved in the complex process of MET, and variations on their locations and interactions have been postulated. Tip links are thought to gate the MET channels either by being directly connected or ‘tethered’ to them or by being anchored next to them (Peng et al., 2011). Protoadherin 15 (PCDH15) and cadherin 23

(CDH23) are thought to form part of the tip links. The upper tip link density (UTLD) is thought to contain Myo7a, harmonin-b and Sans (Grati and Kachar, 2011) and the lower tip-link density is believed to be formed of myosin XVa , whirlin (Delprat et al., 2005) and Eps8 (Manor et al., 2011).

It is generally assumed that in the undisturbed tip link the lower end is composed of PCDH15 and the upper end CDH23 (Kazmierczak et al., 2007). However, when tip links undergo damage, either through sound exposure or experimental manipulation, they are able to spontaneously regenerate. The initial phase of this regeneration process appears to be the formation of a shorter tip link composed solely of PCDH15 at both the upper and lower ends. The MET currents produced by hair cells undergoing this phase of regeneration are of normal magnitude but the adaptation of these currents (dominated by fast adaptation) was reduced and had a much slower time constant. In spite of apparent full tip link recovery and MET current amplitude by 12 hours post damage, until CDH23 levels are fully restored at around the 48 hour time point, adaptation remains abnormal. Indzhykulian et al. (2013) posit that this may be due to the shortened tip links altering the angle of the stereocilia sufficiently to induce this shift in adaptation.

1.2.1 The gating spring

The concept of the gating spring was developed by Corey and Hudspeth (1983). The gating-spring model entails that the MET channel opens due to the tension of the gating spring. Tension increases as the hair bundle moves in the excitatory direction (towards the tallest stereocilia) and decreases as it is deflected in the inhibitory direction. The channel is either opened or closed and changes between these two states rapidly. Even when the gating spring is in its resting state there is still a certain level of probability that the channel will open. This resting open probability is somewhere in the region of 0.1 to 0.5 (Howard and Hudspeth,

1988; Farris et al., 2006; Beurg et al., 2010) but is assumed in the work within this thesis to be 0.3 based on previous work on the neonatal mouse done in the group in which I have worked (Kros et al., 1992; Kros et al., 1996). This means a certain proportion of channels are open at rest, causing a resting current to flow. Increasing tension on the gating spring increases the open probability of the MET channel, without there being a fixed level of tension which will cause the channel to open. The MET channel changes between open and closed very quickly and tension on the tip link at a given time controls the amount of time that the channel is open (Corey and Hudspeth, 1983).

The identity of the gating spring remains unknown. High resolution examination of the tip link using electron microscopy revealed that it is too stiff for purpose (Kachar et al., 2000), so the gating spring is thought to reside at the top or the bottom of the tip link, with the lower end being more likely due to the discovery of an elevated tent-like membrane, apparently responsive to tip link deflection (Powers et al., 2012; Reichenbach and Hudspeth, 2014).

1.2.2 The MET channel pore

Farris et al. (2004) measured the MET channel diameter in isolated auditory papillae of red eared terrapins by applying a range of pharmacological channel blockers to the apical surface of cochlear hair cells. Curare, the largest compound tested, has a maximum diameter region of 17 Å (1.7 nm) and penetrates 45% of the way into the membrane electrical field. In order for this to occur, there must be a channel pore region large enough to accept this blocking part of the compound, resulting in the open channel block. Additionally, the rest of the channel must therefore be smaller but must be large enough to accommodate the minimum diameter of the compound (9 Å for curare). Simple amine compounds (methylammonium, trimethylammonium, tetramethylammonium, triethylammonium, tetraethylammonium, tetrapropylammonium and tetrabutylammonium) were also utilised to study the dimensions of the channel pore. They were able to penetrate a similar distance through the electrical field

of the membrane, with smaller amines generally able to penetrate further than larger ones, leading to the conclusion that this is the distance where the channel diameter becomes smaller. Minimum pore diameter was calculated by I_{amine}/I_{Na} (current able to flow through the channel in the presence of a simple amine compound divided by the current in the presence of sodium) plotted against the calculated dimensions for the compounds they tested, fitted with a curve, the equation of which assumed a circular pore and spherical amines. This yielded a minimum pore diameter estimation of ~12 Å (1.2 nm). Using the equation which assumed the channel pore is cylindrical, they were thus able to calculate an estimate of the MET channel pore length (31 Å or 3.1 nm) based on the single channel conductance of the MET channel and the estimated diameter of the pore. Taken together this led to the conclusion that the MET channel pore varies in size, tapering down from the wider channel mouth of 17 Å to 12 Å further through the channel towards the intracellular face. This provided the evidence for a large electronegative vestibule within the MET channel pore.

Farris et al. (2004) proposed that the MET channel contained a large outer vestibule based on the open channel block witnessed where large molecules entered the channel. To test if there was in fact a vestibule which was concentrating ions thus increasing their availability to carry the MET current, similar to the intracellular vestibule in BK channels (Brelidze et al., 2003), Beurg et al. (2006) utilised an extracellular medium of low ionic strength which, as expected, resulted in reduced MET current sizes in apical and mid-coil IHCs and OHCs. Additionally, they found that there was less reduction in inner than in outer hair cells, offering a factor to account for the witnessed larger single channel MET current size and calcium permeability in apical IHCs. The origin of these differences was proposed to lie in different vestibule isoforms, with the IHC isoform containing more negatively charged residues. They also predicted that the basal OHCs, with the largest single channel conductance, would have a vestibule more similar to IHCs, which have uniform single channel conductance along the cochlear length. The existence of the vestibule may explain the much higher affinity block caused by extracellular

compared with intracellular application of channel blockers such as the aminoglycoside antibiotic dihydrostreptomycin (Marcotti et al., 2005; van Netten et al., 2007).

1.2.3 The MET current

As a non-selective cation channel, the MET channel permits the flow of multiple ions and thus it has been demonstrated that the MET current can be carried by a variety of ions. The most plentiful ion in the vicinity in vivo is K^+ and as a result much of the MET current is carried by it. Ca^{2+}, also carries a proportion of the MET current, although it blocks the channel somewhat and thus its conductance is low relative to its permeability (Corey and Hudspeth, 1979, Ricci et al., 2003).

1.2.4 Fast adaptation

The MET current behaves in such a way that shortly after being evoked it then rapidly decreases in spite of continued stimulation. The current can however be recovered by using greater stimulation. This process is known as adaptation. Both fast (submillisecond) and slow (over tens of milliseconds) adaptation components exist in some systems (Vollrath and Eatock, 2003). In the mammalian system the fast component, occurring on a millisecond or a submillisecond basis, is thought to be the major component involved. It is very widely agreed to be a Ca^{2+} dependent process where Ca^{2+} influences MET channel closure when bound at or near the intracellular face of its channel pore, shifting its operating point. Studying the Ca^{2+} dependence of adaptation has been achieved through the use of varying concentrations of internal and external Ca^{2+} and using Ca^{2+} buffers. Peng et al. (2013) have however recently challenged this model, appearing to show that fast adaptation is independent of Ca^{2+} entry due to their ability to elicit currents which adapt even at positive potentials and in the presence of

the calcium chelator 1,2-bis(o-aminophenoxy) ethane-N,N,N',N'-tetraacetic acid (BAPTA) applied intracellularly.

1.2.5 Slow adaptation

Additionally, a slow component (Wu et al., 1999) which has also been posited to be calcium dependent (Corns et al., 2014) is believed to be involved. After MET channels are opened in response to stereociliary movement in the excitatory direction, the stereociliary attached region at the top of the tip links slides down and tip link tension declines (Wu et al., 1999). Myosins such as myosin 7a, are Ca^{2+} sensitive motor proteins which operate along actin filaments, and several isoforms are present in stereocilia. Thus, myosins and especially myosin IC were key mammalian motor protein candidates (Gillespie and Cyr, 2004), as in the bullfrog (Corey and Hudspeth, 1983), thought to detach and then reattach to the stereocilial actin core, allowing the sliding and climbing action. The finding that myosin 1C is at the upper end of the tip links (Assad and Corey, 1992), whilst the MET channels reside at the lower end (Beurg et al., 2009), makes it seem unlikely to be responsible for slow adaptation, as well as some stating that the resultant motility would be too slow to be responsible for adaptation in the mammalian cochlea (Pickles, 2008). What is also contrary to the idea of myosin 1C involvement is the fact that both fast and slow adaptation have been found to be relatively equally altered by changes in intracellular and extracellular Ca^{2+} concentration (Corns et al., 2014). This makes it seem plausible that both these elements arise from the same structure, in this case the MET channel (Corns et al., 2014). Although, some still believe that myosin 1C is a feasible candidate, citing the relatively small contribution of slow adaptation in OHCs relative to that in vestibular hair cells, suggesting that calcium entry though the MET channel might be able to drive myosin 1c to some degree even though it is at the upper end of the tip link (Pan and Holt, 2015). In vestibular hair cells slow adaptation is the major if not the only adaptation

mechanism and there is good evidence for myosin 1C being the adaptation motor (Holt et al., 2002).

1.2.6 Hair bundle stimulation methods

There are two primary stimulation methods used for electrophysiologically studying MET currents; stimulation with a fluid jet and stimulation with a stiff probe. The method I have used to undertake the work in this thesis is stimulation generated by a fluid jet (FIGURE 1-3). I used this stimulus as it allows for studying of the maximum size of the MET currents, as the flow of the fluid which it generates is evenly directed at the entire bundle (Corns et al., 2014) if correctly placed. Additionally, it provides the required level of pushing forward and pulling backward of stereocilia essential for eliciting excitatory and inhibitory responses. An alternative stimulation method involves using a stiff probe to push directly on a proportion of the stereocilia, dependent upon its shape. It has been suggested that the stiff probe may cause damage to the stereocilia. Alternatively, it may just not stimulate the hair bundle evenly, primarily pushing on the tallest bundle, in turn resulting in a broadened current-displacement (I-X) relationship (Fettiplace and Kim, 2014). This is a particular problem where stimulating IHC bundles as they are more uneven than OHC hair bundles (Fettiplace and Kim, 2014). Indzhykulian et al. (2013) investigated the effects on adaptation of different positioning when using a stiff probe as stimuli to open and close MET channels by pushing on stereocilia. They found that placing the probe at a higher level and pushing only on the tallest front row of stereocilia caused increased, faster adaptation of MET currents than when the probe was placed lower down, giving more even stimulation of all bundles. Nam et al. (2015) compared different types of probes for stereocilia stimulation finding the large rounded probe, that they usually used, elicits currents with increased adaptation compared to the other kinds of probes they tested. They discovered that all the probe types that they tested caused bundle deflection which resulted in a broadened I-X relationship, relative to the ideal bundle deflection that they

modelled. They also found that a large flat probe which specifically stimulates only the shortest rows of stereocilia and a thin probe which only pushes on the tallest stereocilia, resulted in a broadened I-X relationship relative to the normal round probe that they use. They did not, however, make a comparison of stimulation using a fluid jet with the stiff probes that they tested.

Inhibitory stimulation is difficult to achieve with the stiff glass probe as it may detach from the bundle when pulled backwards towards the shortest stereocilia as Nam et al. (2015) found to be the case where they used a thin probe which only made contact with the tallest row of stereocilia. They did nonetheless show that the probes which offered less even bundle stimulation elicited currents which showed reduced, not increased, adaptation relative to the probe that they normally use for such experiments. The distinction between the kind of uneven stimulation provided by these probes was distinct from that demonstrated by Indzhykulian et al. (2013) as one was large and flat pushing only on the shorter bundles and although the other did push exclusively on the tallest stereocilia it was very thin. They additionally noted that the thin probe did not adhere well to the bundle, as the retraction of the bundles in the inhibitory direction did not close the MET channels sufficiently well. However, where they used a silicon bundle shaped probe, with pushed on all bundles more evenly than the normal probe, currents which adapted more quickly and strongly were elicited (Nam et al., 2015). Given that different probe shapes and the height at which they are placed appears to affect adaptation, it seems feasible that using a glass probe instead of a fluid jet may stimulate the bundle in a way which elicits a current which displays apparent enhanced decay which looks like adaptation but is actually an Ca^{2+} independent artefact (Corns et al., 2014). Therefore, the finding of calcium independent adaptation (Peng et al., 2013) is questionable. On the other hand, the faster speed of probe stimulation means the stiff probe can be used for studying the kinetics of the MET current, where fluid jet stimulation may only be capable of relatively slow bundle displacements. It is nevertheless possible to study

adaptation characteristics of the MET current, albeit with some distortion, on a submillisecond time scale (Corns et al., 2014).

On the other hand, the faster speed of probe stimulation means the stiff probe can be used for studying the kinetics of the MET current, where fluid jet stimulation may only be capable of relatively slow bundle displacements. It is nevertheless possible to study adaptation characteristics of the MET current, albeit with some distortion, on a submillisecond time scale (Corns et al., 2014).

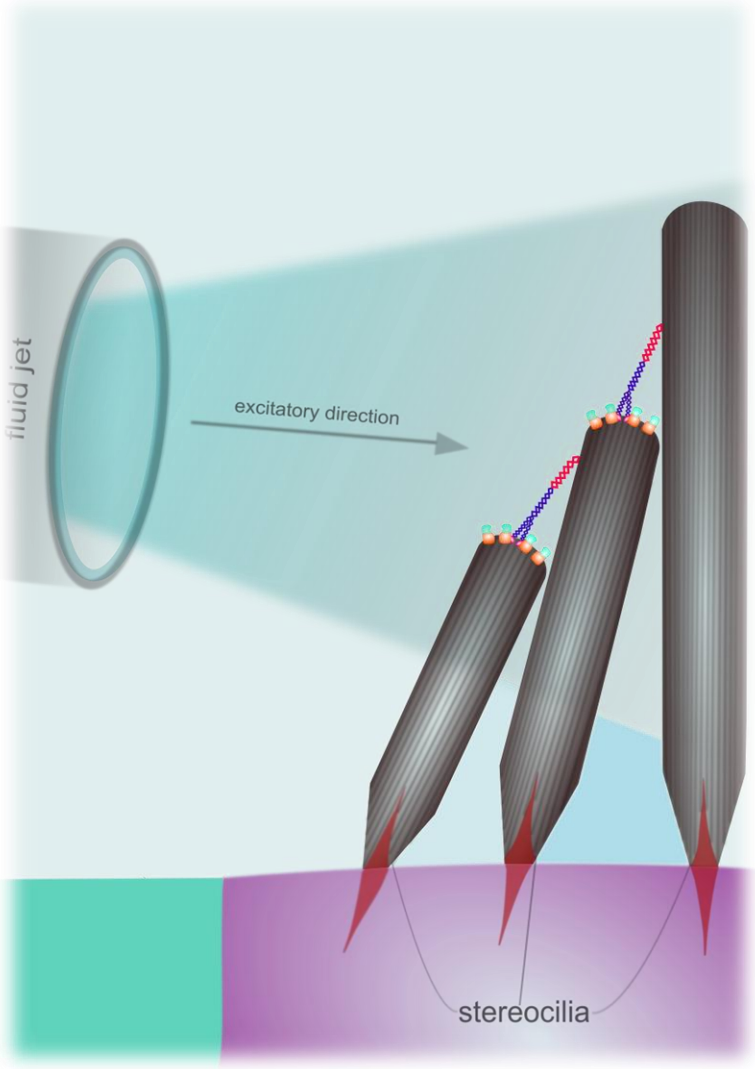

FIGURE 1-3 : Stereocilia atop a hair cell being stimulated by a fluid jet. The fluid moving out of the fluid jet will push the stereocilia in the excitatory direction, towards the tallest stereocilia, opening the majority of MET channels which were not open at rest.

1.3 Mechano-electrical transducer channel channel candidates

After the creation of a large number of Drosophila mutants, the mutations in those demonstrating abnormalities in mechanosensation were studied, including mutations in nompC. In Drosophila possessing nompC mutations, bristle organ MET currents and receptor potentials were lacking. It was subsequently discovered that nompC is a member of the transient receptor potential (TRP) family and is thus now known as TRPN1. TRPN1 has been found to be directly involved in auditory transduction channel gating in Drosophila (Effertz et al., 2012). TRPN1 also localises to the kinociliary tips in zebrafish and is likely thought to play some part in hair cell function as it is present in these cells and TRPN1 removal results in larval deafness (Sidi et al., 2003, Pickles, 2008). This discovery, however, only provided a starting point for the discovery of candidate channels in the mammalian system, as there is no TRPN1 analogue to be found there.

Later the Drosophila Nanchung (Nan) protein was discovered, similar to vanilloid-receptor-related (TRPV) channels. A Nan mutation entirely eliminated sound-evoked potentials, suggesting that it is a crucial component in this process (Kim et al., 2003). TRPV4 is expressed in mammalian hair cells (Ishibashi et al., 2008) and knock out mice have a delayed onset hearing loss but are able to hear for the first 8 weeks of their life, so evidently this channel is not a primary part of the MET channel or the attached complex (Tabuchi et al., 2005).

TRPML3 mutant mice have early onset hearing loss (Palma et al., 2002) and impaired MET, although MET currents with normal polarity and adaptation characteristics are present (Van Aken et al., 2008). This, in addition to the fact that the channels are localised at the base of the stereocilia, makes them poor candidates for components of the MET channel as the MET channels are located at the tops.

TRPA1 channels are activated by pungent compounds such as allyl isothiocyanate (AITC) and play a role in mechanosensation in Drosophila (Walker et al., 2000) and zebrafish (Sidi et al., 2003). TRPA1 was previously thought to be a candidate in the search for the MET channel, as TRPA1 antibody labelling was evident at the tips of the stereocilia and where MET was disrupted this labelling disappeared, additionally TRPA1 disruption interfered with MET (Corey et al., 2004). In spite of this it has now been eliminated as a candidate because TRPA1 knock-out mice show normal MET and hearing (Kwan et al., 2006). Additionally, application of TRPA1 activating pungent compounds does not alter MET (Kwan et al., 2006). TRPA1 channels have an estimated pore size of somewhere in the region of 1.1 nm (Karashima et al., 2010), somewhat smaller than the MET channel pore size estimates made by Farris et al. (2004). In addition to pungent compounds such as AITC and mustard oil, TRPA1 channels can also be activated by endogenous products of lipid peroxidation, such as 4-hydroxynonenal, which are produced as the result of exposure to loud noise and aminoglycosides (Huth et al., 2011). Electrophysiological recordings of TRPA1 channels have shown that they share characteristics of susceptibility and reactivity to permeant blockers with the MET channel. Unpublished data by Karashima and Nillius has shown that DHS blocks the TRPA1 channel in a voltage dependent manner, with stepping the cell to extreme negative potentials resulting in the block being relieved (Nilius et al., 2011).

Texas red conjugated gentamicin (GTTR) and FM1-43 were both found to be capable of entering OHCs, where tip links had been severed by pre-incubation in a calcium-free solution containing the calcium chelator BAPTA (Stepanyan et al., 2011). This only occurred in wild-type and not TRPA1 knockout mice, thus appearing to be a result of TRPA1 activation and subsequent entry through these channels. TRPA1 was activated by the endogenous molecule 4-hydroxynonenal (4-HNE), a phospholipid membrane peroxidation product caused by reactive oxygen species (ROS) reacting with the hair cell membrane in endogenous stress. Creation of

4-HNE can occur after exposure to aminoglycosides, cisplatin (Rybak and Whitworth, 2005) or noise (Yamashita et al., 2004). These results suggest that TRPA1 may provide a secondary route for aminoglycosides entry into hair cells.

The neoteric MET channel candidates are the transmembrane channel (TMC)-like membrane proteins TMC1 and TMC2, which have been localised to cochlear hair cells (Kawashima et al., 2011). However, discovering the elusive MET channel is no easy feat, as it seems that there may be many subunits and additional structural components which form the MET complex (TABLE 1).

Aside from the identity of the MET channel, an additional undiscovered feature of the MET apparatus is how the two identified MET channels, located at the lower ends of the tip links of the second and third rows of stereocilia (Beurg et al., 2009), interact with one another. The question is, is their gating dependent or independent of the gating of one another in a cooperative or anti-cooperative way? The general consensus is that they are independent and that, in single channel recordings, one is indeed witnessing the currents flowing through a single channel (Ricci et al., 2003). However, this may not be the case and ‘single channel recordings’ may instead represent a cohesive current flow through multiple channels (Reichenbach and Hudspeth, 2014).

Candidate Channel	Evidence for mammalian MET channel candidacy	Evidence against candidacy
TRPN1	Direct involvement in auditory transduction channel gating in Drosophila (Effertz et al., 2012). Localises to the kinociliary tips in zebrafish and is likely to play some part in hair cell function as it is present in these cells and TRPN1 removal results in larval deafness (Sidi et al., 2003; Pickles, 2008).	No mammalian TRPN1 analogue (Pickles, 2008).
TRPV4	Expressed in mammalian hair cells (Ishibashi et al., 2008) and knock out mice have delayed onset hearing loss (Tabuchi et al., 2005).	Mutant mice are able to hear for the first 8 weeks of life (Tabuchi et al., 2005).
TRPML3	Mutant mice have early onset hearing loss (Palma et al., 2002) and reduced MET current size (Van Aken et al., 2008).	MET currents with normal polarity and adaptation characteristics are present (Van Aken et al., 2008).
TRPA1	Plays a role in mechanosensation in Drosophila (Walker et al., 2000) and zebrafish (Sidi et al., 2003). TRPA1 antibody labelling at the tips of the stereocilia and where MET was disrupted this labelling disappeared, additionally TRPA1 disruption interfered with MET (Corey et al., 2004).	TRPA1 knock-out mice show normal MET and hearing (Kwan et al., 2006). MET remains unchanged after application of TRPA1 activating pungent compounds (Kwan et al., 2006). Estimated pore size in the region of 1.1 nm (Karashima et al., 2010), smaller than the minimum MET channel pore size of 1.2 nm Farris et al. (2004).
TMC1 + TMC2	Mutations in TMC1 and TMC2 caused hearing loss. TMC1 expression found to occur in the cochlear hair cells and required for the cells to function normally (Kurima et al., 2002). Mice with targeted deletions of TMC1, TMC2 have no evident MET currents (Kawashima et al., 2011). Ca^{2+} permeability and single channel current size are both reduced after altering TMC1 (Pan et al., 2013). TMC1 localised to the stereocilia of hair cells (Kawashima et al., 2011; Beurg et al., 2014), located at the tips of the two shortest rows of stereocilia (Kurima et al., 2015). Block by extracellular and intracellular DHS is reduced in Bth mutant mice, which harbour a point mutation in the gene encoding TMC1 (Corns et al., 2016).	Inverse polarity MET current present in TMC1; TMC2 double mutant mice are present (Kim et al., 2013) with different onset, adaptation and drug block characteristics (Marcotti et al., 2014).

TABLE 1 - MET channel candidates

Met channel candidates are presented with the evidence which validated their candidacy and that which proved that they were not in fact the MET channel.

1.4 Elucidating the properties of the mechano-electrical transducer channel using electrophysiology

Electrophysiological techniques have been used to elucidate the mechanisms by which hair cells function, in terms of the gating mechanisms and activation potentials of the channels contained in their membranes the currents which flow through them, as well as eliminating MET channel candidates. Single channel and macroscopic current recordings can offer different insights.

1.4.1 The location of the MET channel

Fluorescent Ca^{2+} indicator dyes of the Fluo4 family have been utilised to locate the MET channel, as a sufficiently large proportion of the MET current is carried by Ca^{2+} and the intracellular concentration of it in hair cells is relatively low. Stimulating the hair bundles of rat IHCs and OHCs, thus eliciting MET currents, in the presence of the dye whilst using fast confocal imaging allowed Beurg *et al*. (2009) to see where the Ca^{2+} was flowing into the channel and thus where it was located. They discovered that Ca^{2+} signals were far greater and more rapid in the second and third rows of stereocilia when compared with the first row and also indicated that the channels were at the bottom end of the tip links. The channel pore is arguably the channel's defining feature and thus using electrophysiological techniques in combination with channel blockers such as ions or compounds to discover its attributes can be very illuminating.

1.4.2 MET current rectification

Current voltage curves plotted, in 1.3 mM Ca^{2+} stepping the membrane potential of the HCs from -164 to +94 mV in 20 mV steps, show both inward and outward rectification. This occurs because Ca^{2+} and Mg^{2+} plug the channel pore as they flow through it but are increasingly released, permeating the channel, at extreme depolarised (inward current) or hyperpolarised (outward current) potentials, due to the positively charged ions being pulled into the intracellular space or pushed into the extracellular space, respectively (Kros et al., 1992). The MET current was initially thought to be non-rectifying. This was a consequence of conducting experiments where hair cells were not stepped to extreme enough membrane potentials to provide the driving force for rectification to occur and/or the use of intracellular BAPTA, which is a faster acting, stronger Ca^{2+} chelator when compared with others such as EGTA or EDTA, meaning that intracellular Ca^{2+} was not available to cause the rectification characteristics of outward MET currents. Farris et al. (2004) described the MET channel as being 'minimally rectifying', having used 1 mM BAPTA in the intracellular solution and stepping the cells to a maximally hyperpolarised potential of -120 mV, compared with the 1 mM intracellular EGTA and the maximally hyperpolarised membrane potential of -164 mV used in other studies Marcotti et al. (2005) and in this thesis, where characteristic double rectification of the MET current is evident.

Pan et al. (2012) offered a plausible explanation for the fact that some channel blockers block the MET channel far less effectively from in intracellular side than from the extracellular side. Intracellular channel block is inversely voltage dependent, such that maximum block occurs at highly positive potentials, where the polycationic compounds are driven out of the intracellular space into the MET channel pore. At -120 mV they found that the K_D for intracellular FM1-43 was 30x that previously reported by Farris et al. (2004) for extracellular FM1-43. They deemed

access to the internal face of the MET channel was not to be the issue, through the use of fluorescent Alexa 488 tagged dextrans (polysaccharides) in two photon microscopy experiments. These experiments revealed that there was not a diffusion barrier impeding access of the compounds to this region.

Farris et al. (2004) found evidence of the asymmetric MET channel pore size, decreasing from the external mouth of the channel to its internal face. They intracellularly applied two similarly sized molecules, one that was planar and asymmetric (guanidine) and one that was geometrically symmetrical (methyl guanidine). They found that the asymmetric guanidine blocked the channel more effectively and was thus evidently gaining access via its short axis. Intracellularly application of a number of different compounds, which when Farris et al. (2004) applied internally were pushed into the channel at depolarised potentials, allowed them to find that pore size at hyperpolarised potentials was half that at depolarised potentials . Pan et al. (2012), posit the ability of the pore size to change its size dependent on whether Ca^{2+} binding sites are empty or full as Ca^{2+} occludes the MET channel pore. They postulated that the large negatively charged vestibule near the outer face of the channel is responsible for an increased current flow into the MET channel at negative membrane potentials. This in turn causes dehydration and concentration of the ions carrying the current. This is the driving force behind Ca^{2+} removal from the channel, effectively increasing the functional size of the channel pore. At positive membrane potentials, the outward current flow is comparatively reduced as it occurs from the intracellular face of the MET channel, away from the vestibule. Therefore, the driving force is reduced and more Ca^{2+} remains bound in the pore, occluding it, resulting in decreased pore size.

1.5 The Hill coefficient, the two barrier-one binding site model and the nature of different types of MET channel block

In-depth cognisance of the properties of the MET channel pore has been gained through the use of various permeant channel blockers including aminoglycoside antibiotics (Marcotti et al., 2005) and the fluorescent dye FM1-43 (Gale et al., 2001). The Hill coefficient (n_H) is a measure of the degree of cooperativity of the binding process of the blocker to the binding site (Hille, 2001). The slope of the curves which have been fitted with the Hill equation can determine cooperativity of interaction between binding sites within the MET channel pore.

Woodhull, (1973) found that when putting frog nerve cells into a solution with elevated H^+ concentration, H^+ ions would enter, bind and consequently block Na^+ channels in a manner that was dependent upon the membrane potential. This in turn decreased Na^+ permeability. It was noted that seemingly this would need to be the result of the H^+ binding site being a great enough distance across the membrane that changing the voltage across the membrane would influence the movement of ions into the channel. Working with assumptions made based on the apparent nature of the block, a model was fitted from a rate theory of ion kinetics (Eyring and Eyring, 1963; Woodbury, 1971) including two barriers; one on the inside and one on the outside which led to the conclusion that "if a positive ion blocks mainly by entering from the outside… raising the membrane potential relieves the block. If the block is mostly from the [inside]… raising potential increases blocking by driving ions into the blocking position", where the applied voltage fractionally adds to the heights of the energy barriers and to the energy well (binding site). Changing the heights of the energy barriers and the electrical distance of the binding site from the barriers, in the equation, has a significant effect on the level of voltage dependence of the block. Ergo, an increased distance of the binding site, based on the number of positive charges which a compound has, from the outside of the cell results in a steeper voltage dependence (Hille, 2001). In the case of Na^+ ions, raising the membrane

potential resulted in relief of the block and thus H^+ was seen to be blocking from the outside. Woodhull (1973) therefore found that a simpler model, that assumed only entry from the extracellular solution, was sufficient.

DHS is only able to block the open MET channel and this is evident when applying an excitatory mechanical step at -84 mV, as the presence of DHS has no effect on the onset kinetics of the MET current and thereafter settles to a steady state block, increasing with concentration. Stepping the cell to +96 releases the block and when stepping it back to -84 mV, the time constant of the ensuing block is again suggestive of an open channel block (Marcotti et al., 2005). DHS has a Hill coefficient of 1 at all holding potentials and was fitted with a two-barrier one-binding site model (Marcotti et al., 2005). Conversely, FM1-43 is able to reside in both the open and the closed MET channel, as is apparent from the similarity of the kinetics when applying an excitatory or inhibitory step. Gale et al. (2001) used a one barrier model to fit their data on FM1-43 MET channel block, identifying that there were at least two binding sites for FM1-43 in the MET channel pore, based on Hill coefficients (n_H) ranging from 1 at the extreme positive (+96 mV) and negative (-164 mV) membrane potentials to 2 at potentials near 0 mV. Later, the interactional profiles of FM1-43 and DHS with the MET channel were used to further developed the two-barrier one-binding site model to allow for consideration of using it to fit blockers with Hill coefficients other than 1 (van Netten et al., 2007).

The “punch through” effect describes molecules being pulled from the binding site in the channel into the cytoplasm of the cell (van Netten et al., 2007). For DHS this occurs at extreme negative potentials below -80 mV (Marcotti et al., 2005). Failing to step cells down to sufficiently negative membrane potentials previously meant that the punch-through effect was not evident for DHS and it thus was thought for a time to be an impermeant MET channel blocker (Kroese et al., 1989). If the blocker was not permeating through the channel pore, one

would expect to see the block getting increasingly strong without release of block at extreme hyperpolarised potentials. FM1-43 has a somewhat different profile, blocking the MET channel maximally around 0 mV, where n_H = 2. At more positive or negative potentials than this n_H decreases to 1 at the extreme ends. A blocker which was unable to permeate the channel would not demonstrate this apparent decrease in fractional block of the current at increasingly hyperpolarised potentials.

$$\frac{I_{\text{peptide}}}{I_{\text{c}}} = \frac{1}{1 + \left(\frac{[\text{D}]_{\text{o}}}{K_{\text{D}}}\right)^{n_{\text{H}}}}$$

Equation (1): The Hill equation

Equation from Marcotti et al. (2005), for equations and explanations on calculating K_D see Marcotti et al. (2005).

The two-barrier-one-binding-site model suggests that the MET channel has an inner and outer electrical barrier and a binding site within it, representing the "energy minimum in the movement of an ion [through the channel]" (Woodhull, 1973).

Conformational change can result from the binding of ligands to allosteric sites (sites other than the active site) on proteins. The Monod-Wyman-Changeux model describes the cooperativity between binding sites on proteins with multiple subunits by means of allosteric transitions (Monod et al., 1965). When applied to cooperativity of ligand-gated channels, this model does not consider the possibility of any direct interaction between the binding sites on different subunits. Instead the cooperativity arises from binding at one site causing conformational change in the subunit that it's on. The interfaces where the subunits are packed together then cause changes in protein conformation and ultimately affect the binding at another binding site. This is not applicable to the MET channel, which is mechanically gated and any change in the size of the channel pore is thought to occur through Ca^{2+} binding (Pan et

al., 2012). However, as described by Jackson, (2002) the Weber theory (1992), which built upon the Monod-Wyman-Changeux model (Monod et al., 1965), to include consideration of direct interaction between binding sites can offer some insights, as no allosteric transitions are necessary to cause cooperative change in binding sites, but instead distortion at a binding site, induced by binding of ligands, in turn causes distortion at other binding sites altering the affinity of these sites. This is analogous to the binding of compounds with multiple binding sites, in the MET channel. This theory applies the idea of coupling energies which equate to the free energy of one binding site when an additional site is empty or occupied by a given compound. It turns out that where absolute cooperativity is considered; infinite coupling energies become a requisite, an argument for interpreting the Hill coefficient as the minimum number of binding sites and not the absolute number (Jackson, 2002).

1.6 Cooperativity and negative cooperativity

From the Hill coefficient (Hille, 2001) we may firstly be able to infer whether there is a single or multiple binding sites for the compound in question. Secondly, if there are multiple binding sites we can gain a measure of the level of cooperativity between them. A neutral cooperativity of $n_H = 1$ may lead us to believe that there is a single binding site. However, this is only one possible explanation. Withal, a Hill coefficient of one indicates zero or neutral cooperativity, which may in fact represent the fact that there are multiple binding sites with equal affinities which are independent of one another. The $n_H = 1$ which has been found for DHS channel block, however, does not vary with holding potential (Marcotti et al., 2005). Therefore, making the least assumptions it seems fair to posit that there is only one binding site for DHS in the MET channel. Additionally, according to the energy profile presented by Marcotti et al. (2005), because of its electrical distance from the extracellular side this binding

site is likely to be nearer narrow region of the channel pore. Positive cooperativity is indicated by a Hill coefficient of greater than 1, which will obtained from a steeper fitted curve than the former. It means that the binding of one molecule to one binding site, increases the chances of another molecule of the same compound binding to another binding site within the channel. The binding profile of FM1-43 is an interesting example, in so far that it varies with the voltage at which the cell is held during patch clamp manipulation. At the extreme ends of the positive and negative holding potentials, the Hill coefficient is around 1. This varies at positive and negative holding potentials near zero, where the Hill coefficient gets closer to 2 meaning positive cooperativity is dramatically increased. Perhaps the influence of the binding of the first molecule on the other molecules is less at extreme negative or positive potentials due to the net forces pulling the molecules to the inside or outside of the cell.

A Hill coefficient of less than 1 equates to negative cooperativity and interpreting negative cooperativity is more complex. It may result from the existence of distinct binding sites with different binding affinities binding independently. Alternatively, it may mean that the binding of one molecule reduces the likelihood of a second molecule binding (Ferguson et al., 1975; Jackson, 2002). Additional information about the channel is required to work out which of these is more likely potentially achievable by molecular analysis of receptor structure (Jackson, 2002).

2 METHODS

2.1 Cultured cochlea preparation

OHCs from CD1, C57/SV129, TRPC 3/6, TRPC 1/3/6 and TRPC 1/3/5/6 were studied in organotypic cultures. Mice were killed by cervical dislocation in accordance with UK Home Office regulations and with approval of the local ethical committee. The pups were postnatal day 2 (P2) in age at the time of dissection and the cultures were grown on collagen-coated, round glass coverslips for between 1 (P2 + 1) and 3 (P2 + 3) days at 37°C in Maximow slide assemblies in a medium containing 93% DMEM/F12 (v/v), 7% fetal bovine serum (v/v). Cochlear coils were then dissected into apical and basal segments two apical and two basal cochlear coils were placed onto each coverslip. Alternatively, coils were kept whole and a single whole coil was placed onto each coverslip.

2.2 Live cell imaging using a light microscope

In order to observe phosphatidylserine (PS) externalisation (as described by Goodyear et al., 2008), Alexa Fluor 488 conjugated annexin V was added at a dilution of 1:50 when testing each culture. In order to compare their toxicity D-JNKi1 and D-HIV-TAT (D-TAT) were tested at a concentration of 5 µM (based on a previous assessment of the effects of different concentrations of the compounds, at 5 µM a consistent PS externalising affect from apex to base was witnessed). In order to study entry into the cells, Texas Red conjugated D-JNKi1 (TR D-JNKi1) and D-TAT (TR D-TAT) were also used in separate experiments at a concentration of 5µM. A Zeiss AxioPlan II light microscope was used for live imaging. The coverslips with four adherent cochlear cultures, two apical and two basal, were transferred from the Maximow slide assemblies into a glass-bottom, Perspex slide chamber and 0.5 ml of HEPES-buffered (10 mM, pH 7.2) HBHBSS was added. The cultures were located using a 10x lens and then the hair

cells were viewed using a 63x water-immersion lens. Nomarski interference contrast optics were utilised. Images were captured after addition of Alexa Fluor 488 conjugated annexin V and the compound to be tested. Exposure to illumination was restricted to the times necessary to focus and capture the images, in order to prevent phototoxicity and keep photobleaching to a minimum. Images were taken from fields in the middle region of each coil with a Spot RT slider digital camera, fixed exposure times were used: 3 seconds for the green channel and 0.5 seconds for the red channel and the images were then saved and stored on a computer. The FITC (green) filter set was used to visualise annexin V fluorescence (indicating PS externalisation) and the Rhodamine (red) filter set was used for viewing Texas Red fluorescence. See Goodyear et al., 2008.

2.3 Fixation and immunofluorescence labelling

Coverslips with the adherent cultures were firstly removed from the slide chambers and then placed in 35-mm-diameter plastic culture dishes and washed three times with HBHBSS, this represented 20 minutes of exposure to a given compound. Cultures were fixed for 1 hour in 3.7% (v/v) formaldehyde in 0.1 M sodium phosphate buffer (pH 7.4). After fixation, cultures were washed three times in PBS, preblocked and permeabilised for a short 15 minute period in 10% (v/v) horse serum in PBS with 0.1% (v/v) Triton X-100 added. The cultures were then washed three times with PBS, and labelled with rabbit anti-Alexa Fluor 488 IgG at a dilution of 1:100 and Texas Red phalloidin at 1:300 overnight. Then the cultures were washed three times with PBS and the secondary antibody, Alexa Fluor 488-goat anti-rabbit IgG was then added.

2.4 Confocal microscopy

Stained and mounted cultures were viewed with a LSM 510 Meta confocal microscope using a 100x, NA 1.4, oil-immersion lens. Images were acquired with the LSM 510 Meta using the

488 nm Argon laser line in order to excite Alexa Fluor 488 annexin V and the 543 nm HeNe laser line to excite Texas Red. Images were taken at different levels in order to visualise both hair bundle staining with annexin V and loading of Texas Red conjugated compounds into the hair cells.

2.5 Analysis of cell culture microscopy data and figure creation

A series of composite images were created using Photoshop CS2. Pseudo-colouring via Photoshop CS2 was used to illustrate Texas Red (red channel) fluorescence. In order for the difference in fluorescence levels of the Texas Red conjugated D-JNKi1 and D-TAT pseudo-coloured images to be observable and comparable, the contrast and brightness of these images were altered by creating a 'Levels Adjustment Layer' in Photoshop CS2. Within FIGURE 4-4, alterations were kept to the same level in order for the images to remain comparable.

For the purpose of generating numerical data, 10x magnification light micrograph composites of the hair cells were used (FIGURE 4-3). Using Photoshop CS2, measurement of arbitrary grey levels from hair cells responding to treatment with the compound, in a given culture, were taken. Grey levels were measured using Photoshop CS2. The grey level was obtained using the Histogram tool, which provided the arbitrary reading entitled 'mean'. All the hair cells which were externalising PS, to an arbitrary grey level which was calculated to be the threshold as it was above the background fluorescence level, were counted. This level was calculated to be anything above 0.40, using the Histogram tool. This was done for two apical or basal cultures tested and then the values obtained were added together. The average number of hair cells in the apical and basal cultures used were calculated and multiplied by two. The resulting value from the addition of the two cultures added together was then divided by the average total

number of hair cells in a culture of the same type and then this was multiplied by 100 in order to obtain a percentage of cells externalising PS for those cultures.

2.6 Experimental equipment for electrophysiology

The cultured organ of Corti preparations were viewed using an upright light microscope equipped with a x60 water-immersion objective lens and Normarski interference contrast optics utilised as well as a x15 eyepiece. The cultures were sat in a bath chamber, with an inflow and outflow tube to allow constant perfusion of fresh extracellular solution. This sat atop a rotating stage to allow access to the cells from different angles. Cultured preparations were perfused with an extracellular solution in the bath chamber at a rate of 0.12ml/min using a peristaltic pump (Cole-Palmer, IL, USA). Perfused extracellular solution was pre-filtered using a Millipore Millex syringe filter unit and tubes were connected to the inflow and outflow of the bath. To reduce noise picked up by the bath chamber from the peristaltic pump the chamber was grounded through a 63 µF capacitor, connected to the inflow, to the headstage, in parallel with the bath electrode. Hair cells from apical and basal coils at room temperature (~ 21°) were whole-cell voltage clamped and recorded from using the patch-clamp amplifier. The setup, including the microscope, was placed on an air table and inside a Faraday cage to reduce movement and electrical noise.

To deliver compounds to the culture, a gravity fed system was used. This was comprised of filled syringes with taps, connected to tubes which were fed into a system of very fine tubes bound together using dental cement and parafilm, all leading to the same relatively large end (in comparison to the size of the cochlear culture), out of which any of the solutions could flow if the tap connected to the syringe containing it was open. This was placed two and a half turns of the focus knob above the preparation in the bath. Manual control of the syringe taps

allowed for application of and fast changes between solutions. There was always a control solution and 1-3 solutions containing compounds.

The patch electrode, comprised of a silver chloride wire coupled to a polycarbonate electrode holder with a pin headstage connector, connected to a Cairn Optopatch head-stage and an Optopatch patch-clamp amplifier. The signal was filtered through an 8-pole Bessel filter at 2.5 kHz prior to being inputted into a Power1401 data acquisition interface (Cambridge Electronic Design) allowing for analogue to digital conversion.

Using an upright glass puller (Narishige, Tokyo, Japan) cleaning pipettes were pulled from borosilicate glass capillaries and patch pipettes from soda glass capillaries. A cleaning pipette, with an attached syringe to provide suction, made of glass with a tip diameter around 7 µm, filled with extracellular solution, was used to remove supporting cells, in order to expose the basolateral surface of the OHCs. A patch pipette with a resistance of around 1.8-2.8 MΩ was used to patch the basolateral membranes of the OHCs. Patch pipettes were coated, from half way down the shaft to within 100 µm of the tip, with a thin layer of wax (Mr Zogs SexWax, Carpinteria, CA, USA).

2.7 Solution composition for electrophysiology

The patch-pipettes were filled with a caesium chloride based intracellular solution, used in order to block potassium channels, so that potassium currents would not be recorded as this would interfere with MET current visualisation. This solution contained (mM) 135 CsCl, 2.5 $MgCl_2$, 2.5 Na_2ATP, 1 EGTA-CsOH, 5 HEPES, 10 Na_2phosphocreatine. The solution had a final pH of 7.28 and an osmolarity of, ± 5 mOsm kg^{-1}, ~295 mosm kg_{-1}; (10-15 mOsm below extracellular).

The high Na+ extracellular (perilymph mimicking) solution contained (mM) 135 NaCl, 1.3 $CaCl_2$, 5.8 KCl, 0.9 $MgCl_2$, 10 HEPES-NaOH, 5.6 $_D$-glucose, 0.7 NaH_2PO_4 and 2 sodium pyruvate, Eagle's minimum essential medium (MEM) concentrated amino acids and vitamins . The solution had a final pH of 7.48 and an osmolarity of, ± 5 mOsm kg^{-1}, 308 mOsm kg^{-1}. (10-15 mOsm above intracellular).

Control extracellular solution used for drug superfusion was composed of (in mM) 135 NaCl, 1.3 CaCl2, 5.8 KCl, 0.9 $MgCl_2$, 10 HEPES-NaOH, 5.6 $_D$-glucose, 0.7 NaH_2PO_4 and 2 sodium pyruvate. The solution had a final pH of 7.48 and an osmolarity of, ± 5 mOsm kg^{-1}, 305 mOsm kg^{-1}. (10-15 mOsm above intracellular).

For recording the anomalous currents, cells were bathed in a Ca^{2+}-free, BAPTA-containing extracellular solution (in mM: 141 NaCl, 5.8 KCl, 0.7NaH2PO4, 5.6 D-glucose, 10 HEPES NaOH, 5 Na_4BAPTA) for 5 minutes prior to exchanging the bath solution with normal extracellular solution twice.

2.8 Compounds

D-TAT was obtained from Enzo Life Sciences and later was synthesised for us by LifeTein. The stock solution was prepared from 500 µM D-TAT powder which was diluted to 100 µM by weighing out and adding 1 part 500 µM D-TAT to 4 parts H_2O. D-JNKi1 was obtained from Enzo Life Sciences and later was synthesised for us by Invitrogen. Solutions were prepared from 100 µM D-JNKi1 stock solution prepared by weighing out and adding 1 part 500 µM D-JNKi1 powder to 4 parts H_2O. The stock solutions for both peptides were stored in small aliquots which were only freeze-thawed once in order to prevent any degradation caused by the freeze-thawing process. Superfusion stock solution of concentrations varying from 3 nM to 1 µM was prepared daily by adding the 100 µM stock to control extracellular solution.

DHS was obtained from Sigma-Aldrich. FM1-43 was obtained from Life Technologies. Fresh solutions were prepared each day by adding the powder compounds to extracellular solution to make solutions ranging in concentration from 100 µM to 3 mM DHS and 1 µM to 30 µM FM1-43.

2.9 MET current recording in whole cell mode

Hair cells were recorded from using the whole cell patch clamp technique. This was achieved by applying mouth pressure through tubing connected to the patch electrode. Positive pressure allowed for seeing dimpling in the cell membrane of the hair cells. Following this, light suction was applied in order to pull a patch of membrane with the aim of forming a Gigaohm seal. The membrane potential was then stepped to -80 mV and capacitive transients were compensated for. Additional light suction is then applied to break the cell membrane open, allowing for access to the cell so that the intracellular solution in the cell and the patch pipette became continuous: the 'whole cell' configuration is thus established. Compensation for the membrane capacitance (C_m) and series resistance (R_s) was applied and noted, providing information about the cell size and quality of the seal. In order to eliminate the potential disparity in voltage clamp recordings between clamped potential and the actual membrane potential of the cell caused by voltage-drop of membrane currents across R_s, compensation of the latter of between 50% and 80% was applied using the Optopatch patch clamp amplifier. Membrane capacitance (C_m) of outer and inner hair cells varied from 5.5 to 10 pF (with inner hair cells having a larger C_m) and R_s after compensation varied from 0.5 to 2.5 MΩ.

In patch-clamp experiments which aim to measure MET currents, a cesium based intracellular solution was used to block K^+ channels. This is helpful because otherwise the large basolateral currents carried by K^+ that flow upon depolarization would dwarf the MET current recordings.

In the main protocol I have used in this thesis, the cells are stepped from a negative (-164 mV) to a positive (+94 mV) potential in 20 mV incremental voltage steps. However, in order to ascertain if some aspects of the blocking profile of a given drug are related to some second-order component of the drug block which is slow relative to the time scale of the voltage steps in the protocol, it may be useful to use a protocol that steps from a positive to a negative potential. An example of this is where a drug appears to be blocking at positive potentials. One wishes to see if this is the effect of having the drug pulled into the channel over multiple negative voltage steps, or if this block still readily occurs where the first step applied is highly positive. Additionally, voltage steps applied in conjunction with mechanical stimuli in the form of square steps can be used to see the kinetics of channel block.

Eliciting MET currents was achieved by utilising a fluid jet, a borosilicate glass pipette with a diameter of ~10 µm (a larger tip of ~14 µm for recording anomalous currents), attached to a glass encased Piezo driver. The fluid jet was placed at the modiolar side of the hair bundle, optimised for close positioning and diameter in order to maximally stimulate the bundle. A protocol which applied four successive 45 Hz sine waves was used with a driver voltage of 40 V, with a positive driver voltage equating to a force which pushed the bundle in the excitatory direction, towards the tallest row of stereocilia. The voltage applied to the Piezo driver was filtered through an 8-pole low-pass Bessel filter at 1.0 kHz.

During a given experiment, recordings were made before drug application, with positioning and height readjustments made as necessary in order to attempt to obtain recordings of the maximum obtainable MET current amplitude. Compounds were then applied using the gravity fed superfusion system, placed two and half turns of the focus nob above the preparation in all experiments. After the application of the drug via the superfusion system, a small constant negative pressure at the fluid jet ensured it would suck up the compound so that it could be applied at the correct concentration to the MET channel. The sine wave stimulus was applied several times until a consistent level of MET current block was seen. The control solution was

then applied and the same procedure was followed where possible (if the cell continued to be viable) to obtain washout recordings where control ECS was applied to wash the compound away from the hair cells, in an attempt to release any MET channel block.

2.10 Data Acquisition and Analysis

Data was acquired using Signal 4.3 software (Cambridge Electronic Design). Protocols were written to set the command voltage and apply the sine wave stimulus to the hair bundle. The cells were held at -80 mV using an external voltage calibrator. During a given recording the cell was stepped in 20 mV increments from -164 to +94 mV, whilst a sine wave stimuli was applied driving the piezo driver. The sampling rate used was 10 kHz.

The traces were saved as text files in Signal 4.3 and opened in Origin 7.0 for analysis. The peak and trough of the third (FIGURE 2-1) or fourth sine wave were measured for each recording condition with measuring consistency being kept between recordings which were going to be compared (before and during the drug application). If there was evident electrical noise in the traces, an average of two or three sine waves was taken. The trough measurement (the leak) of the sine wave was then taken away from the peak current. Measurements were taken from the control recording prior to the application of a given compound, one of a number of recordings where the compound was being applied and where recording due to cell viability was possible a washout recording.

2.11 Statistical analysis

GraphPad Prism 4 was used for statistical analysis. To look at the effect of location (apical or basal) and voltage (-164 mV through to +94 mV) on mean current amplitudes in chapter 3, a two-way ANOVA followed by Bonferroni's test was used. To compare the mean number of channels in apical and basal OHCs in chapter 3, an unpaired t-test was used. To look at voltage

and concentration dependence in chapter 6, statistical comparisons of mean current amplitudes at the different membrane potentials (-164 mV through to +96 mV) where different concentrations of a given compound were used, were made using a two-way ANOVA followed by Bonferroni's test. <0.05 was used as the criterion for statistical significance. Mean values are quoted ± S.E.M in text and figures. For calculating whether the K_Ds in chapter 4 were significantly different, Origin 7.0 was used. The graphs were plotted using a 95% confidence interval and thus upper and lower limits at this level could be obtained. Where a given pair of limit values (upper and lower) was not within the same range as another this difference had a statistical significance of $P < 0.05$.

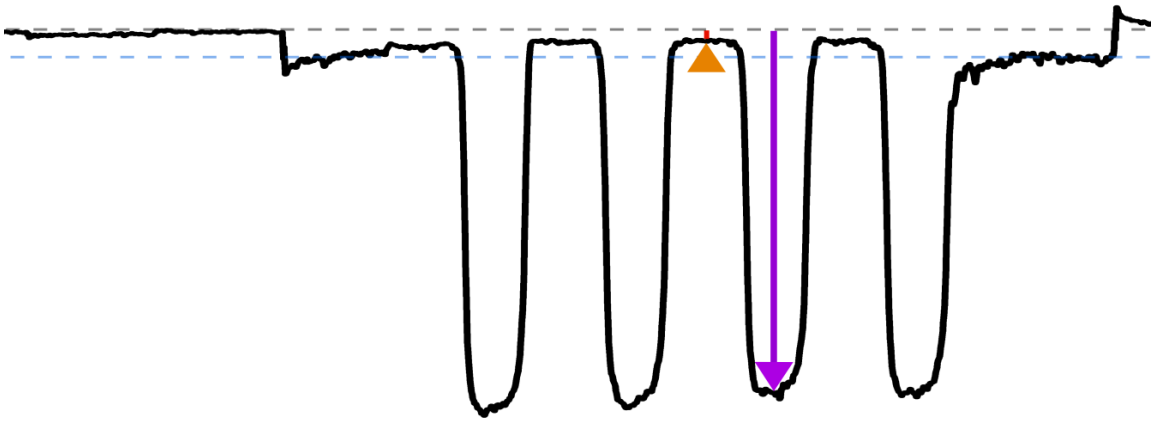

FIGURE 2-1: MET current measurements. Illustration of the regions that MET current 'peak' and 'trough' measurements were taken from. The example trace used here was obtained at a membrane potential of -164 mV. The dashed grey line indicates the zero (baseline) line of the trace. The dashed blue line indicates the level of the current flowing through the MET channels which are open at rest due to their resting open probability. The purple line with the arrowhead indicates the region and what is measured when taking the 'peak' measurement. The orange arrowhead indicates where the trough measurement is taken and the red line indicates the leak current which is deducted from the peak current (peak – trough = measured current size).

3 A GRADIENT IN OUTER HAIR CELL MECHANO-ELECTRICAL TRANSDUCER CHANNEL PROPERTIES FROM APEX TO BASE

3.1 Introduction

There are a number of characteristics which vary from apex to base in the cochlea. Adaptation is faster in basal hair cells compared to apical hair cells (Ricci et al., 2005), the resting open probability of the MET channel decreases from base to apex (Dallos et al., 1982; Johnson et al., 2011), hair bundle height decreases from apex to base whilst the number of stereocilia increases (Roth and Bruns, 1992; Beurg et al., 2006). As basilar membrane flexibility increases and thickness decreases from base to apex, levels of displacement differ such that the basal region is selectively sensitive to high frequency sounds and low frequency sounds are encoded at its apex. There are also variations in the characteristics of the outer hair cells. Single channel conductance of the MET channels is greater in basal hair cells in both rats (Ricci et al., 2003) and mice (Beurg et al., 2006). More recently, a gradient in macroscopic MET currents in the mouse has been found (Kim and Fettiplace, 2013) . Thus, there is evidence for multiple channel isoforms, which account for differences in single channel conductance, potentially in addition to a greater number of MET channels from apex to base contributing to larger macroscopic MET currents.

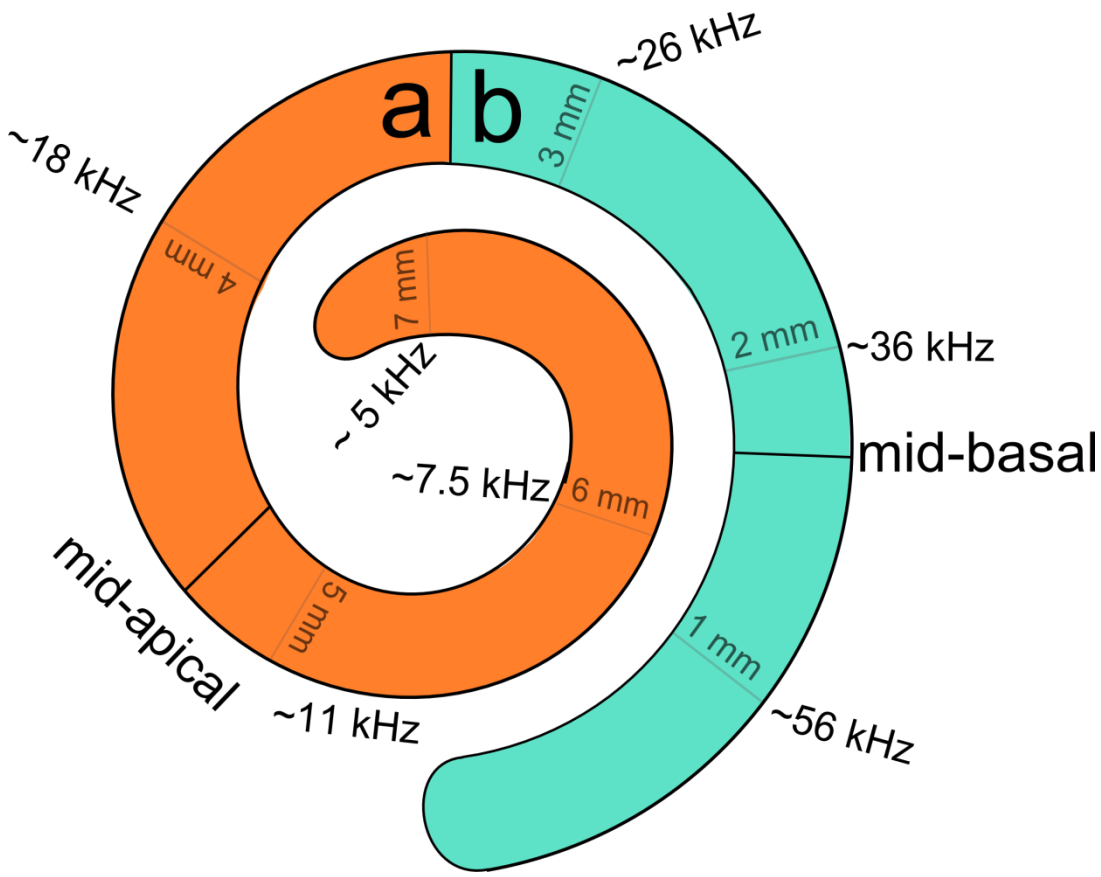

FIGURE 3-1 : Apical and basal regions in the mouse cochlea. Illustration of apical (orange) and basal (aquamarine) cochlear regions, with mid-apical and mid-basal regions indicated. Positions are plotted according to Bekesy (1960) and corresponding frequencies are plotted according to Viberg and Canlon (2004), Müller et al. (2005) as in Sanz et al. (2015).

3.2 Results

Where MET currents were evoked by a fluid jet, whilst hair cells were whole-cell patch clamped, there is an evident difference in the average MET current sizes of mid-apical and mid-basal OHCs. This is congruent with previous data from apical and basal cochlear hair cells illustrating a gradient in both rats (Ricci et al., 2003; Beurg et al., 2006) and mice (Kim et al., 2013), demonstrating differences in single channel current sizes. As well as this, apical and basal MET current peak amplitudes have been characterised as consistently varying in amplitude when compared at different developmental stages (from P1 to P10 in apical OHCs and P1 to P5 in basal OHCs) in mice (Kim and Fettiplace, 2013). Thanks to high n-numbers, my results provide strong evidence of an increase from apex to base in macroscopic MET current size in the P2 (+1-3) mouse cochlear OHCs. A two-way ANOVA test followed by Bonferroni's test, comparing the size of the currents in different locations (apical or basal regions) and at different membrane potentials (-164 mV to +96 mV), revealed that a statistically significant ($P<0.0001$) correlation between the variation of voltage and location, meaning that location had an effect on the amplitude of the current at every membrane potential. Moreover, the variation in current size with location is statistically significant ($P<0.0001$) and thus there is a statistically significant difference between the currents recorded from mid-apical and mid-basal OHCs.

In order to gain an estimate of the amount of MET channels atop apical and basal OHCs, I analysed the macroscopic MET currents recorded from each individual cell in both the apical and basal regions at a membrane potential of -84 mV. I then divided those values with the single channel recordings obtained by Kim et al. (2013) at the same potential of 5.2 pA in apical P4-P5 OHCs and 8.5 pA in basal P3 OHCs. I was then able to calculate a mean number of channels ± S.E.M (TABLE 2). There were found to be 134 ± 6 channels in apical cells (n = 75)

and 102 ± 9 in basal cells (n = 19). There was a significant difference ($P < 0.05$) between these two values, as determined by using an unpaired t-test.

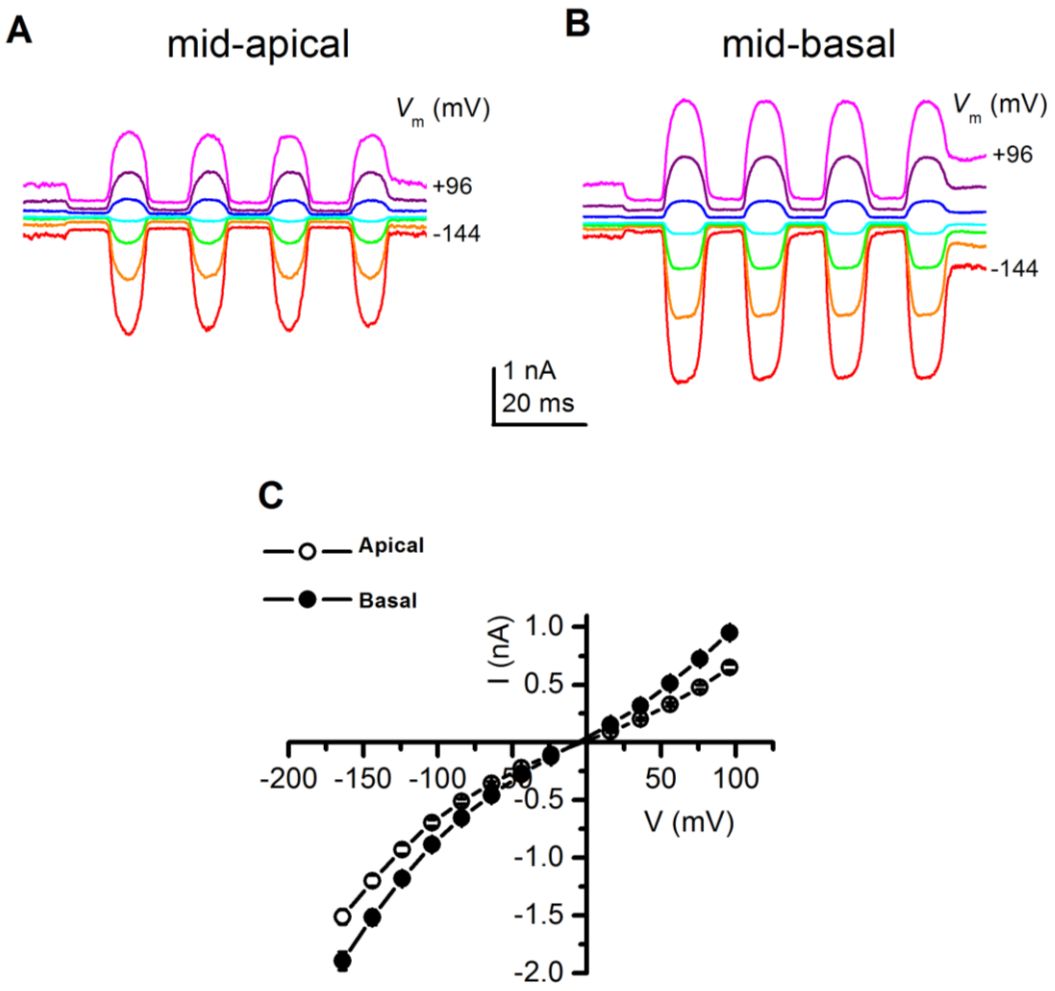

FIGURE 3-2 : Difference in amplitude of apical and basal OHC MET currents. A, B, Illustrative traces from mid-apical (A) and mid-basal (B) OHCs. **C,** Averaged current-voltage curves from mid-apical and mid-basal CD-1 outer hair cells (C). Half the voltage steps used are shown for clarity (-144, -104, -64, -24, +16, +56, +96 mV). Driver voltage (45 Hz sinusoid, 40 V amplitude) plotted above the current traces. At -104 mV the size of mid-apical OHC MET currents was -696 ± 29 pA (mean ± S.E.M., n = 75), this was significantly different ($p < 0.0001$; two-way ANOVA with Bonferroni's test comparing the currents at the different voltage steps and concentrations) from mid-basal coil CD-1 OHCs (-884 ± 41 pA, n = 19). This illustrates the tonotopic gradient in OHCs that is believed to exist.

	Single channel current (pA) at -84 mV	Mean whole cell MET current (pA) at -84 mV	Number of channels (single channel/macroscopic MET current)
Apical OHC At -84 mV	5.2	-510 ± 21	134 ± 6
Basal OHC At -84 mV	8.5	-654 ± 31	102 ± 9
Apical OHC Max macroscopic current at -84 mV	5.2	-877	-877 / 5.2 = 168
Basal OHC Max macroscopic current at -84 mV	8.5	-1173	1173 / 8.5 = 138

TABLE 2 – Number of MET channels in apical and basal OHCs

Single channel current size, whole cell MET current size and number of channels per hair cell. Mean values are quoted ± S.E.M. Macroscopic averages I obtained at-84 mV: averages of -510 ± 21 pA in apical OHCs (n = 75) and -654 ± 31 pA in basal OHCs (n = 19). The largest macroscopic currents recorded at -84 mV: -877 pA in apical OHCs and -1173 pA in basal OHCs. Single channel recordings obtained by Kim et al. (2013): 5.2 ± 0.1 pA in apical P4-P5 OHCs and 8.5 ± 0.2 pA in basal P3 OHCs. Number of channels per hair cell was calculated by dividing whole cell MET current from each individual hair cell, from both the apical and basal regions, by the single channel conductance obtained by Kim et al. (2013) and then obtaining a mean number of channels ± S.E.M. This yielded 134 ± 6 in apical cells (n = 75) and 102 ± 9 in basal cells (n = 19).

3.3 Discussion & conclusions

It has previously been shown that MET current size increases from apex to base in both single channel (Ricci et al., 2003; Beurg et al., 2006; Kim et al., 2013) and macroscopic MET current recordings (Kim and Fettiplace, 2013). This seems to account, at least in part, for the increased susceptibility of basal OHCs to damage by ototoxic agents (Kamimura et al., 1999). The unique insight offered by my data lies in the large number of cells recorded from in two specific areas of the cochlea, namely the mid-apical and mid-basal regions. As there is some variation in the sizes of MET currents recorded, even from hair cells in the same region, in mice of the same age, a large n-number is useful for reliability of the data.

Single channel currents are larger in basal than in apical OHCs indicating that there are different channel isoforms in these cells (Beurg et al., 2006; Kim and Fettiplace, 2013). This is consistent with an increasing pool of evidence that suggests that the MET channel is composed of subunits which can vary dependent upon location along the cochlear, based on increasing channel pore size or the number of negatively charged residues within the channel pore (Beurg et al., 2006; Kim et al., 2013). It has been postulated that it may not only be the increased single channel conductance from apex to base which results in increased macroscopic MET current size; there may also be also a greater number of channels in basal OHCs due to the additional stereocilia found atop OHCs in this region (Fettiplace and Kim, 2014). The data presented here, however, are at odds with the latter assertion. By dividing the macroscopic MET current size from each individual recording in mid-apical and mid-basal OHCs obtained here by the respective average single channel current size obtained by Kim et al. (2013), I have obtained an estimate of the number of channels in apical and basal OHCs (TABLE 2). The data suggest that there are in fact more channels in apical than in basal OHCs. The averages obtained at -84 mV suggest that there are 134 ± 6 channels per apical OHC but only 102 ± 9 per basal OHC. Moreover, the macroscopic MET currents with the highest amplitudes which I

recorded are most representative of the true size of the currents. Therefore, they are representative of the actual number of MET channels which a P2 OHC is likely to possess, as one can assume that the least channels have been lost in these cells and the maximum amount are being stimulated. Using these currents to calculate the number of MET channels yields a noticeably higher value, with an even greater disparity between apical and basal OHCs: 168 in apical OHCs and 138 in basal OHCs (TABLE 2). Therefore, it appears that it is only an increase in single channel conductance from apex to base which results in increased macroscopic MET current amplitude.

4 GRADIENTS IN THE INTERACTION OF THE OTOTOXIC PEPTIDES, D-TAT AND D-JNKI1, WITH THE MECHANO-ELECTRICAL TRANSDUCER CHANNELS IN COCHLEAR OUTER HAIR CELLS

4.1 Aminoglycoside ototoxicity

Ototoxicity is the property of being reversibly or irreversibly toxic to the cochlea or auditory nerve. Noise trauma and the actions of ototoxic compounds such as aminoglycoside antibiotics, cisplatin (and other platinum containing compounds used in chemotherapy), aspirin (as well as other nonsteroidal anti-inflammatory drugs), heavy metals and quinine can all cause ototoxicity (Cheng et al., 2005). Aminoglycosides are not entirely selective for bacterial (prokaryotic) rRNA, also binding to a proportion of cytoplasmic rRNA in eukaryotic cells (Böttger et al., 2001). They damage hair cells via a variety of possible mechanisms, after entering hair cells through the MET channel (Marcotti et al., 2005).

Aminoglycosides are broad-spectrum bactericidal antibiotics that are particularly effective against gram-negative, aerobic bacteria as well as *Mycobacterium tuberculosis* (Kumana and Yuen, 1994). They are used to treat serious illnesses such as cystic fibrosis (Tan et al., 2003), multidrug-resistant tuberculosis (Gonzalo et al., 2014) and septicaemia (Picard et al., 2014). The prevalence of life threatening conditions in developing countries such as South Africa (Petersen and Rogers, 2015) as well as their low cost and efficacy means that they are especially widely used there, as well as still being used in countries with richer economies, albeit more sparingly than in previous decades. Estimates of the number of aminoglycoside induced hearing loss sufferers varies but is somewhere in the region of 17-33% of the people who are given them (Fischel-Ghodsian, 2005).

Lacking the inherent ability to regenerate hair cells that fish (Lombarte et al., 1993) and birds (Weisleder and Rubel, 1993) have, ototoxic agents such as aminoglycosides can result in irreversible damage to mammalian cochlear hair cells and thus to the hearing of individuals. Many attempts have been made at deconstructing the process of hair cell development with a view to understanding (Li et al., 2015), and ultimately harnessing the ability to enable regeneration of hair cells from precursor cells, in the organ of Corti, using reagents. Recruiting

supporting cells as facultative progenitor cells and manipulating cell fates (Fujioka et al., 2015) and the use of manipulated stem cells (Hu and Ulfendahl, 2013) are under investigation.

A number of genes which are involved in the cell death cascade in hair cells, as well as other cell types, have been identified. Caspases are proteases which have been found to play a role in the breakdown of cells. 14 caspase family members have been identified in the human genome (Strasser et al., 2000) and caspase inhibitors appear to convey protection against aminoglycoside ototoxicity (Cunningham et al., 2002, Matsui et al., 2003), although exactly which caspases are involved remains unclear.

Apoptosis, or programmed cell death, is a natural and necessary process which helps to maintain cellular density equilibrium within an organism. Bax is a pro-apoptotic Bcl-2 protein which regulates cell death. Bcl-2 proteins form heterodimers of the proapoptotic, antiapoptotic or neutral variety which provide signals for the cell leading to release of cytochrome-c, a component of the electron transport chain in mitochondria which is involved in the initiation of apoptosis. After hair cell treatment with aminoglycosides, mitochondrial membrane potential loss has been observed and Bax molecules, which promote pore formation in mitochondrial membranes increasing their permeability, result in the loss of the mitochondrial membrane potential (Gross et al., 1998).

The increased formation of ROS in response to oxidative stress is thought to be the main component in aminoglycoside ototoxicity (N. Abi-Hachem et al., 2010), having a number of effects which are disruptive to the cell (Huth et al., 2011). ROS have been found to show elevated levels in hair cells undergoing noise (Ohlemiller et al., 1999), aminoglycoside (Hirose et al., 1999) and cisplatin (Kopke et al., 1997) induced damage. In vivo, antioxidant application which lessens free radical damage, has been shown to protect against ototoxicity (Garetz et al., 1994).

The c-jun NH2-terminal kinase (JNK) pathway is one of the mitogen-activated protein (MAP) pathways, is also important in cell death. JNK phosphorylates and activates c-jun, a transcription factor, which has been found to occur in hair cells treated with aminoglycosides (Matsui et al., 2004). Inhibitors of MAP kinases have been demonstrated to be protective against noise and aminoglycoside induced ototoxicity (Pirvola et al., 2000; Ylikoski et al., 2002), although it has been noted that in large doses some cell penetrating peptides (CPPs) can cause toxicity via membrane perturbation (Saar et al., 2005).

Increased susceptibility to aminoglycoside ototoxicity is thought to result from maternally inherited genetic factors (Hu et al., 1991). A nucleotide 1555 A to G substitution in the mitochondrial 12S rRNA gene has been implicated which, by an as yet not fully understood mechanism, causes tighter binding of aminoglycosides to rRNA (Prezant et al., 1993; Tono et al., 2001; Zhao et al., 2004).

It has recently been discovered that those with the most serious illnesses are more likely to be susceptible to the destructive ototoxic effects of aminoglycosides. Utilising a model of sepsis and inflammation, using bacterial lipopolysaccharides to induce endotoxemia in mice, Koo et al. (2015) discovered that doing so increases the cochlear level of aminoglycosides, via increased trafficking across the blood-labyrinth barrier, thus increasing their adverse effects. Cochlear and serum levels of inflammatory markers were also increased. This enhanced effect, is highly undesirable, since those who are most ill, who need the highest dose and/or longest course of treatment, will be additionally affected in a deleterious manner (FIGURE 4-1).

There is an evident imperative for the discovery and utilisation of preventative measures against aminoglycoside ototoxicity. Attempts to tackle both the ototoxic consequences of aminoglycoside treatment and the increasing problem of drug resistant bacterial strains

rapidly emerging have been made via the creation of non-toxic derivative of the aminoglycoside paromomycin, which were found to be efficacious at treating bacterial infection as well as being highly selective at ribosomal targets (Duscha et al., 2014).

The potential for the use of a calcium chelator such as BAPTA, co-administered with aminoglycosides has been put forward by Vu et al. (2013). Because tip links can readily, spontaneously regenerate upon removal of the calcium chelator, temporarily breaking tip links could prevent aminoglycoside uptake and then tip links could regenerate restoring hearing (Duscha et al., 2014). However, causing complete hearing loss, even if only temporarily, may seem like a troubling prospect in a human subject and the exact timeline of tip link recovery and corresponding potential to elicit MET currents has not yet been documented. Zhao et al. (1996) noted that MET currents were still absent 1 hour after BAPTA treatment in chick basilar papilla. In mouse OHCs, whilst the fast and slow components of transduction were recovered at the first time point measured at 3 hours after BAPTA treatment, only very small MET currents could be observed (Lelli et al., 2010). Indzhykulian et al. (2013) reported that some regenerated tip links could be seen 1 hour after BAPTA treatment. They found that initially a shorter tip link composed of PCDH15 at both the upper and lower ends was formed and whilst there appeared to be a full complement of tip links present 12 hours after BAPTA application, CDH23 levels were only fully restored around 48 hours after BAPTA treatment. MET currents recorded up until this point, whilst normal in magnitude did not adapt as normal MET currents do (Indzhykulian et al., 2013).

As well as treating bacterial infections, the fact that aminoglycosides can bind to a proportion of cytoplasmic rRNA means that they can be used to treat genetic disease that result from nonsense mutations or premature stop codons in cytoplasmic ribosomes by supressing them, allowing for successful protein encoding (Burke and Mogg, 1985; Keeling et al., 2012).

Additionally, it has been found that it is primarily mitochondrial protein synthesis that is inhibited by aminoglycosides (Shulman et al., 2014). Creation of aminoglycosides which selectively inhibit cytoplasmic and not mitochondrial ribosomes seems a promising way of ameliorating ototoxicity for the purpose of treating genetic diseases in this way (Shulman et al., 2014).

Aminoglycosides which have good efficacy but are less able to penetrate the cochlear MET channels have been created. These antibiotics are altered to have fewer positive charges along their length and are thus less able to interact with the negatively charged residues which reside in the MET channel. A patent for these antibiotics was secured (Huth et al., 2015). The large scale potential of using zebrafish for initially screening for compounds which protect against aminoglycoside induced ototoxicity (Owens et al., 2008), makes this a very viable option. Once narrowed down, selected candidates can be assessed on cochlear cultures and their competitive blocking of the MET channel as well as the characteristics of the block can be assessed using electrophysiological techniques.

Streptomycin and dihydrostreptomycin have been estimated to have a diameter of 1.04 nm, gentamicin a diameter of 0.98 nm and neomycin a diameter of 0.96 nm (Alharazneh et al., 2011) and are thus able to pass through the MET channel. It has been found that aminoglycoside antibiotics, FM1-43 and a host of other compounds are MET channel blockers (Gale et al., 2001; Marcotti et al., 2005) and thus MET channels are considered to be necessary for entry of these compounds into the hair cells and the subsequent ototoxic effects (Marcotti et al., 2005; Alharazneh et al., 2011). However, the question as to whether there are other facilitators for the entry of these compounds, such as via TRPA1 channels, remains (Stepanyan et al., 2011). Many possible routes of entry have been proposed including entry directly through nerve terminals which are adjacent to the hair cells (Alharazneh et al., 2011). Another

proposed method of entry is via endocytosis as both the apical and basolateral membrane of cochlear hair cells have been found to contain endocytotic pathways (Lim, 1986, ; Hashino and Shero, 1995). Whilst these other routes of entry may play a small role in the accumulation of aminoglycoside antibiotics in cochlear hair cells, the MET channel is clearly the main route of entry (Marcotti et al., 2005).

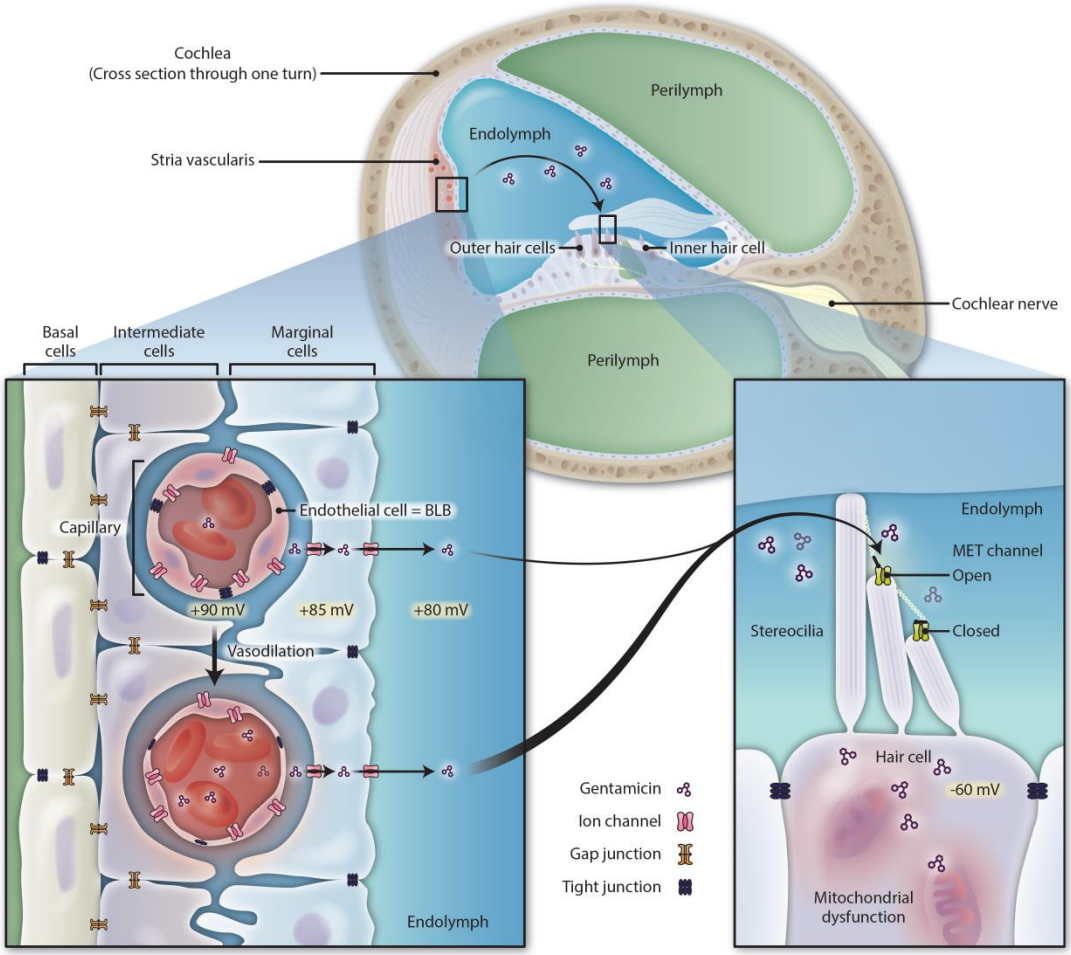

Figure 4-1 : Endotoxemia potentiates aminoglycoside ototoxicity via increased vasodilation. The polycationic aminoglycosides enter through the endothelial cells which line capillary walls via an as yet unknown mechanism, against the electrical gradient of +90 mV of the blood-labyrinth-barrier, then move across marginal cells into the endolymph. Once they have crossed the endolymphatic space to where the hair cells are located, they are able to enter into them via the MET channels atop the stereocilia. From Kros and Desmonds (2015).

4.2 Competitive MET channel blockers

The stryl dye FM1-43, due to its small dimensions (0.78 x 0.5 nm (Gale et al., 2001)) has been demonstrated to enter into hair cells, gaining rapid access via the MET channel in an open state and acting as a permeant channel blocker Gale et al., (2001), as well as entering many other types of sensory cell through non-selective ion channels (Meyers et al., 2003). As well as this FM1-43 has been shown to enter hair cells via other ion channels (Meyers et al., 2003). This entry and subsequent labelling is only evident in sensory cells and thus appears to require a specifically sensory entry point such as the MET channel. Further, the labelling is prolonged and sustained after washing the drug out (Gale et al., 2001 ; Meyers et al., 2003; Marcotti et al., 2005; Goodyear et al., 2008). FM1-43 is not ototoxic, at least at the levels previously tested. It has a K_D of 1.2 μM at a holding potential of 0 mV and has been demonstrated to offer protection against aminoglycoside induced ototoxicity in vivo (Gale et al., 2001).

The ideal channel blocker to compete with ototoxic aminoglycosides would have a high affinity for the MET channel, would not be ototoxic and would also be a blocker which does not permeate through the channel. Annexin V is a calcium-dependent phospholipid binding protein with anticoagulant properties which selectively binds to negatively charged PS. If applied externally to the apical surface of hair cells in the cochlea, the binding of annexin V indicates that PS is present on the outer leaflet of the cell membrane. Annexin V can be used to detect apoptosis of certain cell types (Vermes et al., 1995). Thus, using Annexin V, can assist in assessing the suitability of a compound for competitive blocking potential based on assessing its potential to damage hair cells, using real time using fluorescence imaging (Goodyear et al., 2008). DHS causes rapid and reversible PS-externalisation and blebbing in cochlear hair cells, indicative of the damage occurring. However, PS-externalisation in cochlear

hair cells does not necessarily indicate that they are undergoing apoptosis as externalisation occurs very rapidly and can be reversible (Goodyear et al., 2008).

4.3 Cell penetrating peptides, D-TAT and D-JNKi1

4.3.1 The molecular structure of D-TAT and D-JNKi1

D-TAT is a 12-amino acid peptide (MW 1590 Da) containing 8 potentially positively charged, basic amino acids. An inhibitor of Jun c N-terminal kinase, D-JNKi1 (MW 3822 Da), which is the D-retro inverso form of L-JNKi1 consisting of D-amino acids in reversed sequence, comprises 19 amino acids (4 of which are basic) from the human JNK inhibitory protein, coupled with D-HIV-TAT (making a total of 12 basic amino acids) (FIGURE 4-2).

With D-TAT measuring in at 30 Å and D-JNKi1 at a much larger 80 Å in length, both with more modestly sized end-on diameters of 15 Å; these peptides are sizeable when compared with the largest published MET channel blockers to date. Especially where D-JNKi1 was concerned, these peptides seemed somewhat unlikely to be able to act as permeant blockers of the MET channel. However, the polycationic elongated structure of D-TAT and D-JNKi1 appears to allow them both to be drawn into and permeate the MET channel, in a voltage dependent manner, as I will demonstrate.

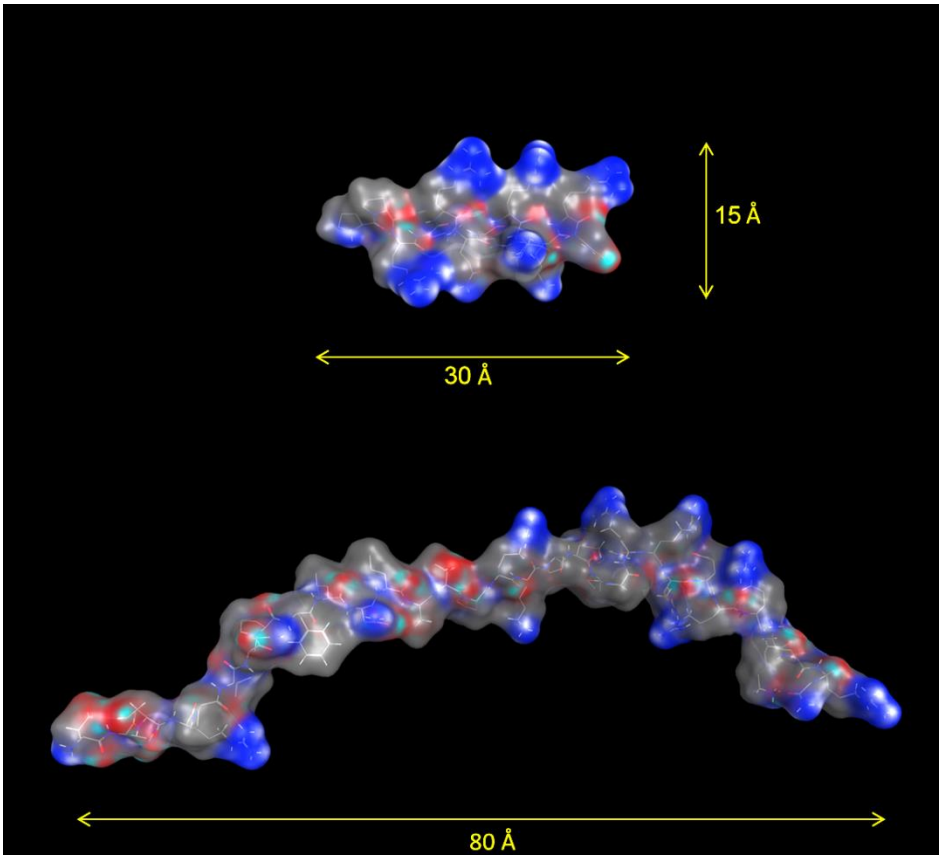

By Prof Simon Ward, University of Sussex (2012).

D-TAT sequence: H-PP-RRRQRRKKRG-NH_2 (MWt 1589.5 Da)

D-JNKi1 sequence: H-DQSRPVQPFLNLTTPRKPR-PP-RRRQRRKKRG-NH_2 (MWt: 3822.3 Da)

FIGURE 4-2 : Modelled molecular structures of D-TAT and D-JNKi1 - Long polycationic structures illustrated. Blue = nitrogen, indicating a basic amino acid, red = oxygen, indicating a neutral amino acid in this instance.

4.3.2 Cell penetrating peptide routes of entry into cells

The routes of entry of CPPs such as HV-TAT into cells have been widely debated and, whilst several routes of entry have been found, much conflicting evidence exists. Mechanisms of uptake of the TAT sequence other than endocytosis have been posited, as it can be internalised at 4˚ C (Vivès et al., 1997), a temperature at which endocytosis cannot occur (Silhol et al., 2002). However, it was subsequently found that endocytosis can facilitate entry (Richard et al., 2005). It has been postulated TAT may instead enter cells via direct translocation through the cell surface membrane (Vivès et al., 1997). Interaction with cell surface glycosaminoglycans (GAGs) is potentially thought to be involved in the translocation of some CPPs (Ziegler, 2008). Creation of a transient pore in the membrane has also been recently proposed. This would involve interaction with positively charged phosphate groups, which would cause a transient change in the cell surface membrane and the creation of the pore, allowing the diffusion of CPPs into the cell along the surface of the transient pore (Herce and Garcia, 2007).

4.3.3 Clinical significance

There is mounting interest in the therapeutic potential of cell penetrating peptides such as D-TAT for drug delivery (Zhang et al., 2012). However, there is now evidence that some retro-inverso cell penetrating peptides are toxic, thus clinical suitability must be carefully scrutinised (Holm et al., 2011). Studies have been conducted on D-JNKi1 (also known by the names XG-102 and AM-111) to evaluate its efficacy at treating several conditions caused by inhibiting the apoptosis caused by the JNK signalling pathway. D-JNKi1 has been demonstrated

to offer protective effects against colitis (Reinecke et al., 2012) and severe cerebral ischemia (Hirt et al., 2004).

In guinea pigs, Eshraghi et al. (2006) asserted that D-JNKI1 prevents trauma-induced delayed hearing loss caused by cochlear implantation. Auditory brainstem response (ABR) thresholds are measurements of auditory evoked potentials in the brain taken using electrodes attached to the head. Distortion product otoacoustic emissions (DPOAE) are a measure of resultant distortion products emanating from the cochlea, after two simultaneous pure tone stimuli are presented. Having recorded these as reliable measures of the effects of the trauma, they found that the characteristic further decrease in DPOAE amplitudes and increase of auditory brainstem response (ABR) thresholds after initial trauma, were prevented. Omotehara et al. (2011) measured ABR changes in gerbils treated with 100 μM AM-111, which were subjected to transient cochlear ischemia, and found that cochlear damage was significantly reduced.

It has been proposed that D-JNKi1 can protect against the ototoxic effects of aminoglycoside antibiotics (Wang et al., 2003), by interfering with the MAPK-JNK signalling pathway, preventing the binding of JNK to c-Jun by directly competing with it and thus preventing cell death (Bonny et al., 2001) or, as I have explored, by acting as a blocker of the MET channel, competing for entry with aminoglycosides. In 2003, a patent was obtained by Bonny for “cell-permeable peptides that bind to JNK proteins and inhibit JNK-mediated effects in JNK-expressing cells” based on the data they acquired in guinea pigs which suggested protection against noise induced hearing loss was offered by these compounds.

In 2007, Suckfuell et al. conducted a phase I/II study on 11 patients who had received noise exposure and thus acoustic trauma less than 24 hours before treatment. They were subjected to intratympanic treatment with 0.4 mg/ml or 2 mg/ml AM-111 (D-JNKi1). Suckfuell et al. (2007) noted that, based on pure tone audiometry, which helps to determine threshold hearing levels by the response of the subject to pure tone stimuli, and DPOAE readings, there

appeared to be a therapeutic effect offered by AM-111. However, they did also note some adverse effects, although they state that none of these were serious (Suckfuell et al., 2007). A follow up, larger phase II study (Suckfuell et al., 2014) was conducted on male and female human subjects between the ages of 18 and 60 with acute sensorineural hearing loss (at least 30 dB and occurring no later than 48 hours prior to treatment). 0.25 ml AM-111 was administered on day 0, through intratympanic injection and again a higher 2 mg/ml and a lower 0.4 mg/ml dose were used on different patient cohorts in order to see if any effects were concentration dependent. This study was more comprehensive and involved a greater number of patients (n = 92); however, they did not find any statistically significant difference between the recovery of the placebo, low dose or high dose groups. In fact, when they quantified the least square means of the three groups, the recovery of the placebo group (24 dB) was better than that of the high dose group (22.5 dB). The recovery of the low dose group was slightly improved at 27 dB. This is interesting as it potentially points towards a therapeutic window, where negative effects are incurred at higher concentrations. They additionally note that further exploratory analyses revealed that in the low dose group recovery occurred more quickly and tinnitus remission in the patients in this group was reported more frequently than in controls. Whilst they state that there did appear to be a degree of recovery offered by AM-111, they admit that they did not find a great level of consistency in their results. They do mention, however, that AM-111 appears safe and well tolerated (Suckfuell et al., 2014). Another study found that XG-102 (D-JNKi1) was safe and well tolerated when intravenously infused into male volunteers (Deloche et al., 2014).

4.4 Results

4.4.1 D-JNKi1 and D-TAT cause PS externalisation in treated cochlear cultures

Cochlear cultures were treated with 5 µM D-TAT or D-JNKi1. Fluorescent Alexa 488 conjugated annexin V binding (added at a dilution of 1:50) was used to probe PS externalisation in hair cells, with PS presence on the outer leaflet of the plasma membrane of the cells indicating cell damage. A Zeiss AxioPlan II light microscope with a water-immersion lens was used for live imaging (see Goodyear et al., 2008). After 20 minutes of exposure to one of the compounds, the coverslips with the adherent cultures were fixed, preblocked and permeablised and then labelled with rabbit anti-Alexa Fluor 488 IgG at a dilution of 1:100 overnight, to increase the fluorescent signal. Texas Red phalloidin at 1:300 was also applied and left overnight to a make cell junctions visible. Then the secondary antibody, Alexa Fluor 488-goat anti-rabbit IgG, was added. Images of the whole coils were then captured using the light microscope and images different cellular levels were also obtained using a LSM 510 Meta confocal microscope with an oil-immersion lens.

The preliminary data (n = 2 for each condition) presented here showed that, at a concentration of 5 µM, D-TAT caused PS-externalisation in 83% of OHCs in apical cochlear cultures and in 97% of OHCs in basal cochlear cultures. At a concentration of 5 µM, D-JNKi1 causes PS-externalisation in 27% of OHCs in apical cochlear cultures and 85% of OHCs in basal cochlear cultures (TABLE 3, FIGURE 4-3). D-TAT caused fairly uniform labelling of externalised PS in IHCs and OHCs from apex to base (FIGURE 4-3 A, C). D-JNKi1 caused greater labelling in basal OHCs, with increasingly sparse labelling towards the apical end of the coil. IHC labelling remained more consistent but also was not evident for the most apical cells (FIGURE 4-3 B, D).

OHCs externalising PS	Culture 1 – Number of OHCs	Culture 2 – Number of OHCs	Total OHCs	% of total
Apical coil total	1620	1570	1595 ± 25	N/A
Basal coil total	830	880	855 ± 25	N/A
D-TAT in apical coil	1388	1258	1323 ± 65	83%
D-TAT in basal coil	835	823	829 ± 6	97%
D-JNKi1 in apical coil	442	420	431 ± 11	27%
D-JNKi1 in basal coil	737	717	727 ± 10	85%

TABLE 3 - Percentage of OHCs externalising PS in apical and basal cochlear cultures

The number of OHCs in two cultures from the apical cochlear coil and two cultures from the basal coil were counted and divided by two to obtain an average number of OHCs in each of these regions. Then the number of OHCs fluorescing due to Alexa 488 conjugated annexin V binding to externalised PS were counted. For each cell, a grey level reading was obtained using the Histogram tool in Photoshop CS2 and a given cell was only counted if it reached above this threshold (see METHODS section 2.5). This again was measured in two cultures for each condition and averaged. These values were then used to obtain the percentage of cells externalising PS in a given condition, n = 2 for all conditions ± S.E.M.

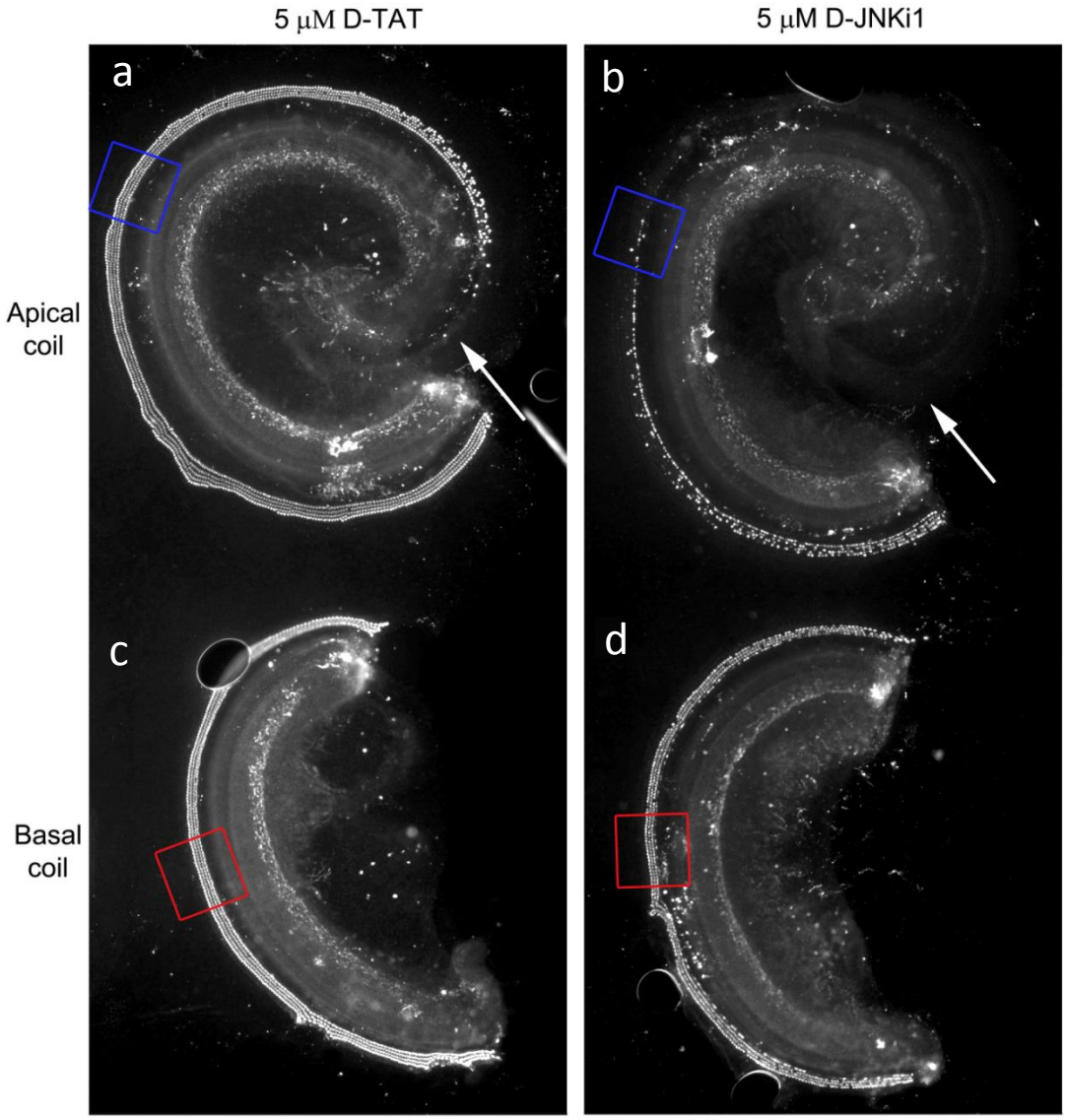

FIGURE 4-3 : Phosphatidylserine externalisation in cochlear. Annexin V labelled cochlear cultures treated with D-TAT or D-JNKi1 - 10x magnification light micrograph montage of images taken using a light microscope. 5 μM D-TAT (a, c), 5 μM D-JNKi1 (b, d) treated apical (a, b) basal (c, d) cochlear coil sections. D-TAT causes externalisation of PS in hair cells further towards the apical end of the cochlear culture (a) than D-JNKi1 (b). Blue squares indicate the mid-apical regions and mid-basal regions are indicated by red squares. Arrows indicate the ends of the apical cochlear cultures.

4.4.2 Texas Red conjugated D-JNKi1 and Texas Red conjugated D-TAT load into hair cells

Texas red conjugated D-TAT (TR D-TAT) and D-JNKi1 (TR D-JNKi1) were used, in the same procedure described in section 4.4.1 and in the METHODS section for D-TAT and D-JNKi1. After the compounds were washed out of the bath after 20 minutes of exposure, the adherent cultures were fixed. The use of these fluorescent conjugated compounds and confocal microscopy allowed for visualisation of them loading into hair cell bodies (FIGURE 4-4). Both compounds did load into hair cells and the loading was consistent with the PS externalisation data. Loading was greater in basal OHCs treated with TR D-TAT or TR D-JNKi1. The greatest level of TR D-TAT loading occurred in basal OHCs (FIGURE 4-4, f), there was somewhat less loading evident in mid-apical OHCs (FIGURE 4-4, d) and less again in OHCs at the apical end of the cochlea (FIGURE 4-4, b). TR D-JNKi1 loading followed a similar pattern, decreasing from base (FIGURE 4-4, e) to mid-apex (FIGURE 4-4, c), but with a greater distinction between apical and basal OHCs. TR D-JNKi1 did not load into the apical end region of the cochlea cultures (FIGURE 4-4, a) as with the pattern of PS externalisation where D-JNKi1 was applied (FIGURE 4-3, b). This makes sense based on the large and even larger dimensions of D-JNKi1 and TR D-JNKi1 respectively, if apical OHC MET channels are smaller in dimension than basal OHCs.

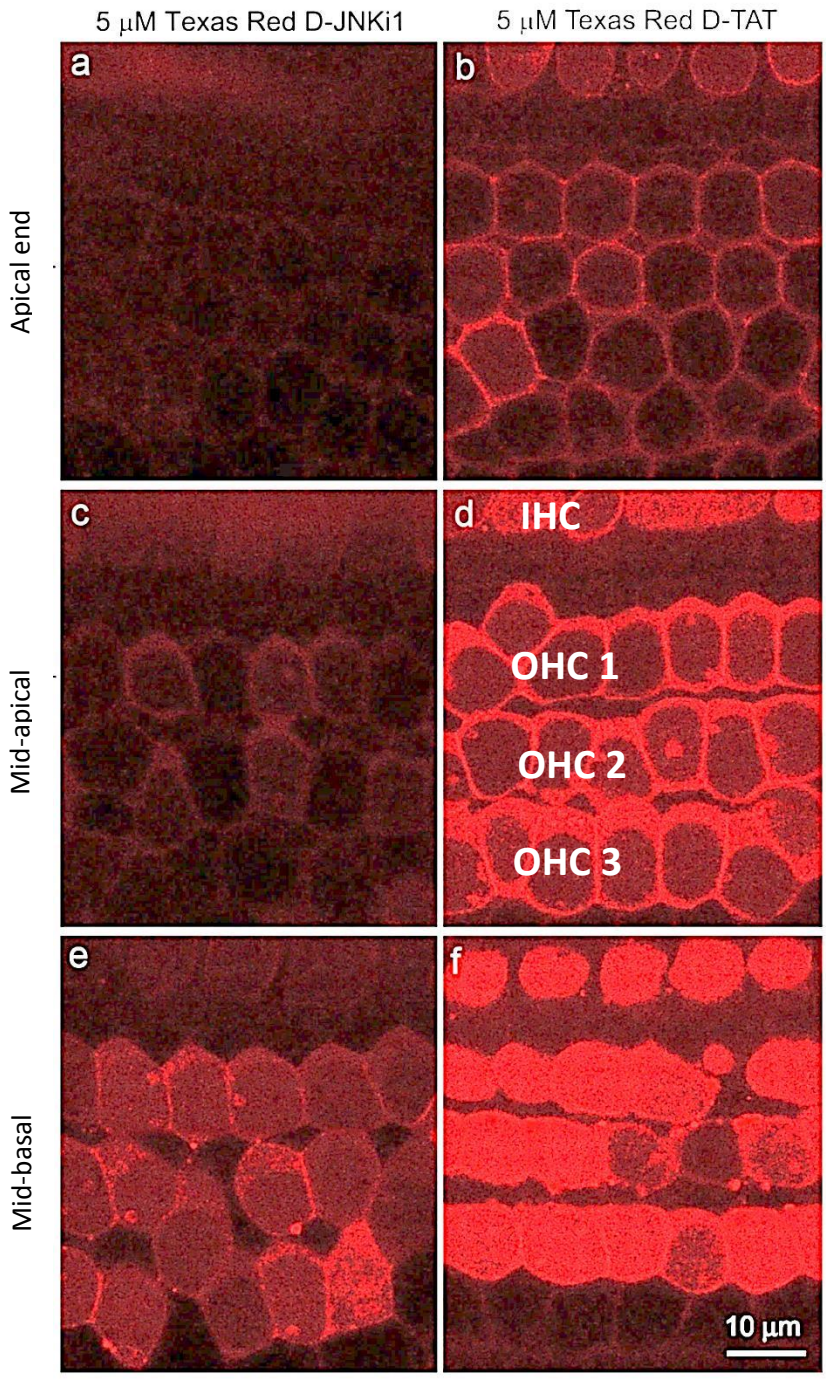

FIGURE 4-4 : Texas Red conjugated D-TAT and D-JNKi1 loading into the hair cells. Confocal micrographs, at the OHC nuclear level: 5 µM TR D-JNKi1 (a, c, e), 5 µM TR D-TAT (b, d, f), the apical end region (a, b), the mid-apical region (c, d), the mid-basal region (e, f). The row of IHCs and the three rows of OHCs are labelled.

4.4.3 D-TAT and D-JNKi1 block mechano-electrical transduction in apical and basal outer hair cells in a reversible, concentration and voltage dependent manner

OHCs were whole cell patch clamped and a 45 Hz sinusoidal force stimulus was used to elicit MET currents. Currents were recorded before and during the application of D-TAT and D-JNKi1 at concentrations ranging from 3 nM to 1 μM. In 65% of cells, where a recording had been made before and during the application of a given compound, I was then able to take a recording where either partial or full washout of the drug was achieved. This was not possible in all cells as sometimes the seal onto the cell was lost before a recording during washout of the compound could be made. Both D-JNKi1 and D-TAT, in spite of their cumbersome size, do block the MET channel. This block, increases with the concentration of the compound used (FIGURE 4-5, 4-6, 4-7, 4-8, 4-9, 4-10). For both compounds the block is also reversible, as upon superfusing a control solution onto the OHCs, these compounds can be washed out of the channel (FIGURE 4-11). The degree to which MET current flow is inhibited by different concentrations of the compounds is dependent upon the membrane potential (FIGURE 4-12, 4-13, 4-14). Current-voltage (IV) curves (FIGURE 4-12) were normalised to represent a proportion of the control MET current (averaged from all controls across all conditions), in order to eliminate the influence of MET current variation on the size of the currents illustrated.

4.4.4 D-JNKi1 and D-TAT are permeant MET channel blockers as block is reduced at positive and extreme negative potentials

MET channel block by D-TAT is increasingly completely released at positive potentials due to its polycationic structure causing it to be repelled from the channel. The block increases at negative potentials, with maximum block occurring at a membrane potential of -104 mV (FIGURE 4-13). Similarly D-JNKi1 increasingly reduces MET current size at more negative

holding potentials until maximum reduction is reached at -104 mV. D-JNKi1 block is also increasingly released at positive membrane potentials but to a lesser extent than of D-TAT, with release of block being less evident with increasing concentrations (FIGURE 4-13). This is probably due to the additional basic amino acids (potentially positive charges) along its length, in addition to its cumbersome size, making it less likely to be dislodged from the MET channel pore.

For both peptides, a partial release of block is evident at extreme negative potentials, lower than -104 mV. This so called 'punch-through' effect (van Netten et al., 2007) indicates that the channel is being cleared by D-TAT or D-JNKi1 being pulled into the hair cells due to the highly negative driving force pulling the polycationic molecules into the intracellular space. This is the hallmark of a permeant channel block (FIGURE 4-13, 4-14).

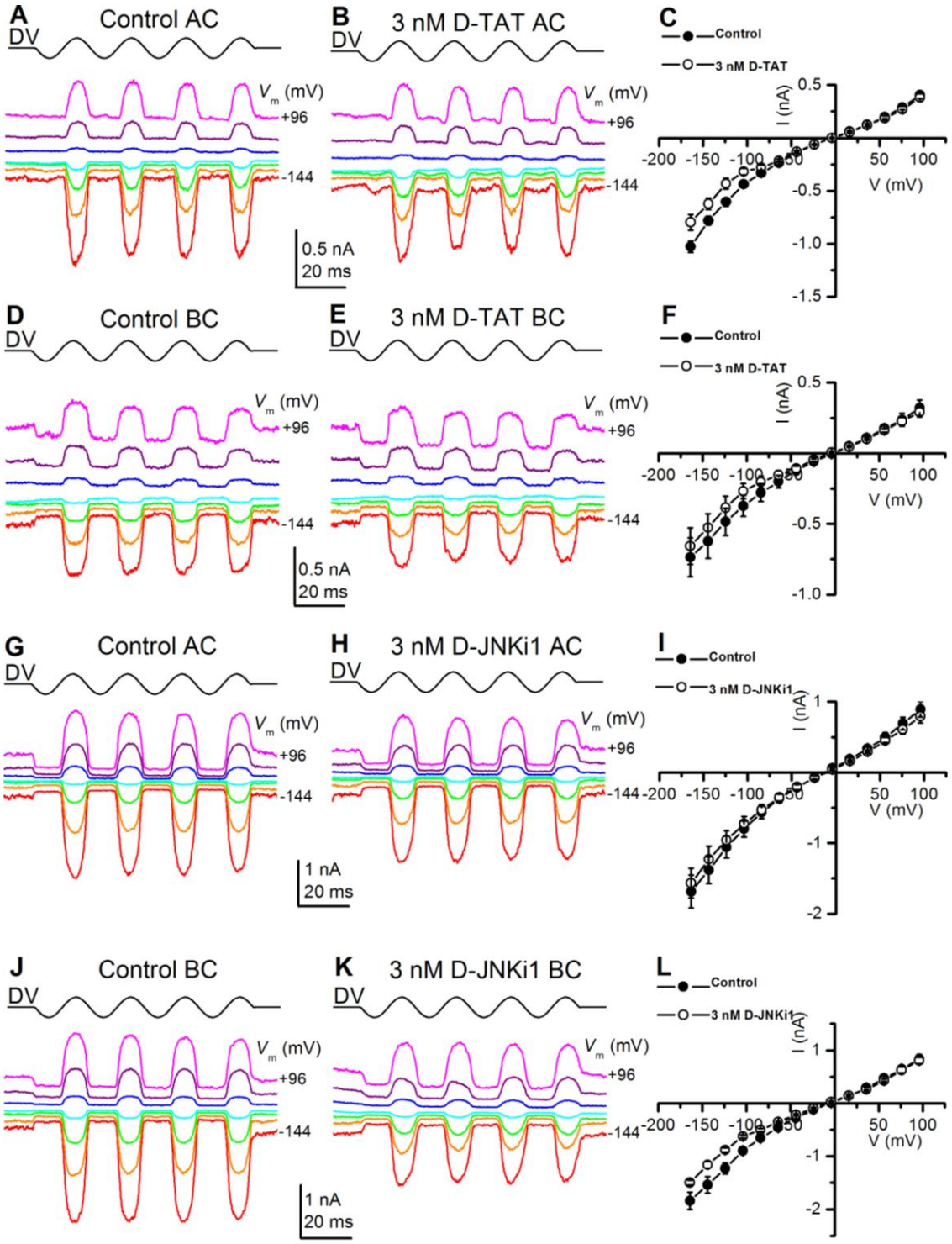
A
Control AC
DV
B
3 nM D-TAT AC
DV
C
Control
3 nM D-TAT
D
Control BC
DV
E
3 nM D-TAT BC
DV
F
Control
3 nM D-TAT
G
Control AC
DV
H
3 nM D-JNKi1 AC
DV
I
Control
3 nM D-JNKi1
J
Control BC
DV
K
3 nM D-JNKi1 BC
DV
L
Control
3 nM D-JNKi1
V_m (mV)
+96
-144
0.5 nA
20 ms
1 nA
20 ms
I (nA)
V (mV)
-200
-150
-100
-50
50
100
0.5
-0.5
-1.0
-1.5
1
-1
-2

FIGURE 4-5 : Block of apical and basal OHC MET currents by 3 nM D-TAT or 3 nM D-JNKi1. A, B, D, E, G, H, J, K, MET currents recorded from apical (A, B, G, H) and basal (D, E, J, K) P2 CD-1 OHCs before and during superfusion with a solution containing 3 nM D-TAT (A, B, D, E) or 3 nM D-JNKi1 (G, H, J, K). Membrane potential stepped between -164 mV and +96 mV in 20 mV increments from a holding potential of -84 mV. Half the voltage steps used are shown for clarity (-144, -104, -64, -24, +16, +56, +96 mV). Driver voltage (45 Hz sinusoid, 40 V amplitude) plotted above the current traces. **C, F, I, L,** Average current-voltage curves of apical (C, I) and basal (F, L) OHCs before and during superfusion of a solution containing 3 nM D-TAT (C, F) and 3 nM D-JNKi1 (I, L). Numbers of cells C:5, F:3, I:3, L:3.

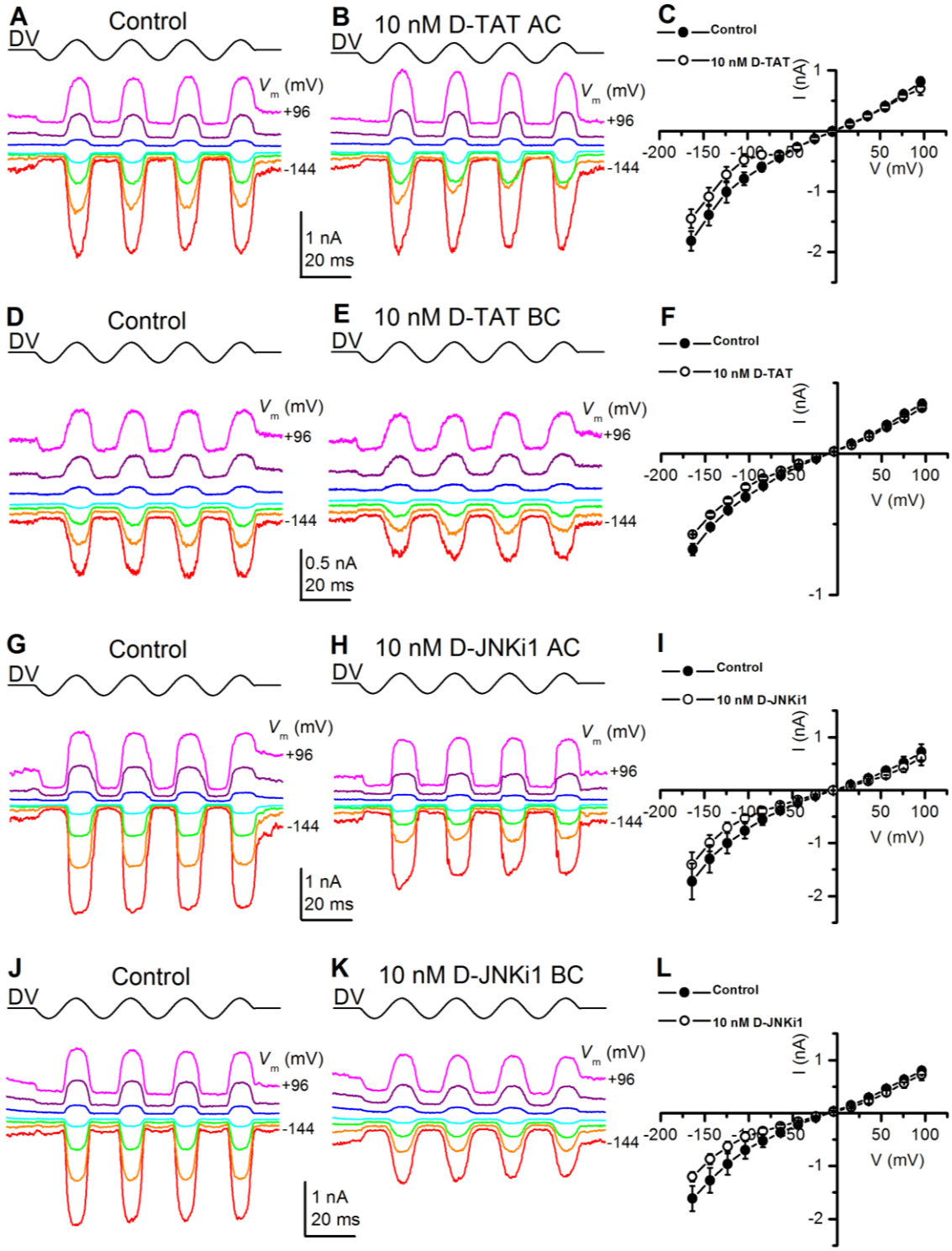
A
Control
DV
V_m (mV)
+96
-144
1 nA
20 ms
B
10 nM D-TAT AC
DV
V_m (mV)
+96
-144
C
Control
10 nM D-TAT
I (nA)
V (mV)
D
Control
DV
V_m (mV)
+96
-144
0.5 nA
20 ms
E
10 nM D-TAT BC
DV
V_m (mV)
+96
-144
F
Control
10 nM D-TAT
I (nA)
V (mV)
G
Control
DV
V_m (mV)
+96
-144
1 nA
20 ms
H
10 nM D-JNKi1 AC
DV
V_m (mV)
+96
-144
I
Control
10 nM D-JNKi1
I (nA)
V (mV)
J
Control
DV
V_m (mV)
+96
-144
1 nA
20 ms
K
10 nM D-JNKi1 BC
DV
V_m (mV)
+96
-144
L
Control
10 nM D-JNKi1
I (nA)
V (mV)

FIGURE 4-6 : Block of apical and basal OHC MET currents by 10 nM D-TAT or 10 nM D-JNKi1. A, B, D, E, G, H, J, K, MET currents recorded from apical (A, B, G, H) and basal (D, E, J, K) P2 CD-1 OHCs before and during superfusion with a solution containing 10 nM D-TAT (A, B, D, E) or 10 nM D-JNKi1 (G, H, J, K). Membrane potential stepped between -164 mV and +96 mV in 20 mV increments from a holding potential of -84 mV. Half the voltage steps used are shown for clarity (-144, -104, -64, -24, +16, +56, +96 mV). Driver voltage (45 Hz sinusoid, 40 V amplitude) plotted above the current traces. **C, F, I, L,** Average current-voltage curves of apical (C, I) and basal (F, L) OHCs before and during superfusion of a solution containing 10 nM D-TAT (C, F) and 10 nM D-JNKi1 (I, L). Numbers of cells C:4, F:2, I:3, L:4.

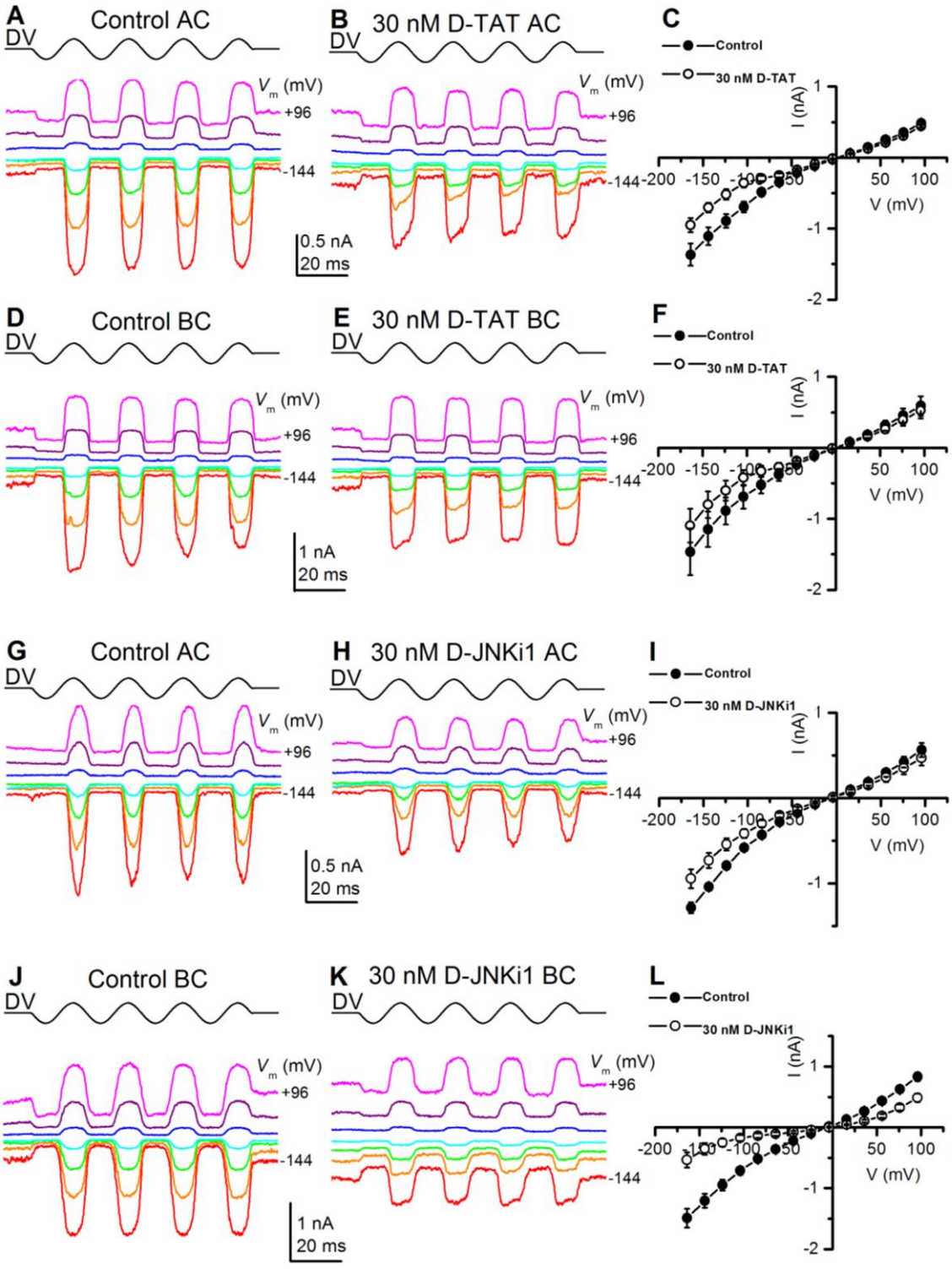
A
Control AC
DV
V_m (mV)
+96
-144
0.5 nA
20 ms
B
30 nM D-TAT AC
DV
V_m (mV)
+96
-144
C
Control
30 nM D-TAT
I (nA)
V (mV)
D
Control BC
DV
V_m (mV)
+96
-144
1 nA
20 ms
E
30 nM D-TAT BC
DV
V_m (mV)
+96
-144
F
Control
30 nM D-TAT
I (nA)
V (mV)
G
Control AC
DV
V_m (mV)
+96
-144
0.5 nA
20 ms
H
30 nM D-JNKi1 AC
DV
V_m (mV)
+96
-144
I
Control
30 nM D-JNKi1
I (nA)
V (mV)
J
Control BC
DV
V_m (mV)
+96
-144
1 nA
20 ms
K
30 nM D-JNKi1 BC
DV
V_m (mV)
+96
-144
L
Control
30 nM D-JNKi1
I (nA)
V (mV)

FIGURE 4-7 : Block of apical and basal OHC MET currents by 30 nM D-TAT or 30 nM D-JNKi1. A, B, D, E, G, H, J, K, MET currents recorded from apical (A, B, G, H) and basal (D, E, J, K) P2 CD-1 OHCs before and during superfusion with a solution containing 30 nM D-TAT (A, B, D, E) or 30 nM D-JNKi1 (G, H, J, K). Membrane potential stepped between -164 mV and +96 mV in 20 mV increments from a holding potential of -84 mV. Half the voltage steps used are shown for clarity (-144, -104, -64, -24, +16, +56, +96 mV). Driver voltage (45 Hz sinusoid, 40 V amplitude) plotted above the current traces. **C, F, I, L,** Average current-voltage curves of apical (C, I) and basal (F, L) OHCs before and during superfusion of a solution containing 30 nM D-TAT (C, F) and 30 nM D-JNKi1 (I, L). Numbers of cells C:5, F:3, I:4, L:5.

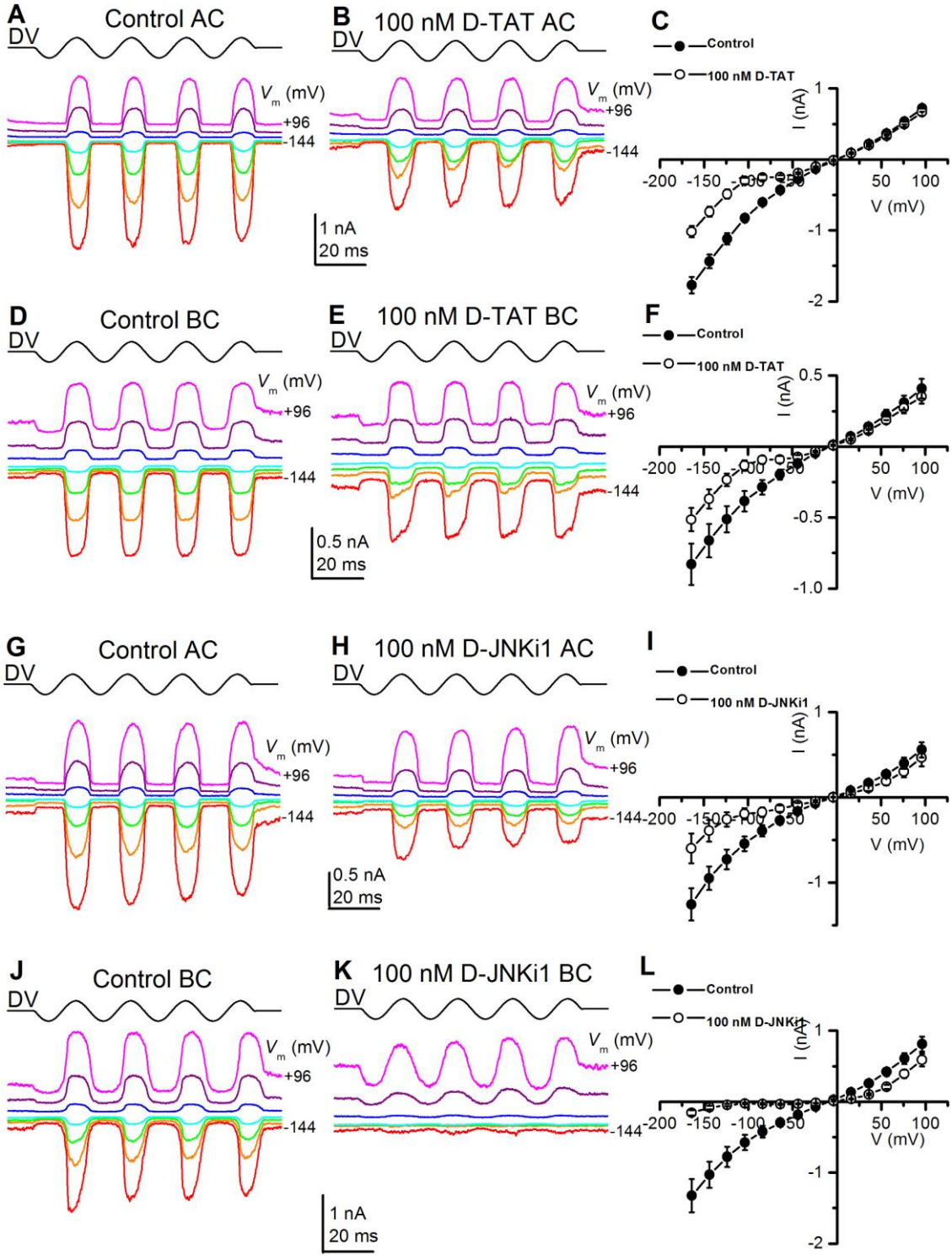
A
Control AC
DV
V_m (mV)
+96
-144
1 nA
20 ms
B
100 nM D-TAT AC
DV
V_m (mV)
+96
-144
C
Control
100 nM D-TAT
I (nA)
V (mV)
D
Control BC
DV
V_m (mV)
+96
-144
0.5 nA
20 ms
E
100 nM D-TAT BC
DV
V_m (mV)
+96
-144
F
Control
100 nM D-TAT
I (nA)
V (mV)
G
Control AC
DV
V_m (mV)
+96
-144
0.5 nA
20 ms
H
100 nM D-JNKi1 AC
DV
V_m (mV)
+96
-144
I
Control
100 nM D-JNKi1
I (nA)
V (mV)
J
Control BC
DV
V_m (mV)
+96
-144
1 nA
20 ms
K
100 nM D-JNKi1 BC
DV
V_m (mV)
+96
-144
L
Control
100 nM D-JNKi1
I (nA)
V (mV)

FIGURE 4-8 : Block of apical and basal OHC MET currents by 100 nM D-TAT or 100 nM D-JNKi1. A, B, D, E, G, H, J, K, MET currents recorded from apical (A, B, G, H) and basal (D, E, J, K) P2 CD-1 OHCs before and during superfusion with a solution containing 100 nM D-TAT (A, B, D, E) or 100 nM D-JNKi1 (G, H, J, K). Membrane potential stepped between -164 mV and +96 mV in 20 mV increments from a holding potential of -84 mV. Half the voltage steps used are shown for clarity (-144, -104, -64, -24, +16, +56, +96 mV). Driver voltage (45 Hz sinusoid, 40 V amplitude) plotted above the current traces. **C, F, I, L,** Average current-voltage curves of apical (C, I) and basal (F, L) OHCs before and during superfusion of a solution containing 100 nM D-TAT (C, F) and 100 nM D-JNKi1 (I, L). Numbers of cells C:14, F:6, I:5, L:8.

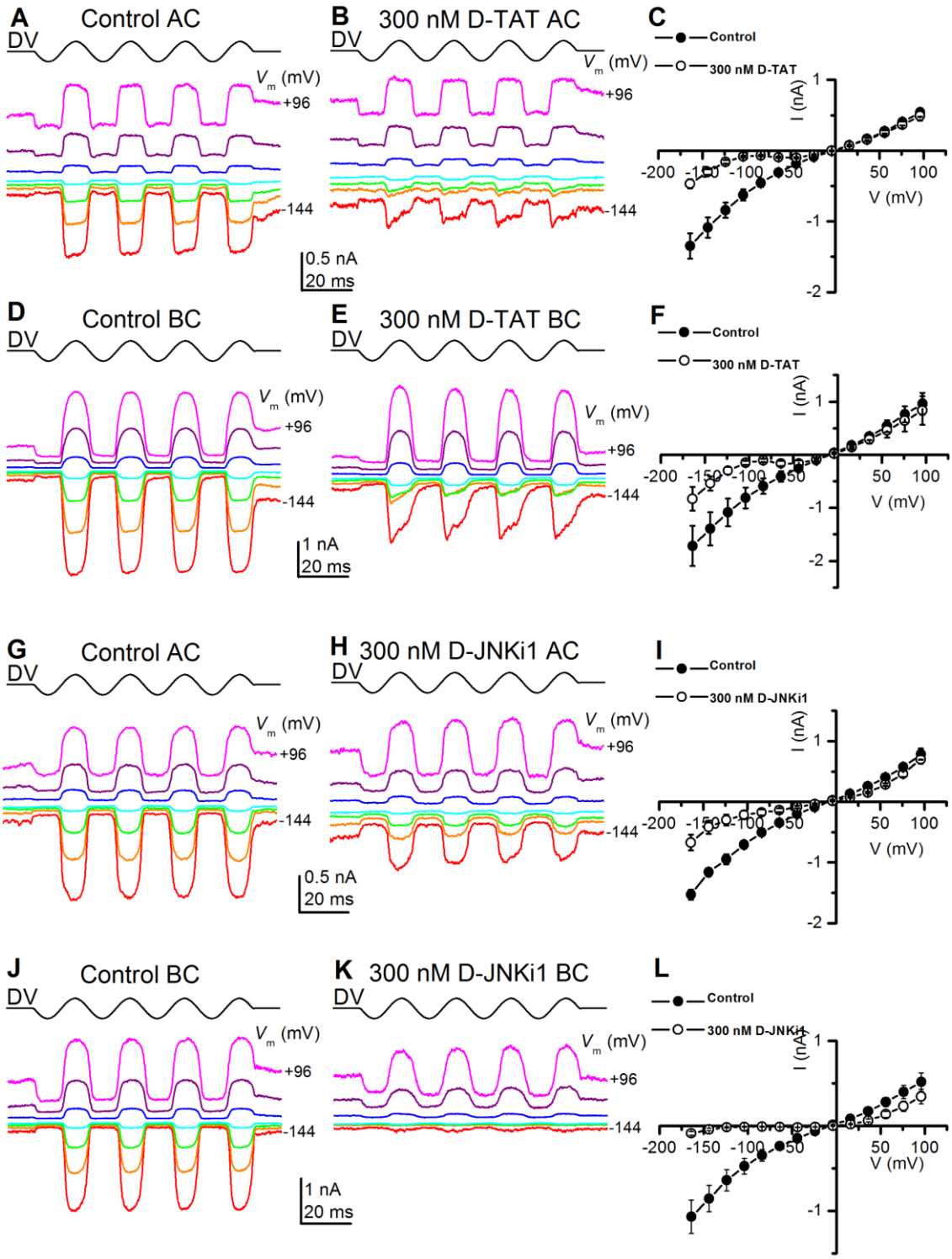
A
Control AC
DV
V_m (mV)
+96
-144
0.5 nA
20 ms
B
300 nM D-TAT AC
DV
V_m (mV)
+96
-144
C
Control
300 nM D-TAT
I (nA)
V (mV)
D
Control BC
DV
V_m (mV)
+96
-144
1 nA
20 ms
E
300 nM D-TAT BC
DV
V_m (mV)
+96
-144
F
Control
300 nM D-TAT
I (nA)
V (mV)
G
Control AC
DV
V_m (mV)
+96
-144
0.5 nA
20 ms
H
300 nM D-JNKi1 AC
DV
V_m (mV)
+96
-144
I
Control
300 nM D-JNKi1
I (nA)
V (mV)
J
Control BC
DV
V_m (mV)
+96
-144
1 nA
20 ms
K
300 nM D-JNKi1 BC
DV
V_m (mV)
+96
-144
L
Control
300 nM D-JNKi1
I (nA)
V (mV)

FIGURE 4-9 : Block of apical and basal OHC MET currents by 300 nM D-TAT and 300 nM D-JNKi1. A, B, D, E, G, H, J, K, MET currents recorded from apical (A, B, G, H) and basal (D, E, J, K) P2 CD-1 OHCs before and during superfusion with a solution containing 300 nM D-TAT (A, B, D, E) or 300 nM D-JNKi1 (G, H, J, K). Membrane potential stepped between -164 mV and +96 mV in 20 mV increments from a holding potential of -84 mV. Half the voltage steps used are shown for clarity (-144, -104, -64, -24, +16, +56, +96 mV). Driver voltage (45 Hz sinusoid, 40 V amplitude) plotted above the current traces. **C, F, I, L,** Average current-voltage curves of apical (C, I) and basal (F, L) OHCs before and during superfusion of a solution containing 100 nM D-TAT (C, F) and 100 nM D-JNKi1 (I, L). Numbers of cells C:14, F:6, I:6, L:10.

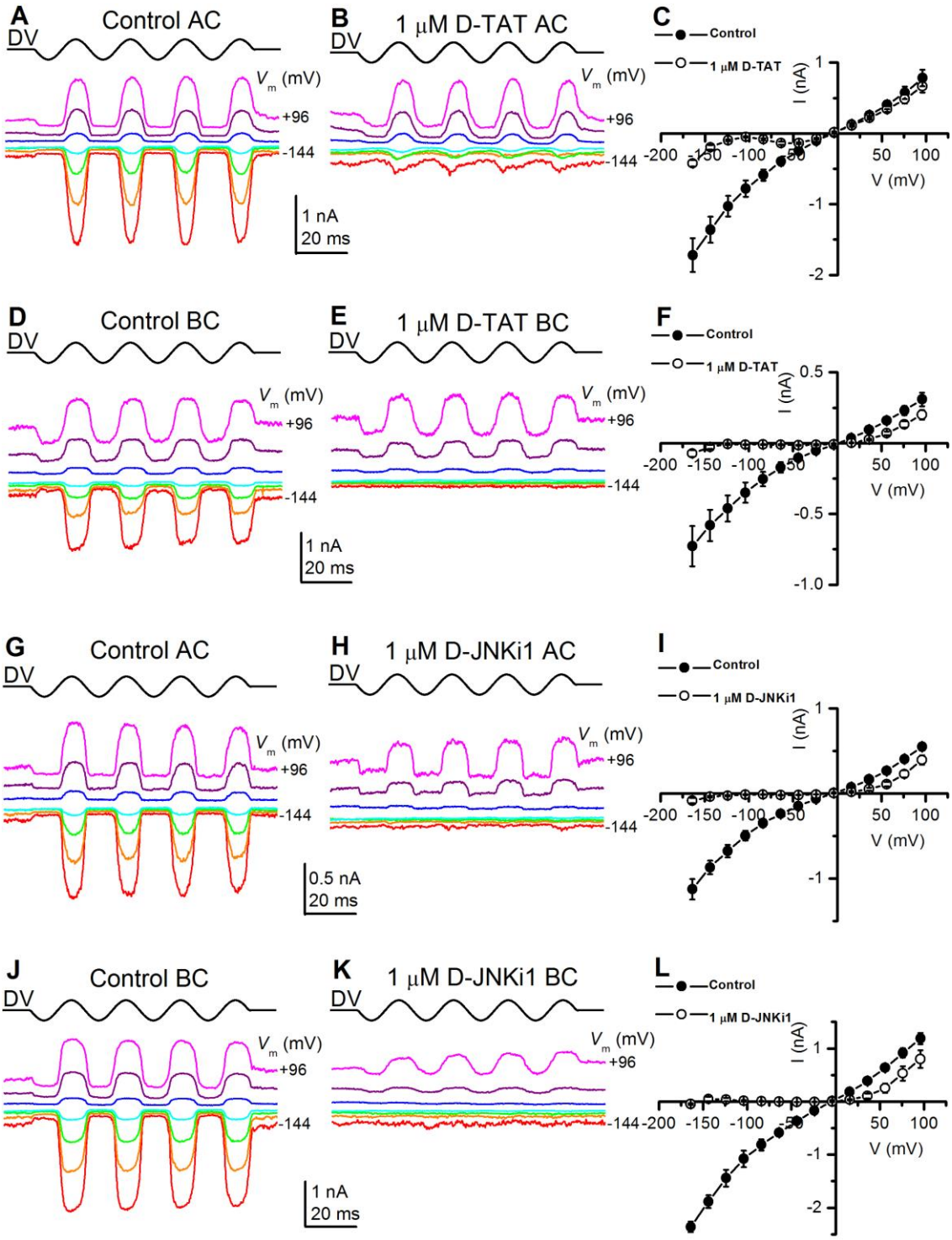
A
Control AC
DV
V_m (mV)
+96
-144
1 nA
20 ms
B
1 μM D-TAT AC
DV
V_m (mV)
+96
-144
C
Control
1 μM D-TAT
I (nA)
V (mV)
D
Control BC
DV
V_m (mV)
+96
-144
1 nA
20 ms
E
1 μM D-TAT BC
DV
V_m (mV)
+96
-144
F
Control
1 μM D-TAT
I (nA)
V (mV)
G
Control AC
DV
V_m (mV)
+96
-144
0.5 nA
20 ms
H
1 μM D-JNKi1 AC
DV
V_m (mV)
+96
-144
I
Control
1 μM D-JNKi1
I (nA)
V (mV)
J
Control BC
DV
V_m (mV)
+96
-144
1 nA
20 ms
K
1 μM D-JNKi1 BC
DV
V_m (mV)
+96
-144
L
Control
1 μM D-JNKi1
I (nA)
V (mV)

FIGURE 4-10 : Block of apical and basal OHC MET currents by 1 µM D-TAT and 1 µM D-JNKi1. A, B, D, E, G, H, J, K, MET currents recorded from apical (A, B, G, H) and basal (D, E, J, K) P2 CD-1 OHCs before and during superfusion with a solution containing 1 µM D-TAT (A, B, D, E) or 1 µM D-JNKi1 (G, H, J, K). Membrane potential stepped between -164 mV and +96 mV in 20 mV increments from a holding potential of -84 mV. Half the voltage steps used are shown for clarity (-144, -104, -64, -24, +16, +56, +96 mV). Driver voltage (45 Hz sinusoid, 40 V amplitude) plotted above the current traces. **C, F, I, L,** Average current-voltage curves of apical (C, I) and basal (F, L) OHCs before and during superfusion of a solution containing 1 µM D-TAT (C, F) and 1 µM D-JNKi1 (I, L). Numbers of cells C:8, F:5, I:5, L10.

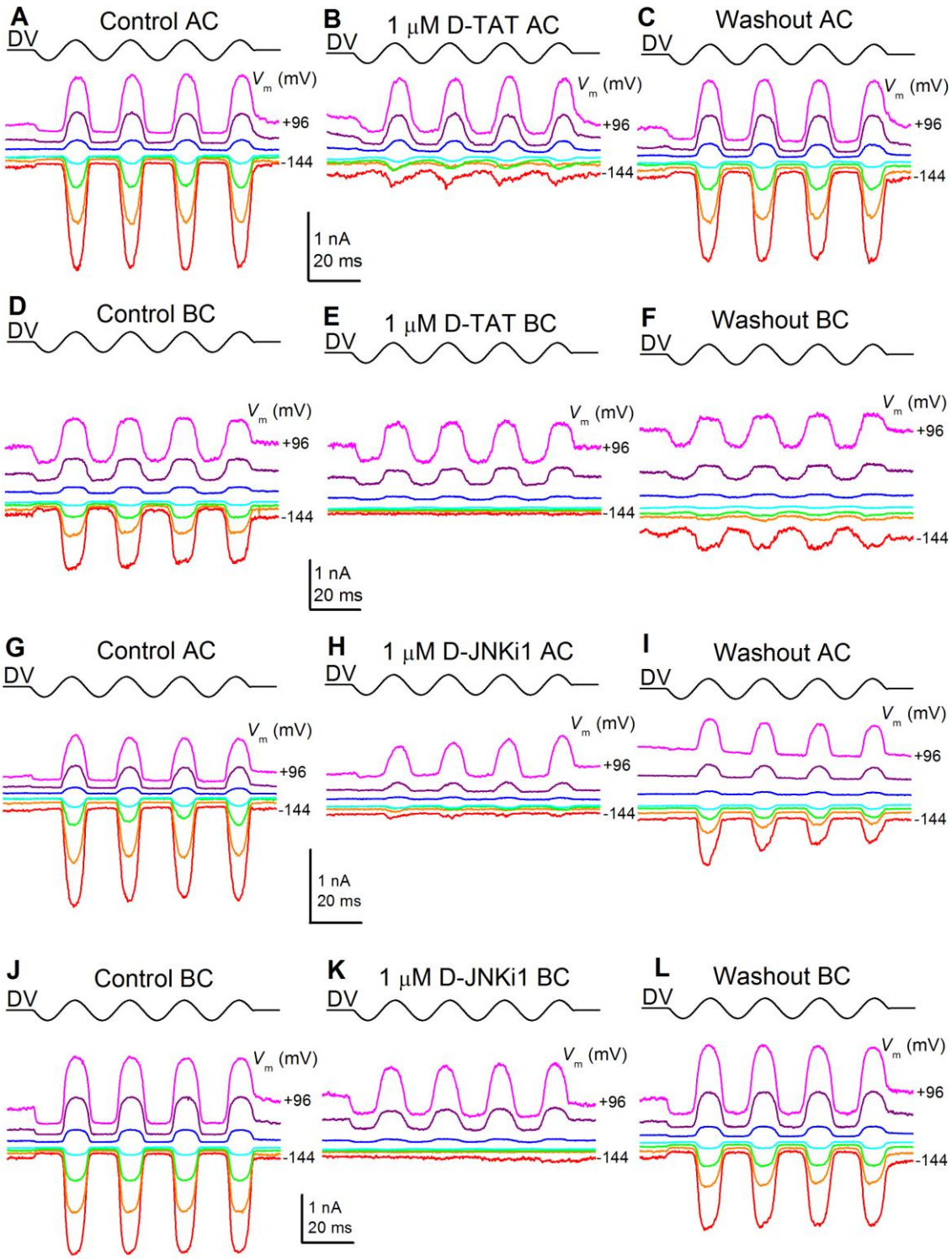
A
Control AC
DV
B
1 μM D-TAT AC
DV
C
Washout AC
DV
V_m (mV)
+96
-144
1 nA
20 ms
D
Control BC
DV
E
1 μM D-TAT BC
DV
F
Washout BC
DV
G
Control AC
DV
H
1 μM D-JNKi1 AC
DV
I
Washout AC
DV
J
Control BC
DV
K
1 μM D-JNKi1 BC
DV
L
Washout BC
DV

FIGURE 4-11 : Block and washout of 1 µM D-TAT or 1 µM D-JNKi1. MET currents from P2 CD-1 OHC before (A, D), during (B, E) and after (C, F) superfusion with a solution containing 1 µM D-TAT and 1 µM D-JNKi1. Membrane potential stepped between -164 mV and +96 mV in 20 mV increments from a holding potential of -84 mV. Driver voltage (45 Hz sinusoid, 40 V amplitude) plotted above the current traces.

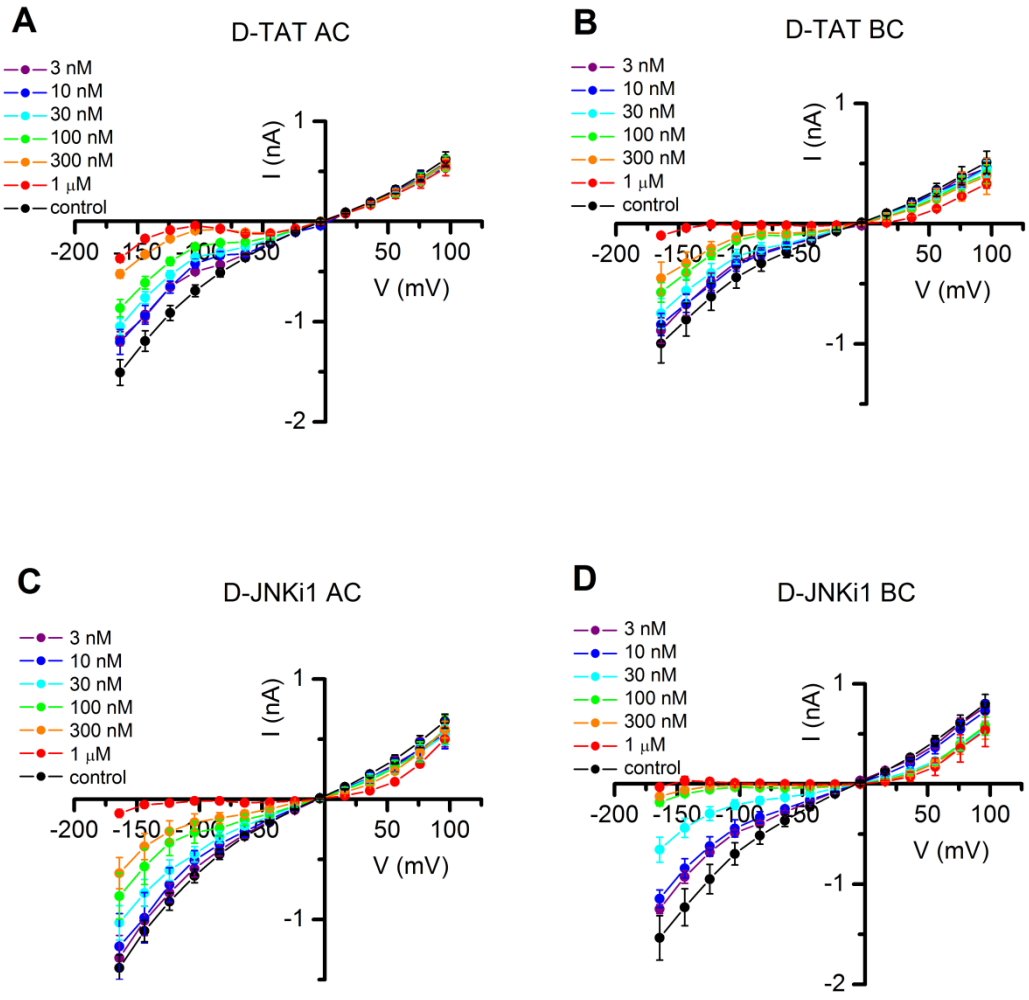
A
D-TAT AC
3 nM
10 nM
30 nM
100 nM
300 nM
1 μM
control
I (nA)
V (mV)
B
D-TAT BC
C
D-JNKi1 AC
D
D-JNKi1 BC

FIGURE 4-12 : A, B, C, D, Current-voltage curves plotted at concentrations from 3 nM – 1 µM D-TAT or D-JNKi1 in OHCs. Apical D-TAT (A), Basal D-TAT (B), Apical D-JNKi1 (C), Basal D-JNKi1 (D). MET Currents and S.E.M. were normalised to represent a proportion of the averaged control current presented (from all control cells for a given condition e.g. apical D-TAT) as opposed to the averaged control for each concentration. N-numbers: Apical D-TAT: control: 42 , 3 nM: 5, 10 nM: 4, 30 nM: 5, 100 nM: 14, 300 nM: 14, 1 µM: 8. Basal D-TAT: control: 25, 3 nM: 3, 10 nM: 2, 30 nM: 3, 100 nM: 6, 300 nM: 6, 1 µM: 5. Apical D-JNKi1: control: 26, 3 nM: 3, 10 nM: 3, 30 nM: 4, 100 nM: 5, 300 nM: 6, 1 µM: 5. Basal D-JNKi1: control: 34, 3 nM: 3, 10 nM: 4, 30 nM: 7, 100 nM: 8, 300 nM 10:, 1 µM: 4.

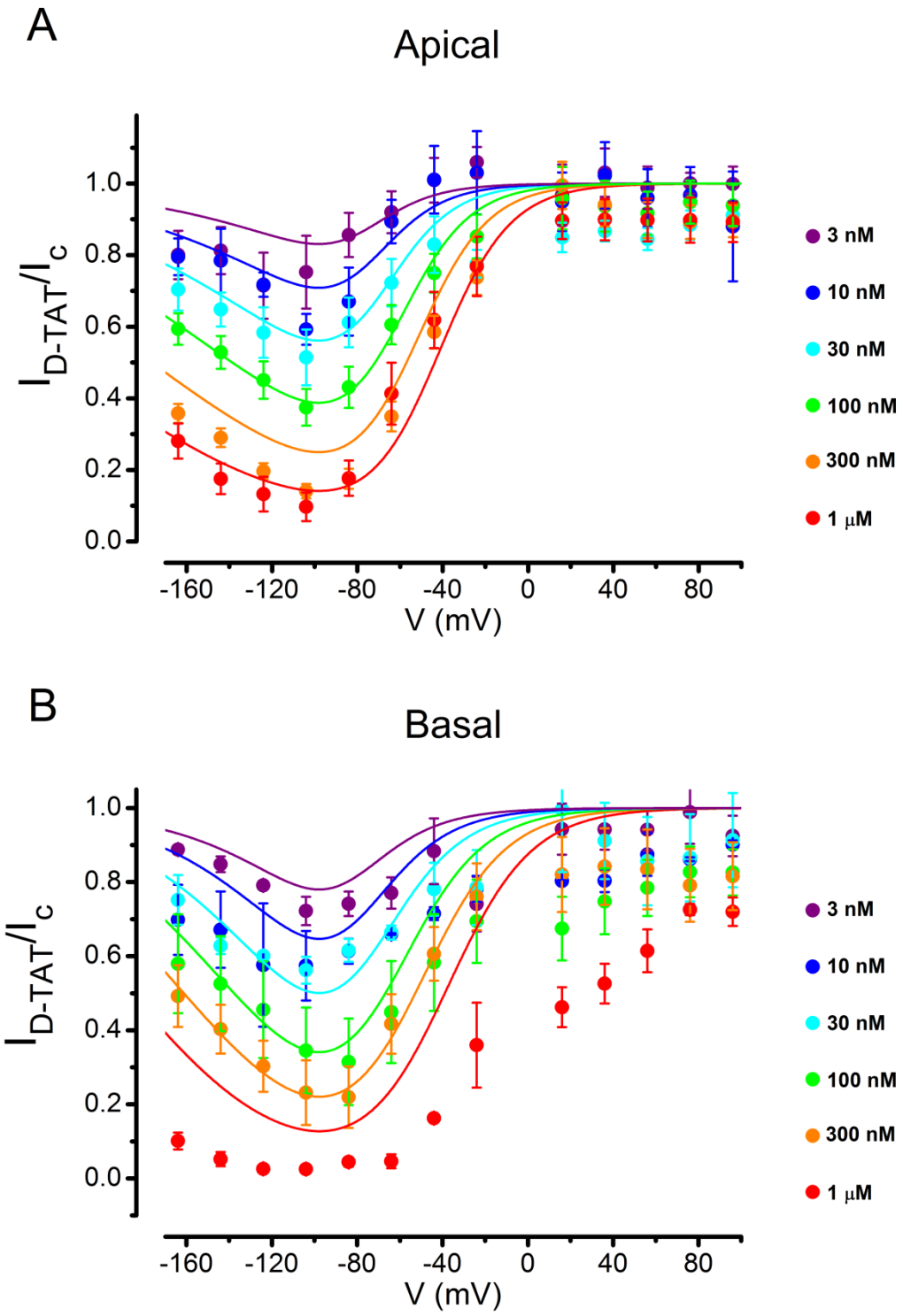
A
Apical
$I_{D\text{-}TAT}/I_c$
1.0
0.8
0.6
0.4
0.2
0.0
-160
-120
-80
-40
0
40
80
V (mV)
3 nM
10 nM
30 nM
100 nM
300 nM
1 μM
B
Basal
$I_{D\text{-}TAT}/I_c$
1.0
0.8
0.6
0.4
0.2
0.0
-160
-120
-80
-40
0
40
80
V (mV)
3 nM
10 nM
30 nM
100 nM
300 nM
1 μM

FIGURE 4-13 : Fractional block of OHC MET currents by D-TAT. A, B, MET currents as a fraction of the current in the control solution recorded from apical (A) and basal (B) OHCs before and during superfusion with D-TAT at concentrations from 3 nM to 1 µM. Numbers of cells from low to high concentrations A:6,4,5,14,14,8, B: 3,2,3,6,6,7. Fitted curves plotted according to equations (1) and (2) in Marcotti et al. (2005).

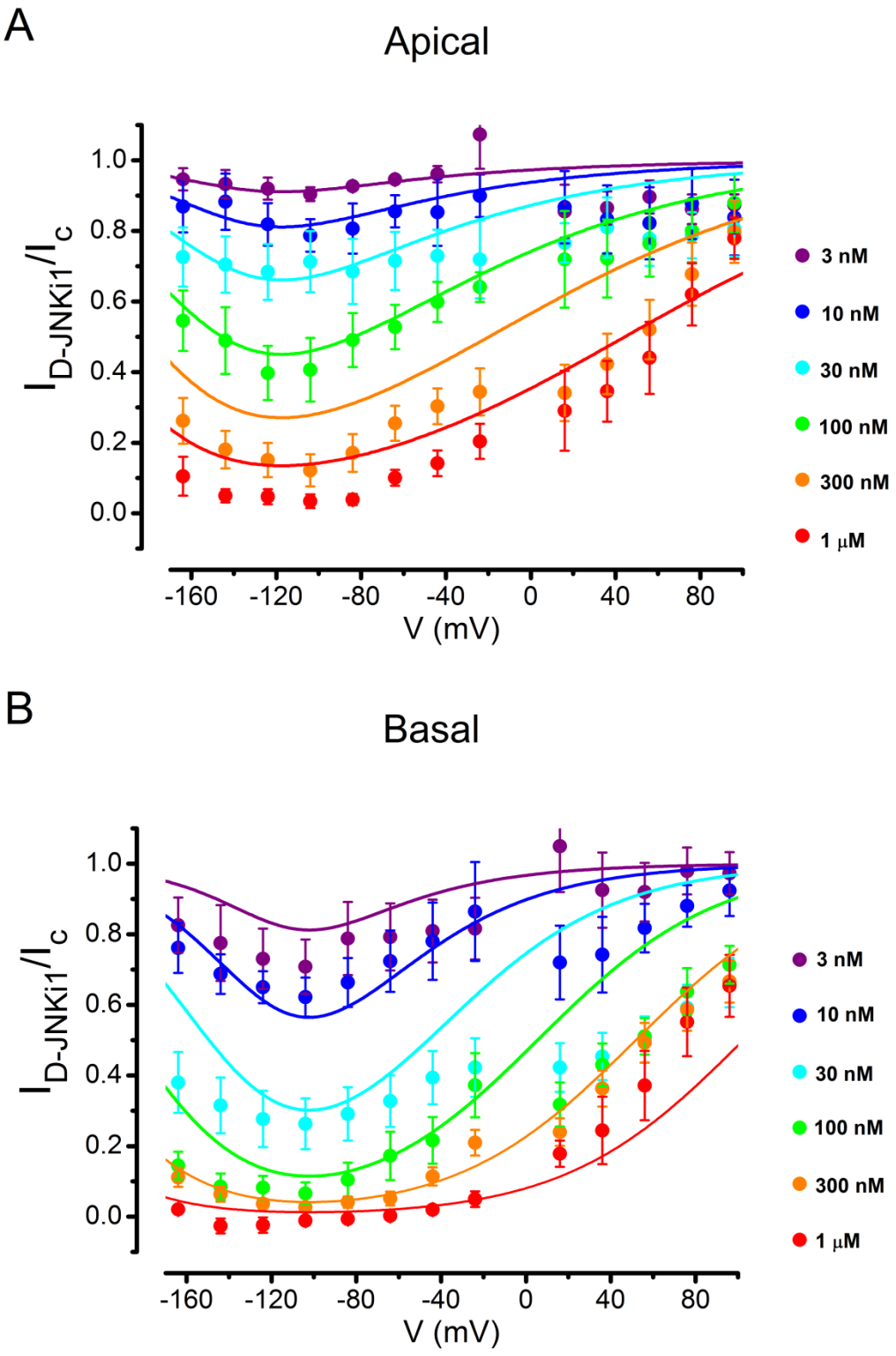
A
Apical
$I_{D\text{-}JNKi1}/I_c$
1.0
0.8
0.6
0.4
0.2
0.0
-160
-120
-80
-40
0
40
80
V (mV)
3 nM
10 nM
30 nM
100 nM
300 nM
1 μM
B
Basal
$I_{D\text{-}JNKi1}/I_c$
1.0
0.8
0.6
0.4
0.2
0.0
-160
-120
-80
-40
0
40
80
V (mV)
3 nM
10 nM
30 nM
100 nM
300 nM
1 μM

FIGURE 4-14 : Fractional block of OHC MET currents by D-JNKi1. A, B, MET currents as a fraction of the current in the control solution recorded from apical (A) and basal (B) OHCs before and during superfusion with D-JNKi1 at concentrations from 3 nM to 1 µM. Numbers of cells from low to high concentrations A:8,4,5,8,8,7, B:3,4,7,8,10,4. Fitted curves plotted according to equations (1) and (2) in Marcotti et al. (2005).

4.4.5 There is a clear apical to basal gradient in the MET channel block caused by D-JNKi1 but not D-TAT

D-JNKi1 causes PS externalisation up to the middle of the apical coil (FIGURE 4-3 b) and the loading of TR D-JNKi1 also follows this pattern (FIGURE 4-4 c). Compatible with this D-JNKi1 shows a variable level of permeant block of the MET channel of a given OHC dependent upon its position along the cochlea. At -104 mV the D-JNKi1 K_D in apical OHCs is 12 nM, considerably lower compared with apical OHCs with a K_D of 61 nM, probably due to increased affinity of the peptide for the basal channel vestibule. Conversely, the K_D of D-TAT is 27 nM in both apical and basal OHCs (FIGURE 4-15) but there does appear to still be a gradient in TR D-TAT loading (FIGURE 4-4 d, f).

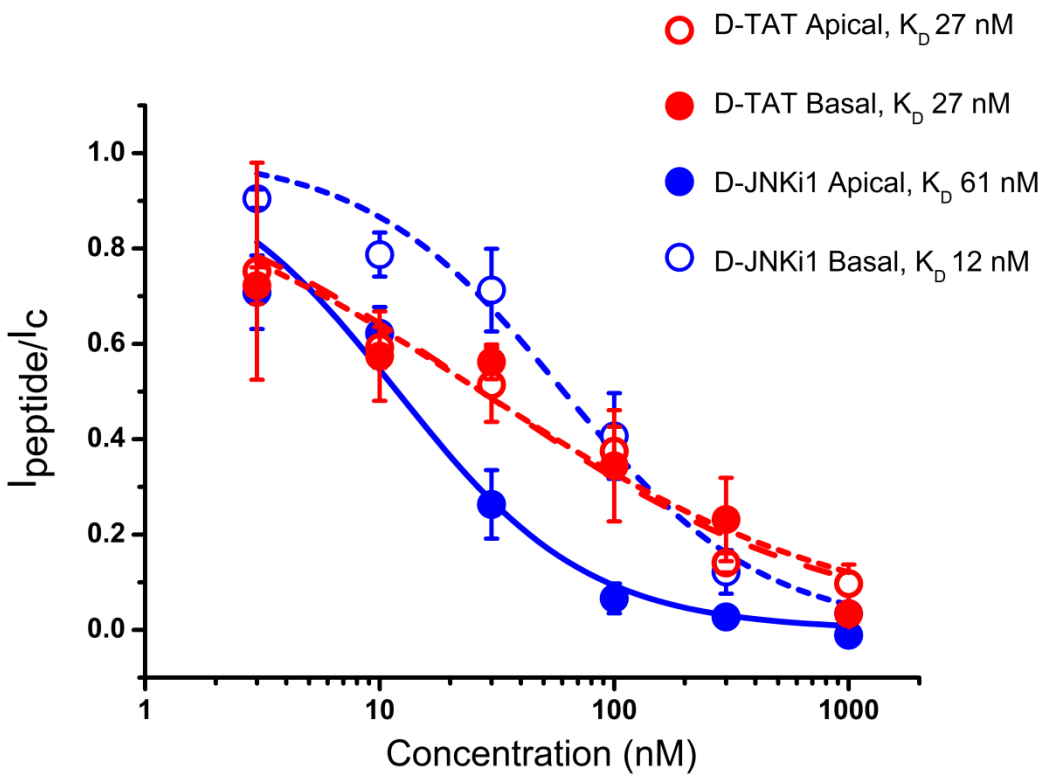
D-TAT Apical, K_D 27 nM
D-TAT Basal, K_D 27 nM
D-JNKi1 Apical, K_D 61 nM
D-JNKi1 Basal, K_D 12 nM
I_peptide/I_c
1.0
0.8
0.6
0.4
0.2
0.0
1
10
100
1000
Concentration (nM)

FIGURE 4-15 : Dose-response curves at -104 mV, illustrating block of apical and basal OHC MET currents by D-TAT and D-JNKi1. D-TAT treated mid-apical OHCs: red open symbols fitted with red dashed line fitted to the Hill equation (see Materials and Methods), K_D = 27 ± 6 nM and n_H = 0.59 ± 0.08. Number of cells from left to right: 3 nM (n = 5), 10 nM (n = 4), 30 nM (n = 5), 100 nM (n = 14), 300 nM (n = 14), 1 µM (n = 8). D-TAT treated mid-basal OHCs: red closed symbols fitted with continuous line to the Hill equation, K_D = 27 nM ± 10 and n_H = 0.55 ± 0.12. Number of cells from left to right: 3 nM (n = 3), 10 nM (n = 2), 30 nM (n = 3), 100 nM (n = 6), 300 nM (n = 6), 1 µM (n = 5). D-JNKi1 treated mid-apical OHCs: blue open symbols fitted with blue dashed line to the Hill equation, with K_D = 61 nM ± 10 and n_H = 1.03 ± 0.15. Number of cells from left to right: 3 nM (n = 3), 10 nM (n = 3), 30 nM (n = 4), 100 nM (n = 5), 300 nM (n = 6), 1 µM (n = 5). D-JNKi1 treated mid-basal OHCs: blue closed symbols fitted with blue continuous line to the Hill equation, with K_D = 12 nM ± 2 and n_H = 1.07 ± 0.13. Number of cells from left to right: 3 nM (n = 3), 10 nM (n = 4), 30 nM (n = 5), 100 nM (n = 8), 300 nM (n = 10), 1 µM (n = 4). The K_Ds of D-TAT in mid-apical and mid-basal OHCs were not significantly different. The K_Ds of D-TAT in mid-apical and mid-basal OHCs were significantly different as calculated by looking at the upper and lower limits at a confidence interval of 95%, no overlap in the range of two sets of values from the lower to upper limit indicating a statistically significant difference of $p < 0.05$.

4.4.6 D-TAT has fairly uniform negative cooperativity with its binding site and the cooperativity of D-JNKi1 is neutral at negative membrane potentials.

The K_Ds for D-TAT and D-JNKi1, fitted with equation (1), were evidently voltage dependent (FIGURE 4-13, 4-14, 4-16, 4-17, 4-18, 4-19). The Hill coefficients for D-TAT in both apical and basal OHCs, at voltages -164 mV through -64 mV, varied very little from 0.49 – 0.64, all showing negative cooperativity (FIGURE 4-16, 4-17). The Hill coefficients for D-JNKi1 in apical and basal OHCs measured at membrane potentials from -164 mV to -64 mV, remained steadily neutrally cooperative (near 1) ranging between 0.87 and 1.03 in apical OHCs (FIGURE 4-17) and 1.01 and 1.09 in basal OHCs (FIGURE 4-18).

A two-barrier one-binding-site model has been used to fit the data, based on the concentration and voltage dependent nature of D-TAT and D-JNKi1, yielding an energy profile for the two peptides (FIGURE 4-20). The energy profile for basal D-JNKi1 has a binding site with a relative electrical distance from the extracellular side of 0.40, with an energy well at the binding site of -16.50 kT below the free energy of the minima (at the intracellular and extracellular spaces surrounding the channel). This is slightly greater in electrical distance from the extracellular side than the binding site for apical D-JNKi1 (0.28), which additionally has less deep energy well at -15.50 kT. The profiles of D-TAT have a binding site with a greater relative electrical distance from the extracellular side than D-JNKi1 of 0.78 in apical OHC MET channels and 0.66 in basal OHCs. Moreover, the binding sites have a far shallower energy well of -5.52 kT in apical OHCs and -5.64 kT in basal OHCs. The profile for apical and basal D-TAT is very similar with the first energy barrier at a distance of 0 from the extracellular side: 15.20 kT in the apical and 15.90 kT in basal OHCs, and the second energy barriers at a distance of 1: 21.60 kT in the apical OHCs and 21.80 kT in the basal OHCs. There is a distinct difference between the height of the energy barriers in the profiles of D-JNKi1 in apical and basal OHC

MET channels. The energy profile for apical D-JNKi1 has noticeably higher barriers with more free energy. For apical D-JNKi1 the height of the first barrier (again at 0) is 11.60 kT and the height of the second (also at 1) is 18.20 kT and for basal D-JNKi1 it is 8.95 kT and 14.55 kT respectively, with noticeably less free energy.

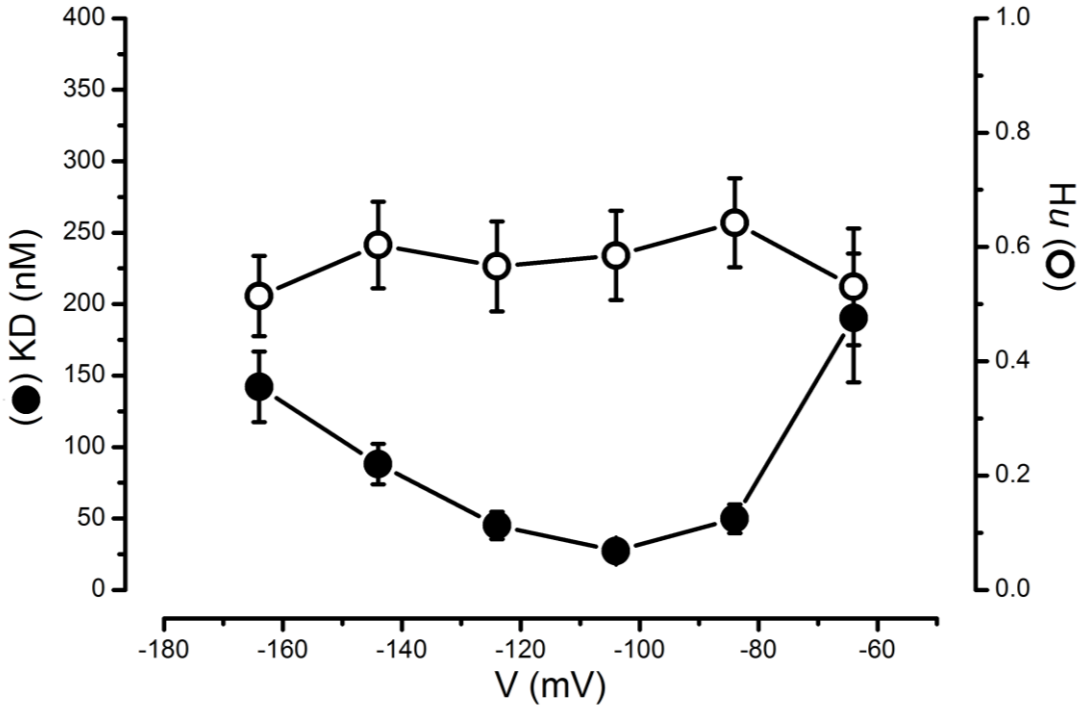

FIGURE 4-16 : Average K_D and n_H for D-TAT treated apical OHCs plotted as a function of membrane potential from -164 mV to -64 mV, including those shown at -104 mV in FIGURE 4-15. Number of cells that went into each dose-response curve used for obtaining the K_Ds and n_Hs (H*u*): 3 nM (n = 5), 10 nM (n = 4), 30 nM (n = 5), 100 nM (n = 14), 300 nM (n = 14), 1 µM (n = 8). At -164: K_D = 142 ± 25, n_H = 0.51 ± 0.07. -144: K_D = 88 ± 14, n_H = 0.60 ± 0.08. -124: K_D = 45 ± 10, n_H = 0.57 ± 0.08.- 104: K_D = 27 ± 6, n_H = 0.59 ± 0.08, -84: K_D = 49 ± 10, n_H = 0.64 ± 0.08. -64: K_D = 190 ± 45, n_H = 0.53 ± 0.10. The fit through the K_D data points is according to equation (1).

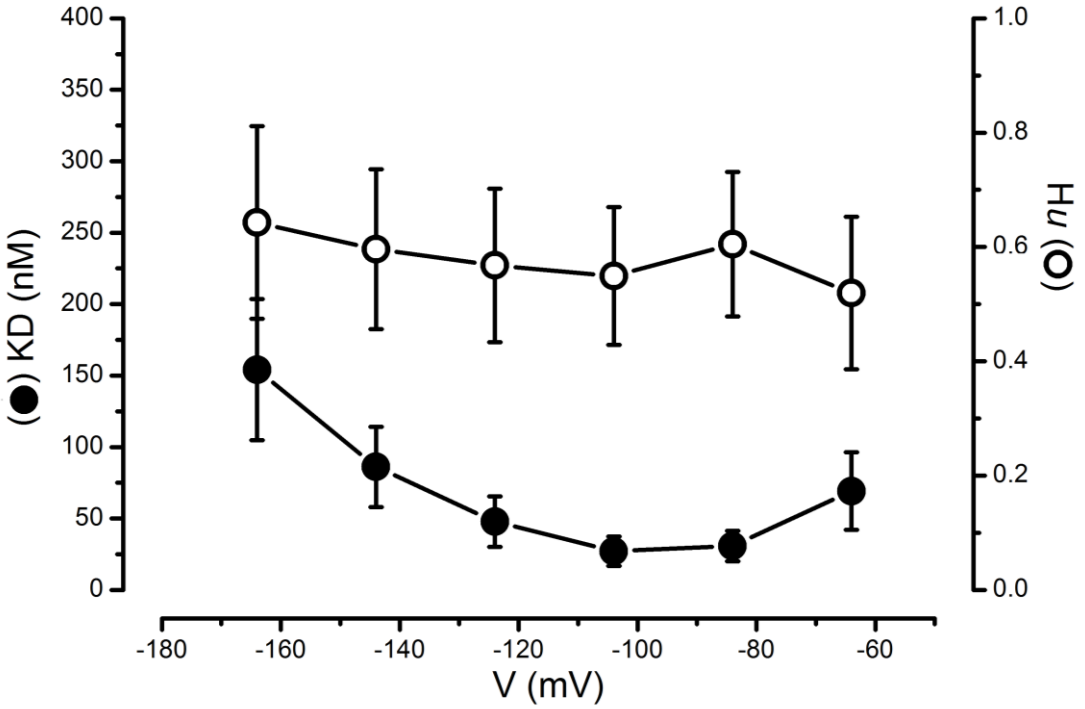

FIGURE 4-17 : Average K_D and n_H for D-TAT treated basal OHCs plotted as a function of membrane potential, from -164 mV to -64 mV, including those shown at -104 mV in FIGURE 4-15. Number of cells that went into each dose-response curve used for obtaining the K_Ds and n_Hs (H*u*): 3 nM (n = 3), 10 nM (n = 2), 30 nM (n = 3), 100 nM (n = 6), 300 nM (n = 6), 1 µM (n = 5). At -164: K_D = 154 ± 49 , n_H = 0.64 ± 0.17. -144: K_D = 87 ± 28 , n_H = 0.59 ± 0.14. -124: K_D = 48 ± 21 , n_H = 0.57 ± 0.13.- 104: K_D = 27 ± 10, n_H = 0.55 ± 0.12, -84: K_D = 31 ± 11, n_H = 0.60 ± 0.13 -64: K_D = 69 ± 27, n_H = 0.51 ± 0.13. The fit through the K_D data points is according to equation (1).

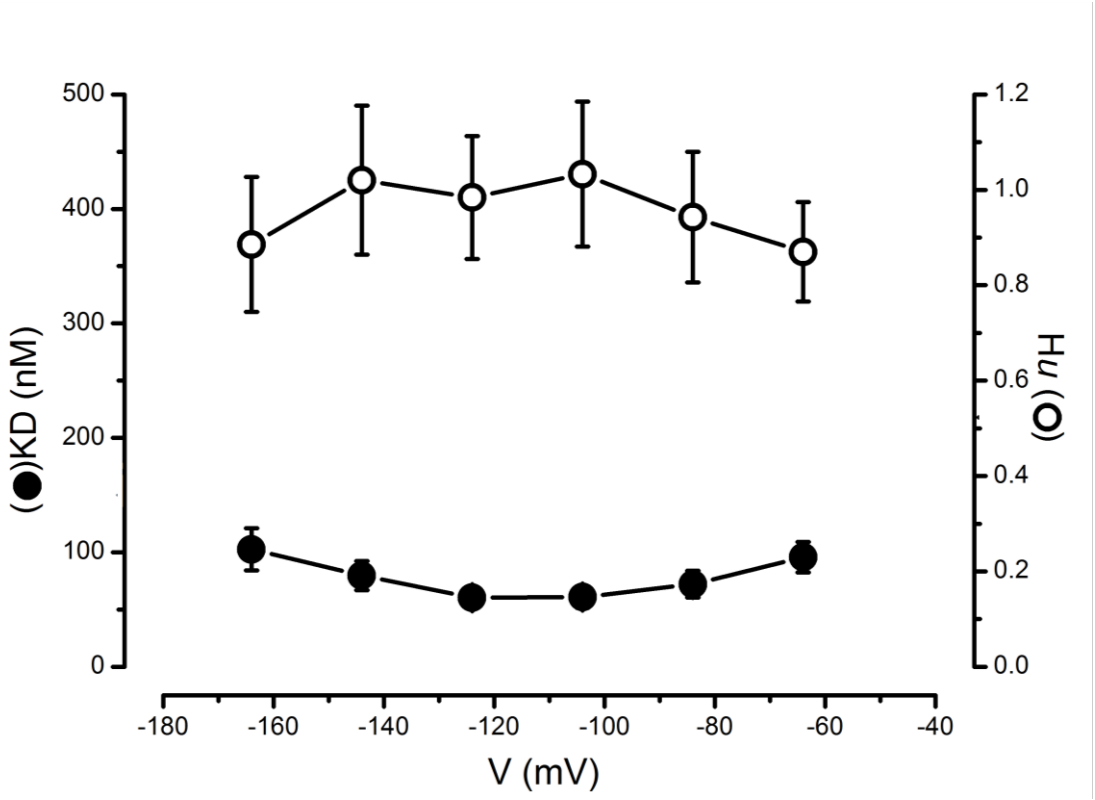

FIGURE 4-18 : Average K_D and n_H for D-JNKi1 treated apical OHCs plotted as a function of the membrane potential, from -164 mV to -64 mV, including those shown at -104 mV in FIGURE 4-15. Number of cells used to create each dose-response curve from which measurements of K_Ds and n_Hs (H*u*) were obtained: 3 nM (n = 3), 10 nM (n = 3), 30 nM (n = 4), 100 nM (n = 5), 300 nM (n = 6), 1 µM (n = 5). At -164: K_D = 103 ± 18, n_H = 0.89 ± 0.14. -144: K_D = 80 ± 13, n_H = 1.02 ± 0.16. -124: K_D = 60 ± 9, n_H = 0.98 ± 0.13 . - 104: K_D = 61 ± 10, n_H = 1.03 ± 0.15, -84: K_D = 72 ± 12, n_H = 0.94 ± 0.14. -64: K_D = 96 ± 13, n_H = 0.87 ± 0.10. The fit through the K_D data points is according to equation (1).

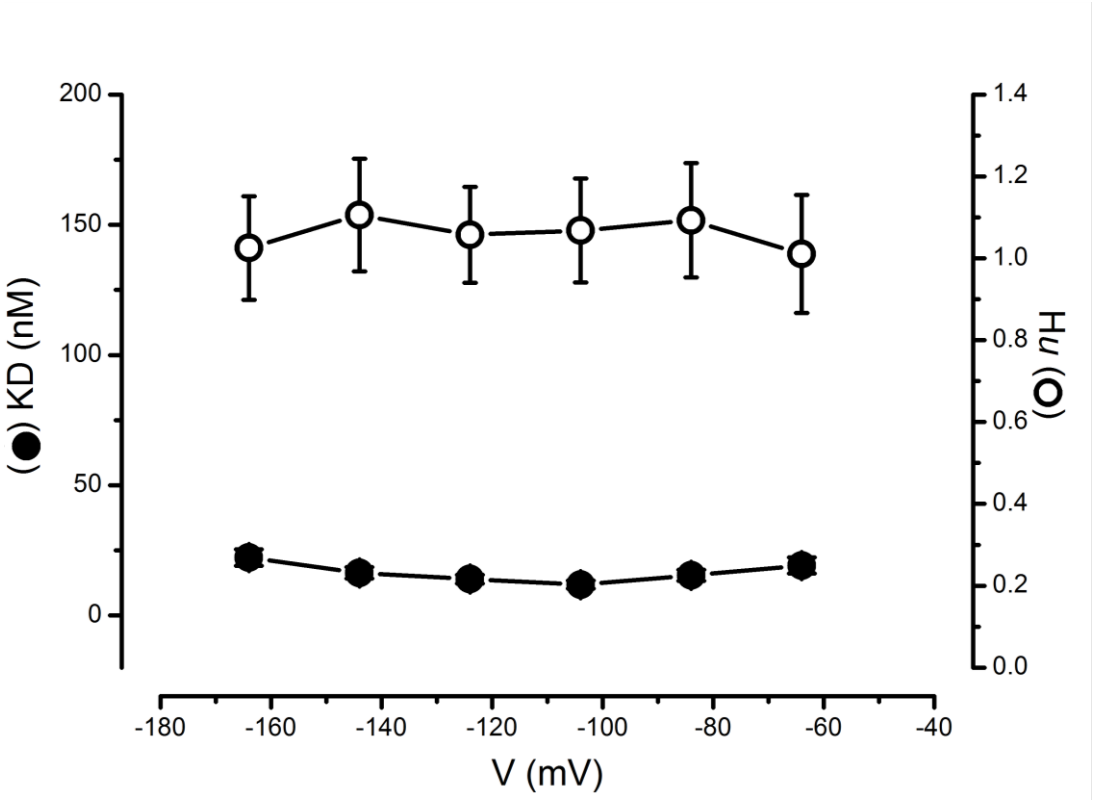

FIGURE 4-19 : Average K_D and n_H for D-JNKi1 treated basal OHCs plotted as a function of membrane potential, from -164 mV to -64 mV, including those shown at -104 mV in FIGURE 4-15. Number of cells used to create dose response curves for each holding potential from which K_D and n_H (H*u*) measurements were obtained: 3 nM (n = 3), 10 nM (n = 4), 30 nM (n = 5), 100 nM (n = 8), 300 nM (n = 10), 1 µM (n = 4). At -164: K_D = 22 ± 3, n_H = 1.03 ± 0.13. -144: K_D = 16 ± 2, n_H = 1.11 ± 0.14. -124: K_D = 14 ± 2, n_H = 1.06 ± 0.12. - 104: K_D = 12 ± 2, n_H = 1.07 ± 0.13, -84: K_D = 15 ± 3, n_H = 1.09 ± 0.14. -64: K_D = 19 ± 3, n_H = 1.02 ± 0.14. The fit through the K_D data points is according to equation (1).

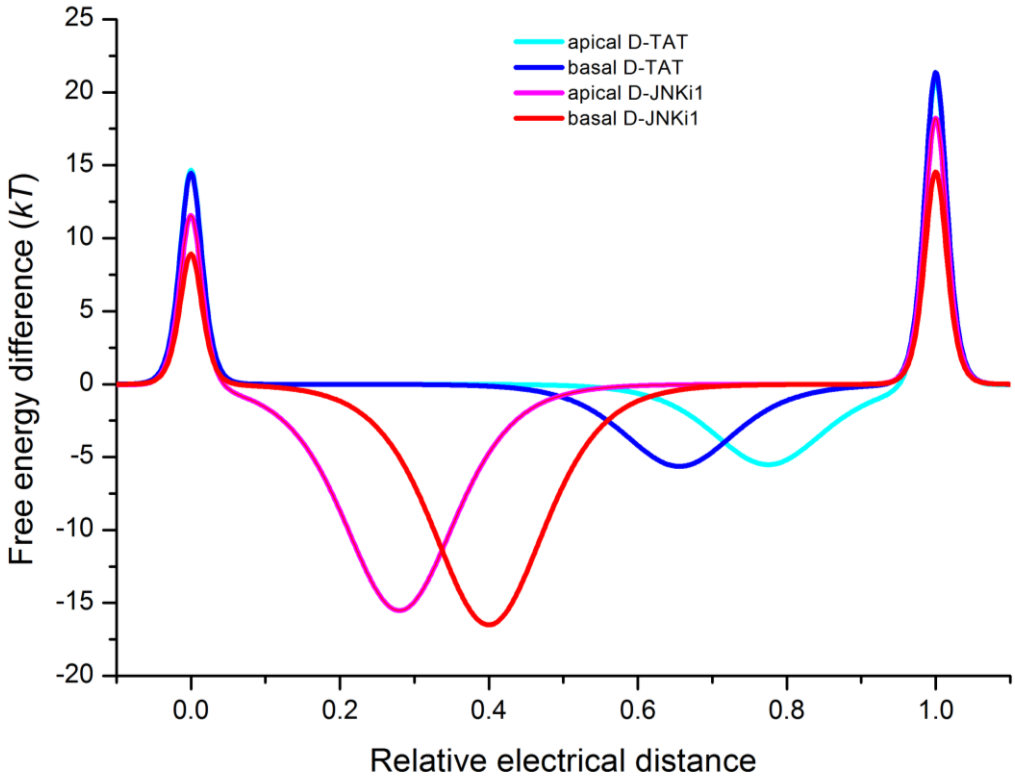

Kros, C. & van Netten, S., unpublished.

FIGURE 4-20 : Energy profiles of the two-barrier one-binding site model used to describe the blockage and permeation of the hair cell transducer channel by D-TAT and D-JNKi1. The energy profiles have been estimated where Vm = 0 mV. The two barriers, one on the extracellular side and one on the intracellular side of the MET channel are at a relative electrical distance of 0 and 1 measured from the extracellular side. The estimated free energies (above the minima free energy level at the intracellular and extracellular sides) of the first barrier are as follows: apical D-TAT: 15.20 kT, basal D-TAT: 15.90 kT, apical D-JNKi1: 11.60 kT, basal D-JNKi1: 8.95 kT. For the second barrier: apical D-TAT: 21.60 kT, basal D-TAT: 22.80 kT, apical D-JNKi1: 18.20 kT, basal D-JNKi1 14.55 kT. Between the two barriers lies the D-TAT and D-JNKi1 binding sites, varying based on apical or basal MET channel location. These have free energies below the minima of: apical D-TAT: -5.52 kT (distance of 0.78), basal D-TAT: -5.64 kT (distance of 0.66), apical D-JNKi1: -15.50 kT (distance of 0.28) basal D-JNKi1: -16.50 kT (distance of 0.4). k = Boltzmann factor, T = temperature.

$$C + B_o \underset{k_{-1}}{\overset{k_1}{\Leftrightarrow}} CB \underset{k_{-2}}{\overset{k_2}{\Leftrightarrow}} C + B_i$$

Equation (2) entry and exit rate constants

From (van Netten and Kros, 2007).

Entry rates for D-TAT and D-JNKi1 into apical and basal MET channel isoforms and their energy profiles were calculated as described by Van Netten and Kros (2007), an expanded version of that used by Marcotti et al. (2005) for DHS entry, in that it allows for Hill coefficients different from 1.

Equation (2) describes the rate of entry into and out of the channel and into and out of the cell, in terms of their rate constants. The forward constant k_1 describes movement into the channel, k_2 relates to movement from the channel to the inside of the cell. The reverse rate constants describe movement from the inside of the cell into the channel (k_{-2}) and from the channel into the extracellular space (k_{-1}).

Compound (region)	**E_1 (kT) – d_1**	**E_2 (kT) – d_b**	**E_b (kT) – d_2**	**100 nM (1/s)**	**1 µM (1/s)**
D-TAT (AC)	15.20 – 0.00	21.60 – 1.00	-5.52 – 0.78	1580	2680
D-TAT (BC)	15.90 – 0.00	22.80 – 1.00	-5.64 – 0.66	1540	2670
D-JNKi1 (AC)	11.60 – 0.00	18.20 – 1.00	-15.50 – 0.28	44	72
D-JNKi1 (BC)	8.95 – 0.00	14.55 – 1.00	-16.50 – 0.40	366	455

TABLE 4 - Energy profile and entry rate data

E_1 = first energy barrier, E_2 = second energy barrier, E_b = binding site energy, d = depth.

The obtained data for D-TAT and D-JNKi1 block of OHCs were fitted with the two barrier one binding site model. Calculations of entry into the cells were based on a driving force of -150 mV, the physiological driving force across the MET channel, as this is the difference between the endocochlear potential (-80 mV) and the resting potential inside of the OHC (-70 mV). The rate constants (k_1, k_2, k_{-1}, k_{-2}) were measured at -84 mV, the potential at which the cells were held. To enable calculating k_1 time constants of drug block to step responses at the holding potential of -84 mV were measured at two concentrations for each drug and cochlear location (data collected by Dr N. Kirkwood). The number of channels per hair cell (C) was as calculated in Chapter 3 (TABLE 2): 98 in apical OHCS and 77 in basal OHCs, and the p_{open} value was set as 0.3 (Marcotti et al., 2005; Johnson et al., 2011).

At 1 µM the entry rate of D-TAT is 2680 molecules/s into apical OHCs and marginally less than that for basal OHCs (2670/s). D-JNKi1, in consonance with its larger dimensions enters much more slowly, with an apical to basal gradient evident, as for the loading of TR D-JNKi1 (FIGURE 4-4). At an extracellular concentration of 1 µM, D-TAT enters apical OHCs at a rate of 72/s and basal OHCs at a rate of 455/s.

4.5 Discussion

4.5.1 D-TAT and D-JNKi1 are both high affinity, voltage dependent, permeant blockers of the MET channel

With very low K_Ds, D-TAT and D-JNKi1 are the highest affinity MET channel blockers profiled to date. The block that both of these compounds offer is clearly of a voltage dependent nature. As the Texas-Red conjugate loading data illustrate both D-TAT and D-JNKi1 enter into hair cells, permeating through the MET channel.

The voltage dependence of the block is due to the polycationic compounds being sensitive to the membrane potential of the cell. Therefore, at very hyperpolarised potentials the MET channel may either be fully blocked or the block will be partially released due to the compound being pulled through into intracellular space of the hair cell (Woodhull, 1973; Marcotti et al., 2005). Entry into the OHCs is further substantiated by the electrophysiological evidence of permeant block of the MET channel, as there is a release of block at hyperpolarised potentials more negative than -104 mV. Moreover, it is thus clear that the MET channel is the primary route of entry taken by these peptides.

4.5.2 A gradient in the MET channel pore properties is apparent and a re-estimate of MET channel pore size(s) necessary

The higher affinity of D-JNKi1 relative to D-TAT block in basal OHCs may be due to the additional potentially positive charges (basic amino acids) along its length interacting with the negatively charged residues within the MET channel vestibule. Moreover, a gradient in the properties of the MET channel pore is evident, resulting in a decreasing ability of D-JNKi1 to

block the channel and permeate into the OHCs from base to apex. The D-JNKi1 gradient is distinct; consistent with the basal vestibule having greater dimensions than that the apical vestibule, as is apparent from the energy profile data which yields energy barriers of a decreased height for D-JNKi1 in basal OHC MET channels. Similarly, the lower energy barrier at the intracellular face of the channel is compatible with the exit from the narrow region of the pore into the cell being wider in the MET channels of basal OHCs. This is in agreement with the evidence of a corresponding gradient in single channel conductance (Beurg et al., 2006; Kim et al., 2013). The energy well of the D-JNKi1 binding site in the basal MET channel is slightly deeper (16.50 kT) than that in the apical (15.50 kT) MET channel suggesting that there may be a small number of additional positive residues in the basal MET channel vestibule, allowing D-JNKi1 to bind more tightly. In turn, this increases the blocking potential of D-JNKi1 in basal OHCs, meaning it has a lower K_D. However, due to the similarity of the D-JNKi1 binding site energy wells in apical and basal OHCs, this is likely to only have a small effect on the increased affinity of D-JNKi1 to basal OHC MET channels relative to the heights of the energy barriers.

An intrinsic difference in susceptibility to free radical damage between apical and basal OHCs has been proposed based on the fact that levels of the antioxidant glutathione were lower in basal OHCs and the number of surviving cells could be increased by addition of radical scavengers (Sha et al., 2001). Early studies indicated that basal OHCs were affected but further towards the apex they did not become as damaged by aminoglycosides, additionally IHCs appeared to be less susceptible to damage by aminoglycosides than OHCs in vivo in guinea pigs (Davis et al., 1958; Ward and Fernandez, 1961; (Brummett et al., 1972); Ylikoski 1973), in mice in vitro (Richardson and Russell, 1991) and in humans (Huizing and Groot, 1987). The precise defensive mechanism(s) of IHCS that result in this pattern are as yet unknown. Consistent with this, IHCs appear to be inherently more resistant to free radical damage (Sha et al., 2001). Additionally, it has been found that there is a gradient in susceptibility to aminoglycosides such

that the first (innermost) row of OHCs is most affected and the IHCs are relatively resistant (Schacht et al., 2012).

Importantly, due to the large size of D-JNKi1, in light of the finding that it is a permeant blocker of the MET channel, a re-estimate the size of the narrow region of the MET channel pore seems necessary as the D-TAT end of D-JNKi1 at its widest is 15 Å, larger than the currently estimated 12.5 Å (Farris et al., 2004).

4.5.3 Energy profiles, apical and basal MET channel isoforms

The energy profiles of D-TAT and D-JNKi1 tell us about their interaction with the MET channel and reveal that they occupy binding sites in different parts of the channel pore. The electrical distance of the binding sites for the two vary sufficiently that this seems a fair assumption, given what we currently believe about the structure of the MET channel. The electrical distance of the D-JNKi1 binding site is 0.28 in apical cells and 0.40 in basal cells and thus D-JNKi1 appears to be binding in the highly electronegative vestibule, whilst the binding site for D-TAT is at a distance of 0.78 in apical cells and 0.66 in basal cells and thus seems to occupy a binding site nearer the narrow region of the channel pore, further towards the intracellular face of the channel. Moreover, the strong binding of D-JNKi1 in the vestibule is illustrated by the deep well of free energy at the binding site (FIGURE 4-19).

D-JNKi1 has larger energy barriers of 11.60 kT (E_1) and 18.20 kT (E_2) in apical OHCs vs 8.95 kT (E_1) and 14.55 kT (E_2) in basal OHCs. The higher barriers impede the ability of D-JNKi1 to enter into the MET channel and then to permeate into the channel. This seems to indicate that the apical MET channel is smaller than the basal isoform. This is congruent with there being no difference in the affinity of D-TAT binding between apex and base, as its smaller dimensions and binding in the near the narrow part of the channel pore, mean that the size of the channel should intuitively have less effect on its binding affinity.

The entry rate of compounds into the hair cells is increasingly limited by energy barriers with more free energy and stronger binding sites (van Netten et al., 2007). The limiting factors for entry of D-TAT into apical and basal MET channels are similar as heights of the energy barriers (E_1: 15.20 kT in apical and 15.90 kT in basal; E_2: 21.60 kT and 22.80 kT, respectively) and the free energy of the binding sites (-5.52 kT and -5.64 kT, respectively). In line with this the entry rates are similar (at 100 nM: 1580 molecules/s in apical and 1540/s in basal; at 1 μM 2680 in apical and 2670 in basal), as predicted by the similar TR D-TAT loading into apical and basal OHCs (FIGURE 4-4). The binding site(s) for D-JNKi1 in the basal MET channel isoform have a slightly deeper energy well of -16.50 kT vs -15.50 kT in the apical isoform, causing D-JNKi1 to bind with somewhat greater affinity. Additionally the smaller energy barriers of the energy profile of D-JNKi1 interacting with the basal MET channel isoform (8.95, 14.60) vs the apical isoform (11.60, 18.20), indicate that the basal MET channel has larger dimensions, allowing D-JNKi1 to enter basal OHCs more rapidly (455/s at an extracellular concentration of 100 nM) compared with apical OHCs (72/s at 100 nM). The more rapid entry rate of D-JNKi1 into basal OHC MET channels is in agreement with the greater loading of TR D-JNKi1 into OHCs compared with apical OHCs (FIGURE 4-4 C, E). Furthermore, the similarity of the entry rate of D-TAT into apical and basal OHCs is also in agreement with the TR D-TAT loading data, where loading is similar, although the slight difference in entry rates mean there is still a degree of difference in fluorescence in the cell bodies of the apical (FIGURE 4-4 D) and basal OHCs (FIGURE 4-4 F).

The entry rate of D-TAT is similar for apical and basal OHCs. Surprisingly, it is slightly greater in apical OHCs at an extracellular concentration of 1 μM, 2680 molecules per second vs 2670/s in basal OHCs. This is also the case at 100 nM where the entry rate in apical OHCs (1580/s) is more rapid than in basal OHCs (1540/s). The entry rate of D-JNKi1 into OHCs is much slower than that of D-TAT, with a distinctively slower entry rate into apical OHCs (44/s at 100 nM and 72/s at 1 μM) and basal (366/s at 100 nM and 455/s at 1 μM). This illustrates that there is a non-linear relationship between increased extracellular concentration and entry rate. It has

been highlighted that entry rates of ototoxic compounds are important because inherent protective mechanisms against free radical damage (Sha et al., 2001) will be less likely to be counteract ototoxic effects where more rapid accumulation within the cells occurs (Alharazneh et al., 2011). Damage repair mechanism of reversible hair cell damage will stand a greater chance of protecting cells against compounds with more limited rates of entry.

The fact that D-JNKi1 binds with high affinity, especially in the basal MET channel and lingers in the channel pore, entering into the cell slowly, means that it is a good competitive MET channel blocker for aminoglycoside antibiotics such as DHS. DHS was found to have an entry rate of 9000 molecules per second when tested under similar conditions to those of my experiments, albeit in the presence of 0.1 mM extracellular Ca^{2+}, (0.05 fmol per hour), which was calculated to equate to 3 fA of the current flowing through MET channels of apical-coil OHCs, a minute proportion of the entire MET current. Thus, where entering through MET channels open at rest it would take 80 seconds to reach a 1 µM intracellular concentration (Marcotti et al., 2005). Using D-JNKi1 as a competitive blocker would, however, depend on being able to find a therapeutic concentration at which it is an efficacious channel blocker but ototoxic effects are ameliorated.

4.5.4 The levels of cooperativity of D-TAT and D-JNKi1 with their MET channel binding sites allow further inferences to be made about the nature of the apical and basal MET channel isoforms

A measure of the level of cooperativity of the MET channel binding sites with D-TAT and D-JNKi1 has been obtained from the Hill coefficient gained from the dose response curves at each holding potential. The principle of cooperativity describes the interaction of binding sites with one another. Where the MET channel is a concerned, a Hill coefficient of 1 is indicative of

the fact that there is one binding site for one molecule of a particular compound or multiple binding sites with equal affinity which do not interact, a Hill coefficient of more than 1 is suggestive of positive cooperativity between binding sites and thus the existence of multiple binding sites (Wyman, 1990, Krusek, 2004).

D-JNKi1 shows consistently neutral cooperativity. The n_H of apical D-JNki1 ranges from 0.87 to 1.03 and the n_H of basal D-JNKi1 ranges from 1.01 to 1.10 at membrane potentials from -164 to -64.

A hill coefficient of less than 1, signifying negative cooperativity, necessitates the existence of two or more binding sites within the channel. However, it does not necessarily indicate that the binding of a compound at one binding site negatively impacts binding at another site. Instead this is one of two possibilities, where negative cooperativity is concerned, the second being that the binding affinities for both sites are different (Ferguson et al., 1975; Wyman, 1990; Jackson, 2002).

The cooperativity of D-TAT with both the apical and basal MET channel pore binding site(s) is consistently negative - apical n_H ranging from 0.49 to 0.64 and basal n_H ranging from 0.63 to 0.79. This suggests that there are two D-TAT binding sites within the MET channel pore. Further, the negative cooperativity indicates either binding of a D-TAT molecule at one site preventing the binding of additional D-TAT molecules, or that the binding sites have different affinities, resulting in the negative cooperativity between the two.

The membrane potential of the OHC has a greater effect on the free energy of areas nearer the intracellular face of the channel such as the narrow part of the channel pore and the internal barrier. Additional energy profile modelling for D-JNKi1 at membrane potentials other than 0 mV has shown that at more positive potentials the barrier on the innermost side of the channel becomes higher whilst the free energy of the outermost barrier in the channel is relatively unaffected.

In spite of the fact that D-JNKi1 does block the MET channel to some degree at positive membrane potentials, the model used for obtaining the K_D and n_H was not found suitable for fitting the data at these potentials. This is probably due to the K_Ds at these potentials being out of the range of the concentrations I have tested. Whilst there is no doubt that there is some degree of channel block by D-JNKi1 at positive potentials, overall it is quite variable (FIGURE 4-14). This may be the result of incomplete washout between recordings, due to D-JNKi1 lingering in the channel due to its large size and high affinity with its binding site(s). This would be less evident at negative membrane potentials as the block is much stronger.

The principle of Occam's Razor is stated as "pluralitas non est ponenda sine necessitate" (plurality should not be posited without necessity) (William of Occam, 14th century; Encyclopedia Britannica). In attempting to posit explanations for this this data I will use this merely as a useful guideline, by way of explaining what seems like an intuitive likelihood. However, I wish to make it apparent that I take into account criticisms of this principle such as that of Emanuel Kant who offered his challenge, "entium varietates non temere esse minuendas" (the variety of beings should not be rashly diminished) (Emanuel Kant, 1781; translation 1929). Nevertheless, given that I have attempted to analyse the data in a way which aims to explore it thoroughly and without exclusion, I feel that the explanation which requires the fewest assumptions is appropriate in this instance. In the case of D-JNKi1, due to its large dimensions, it seems most straightforward to posit that the neutral cooperativity in both apical and basal MET channel isoforms (n_H = ~1) equates to there being a single binding site within both apical and basal MET channel isoforms. The negative cooperativity of D-TAT, defined by an n_H of consistently less than 1, indicates the presence of multiple binding sites. These sites either influence one another such that binding at one site prevents binding at another or they have different affinities for D-TAT. Using rationale informed by parsimony here is certainly more difficult as whilst the former requires less

categories (types of binding site with different affinities), it may be more mechanistically complex. Therefore, I do not feel I can make an assessment based on the binding curves alone.

4.6 Conclusions

In spite of being ototoxic at the relatively high concentrations (0.5 µM or greater), more recent results have shown that there appears to be a therapeutic window; D-TAT and D-JNKi1 are otoprotective, conveying protection against aminoglycoside antibiotics, at much lower concentrations. This indicates that there may be potential for use of one of these peptides in a clinic context. Alternatively, they may provide a starting point for finding a similar high affinity blocker; a modified or similar molecularly structured compound which conveys otoprotection. Ideally, this compound would be able to block but not permeate the MET channel, as this would help in avoiding any potential negative effects caused after entering into the hair cells.

These peptides are interesting in terms of what they elucidate about the MET channel isoforms. They are larger than the currently estimated narrow region of the MET channel pore (12.5 Å) and are able to permeate through it. Therefore, the width of this area must be in the region of the end on diameter of the two compounds: 15 Å. This means that the MET channel pore size needs to be re-estimated. The difference in susceptibility of apical and basal OHCs to D-JNKi1 falls in line with the idea that different channel isoforms exist.

The negative cooperativity of D-TAT with the channel suggests that there are at least two binding sites in the MET channel which it is able to occupy. The neutral cooperativity of D-JNKi1 suggests that there may only be one binding site in the channel, however, as previously discussed, the Hill coefficient represents the minimum number of binding sites. The idea that more D-TAT than D-JNKi1 molecules can be accommodated in the MET channel accords with its smaller dimensions but may indicate that the MET channel pore is even larger than 15 Å.

The energy profiles presented indicate that D-TAT binds near the narrow region of the MET channel pore, as DHS appears to (Marcotti et al., 2005), whilst D-JNKi1 seems to bind in the

vestibule. It was previously found by van Netten et al. (2007) that there appear to be two distinct binding sites within the MET channel pore, one for DHS and another for amiloride and benzamil. Energy profile modelling (van Netten et al., 2007) of DHS showed that it bound at a distance of 0.80 from the extracellular face whilst, using data from Rüsch et al. (1994), they found that amiloride bound at a distance of 0.44 and benzamil at 0.55 . The fact that there appear to be these two distinct binding site regions combined with the fact that there is a different profile for D-JNKi1 binding in apical and basal OHC MET channels provides some further insights into the structure of the MET channel. The MET channel appears to be formed of subunits (Beurg et al., 2006), the pore containing the large electronegative vestibule and the narrow channel pore region; a variation of subunits along the length of the cochlea creating different isoforms. The higher barriers for D-JNKi1 in apical OHCs indicate that the apical MET channel isoform has smaller dimensions than the basal MET channel isoform. If this is the case then the basal channel must be even larger than 15 Å (the minimum end-on diameter of the compounds tested) as they are able to permeate the smaller apical channel.

5 BLOCKING OF THE MECHANO-ELECTRICAL TRANSDUCER CHANNELS IN COCHLEAR INNER HAIR CELLS BY D-TAT AND D-JNKI1

5.1 Lack of gradient from apex to base in IHCs

As the bona fide sensory cells of the cochlear, inner hair cells are connected to ~95% of the afferent nerve fibres (Spoendlin, 1972) which send information to the central nervous system/ As well as this there are some efferent neurons which synapse onto the afferent connections (Pickles, 2008). The stereocilia of the IHCs not in contact with the tectorial membrane as OHCs are and respond to basilar membrane motion after it has been altered by the tectorial membrane and OHC motion (Lim, 1986). IHCs have a larger single channel conductance (Beurg et al., 2006), but smaller macroscopic MET current size (Kros et al., 1992) than those of apical and basal OHCs. It has been suggested that IHC MET channels contain a vestibule with more negatively charged residues within it, explaining the greater single channel conductance (Beurg et al., 2006). Unlike for OHCs, there is no evidence of a gradient in IHC MET current size. Single channel recordings show that single channel conductance is the same size in apical and basal IHCs (Beurg et al., 2006). Congruently, macroscopic IHC currents have been found to be relatively uniform in size (Kim and Fettiplace, 2013).

5.2 Results

5.2.1 D-TAT and D-JNKi1 act as permeant IHC MET channel blockers

The block of IHC MET currents by D-TAT and D-JNKi1 is very similar to that in OHCs. D-TAT and D-JNKi1 are both permeant blockers of neonatal IHC MET channels. Where greater concentrations of the peptides are applied the block witnessed is stronger and thus the block is concentration dependent (FIGURE 5-1, 5-2, 5-3). Both compounds block the MET channel in a voltage dependent manner, being released at increasingly positive potentials, with maximum channel block at -104 mV. The block of both compounds is released at extremely hyperpolarised potentials indicating that the molecules are able to permeate the IHC MET channels, dragged through the channel pore because of the hyperpolarised membrane potential below -104 mV (FIGURE 5-4, 5-5). This is in line with the TR-conjugate loading data, which illustrates that both compounds are able to load into IHCs (FIGURE 4-4).

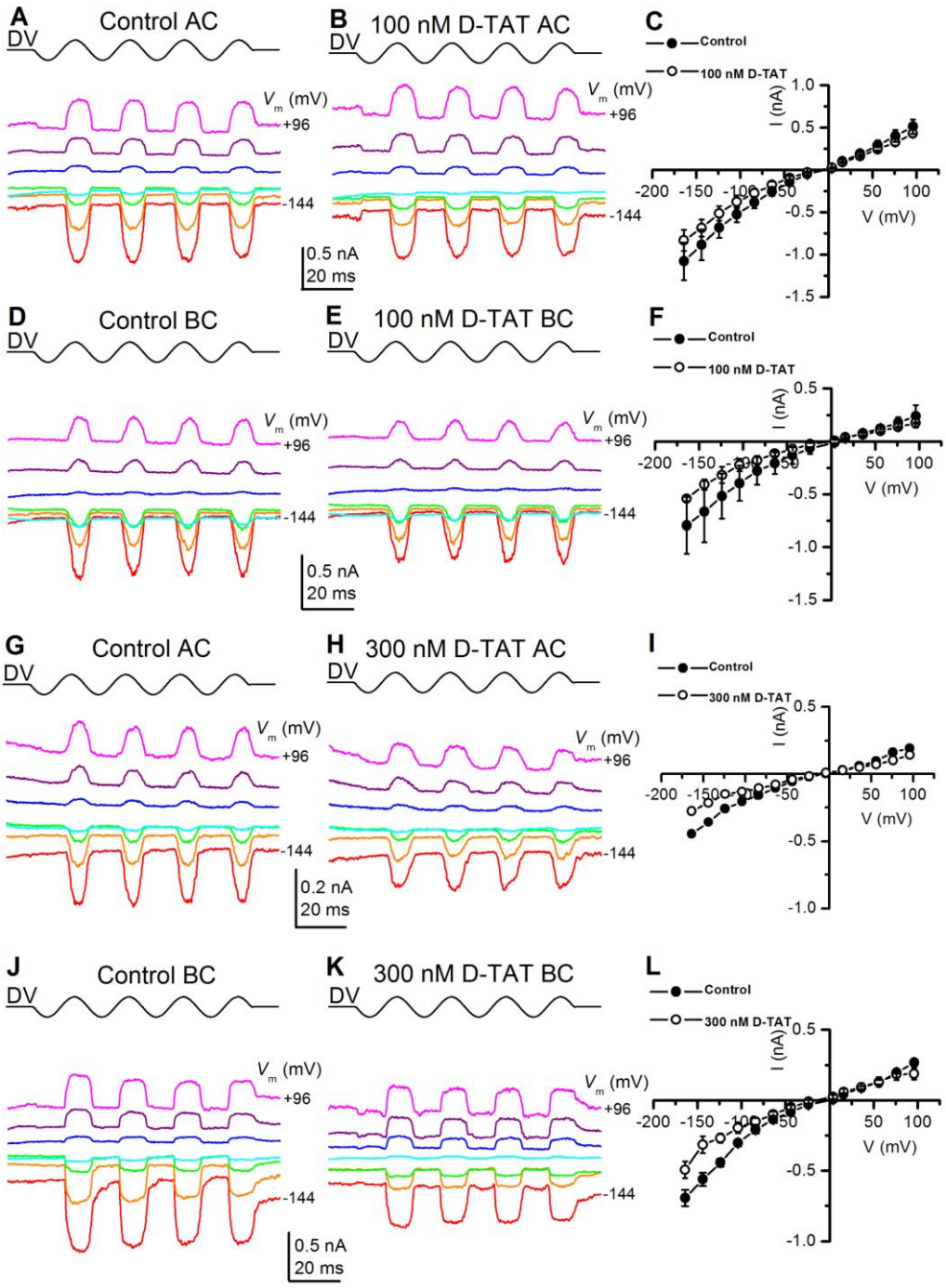
A
Control AC
DV
B
100 nM D-TAT AC
DV
C
Control
100 nM D-TAT
I (nA)
V (mV)
V_m (mV)
+96
-144
0.5 nA
20 ms
D
Control BC
E
100 nM D-TAT BC
F
G
Control AC
H
300 nM D-TAT AC
I
0.2 nA
J
Control BC
K
300 nM D-TAT BC
L

FIGURE 5-1 : Block of apical and basal IHC MET currents by 100 nM and 300 nM D-TAT and apical OHCs by 1 µM D-TAT. A, B, D, E, G, H, J, K, M, N MET currents recorded from apical (A, B, G, H, M, N) and basal (D, E, J, K) P2 CD-1 OHCs before and during superfusion with a solution containing 100 nM (A, B, D, E) or 300 nM (G, H, J, K) D-TAT. Membrane potential stepped between -164 mV and +96 mV in 20 mV increments from a holding potential of -84 mV. Half the voltage steps used are shown for clarity (-144, -104, -64, -24, +16, +56, +96 mV). Driver voltage (45 Hz sinusoid, 40 V amplitude) plotted above the current traces. **C, F, I, L, O** Average current-voltage curves of apical (C, I) and basal (F, L) IHCs before and during superfusion of a solution containing 100 nM (C, F) and 300 nM D-TAT (I, L). Number of cells C:3, F:3, I:2, L:5, O: 4.

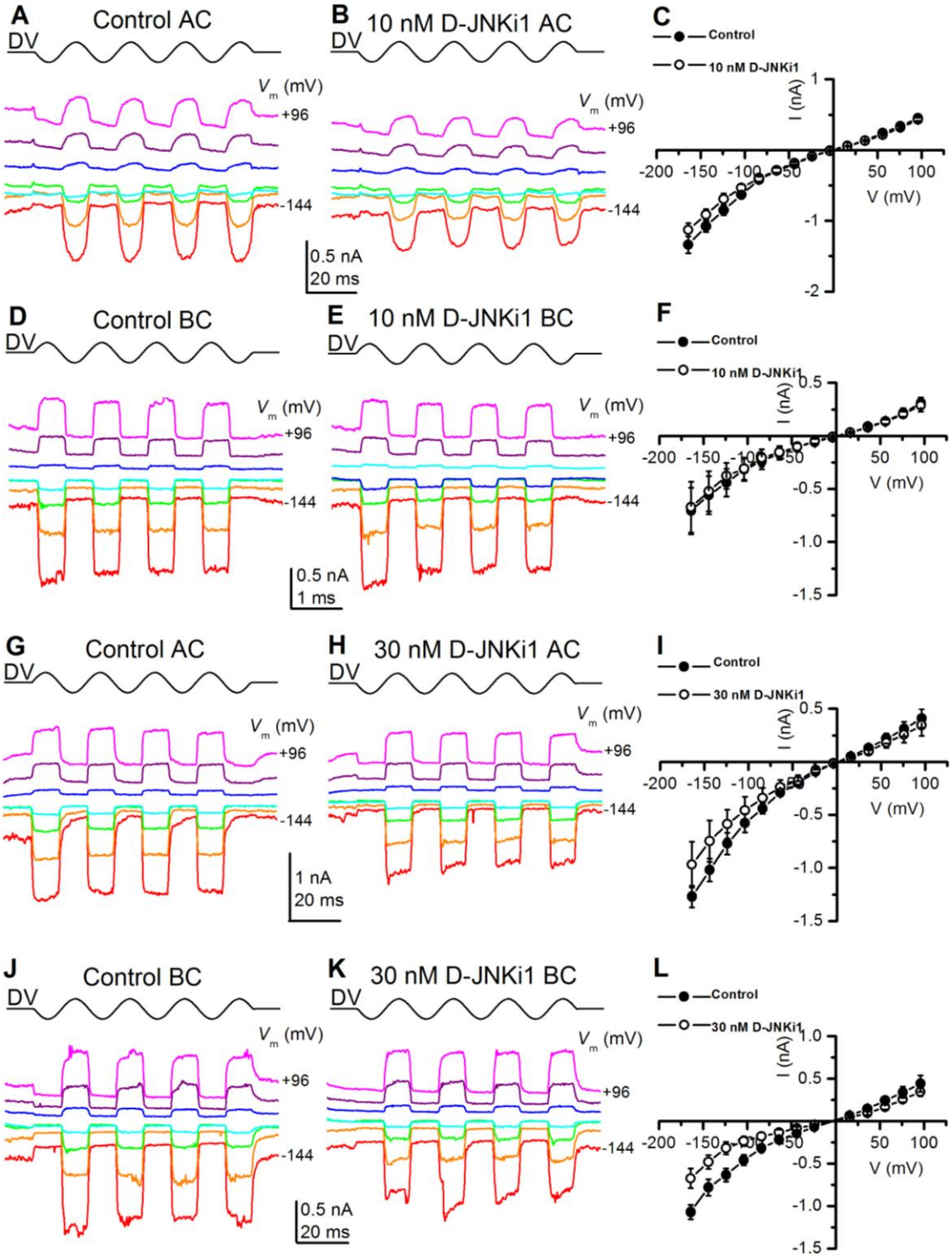
A
Control AC
DV
V_m (mV)
+96
-144
0.5 nA
20 ms
B
10 nM D-JNKi1 AC
DV
V_m (mV)
+96
-144
C
Control
10 nM D-JNKi1
I (nA)
V (mV)
D
Control BC
DV
V_m (mV)
+96
-144
0.5 nA
1 ms
E
10 nM D-JNKi1 BC
DV
V_m (mV)
+96
-144
F
Control
10 nM D-JNKi1
I (nA)
V (mV)
G
Control AC
DV
V_m (mV)
+96
-144
1 nA
20 ms
H
30 nM D-JNKi1 AC
DV
V_m (mV)
+96
-144
I
Control
30 nM D-JNKi1
I (nA)
V (mV)
J
Control BC
DV
V_m (mV)
+96
-144
0.5 nA
20 ms
K
30 nM D-JNKi1 BC
DV
V_m (mV)
+96
-144
L
Control
30 nM D-JNKi1
I (nA)
V (mV)

FIGURE 5-2 : Block of apical and basal IHC MET currents by 10 nM and 30 nM D-JNKi1. A, B, D, E, G, H, J, K, MET currents recorded from apical (A, B, G, H) and basal (D, E, J, K) P2 CD-1 OHCs before and during superfusion with a solution containing 10 nM (A, B, D, E) or 30 nM (G, H, J, K) D-JNKi1. Membrane potential stepped between -164 mV and +96 mV in 20 mV increments from a holding potential of -84 mV. Half the voltage steps used are shown for clarity ((-144, -104, -64, -24, +16, +56, +96 mV). Driver voltage (45 Hz sinusoid, 40 V amplitude) plotted above the current traces. **C, F, I, L,** Average current-voltage curves of apical (C, I) and basal (F, L) IHCs before and during superfusion of a solution containing 10 nM D-JNKi1 (C, F) and 30 nM D-JNKi1 (I, L). Numbers of cells C:3, F:3, I:4, L:4.

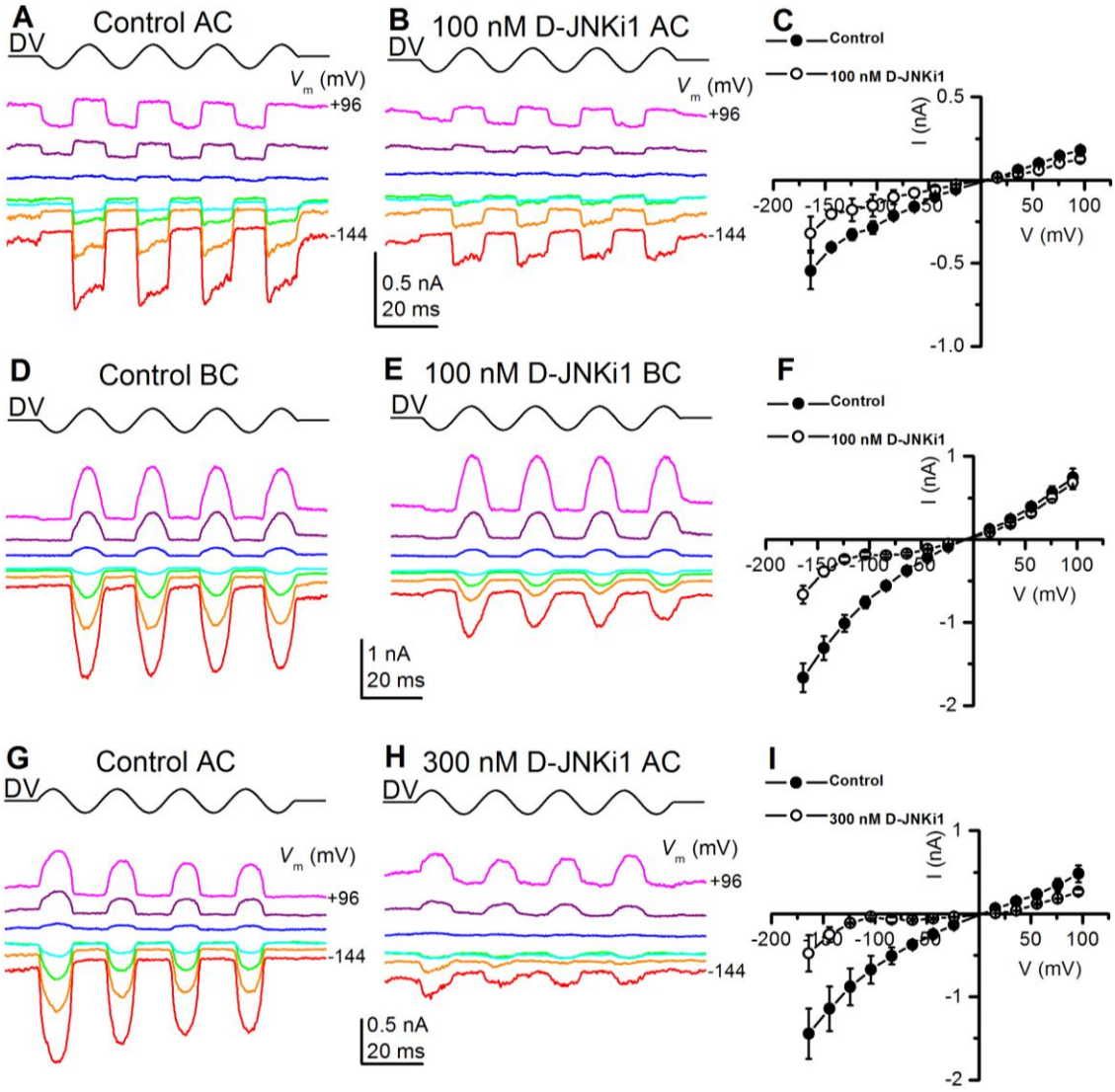
A
Control AC
DV
V_m (mV)
+96
-144
B
100 nM D-JNKi1 AC
DV
V_m (mV)
+96
-144
0.5 nA
20 ms
C
Control
100 nM D-JNKi1
I (nA)
V (mV)
D
Control BC
DV
E
100 nM D-JNKi1 BC
DV
1 nA
20 ms
F
Control
100 nM D-JNKi1
I (nA)
V (mV)
G
Control AC
DV
V_m (mV)
+96
-144
H
300 nM D-JNKi1 AC
DV
V_m (mV)
+96
-144
0.5 nA
20 ms
I
Control
300 nM D-JNKi1
I (nA)
V (mV)

FIGURE 5-3 : Block of apical IHC MET currents by 100 µM and 300 µM D-JNKi1 and basal IHC MET currents by 100 nM D-JNKi1. A, B, D, E, G, H, MET currents recorded from apical (A, B, G, H) and basal (D, E, J, K) P2 CD-1 OHCs before and during superfusion with a solution containing 100 µM (A, B, D, E) or 300 µM D-JNKi1 (G, H). Membrane potential stepped between -164 mV and +96 mV in 20 mV increments from a holding potential of -84 mV. Half the voltage steps used are shown for clarity. Driver voltage (45 Hz sinusoid, 40 V amplitude) plotted above the current traces. **C, F, I,** Average current–voltage curves of apical (C, I) and basal (F) OHCs before and during superfusion of a solution containing 100 µM D-JNKi1 (C, F) and 300 µM D-JNKi1 (I). Numbers of cells C:2, F:5, I:2.

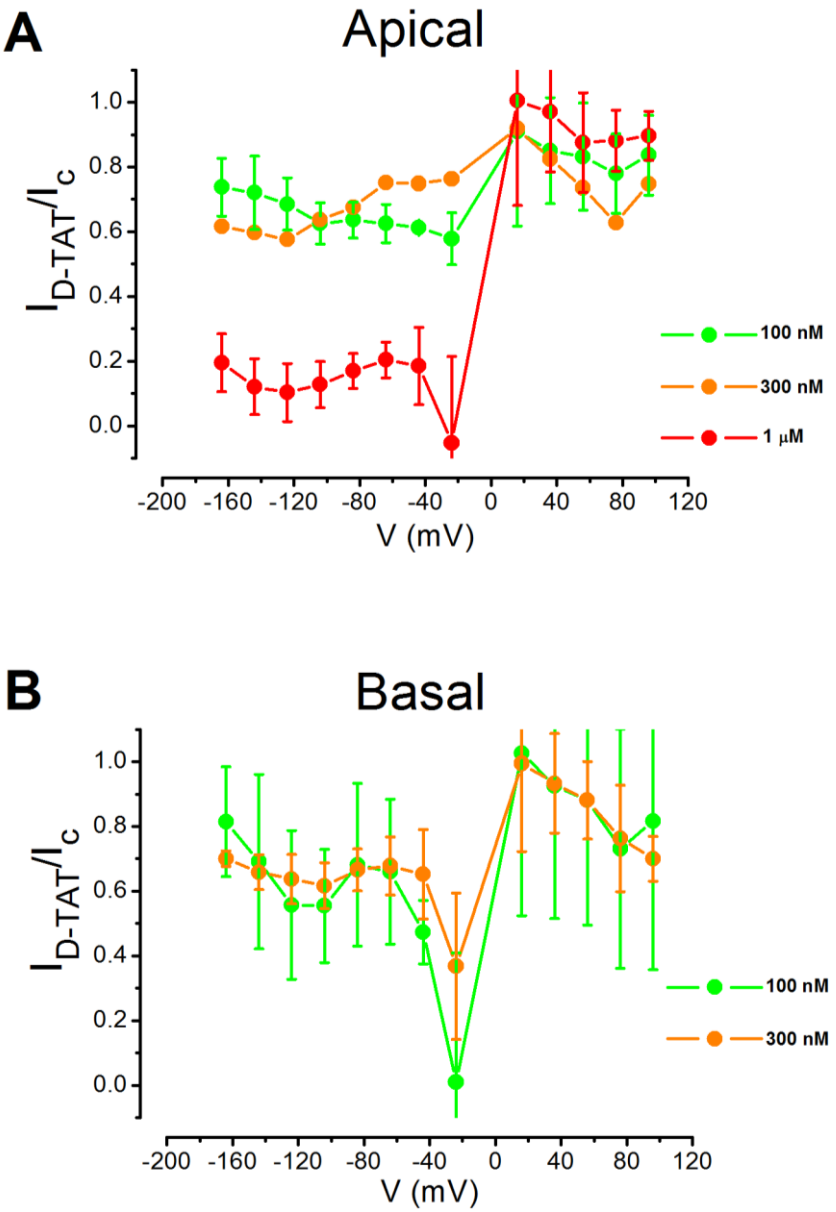

FIGURE 5-4 : Fractional block of IHC MET currents by D-TAT. A, B, MET currents as a fraction of the current in the control solution recorded from apical (A) and basal (B) IHCs before and during superfusion with D-JNKi1 at concentrations from 100 nM to 1 µM. Numbers of cells A: 100 nM (n = 3), 300 nM (n = 1) and 1 µM (n = 4). B: 100 nM (n = 3), 300 nM (n = 5).

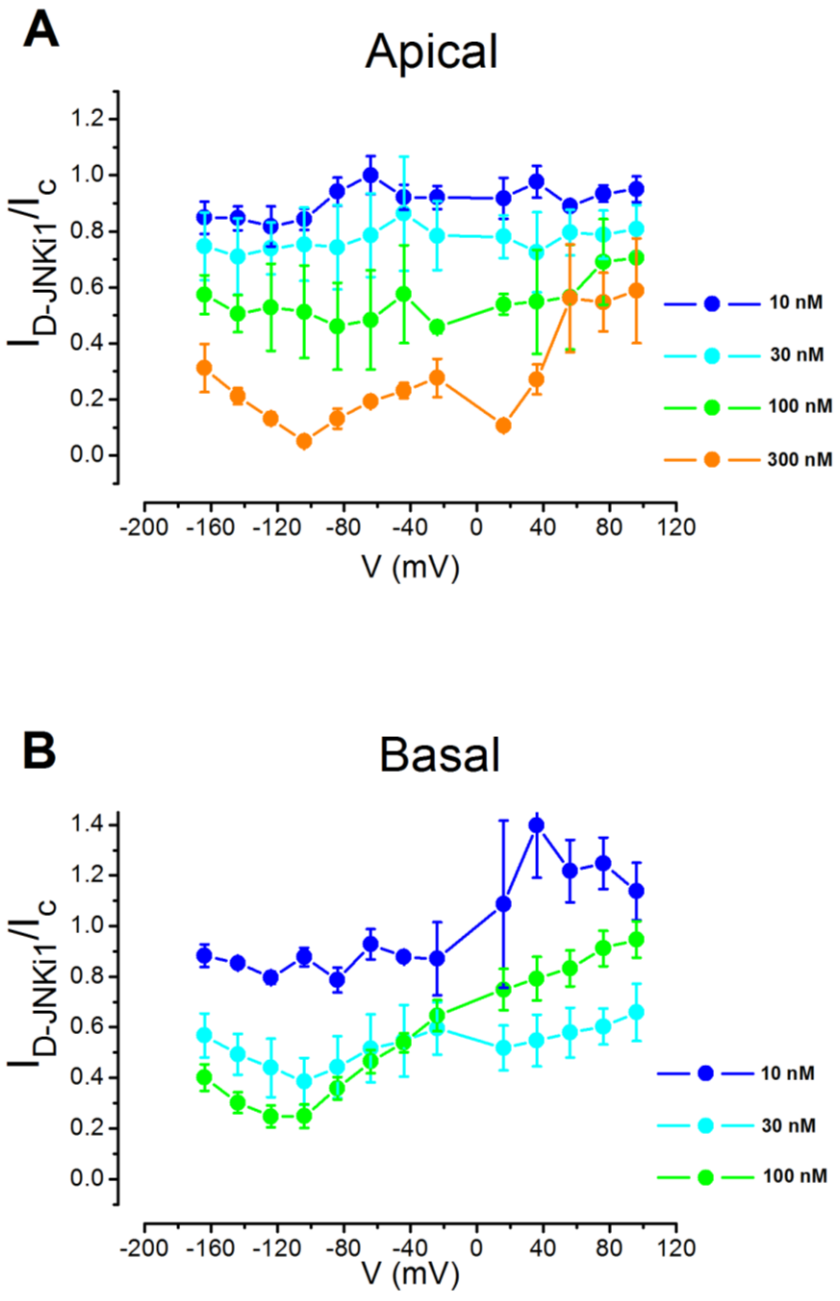

FIGURE 5-5 : Fractional block of IHC MET currents by D-JNKi1. A, B, MET currents as a fraction of the current in the control solution recorded from apical (A) and basal (B) IHCs before and during superfusion with D-JNKi1 at concentrations from 10 nM to 300 nM. Numbers of cells A: 10 nM (n = 3), 30 nM (n = 4), 100 nM (n = 2), 300 nM (n = 2).B: 10 nM (n = 3), 30 nM (n = 4), 100 nM (n = 5).

5.2.2 An apical to basal gradient of D-JNKi1 MET channel block and entry into IHCs

There does not appear to be a significant difference between the block caused by D-TAT in apical and basal IHCs, just as in OHCs, whilst entry into basal hair cells is more rapid as is evident from the TR D-TAT loading data. Compellingly, there is a gradient in D-JNKi1 permeant channel block, its permeation rate into hair cells and TR D-JNKi1 loading (FIGURE 4-4). The K_D (at -104 mV) in apical IHCs is 76 nM, whilst it is less than half that (30 nM) in basal IHCs. The K_D for D-TAT in apical IHCs is 241 nM and whilst there is insufficient data to measure the basal K_D, the fractional blocks at -104 mV for apical and basal IHCs where 100 nM (0.63 ± 0.06 and 0.64 ± 0.06 respectively) and 300 nM D-TAT (0.64 and 0.62 ± 0.07 respectively) were used were very similar (FIGURE 5-4). D-TAT was neutrally cooperative with the apical MET channel isoform (n_H = 0.98 at -104 mV, FIGURE 5-6), whilst D-JNKi1 appeared somewhat positively cooperative with both apical and basal MET channel isoforms (n_H = 1.18 at -104 mV for both, FIGURE 5-6), potentially indicating that it has multiple binding sites in the apical and basal IHC MET channel isoforms. This would necessitate them being substantially larger than the currently estimated OHC MET channel size, however. Given the relatively small number of recordings from IHCs, it is safe to say that n_H is close to one for both D-TAT and D-JNKi1.

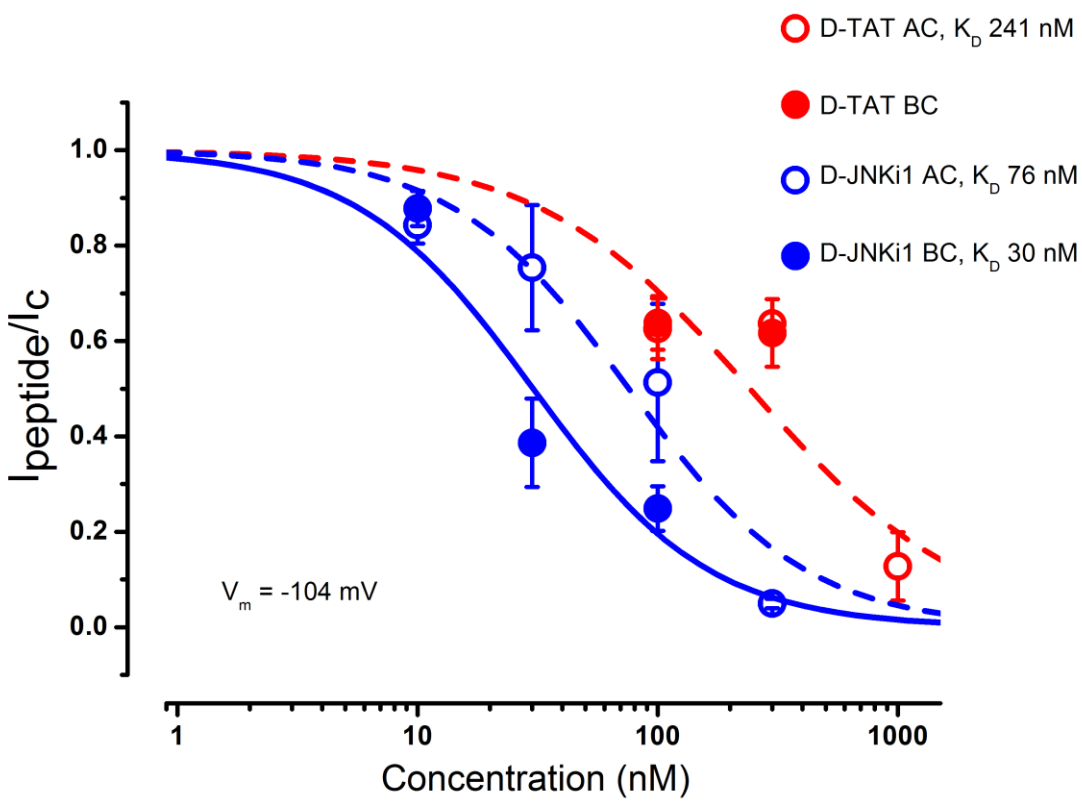
D-TAT AC, K_D 241 nM
D-TAT BC
D-JNKi1 AC, K_D 76 nM
D-JNKi1 BC, K_D 30 nM
Ipeptide/Ic
1.0
0.8
0.6
0.4
0.2
0.0
V_m = -104 mV
1
10
100
1000
Concentration (nM)

FIGURE 5-6 : Dose-response curves at -104 mV, illustrating that D-TAT appears to block of apical and basal IHC MET currents equally well but there is a tonotopic gradient for D-JNKi1. D-TAT treated mid-apical OHCs: red open symbols fitted with red dashed line to the Hill equation, with K_D = 241 nM ± 66 and n_H = 0.98 ± 0.28. Number of cells from left to right: 100 nM (n = 3), 300 nM (n = 2), 1 μM (n = 4). D-TAT treated mid-basal OHCs: red closed symbols. Number of cells from left to right: 100 nM (n = 3), 300 nM (n = 5). D-JNKi1 treated mid-apical IHCs: blue open symbols fitted with blue dashed line fitted to the Hill equation (see Materials and Methods), with K_D = 76 nM ± 20 and n_H = 1.18 ± 0.33. Number of cells from left to right: 10 nM (n = 3), 30 nM (n = 4), 100 nM (n = 2), 300 nM (n = 2). D-JNKi1 treated mid-basal IHCs: blue closed symbols fitted with continuous blue line to the Hill equation, with K_D = 30 nM ± 5.57 and n_H = 1.18 ± 0.26. Number of cells from left to right: 10 nM (n = 3), 30 nM (n = 4), 100 nM (n = 5). The difference between the K_Ds of D-JNKi1 in mid-apical and mid-basal OHCs was not quite significantly difference at a 95% confidence interval.

5.3 Discussion & conclusions

Although the difference in K_Ds of D-JNKi1 in apical and basal IHCs was not found to be quite statistically significant at a confidence interval of 95%, the fact that there appears to be some form of gradient in D-JNKi1 MET channel block in IHCs is interesting since there is no evidence to suggest that there is a gradient in single channel current amplitude (Beurg et al., 2006). My data does seem to show a difference in the blocking efficacy of D-JNKi1 in apical and basal IHCs. This suggests that whilst they possess different isoforms of the channel which are blocked in a distinctive manner by channel blockers, single channel conductance is unaffected and thus is uniform along the length of the cochlea. The K_D in the apical IHCs is very close to that for the OHCs in the same region: 76 nM vs 74 nM. The basal IHC MET channel isoforms appear to have a lower affinity for D-JNKi1, than those of OHCs in the same position, with a K_D of 30 nM, more than double that in mid-basal OHCs (12 nM). This nonetheless is illustrative of the fact that IHCs are not necessarily more resistant to the entry of all ototoxic compounds. This is especially apparent, when taken in conjunction with the evidence of TR D-TAT and TR D-JNKi1 loading into IHCs (FIGURE 4-4) and the permeant nature of the MET channel block achieved by these compounds (FIGURE 5-4, 5-5). TR D-TAT loading inside IHC cell bodies extends further towards the cochlear apex than OHC labelling (FIGURE 4-3) and is thus more uniform, suggesting a gradient which is different from and less pronounced than the OHC gradient. Any resistance to damage (Davis et al., 1958; Ward and Fernandez, 1961; (Brummett et al., 1972; Ylikoski 1973; Richardson and Russell, 1991; Huizing and Groot, 1987) must be conveyed at a later stage by resistance to free radical damage or a more efficient repair mechanism. Additionally they may be protected by the OHCs, where these are present, but some as yet unknown mechanism (Brown and Feldman, 1978). D-TAT however, was ten-fold less effective at blocking the IHC MET channel, with a K_D of 241 nM in mid-apical IHCs vs 25 nM

in the OHCs in the same region of the cochlea, so there are evidently some compounds which are unable to penetrate the IHC MET channel as effectively as the OHC MET channel.

6 DIFFERENTIAL BLOCKING OF ANOMALOUS MECHANOSENSITIVE CURRENT WITH DIHYDROSTREPTOMICIN AND FM1-43 IN COCHLEAR OUTER HAIR CELLS PRETREATED WITH BAPTA

6.1 The anomalous mechanosensitive current

An anomalous mechanosensitive current has been observed which resembles the MET current but which is usually elicited by inverse polarity stimuli (Alagramam et al., 2011; Kim et al., 2013; Marcotti et al., 2014). The anomalous current also differs from the MET current in its "adaptation" characteristics, as what looks like adaptation appears to be calcium independent and does not exhibit the characteristic inward and outward rectification that the MET current does (Marcotti et al., 2014). Moreover, there is no evident resting current and the anomalous current has a delayed onset after the stimulus is applied (Marcotti et al., 2014). Whilst the nature of the anomalous current is being explored, where it arises from is still unknown.

6.1.1 The anomalous current in knockout and mutant mice

6.1.1.1 Pcdh15 and cdh23 mutant mice

Anomalous currents have been found to occur in a type of PCDH15 (av3J/av3J) as well as a CDH23 mutant (v2J/v2J) mouse (Alagramam et al., 2011). Both of these mutants have point mutations which cause a premature stop codon to be created in the transcripts of the genes which encode respective aforementioned tip link components. Electrophysiological recordings revealed that resting currents were absent in these mice. The anomalous currents were mostly elicited by stimuli in the negative direction away from the tallest stereocilia and their amplitude was much reduced, especially at negative membrane potentials, where normal sinusoidal stimuli (35 V driver voltage) was used. It was noted that it was possible to elicit the largest currents at positive holding potentials. Congruent with the presence of anomalous currents in these mice, their hair cells have greatly disrupted bundles with almost no evident tip link like links. Additionally and compellingly, a further mutant mouse that was tested had an in-frame deletion "which is predicted to remove most of the 9th cadherin ectodomain from

PCDH15". This mutation resulted in a far lesser degree of bundle disruption, with far more tip links remaining intact. In line with one potential theory about the necessity of tip links (or attached MET component such as TMHS) for normal MET current generation, these mice show normal MET currents, although they do appear somewhat reduced (Alagramam et al., 2011). Since the proportion of tip links is nonetheless reduced, it is unclear why, if lacking tip links is necessary for anomalous current generation, there is not any evident anomalous current in addition to the MET current apparent in these mice. Perhaps the stimulation applied was not great enough or greater n-numbers would have yielded recordings with such a profile. This too may explain the results in av3J and v2J mice, where large anomalous currents could be elicited at positive potentials but not at negative potentials, with stimuli of a normal magnitude. They did however note an instance of a av3J/av3J OHC where larger currents could be elicited when the stereocilia were stimulated with stronger sinusoidal stimuli (45 V driver voltage). In my experience, greater stimulation and repeating the stimuli over a prolonged period of time is sometimes necessary to elicit the anomalous currents, especially at the negative potentials.

6.1.1.2 Shaker 6J mice

Without acknowledging the opposite polarity of the currents, in characterising transduction in myo7a^{6J} mutants, Kros et al. (2002) found that with greater stimulation, beyond the normal physiological range, MET-like currents could be elicited in these mice. They later realised that these were opposite in polarity and strikingly similar to the currents they could elicit in BAPTA pretreated hair cells in CD1 mice (Marcotti et al., 2014).

6.1.1.3 TMC1 and TMC2

It was discovered that mutations in TMC protein isoforms TMC1 and TMC2 caused hearing loss, after positional cloning of hereditary deafness genes. TMC1 expression was found to occur in the cochlear hair cells and was identified to be required for the cells to function normally (Kurima et al., 2002). These channels subsequently became of great interest in the ongoing hunt for the MET channel candidates.

Experiments by Kawashima et al. (2011) initially showed that hair cells of mice with targeted deletions of TMC1, TMC2 mice had no evident MET currents. Later they discovered that Ca^{2+} permeability and single channel current size are both reduced after altering TMC1 by making a methionine to lysine substitution at position 412 (Pan et al., 2013) suggesting that TMC1 was in fact the MET channel itself.

TMC1 + TMC2 double knockout mice have severe balance deficits and are completely deaf. The presence of the anomalous MET current in these mice has been used to argue that these are not part of the main MET channel machinery. However, in light of the fact that the anomalous current appears to have such different characteristics, this argument does not stand up to critique.

Kim et al. (2013) found evidence of inverse polarity MET current in TMC1; TMC2 double mutant mice, stating that TMC1 was the MET channel, due to their belief that the characteristics of both currents, such as conductance, were sufficiently similar in spite of the reverse polarity of the current. Furthermore, they stated that the susceptibility of the channel to FM1-43 and DHS was the same as for the normal MET channel. Although, after the publication of the data I collected which was presented in Marcotti et al. (2014) they reassessed this assertion and repeated their experiments, subsequently finding that DHS is in fact far less proficient at blocking the anomalous current compared with the MET current

(Beurg et al., 2014). The interpretation was that the TMC channels are some kind of necessary precursor to the localising and realisation of MET channel functionality but not part of the channel itself. Furthermore, they acknowledged that drawing large compounds such as DHS into the channel may require the MET channel vestibule (Beurg et al., 2006) which could feasibly be formed of TMC1 and TMC2 (Beurg et al., 2014b).

The use of antibody labelling enabled TMC1 to be localised to the stereocilia of hair cells (Kawashima et al., 2011; (Beurg et al., 2014a). More recently Kurima et al. (2015) found that TMC1 and TMC2 are located at the tips of the two shortest rows of stereocilia, also by using antibody labelling and the creation of transgenic mice which express fluorphore-tagged TMC proteins, TMC1-mCherry and/or TMC2-AcGFP, under their native promoters. They assessed the ability of TMC1-mCherry and TMC2-AcGFP to restore MET currents in transgenic P3 and P7 mice. They confirmed the functionality of the TMC1-mCherry was in line with the native TMC1 protein as the presence of TMC1-mCherry was able to restore hearing and normal MET currents in the mice. They also confirmed the incapability of TMC2 to compensate for lack of TMC1 in these mice, as hearing was not restored where only TM2-AcGFP was present, although partial MET current restoration does indicate its ability to partially compensate for TMC1. In developing (P3) mice MET currents of normal magnitude in OHCs and near normal magnitude in IHCs were present where both transgenes were expressed. Where only TMC1-mCherry was expressed, currents were restored to some extent but were significantly smaller the native MET currents, especially in IHCs. TMC2-AcGFP expressed on its own, resulted in restored MET currents with a higher magnitude than for TMC1-mCherry in developing mice. Taken together, these are illustrative of the interplay of the two proteins in the developing cochlea. In mature (P7) IHCs, the expression of TMC2-AcGFP in addition to TMC1-mCherry, resulted in being able to elicit MET currents of amplitudes nearer the native size, compared with TMC1-mCherry alone. However, in OHCs, TMC2-AcGFP expression had no effect. This is

illustrative of increasing lack of expression of TMC2 as the cochlea matures (after an initial postnatal increase), in line with previous findings (Kawashima et al., 2011).

Kurima et al. (2015) have discovered that TMC1 and TMC2 are localised along the length of the stereocilia in the developing cochlea. As the hair cells develop, TMC1 and TMC2 are increasingly localised only at the tips of the two shortest stereocilial rows, where the MET channels are thought to reside. Additionally, whilst TMC1 expression is maintained in maturity (P10) TMC2 expression is mostly only evident in the developing cochlea after an initial increase up until P3. Perhaps it is activating the channels, in the absence of tip links, which are localised along the length of the stereocilia during development and consequently being able to record from them, which underlies the anomalous current. An intriguing point is that TMC1-mCherry and TM2-AcGFP puncta remain located in some places along the stereocilia of mature mice, indicating that a reserve pool of MET channels may reside here. This is in concert with the finding that the anomalous current can be elicited in mice up to the P10, which was the latest age tested (Marcotti et al., 2014).

A further addition to the complete picture of the MET channel complex is that there is an implicated role of Lipoma HMGIC fusion partner-like 5 (LHFPL5) (Beurg et al., 2014a), also known by the name TMHS, the absence of which has also been found to disrupt hair cell MET in a similar way. Homozygous null mutants, LHFPL5$^{-/-}$, mice have anomalous currents, decreased single channel conductance and lack the apical to basal gradient found in normal hair cells. Immunolabeling revealed that the stereocilary regions of LHFPL5$^{-/-}$ mice lacked TMC1. They thus state that LHFPL5 is responsible for the correct localisation of TMC1. Moreover, without LHFPL5, a MET complex can still be formed but is instead located at a different region, where stimulation of the bundle in the opposite direction elicits current flow.

The transmembrane protein TMIE has been shown, using protein interaction techniques, to have direct interactions with PCDH15 and LHFPL5. The hair cells of TMIE -/- mice also show

inverse polarity transduction (Zhao et al., 2014). They additionally noted that the presence of currents elicited by inverse polarity stimuli are likely to be representative of the presence of the MET channel in the aforementioned TMC knockouts and thus TMC1 and TMC2 are unlikely to form the MET channel. It seems parsimonious to me that TMIE and LHFPL5 form the part of the MET complex that connects PCDH15 to the MET channel itself.

Kawashima et al. (2014) went on to reiterate and reaffirm that TMC1 and TMC2 may still viably be the MET channel, as the unique characteristics of the anomalous current may in fact mean that is generated by a distinct mechanosensitive channel.

6.1.2 The anomalous current in hair cells pretreated with BAPTA

Tip links are a crucial part of the normal transduction apparatus, creating cohesive movement between stereocilia. Calcium chelators such as BAPTA disrupt tip links which are vital to MET channel function (Assad et al., 1991). When pre-treated with calcium chelators, FM1-43 hair cell entry is prohibited along the length of the cochlea (Gale et al., 2001). When treated with aminoglycosides, after breaking tip links with a BAPTA, most apical coil hair cells, as well as a proportion of basal coil hair cells do not externalise PS as loading into the hair cells is prevented (Goodyear et al., 2008). The anomalous current can be elicited IHCs and OHCs pretreated with BAPTA, in most cases by inverse polarity stimuli (Marcotti et al., 2014).

6.1.3 The anomalous current in normal hair cells

As reported in Marcotti et al. (2014), the anomalous current can be elicited in untreated cells which have not knowingly been damaged or had their tip links pharmacologically or

mechanically ablated. These can appear whilst reasonably large MET currents are also still present, as the MET currents begin to decrease, or on their own where no MET currents are apparent. A simple explanation may be to assume different degrees of damage have been done to tip links and that the anomalous current represents arises from the damaged proportion. However, given the variety of circumstances where anomalous currents have been witnessed, this does not seem very plausible.

6.2 Terminology: the anomalous current and the protochannel from which it arises

Throughout this chapter, as in (Marcotti et al., 2014), I will refer to the current in question as the "anomalous current". In Marcotti et al. (2014) we propose that the channel through which the anomalous current flows is from a reserve pool of mechanosensitive precursor channels, therefore I will refer to this channel here as the "mechanosensitive protochannel" or "protochannel". The witnessed difference in characteristics between the MET current and the anomalous current are thought to arise from a difference in the component subunits from which the channels are formed and the lack of gating by tip links (Beurg et al., 2014b).

6.3 Characterising the anomalous current using channel blockers

6.3.1 FM1-43

Many known MET channel blockers have a blocking profile which has been characterised using patch clamping techniques. Therefore, using these channel blockers can aid in ascertaining

whether this aspect of the protochannel is similar to or different from the MET channel. As a high affinity MET channel blocker which has been well characterised (Gale et al., 2001), with a relatively small size which is estimated at 0.78 x 0.5 nm (Gale et al., 2001) when compared with aminoglycosides, which have diameters ranging from in the region of 0.96 -1.04 nm (Alharazneh et al., 2011), FM1-43 seemed a good candidate to attempt to block the underlying channel and characterise the anomalous current with.

6.3.2 DHS

DHS is another well characterised MET channel blocker, with a different blocking profile to FM1-43, therefore another good candidate to allow for making comparisons between the MET current and the anomalous current. DHS has an end-on diameter of 0.8 nM (Marcotti et al., 2005). It is an open MET channel blocker, whilst FM1-43 is a closed MET channel blocker, able to reside in the closed MET channel. Additionally it had previously been reported that DHS offered a comparable degree of block of the anomalous current and the MET current (Kim et al., 2013).

6.4 Results

6.4.1 FM1-43 acts as concentration dependent blocker of the anomalous current, with some evidence of voltage dependent block but with altered voltage dependence.

After a 5 minute BAPTA pretreatment to break tip links (see METHODS), P2 CD1 OHCs were whole-cell patch clamped and solutions containing concentrations ranging from 1µM to 30 µM FM1-43 or 100 µM to 10 mM DHS were superfused onto the cochlear hair cells in culture, whilst the incremental voltage step protocol was run, in 20 mV steps from -164 mV to +96 mV. Traces were collected before, during and, where the patch seal lasted for long enough, after superfusion with any given concentration.

The bundle stimulation required to record anomalous currents was unlike that used to evoke normal MET currents: a much more forceful stimulus was necessary, as noted by Marcotti et al. (2014). This was achieved by the use of a fluid jet with a larger tip diameter (~14 µm), positioned nearer the bundle than for a normal MET current recording. These currents appeared to materialise over time and increased in size, as more recordings were made. The currents recorded ranged in size dramatically from very small to larger than the normal MET current size.

The anomalous currents have a 'peaky' appearance, especially at negative membrane potentials, compared with the more rounded form of the MET current. They have late onset kinetics, declining more rapidly than the MET current at negative membrane potentials and little or no resting current is evident (FIGURE 6-1, 6-2) as reported in (Marcotti et al., 2014). The anomalous current does not display the inward and outward double-rectification characteristics (FIGURE 6-3) that is a feature of the normal MET current (FIGURE 6-4),

indicating that it may have different ion permeation properties, also as previously reported in Marcotti et al. (2014).

The recording made after the application of 30 µM FM1-43 (FIGURE 6-2, K) is interesting because of the apparent doubling of currents, elicited with both positive (towards the tallest stereocilia) and negative (towards the shortest stereocilia) deflections of the bundle. The characteristics of the currents suggest that they are both anomalous currents, with no evidence of resting transducer current, slow onset kinetics and a peaky appearance. This appearance of these doubled currents was previously reported, in line with the fact that currents, whilst usually elicited by stimuli in the negative direction, can on occasion be elicited by pushing the bundle in either direction (Marcotti et al., 2014). As this was a noted feature of only a single recording this is anecdotal evidence, but it is none the less worth highlighting.

FM1-43 blocks the anomalous current, the block is dependent upon the membrane potential and the degree of block becomes greater with higher concentrations in apical OHCs (FIGURE 6-1). These findings were confirmed using a two-way ANOVA test followed by Bonferroni's test ($P<0.0001$ for both). In basal OHCs (FIGURE 6-2), a two-way ANOVA confirmed the suspected concentration dependence of the block ($P<0.001$), however voltage dependence was not quite significant ($P = 0.0882$).

The block by 10 µM FM1-43 of the anomalous (FIGURE 6-1, 6-2, 6-3, 6-5) and MET currents (FIGURE 6-4, 6-6) is of a similar magnitude. In apical OHCs there was 0.36 ± 0.10 ($n = 3$) of the anomalous current remaining (FIGURE 6-5, A) and 0.47 ± 0.07 ($n = 5$) in basal OHCs (FIGURE 6-5, B) at -104 mV. For the MET current the block was 0.36 ± 0.04 ($n = 3$) in apical OHCs (FIGURE 6-6, A) and 0.41 ± 0.14 ($n = 3$) in basal OHCs (FIGURE 6-6, B) at -104 mV.

A comprehensive study of the block of the MET current by FM1-43 by Gale et al. (2001) found the maximum block to be at intermediate potentials, with block decreasing as the membrane potential was stepped away from 0 mV, in either the direction of negative or positive

membrane potentials. Whilst FM1-43 does block the anomalous current in a voltage dependent manner at least in apical OHCs, the block does not exhibit the same voltage dependence (FIGURE 6-5) as FM1-43 block of the normal MET current, with maximum block at -104 mV, not near 0 mV as in FIGURE 6-6 and Gale et al. (2001). As the maximum degree of MET current block offered by FM1-43 is around 0 mV, for comparison with the maximum block of the MET current we can take a measurement of the fractional proportion of current remaining at -24 mV (the closest measurable membrane potential, due to noise limiting the ability to measure the small currents at -4 mV), which is 0.19 ± 0 (n = 3) in apical OHCs (FIGURE 6-6, A) and in basal OHCs it is 0.41 ± 0.25 (n = 3) (FIGURE 6-6, B).

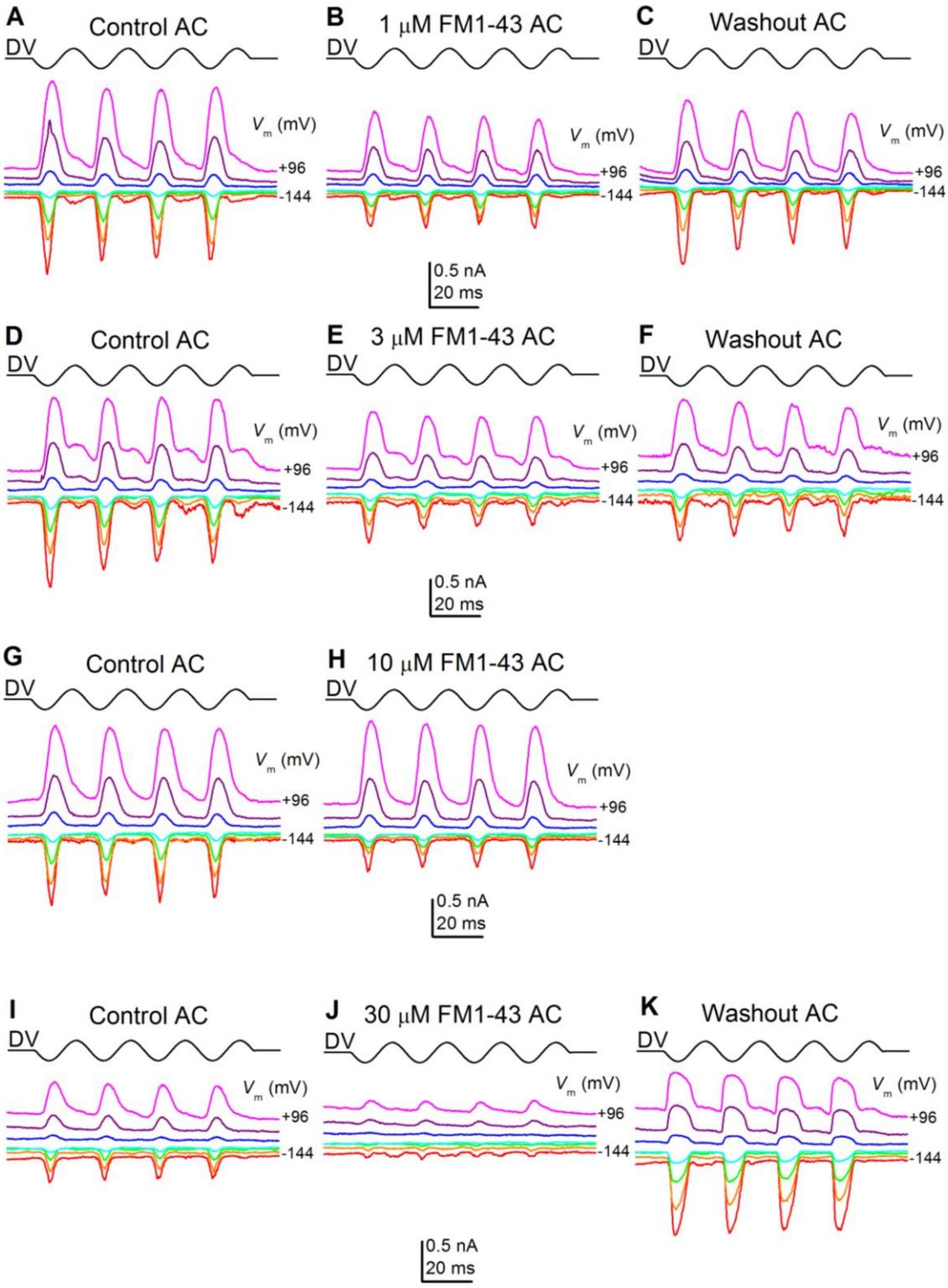
A
Control AC
DV
B
1 μM FM1-43 AC
DV
C
Washout AC
DV
V_m (mV)
+96
-144
0.5 nA
20 ms
D
Control AC
DV
E
3 μM FM1-43 AC
DV
F
Washout AC
DV
G
Control AC
DV
H
10 μM FM1-43 AC
DV
I
Control AC
DV
J
30 μM FM1-43 AC
DV
K
Washout AC
DV

FIGURE 6-1 : Block of anomalous currents in apical OHCs by different concentrations of FM1-43. A, B, C, D, E, F, G, H, I, J, K, anomalous currents recorded from apical OHCs from BAPTA pre-treated CD-1 P2 mice, before (A, D, G, I), during application of 1 µM (B) 3 µM (E), 10 µM (H) and 30 µM (J) FM1-43 and after washout (C, F, K). Membrane potential stepped between -164 mV and +96 mV in 20 mV increments from a holding potential of -84 mV. Half the voltage steps used are shown for clarity. Driver voltage (45 Hz sinusoid, 40 V amplitude) plotted above the current traces.

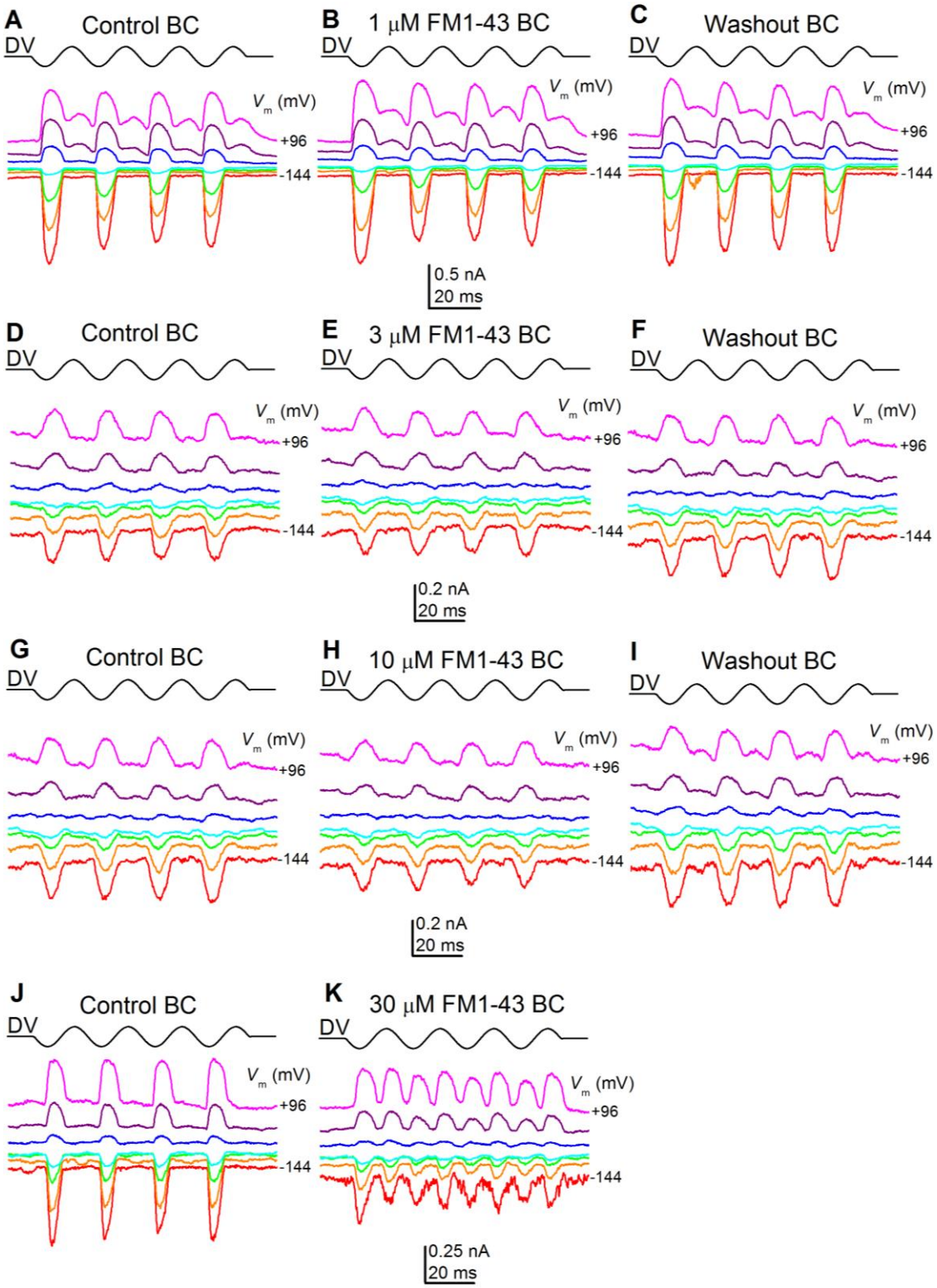
A
Control BC
DV
B
1 μM FM1-43 BC
DV
C
Washout BC
DV
V_m (mV)
+96
-144
0.5 nA
20 ms
D
Control BC
DV
E
3 μM FM1-43 BC
DV
F
Washout BC
DV
0.2 nA
20 ms
G
Control BC
DV
H
10 μM FM1-43 BC
DV
I
Washout BC
DV
0.2 nA
20 ms
J
Control BC
DV
K
30 μM FM1-43 BC
DV
0.25 nA
20 ms

FIGURE 6-2 : Block of anomalous currents in basal OHCs by different concentrations of FM1-43. A, B, C, D, E, F, G, H, I, J, K anomalous currents recorded from basal OHCs from BAPTA pre-treated CD-1 P2 mice, before (A, D, G, J), during application of 1 µM (B) 3 µM (E), 10 µM (H) and 30 µM (K) FM1-43 and after washout (C, F, I). Membrane potential stepped between -164 mV and +96 mV in 20 mV increments from a holding potential of -84 mV. Half the voltage steps used are shown for clarity. Driver voltage (45 Hz sinusoid, 40 V amplitude) plotted above the current traces.

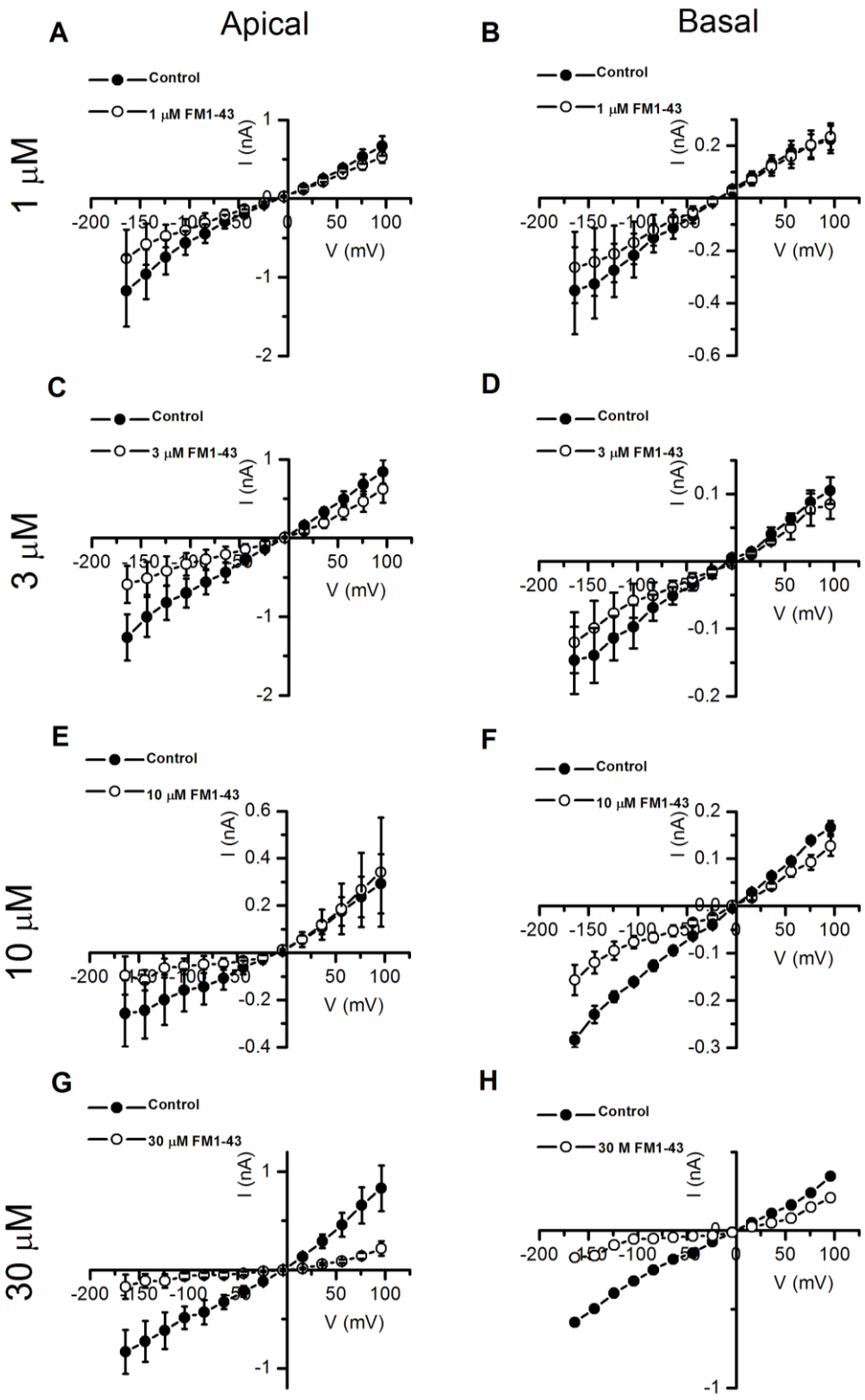
Apical
Basal
A
B
C
D
E
F
G
H
1 μM
3 μM
10 μM
30 μM
Control
1 μM FM1-43
3 μM FM1-43
10 μM FM1-43
30 μM FM1-43
30 M FM1-43
I (nA)
V (mV)

FIGURE 6-3 : FM1-43 current-voltage curves, FM1-43 blocks the anomalous current at negative and to a lesser extent at positive potentials. The anomalous current does not display double-rectification characteristics. A, B, C, D, E, F, G, H, Average current-voltage curves of anomalous currents from BAPTA pre-treated apical (A, C, E, G) and basal (B, D, F, H) OHCs before and during superfusion of a solution containing 1 µM (A, B), 3 µM (C, D), 10 µM (E, F), 30 µM (G, H) FM1-43. Number of cells: Apical: 1 µM (n = 3), 3 µM (n = 3), 10 µM (n = 3), 30 µM (n = 3). Basal: 1 µM (n = 6), 3 µM (n = 4), 10 µM (n = 5), 30 µM (n = 1).

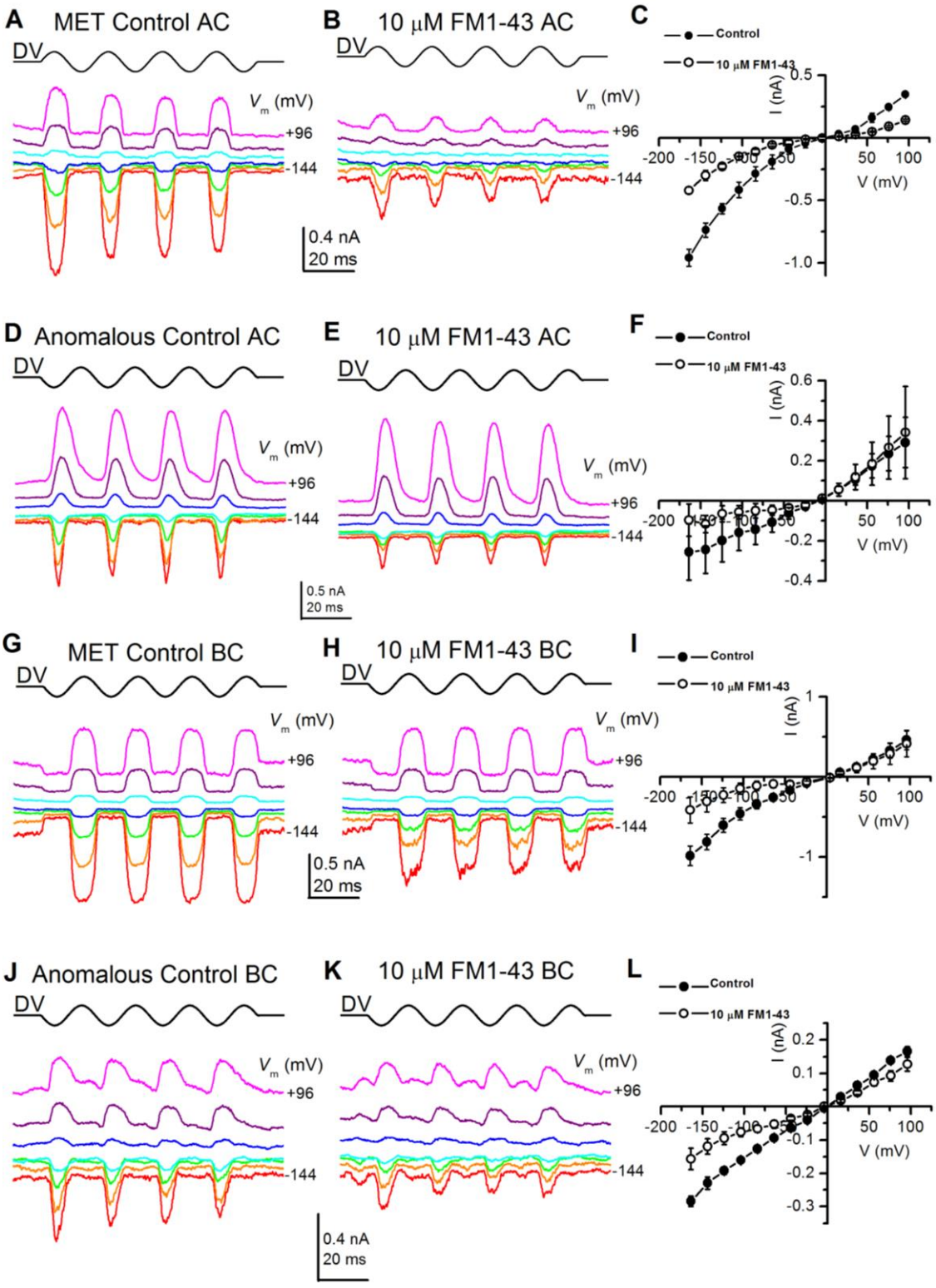
A MET Control AC
DV
V_m (mV)
+96
-144
0.4 nA
20 ms
B 10 μM FM1-43 AC
DV
V_m (mV)
+96
-144
C
Control
10 μM FM1-43
I (nA)
V (mV)
D Anomalous Control AC
DV
V_m (mV)
+96
-144
0.5 nA
20 ms
E 10 μM FM1-43 AC
DV
V_m (mV)
+96
-144
F
Control
10 μM FM1-43
I (nA)
V (mV)
G MET Control BC
DV
V_m (mV)
+96
-144
0.5 nA
20 ms
H 10 μM FM1-43 BC
DV
V_m (mV)
+96
-144
I
Control
10 μM FM1-43
I (nA)
V (mV)
J Anomalous Control BC
DV
V_m (mV)
+96
-144
0.4 nA
20 ms
K 10 μM FM1-43 BC
DV
V_m (mV)
+96
-144
L
Control
10 μM FM1-43
I (nA)
V (mV)

FIGURE 6-4 : FM1-43 block of anomalous currents in apical and basal OHCs is similar to control MET currents in apical OHCs. A, B, D, E, G, H, J, K. currents recorded from apical (A, B, D, E) and basal (G, H, J, K) OHCs from BAPTA pre-treated CD-1 P2 mice (D, E, J, K), before (D, J), during application of 10 µM FM1-43 (E, K) compared with control MET currents (A, B, G, H) before (A, B) and during application of 10 µM FM1-43 (G, H) in normal P2 OHC MET channels. **C, F, I, L,** Average current-voltage curves of MET currents before and during superfusion with 10 µM FM1-43 (C, I) and anomalous currents before and during superfusion with 10 µM FM1-43 (F, L). C: n = 3, F: n = 3, I: n = 4, L: n = 5.

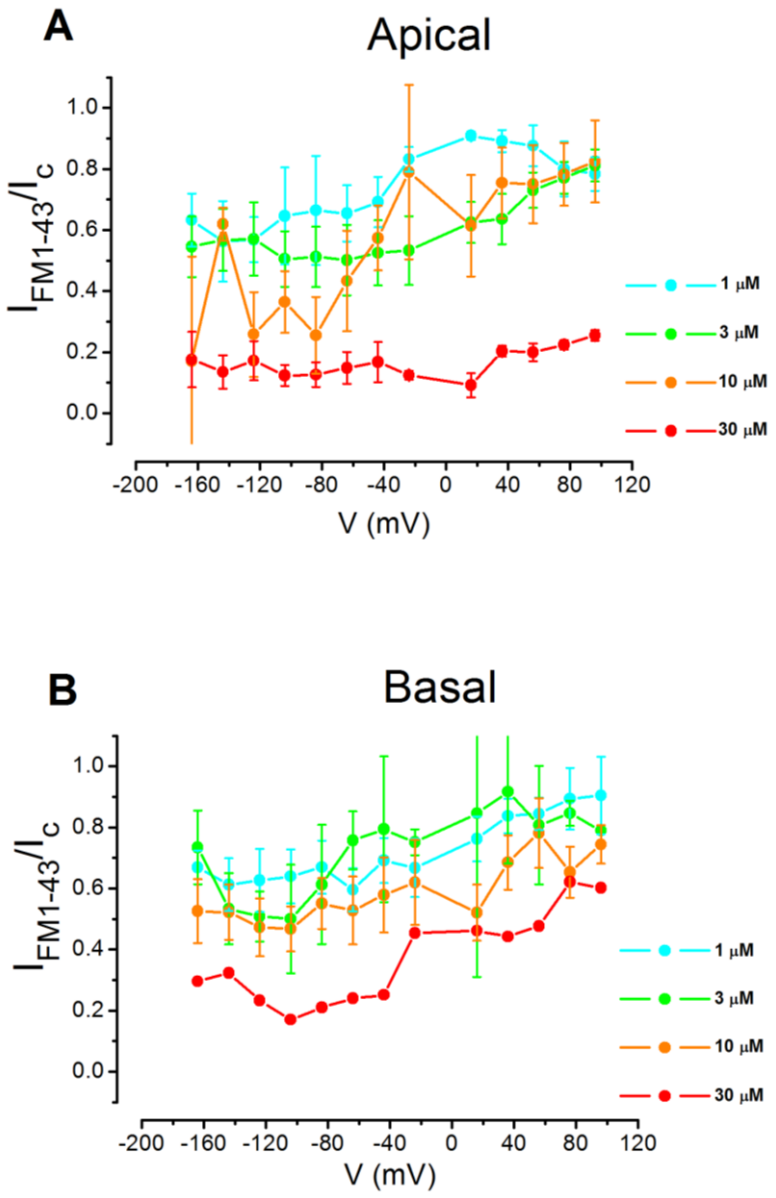

FIGURE 6-5 : Fractional block of anomalous currents in BAPTA pretreated OHCs by FM1-43. FM1-43 blocks the anomalous current in a voltage dependent manner, with maximum block at -104 mV. A, B, Anomalous currents in the presence of 1 µM to 30 µM FM1-43, as a fraction of the currents in the control solution, from apical (A) and basal (B) OHCs. Numbers of cells A: 1 µM (n = 3), 3 µM (n = 3), 10 µM (n = 3), 30 µM (n = 3) B: 1 µM (n = 6), 3 µM (n = 4), 10 µM (n = 5), 30 µM (n = 1).

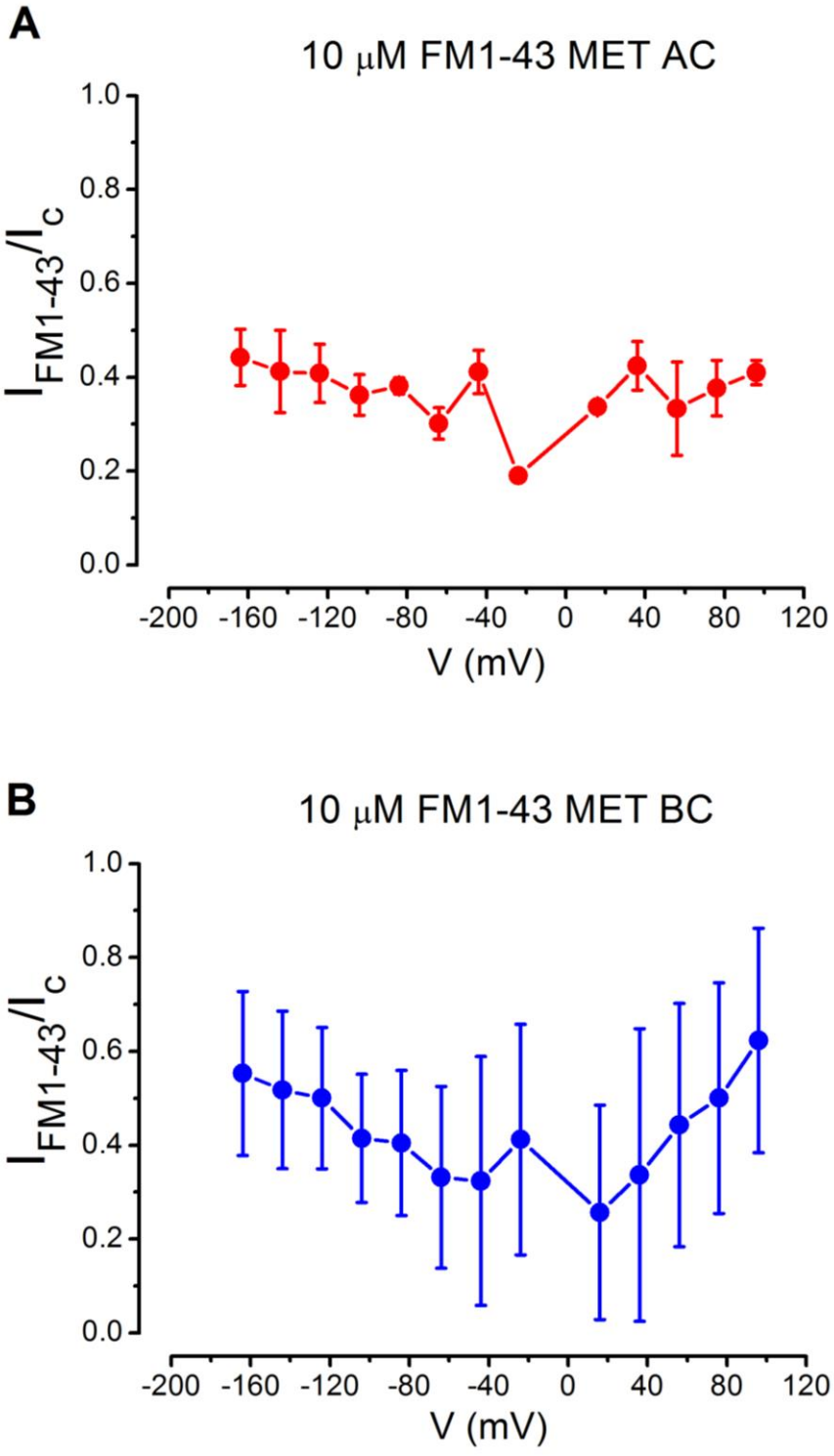

FIGURE 6-6 : 10 μM FM1-43 fractional block of MET current. Block by FM1-43 in apical and basal control OHC MET currents is similar. A, B, Fractional blocks by FM1-43 in control OHCs. 10 μM FM1-43 treated apical OHCs (A), n = 3. 10 μM FM1-43 treated basal OHCs (B), n = 3.

6.4.2 DHS acts as concentration and voltage dependent blocker of the anomalous current in apical OHCs but is two orders of magnitude less efficacious

The block the anomalous currents in apical OHCs by DHS was evidently concentration dependent (FIGURE 6-7, 6-9 A, B, D, F, H) substantiated by using a two-way ANOVA followed by Bonferroni's test ($P<0.0001$ for both), as is the block of the MET current (FIGURE 6-10; Marcotti et al., 2005). Additionally, also in line with DHS block of the MET current (6-12, A) the block of the anomalous current was voltage dependent (FIGURE 6-11, A) in apical OHCs. However, the concentration ($P=0.1067$; FIGURE 6-8, 6-9 C, E, G) and voltage dependence ($P=0.6871$; FIGURE 6-11, B) of the DHS block of the anomalous current in basal OHCs were not significant as determined by conducting a two-way ANOVA followed by Bonferroni's test. This may be because of the low numbers of cells from which recordings were obtained. Further experiments would be required to ascertain whether or not the block in this region is concentration and voltage dependent. Withal, it seems parsimonious to suggest that a larger data set might show concentration and voltage dependence here, given the concentration and voltage dependence of the DHS block in apical OHCs and in apical and basal OHCs treated with FM1-43.

DHS seemed an ideal additional candidate as it has a very different MET channel blocking profile to FM1-43, only blocking the MET current at negative membrane potentials. However, the anomalous current fractional blocking profiles of FM1-43 and DHS turned out to be similar in terms of voltage dependence, maximum block for both at -104 mV (FIGURE 6-5, 6-11). In apical OHCs, the block by DHS of the anomalous current displays the same voltage dependence as in normal OHCs, with maximum block around -104 mV (6-11, 6-12). Maximum block quoted at -84 mV in Marcotti et al. (2005) (FIGURE 6-8).

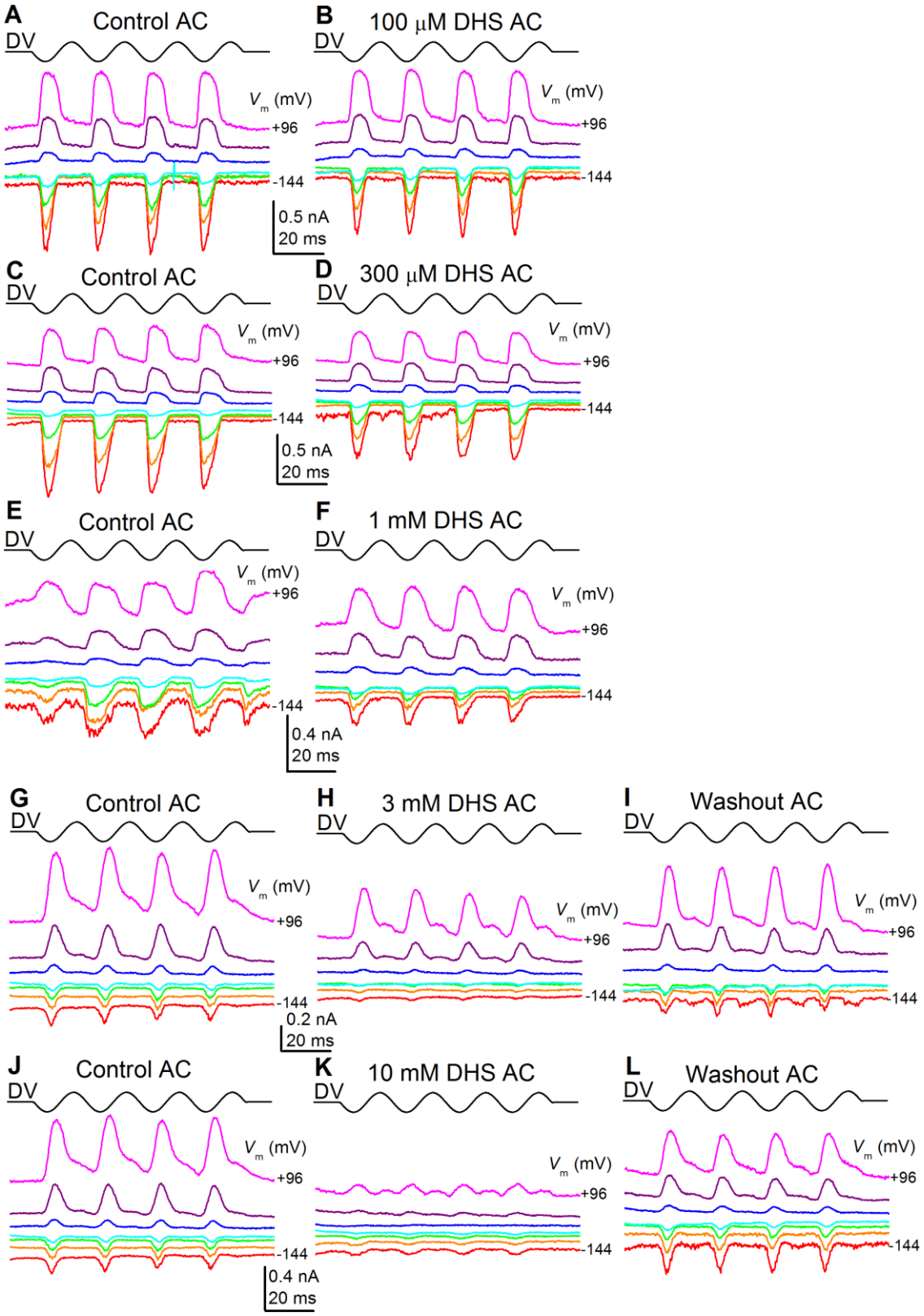
A
Control AC
DV
V_m (mV)
+96
-144
0.5 nA
20 ms
B
100 μM DHS AC
DV
V_m (mV)
+96
-144
C
Control AC
DV
V_m (mV)
+96
-144
0.5 nA
20 ms
D
300 μM DHS AC
DV
V_m (mV)
+96
-144
E
Control AC
DV
V_m (mV)
+96
-144
0.4 nA
20 ms
F
1 mM DHS AC
DV
V_m (mV)
+96
-144
G
Control AC
DV
V_m (mV)
+96
-144
0.2 nA
20 ms
H
3 mM DHS AC
DV
V_m (mV)
+96
-144
I
Washout AC
DV
V_m (mV)
+96
-144
J
Control AC
DV
V_m (mV)
+96
-144
0.4 nA
20 ms
K
10 mM DHS AC
DV
V_m (mV)
+96
-144
L
Washout AC
DV
V_m (mV)
+96
-144

FIGURE 6-7 : Block of anomalous currents in apical OHCs by different concentrations of DHS. DHS is two orders of magnitude less efficacious at blocking anomalous currents in apical OHCs compared with MET currents. A, B, C, D, E, F, G, H, I, J, K, L, anomalous currents recorded from apical OHCs from BAPTA pre-treated CD-1 P2 mice, before (A, C, E, G, J), during application of 100 µM (B) 300 µM (D), 1 mM (F), 3 mM (H) and 10 mM (K) DHS and after washout (I, L). Membrane potential stepped between -164 mV and +96 mV in 20 mV increments from a holding potential of -84 mV. Half the voltage steps used are shown for clarity. Driver voltage (45 Hz sinusoid, 40 V amplitude) plotted above the current traces.

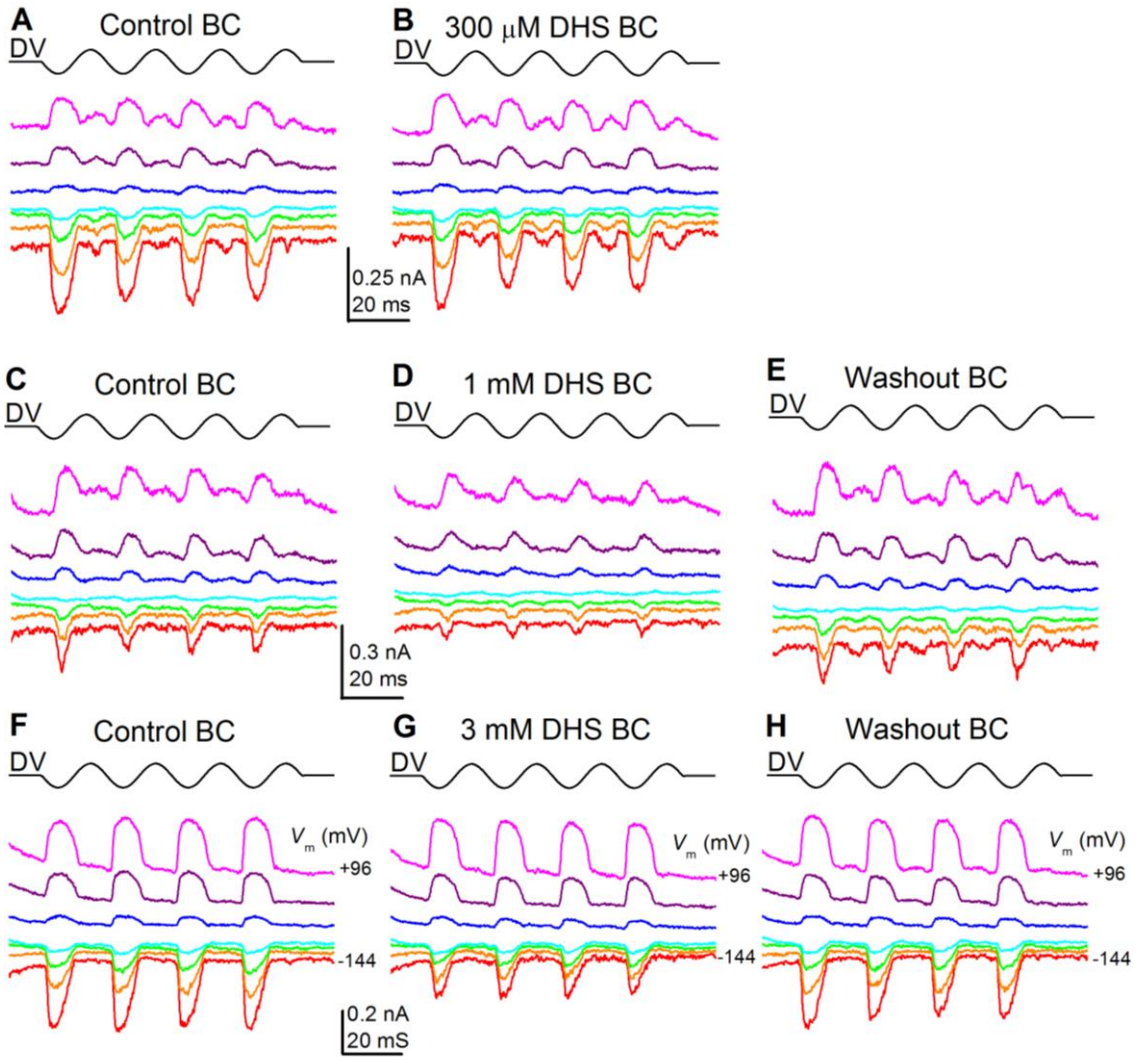
A
Control BC
DV
B
300 μM DHS BC
DV
0.25 nA
20 ms
C
Control BC
DV
D
1 mM DHS BC
DV
E
Washout BC
DV
0.3 nA
20 ms
F
Control BC
DV
G
3 mM DHS BC
DV
H
Washout BC
DV
Vm (mV)
+96
-144
0.2 nA
20 mS

FIGURE 6-8 : Block of anomalous currents in basal OHCs by different concentrations of DHS. DHS block of basal OHCs anomalous currents is two orders of magnitude less strong than that of MET currents. A, B, C, D, E, F, G, H, anomalous currents recorded from basal OHCs from BAPTA pre-treated CD-1 P2 mice, before (A, C, F), during application of 300 µM (B), 1 mM (D), 3 mM (G) DHS and after washout (E, H). Membrane potential stepped between -164 mV and +96 mV in 20 mV increments from a holding potential of -84 mV. Half the voltage steps used are shown for clarity. Driver voltage (45 Hz sinusoid, 40 V amplitude) plotted above the current traces.

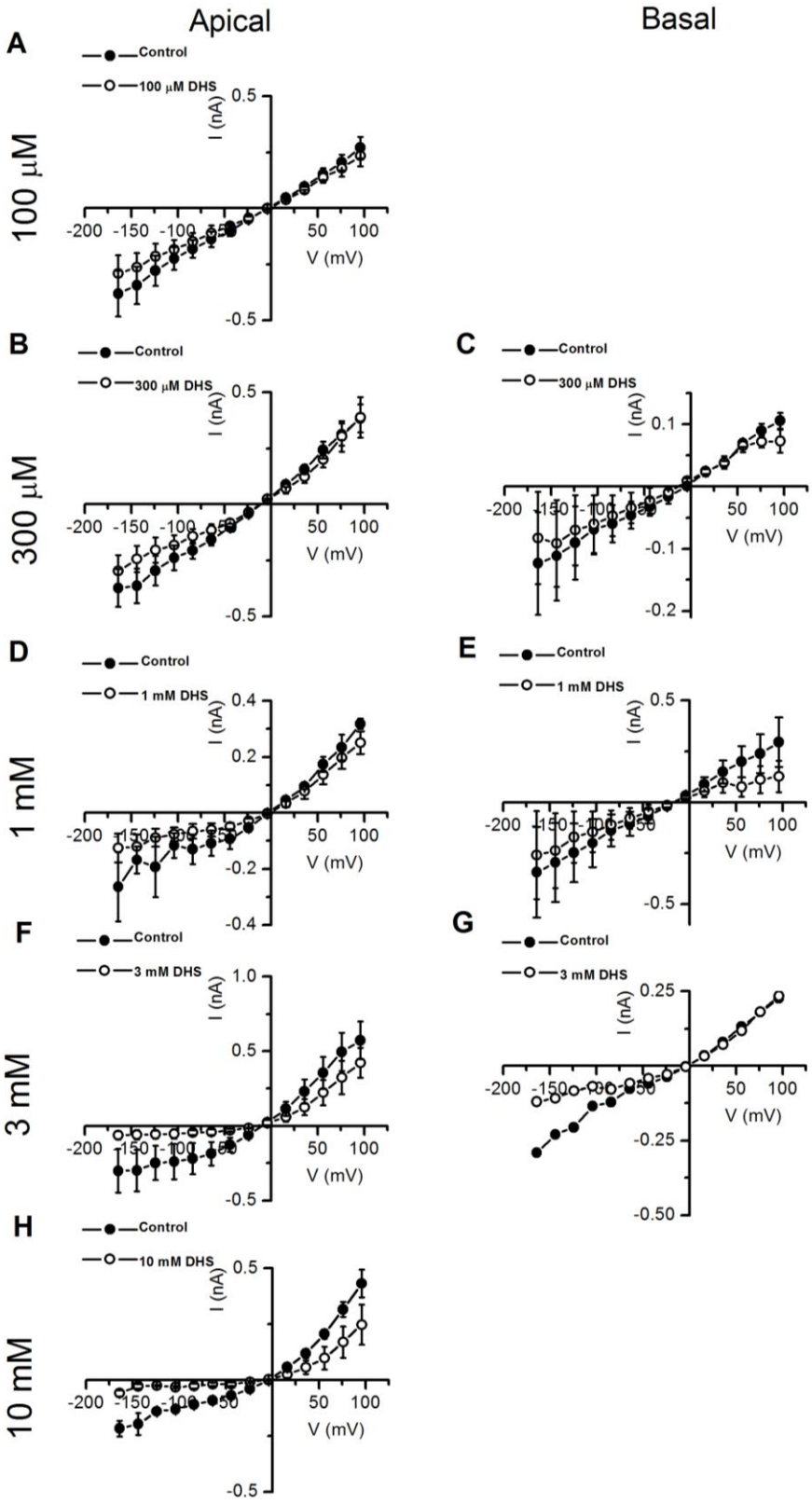
Apical
Basal
A
100 µM
Control
100 µM DHS
B
300 µM
300 µM DHS
C
D
1 mM
1 mM DHS
E
F
3 mM
3 mM DHS
G
H
10 mM
10 mM DHS
I (nA)
V (mV)

FIGURE 6-9 : DHS current-voltage curves. DHS blocks the anomalous current at negative potentials, with no evident difference between block in apical and basal OHCs. The anomalous current does not display double-rectification characteristics. A, B, C, D, E, F, G, H, Average current-voltage curves of anomalous currents from BAPTA pre-treated apical (A, B, D, F, H) and basal (C, E, G) OHCs before and during superfusion of a solution containing 100 µM (A), 300 µM (B, C), 1 mM (D, E), 3 mM (F, G) and 10 mM (H) DHS. Number of cells, apical: 100 µM (n = 4), 300 µM uM (n = 6), 1 mM (n = 2), 3 mM (n = 4), 10 mM (n = 2), basal: 300 µM (n = 4), 1 mM (n = 4), 3 mM (n = 1).

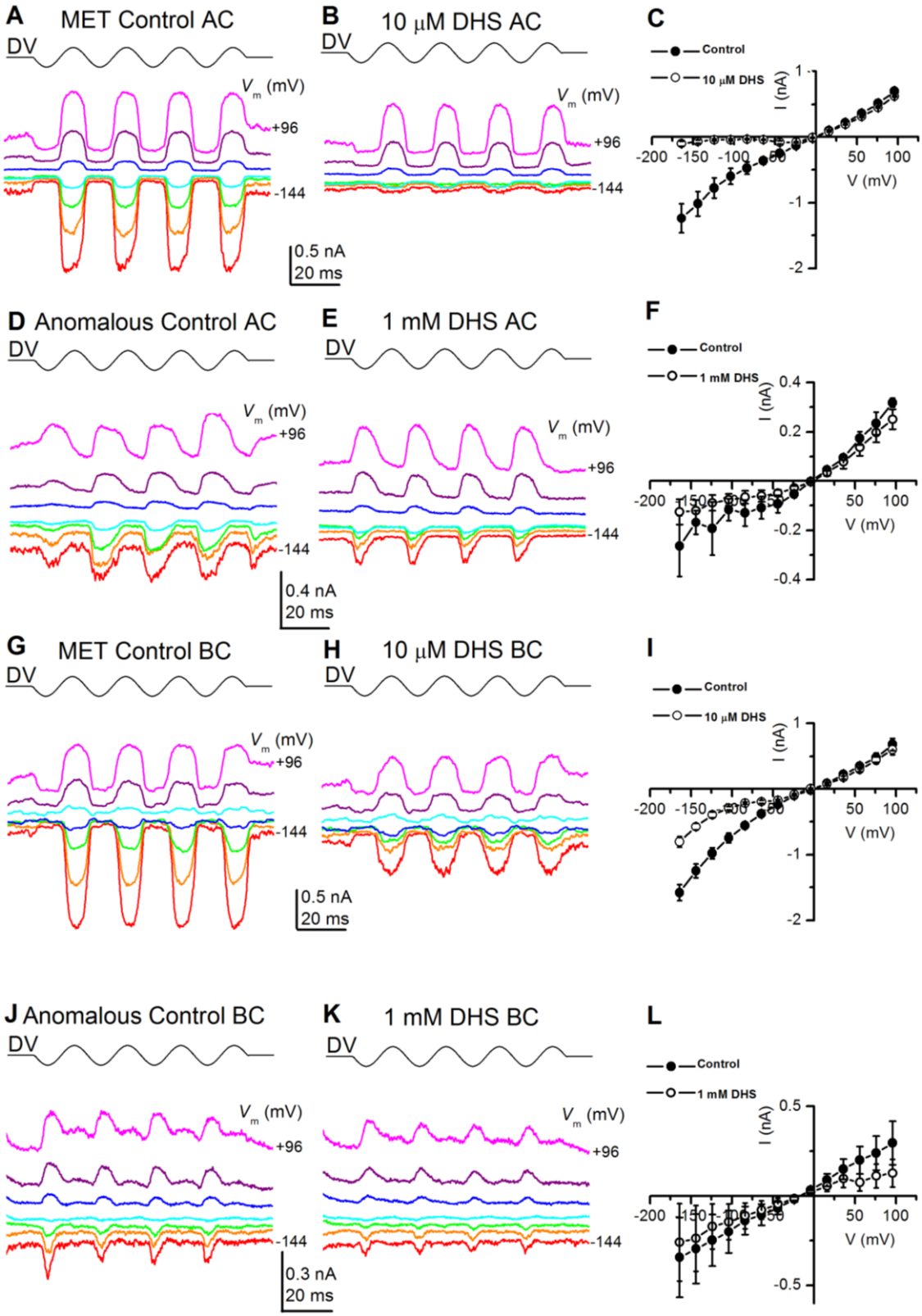
A MET Control AC
DV
V_m (mV)
+96
-144
0.5 nA
20 ms
B 10 μM DHS AC
DV
V_m (mV)
+96
-144
C
Control
10 μM DHS
I (nA)
V (mV)
D Anomalous Control AC
DV
V_m (mV)
+96
-144
0.4 nA
20 ms
E 1 mM DHS AC
DV
V_m (mV)
+96
-144
F
Control
1 mM DHS
I (nA)
V (mV)
G MET Control BC
DV
V_m (mV)
+96
-144
0.5 nA
20 ms
H 10 μM DHS BC
DV
I
Control
10 μM DHS
I (nA)
V (mV)
J Anomalous Control BC
DV
V_m (mV)
+96
-144
0.3 nA
20 ms
K 1 mM DHS BC
DV
V_m (mV)
+96
-144
L
Control
1 mM DHS
I (nA)
V (mV)

FIGURE 6-10 : DHS block of the MET current compared with the anomalous current. DHS block of anomalous currents is two orders of magnitude less strong than that of control MET currents in apical OHCs. A, B, D, E, G, H, J, K. currents recorded from P2 CD1 OHCs (D, E, J, K), before (A, G), during application of 10 µM DHS(B, H) compared with superfusion with the two orders of magnitude greater 1 mM DHS (E, K) on the anomalous current in the BAPTA pre-treated OHC, before recordings (D, J). Apical (A, B, D, E) and basal (G, H, J, K) cells illustrated. **C, F, I, L.** Average current–voltage curves of MET currents before and during superfusion with 10 µM DHS (C, I) and anomalous currents before and during superfusion with 1 mM DHS (F, L).

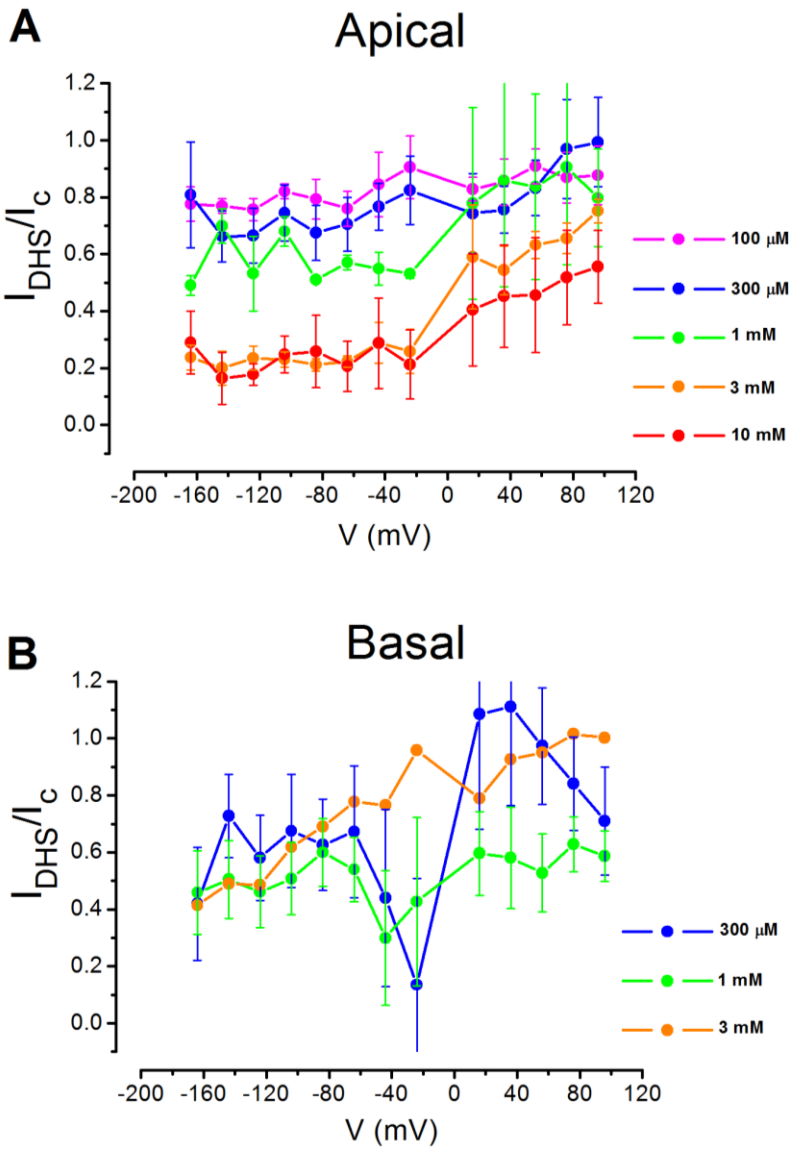

FIGURE 6-11 : **DHS fractional blocks. DHS blocks the anomalous current in a voltage dependent manner, with maximum block at -104 mV, block is not released at more negative membrane potentials than this, indicating that DHS does not act as a permeant blocker here. Fractional block of anomalous currents in BAPTA pre-treated OHCs by DHS. A, B,** Anomalous currents in the presence of 100 µM to 10 mM DHS, as a fraction of the currents in the control solution, from apical (A) and basal (B) OHCs. Numbers of cells A: 100 µM (n = 4), 300 µM (n = 6), 1 mM (n = 2), 3 mM (n = 4), 10 mM (n = 2). B: 300 µM (n = 4), 1 mM (n = 4), 3 mM (n = 1).

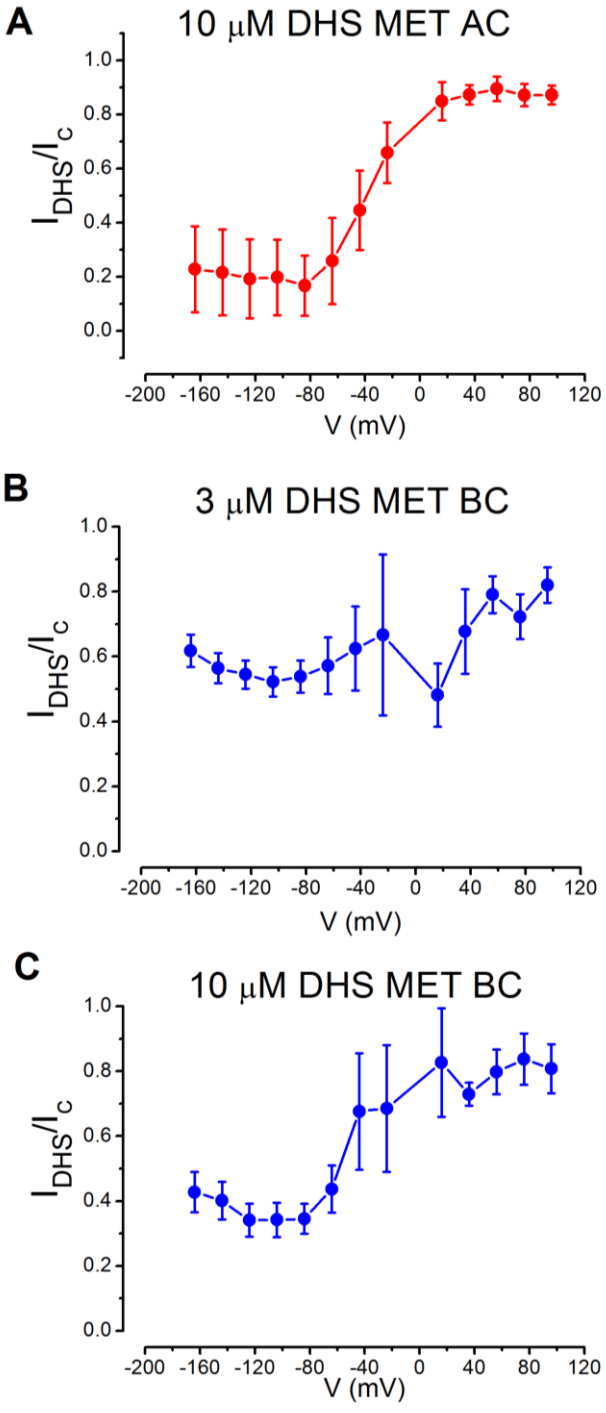

FIGURE 6-12: A, B, C, Fractional blocks by DHS of MET currents in control OHCs. 10 μM DHS treated apical (A) 3 μM DHS treated basal (B) 10 μM DHS treated basal (C) OHCs. 10 μM apical: n = 4 , 3 μM basal: n = 5, 10 μM basal: n = 6.

6.4.3 FM1-43 appears to be a permeant blocker of the protochannel, whilst DHS does not appear to permeate

Whilst the voltage dependence of FM1-43 block of the anomalous current was different to MET current block, block of the anomalous current is still reduced at extreme negative and positive potentials (FIGURE 6-5), just as for the MET current (FIGURE 6-6; Gale et al. (2001)). The release of block at extreme negative potentials, which occurs at membrane potentials which are more hyperpolarised than -104 mV, is characteristic of permeant block. This is in line with the finding by Gale et al. (2001) in myo7a^{6J} mice in which, unlike in normal OHCs, FM1-43 uptake does not occur due to the highly disorganised bundles, lack of tip links and thus lack of normal MET currents. With highly disorganised hair bundles, the hair cells of these mice just display the anomalous current, which can only be elicited by stimulation beyond the normal physiological range. The arising currents appear similar in so far that they are also elicited by inverse stimuli and have additional characteristics which appear alike, such as a peaky appearance and late onset. Gale et al. (2001) demonstrated that stimulating the myo7a^{6J} hair bundles beyond the normal physiological range allows FM1-43 to enter the hair cells. Therefore, one might hypothesise that the anomalous currents in these mice and BAPTA pre-treated CD1 mice arise from the same or similar source.

Whilst the block by DHS is voltage dependent, blocking more strongly at hyperpolarised potentials, with maximum block near -104 mV, DHS block of the anomalous current does not show clear evidence of release at extreme negative potentials in apical or basal MET channel isoforms (FIGURE 6-11). Whereas, characteristic permeant block is evident where DHS blocks the MET current (FIGURE 6-12). This suggests that, unlike for the MET channel, DHS is unable to permeate the protochannel.

6.4.4 FM1-43 blocks the anomalous and MET currents to a similar degree, whilst DHS block is two orders of magnitude less effective at blocking the anomalous current.

Gale et al. (2001) measured the K_D of FM1-43 at -4 mV, as maximum block was near 0 mV. Here, I find that the maximum block achieved is at around -104 mV therefore that is where the K_D has been measured. A previous study by Kim et al., 2013 also measured the K_D at -104 mV although they did not state why, although this was presumably because they found that the maximum block was also at this potential. A K_D of 2.88 µM in apical OHCs and in basal OHCs a K_D of 3.87 µM (FIGURE 6-13) has been calculated at -104 mV, similar to the K_D previously reported for FM1-43 of the normal MET current at -4 mV of 1.2 µM (Gale et al., 2001). In the control experiments that I conducted on normal untreated OHCs where 10 µM of FM1-43 was applied, the fraction of the current remaining in apical (FIGURE 6-10, A) at 0.36 ± 0.04 (n = 3) and very similarly 0.41 ± 0.14 in basal OHCs (n = 3) (FIGURE 6-10, B), suggesting that the K_D will be somewhat higher than previously reported Gale et al. (2001). Further experiments would be needed to generate a dose response curve in order to ascertain the actual K_D.

DHS blocks the anomalous current in apical OHCs with a K_D of 1.24 mM at a membrane potential of -104 mV and basal OHCs with a K_D of 1.04 mM at -104 mV (FIGURE 6-14), at more than 100x greater than 7 µM at -84 mV (1.3 mM Ca^{2+}) in apical OHCs previously reported (Marcotti et al., 2005) and the control experiments I conducted, the K_D in basal cells appears to be somewhere between 3 µM and 10 µM at -104 mV, whilst data from apical OHC treatment with 10 µM DHS, suggests the block in the apex may surprisingly be stronger, with a fraction of 0.17 ± 0.11 (n = 4) (FIGURE 6-12, A) compared with 0.34 ± 0.05 (n = 6) of the current remaining at -104 mV (FIGURE 6-12, C), although the standard error is quite large and thus more data is necessary to ascertain if this is the case.

6.4.5 No apical to basal gradient in channel block of the anomalous current is evident and a difference in pore properties between the normal MET channel and the protochannel is apparent

All the range of different sized anomalous currents appear to occur in hair cells along the length of the cochlea and in consonance with this there is no significant difference in the level of the block by either FM1-43 (FIGURE6-13) or DHS (FIGURE 6-14) between apical and basal OHCs. There is, however, an apparent difference between DHS block of normal OHC MET currents, with greater block of apical (0.20 ± 0.14 of the current remaining at -104 mV) than basal (0.34 ± 0.05 remaining at -104 mV) currents (FIGURE 6-12).

The DHS half blocking concentration of anomalous current is two orders of magnitude greater than of the MET current. The much lower affinity block by DHS of the anomalous current relative to the MET current again indicates a difference in pore properties of the protochannel channel. A possibility is that it lacks the highly negatively charged channel vestibule which may be important for interaction with some permeant blockers (Beurg et al., 2014b).

The n_H for apical DHS is consistently negatively cooperative ranging from 0.39-0.97 (FIGURE 6-15), whilst for MET currents treated with DHS, there is a neutral cooperativity of 1 at all potentials (Marcotti et al., 2005). DHS is also negatively cooperative with its binding sites in the basal protochannel (n_H = 0.60 in basal OHCs at -104 mV, FIGURE 6-14), unlike with the MET channel (n_H = 1, (Marcotti et al., 2005)).This is illustrative of a difference in the binding site(s) for DHS between the MET channel and the protochannel. The negative cooperativity further indicates that there are at least two binding sites for DHS in the protochannel pore.

Due to the difference in voltage dependence of the FM1-43 block of the anomalous current, compared with the normal MET current, the n_H profile is completely altered. Negative

cooperativity is evident (n_H = 0.76 at -104 mV in apical OHCs and n_H = 0.51 in basal OHCs at -104 mV, FIGURE 6-13), very different to the blocking profile of the normal MET current, where n_H is 1 at the extreme negative potentials, gradually increasing to its maximum of 2 near 0 mV, then decreasing to 1 again at more positive potentials. The negative cooperativity does however suggest that there are also at least two FM1-43 binding sites in the protochannel.

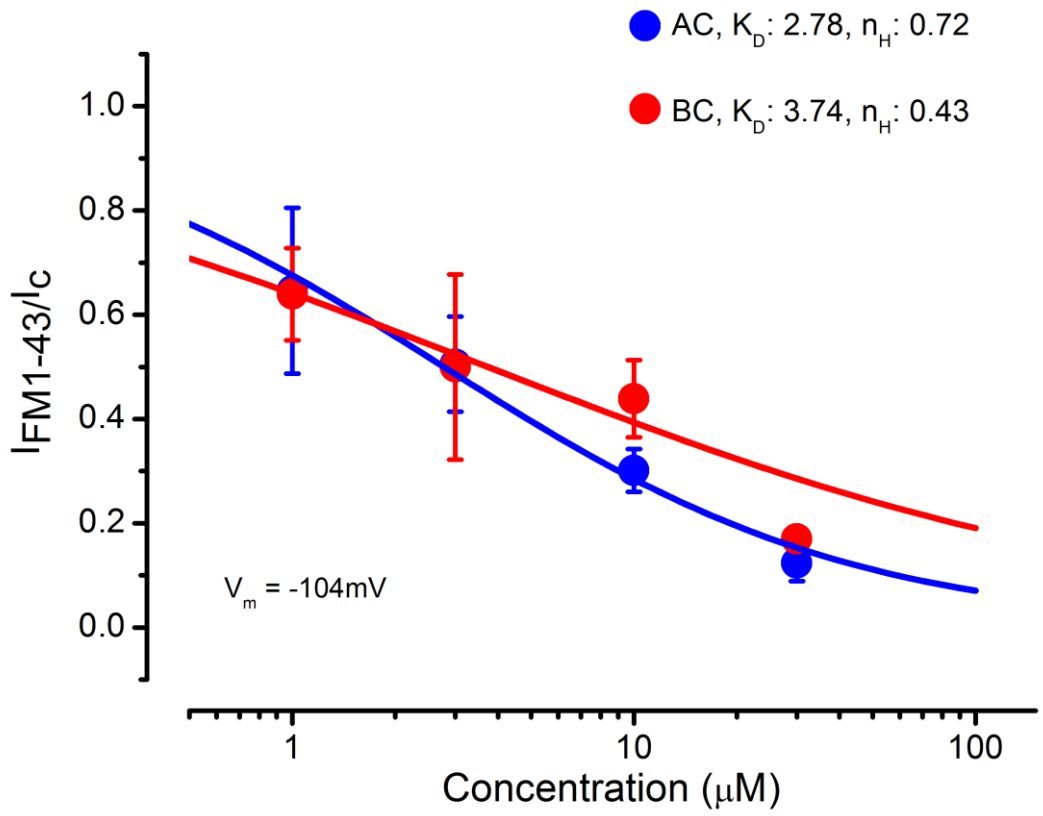

FIGURE 6-13 : **FM1-43 dose response curves. FM1-43 blocks anomalous currents in apical and basal OHCs to a similar degree.** Dose-response curves at -104 mV in BAPTA pre-treated CD-1 OHCs. FM1-43 treated apical OHCs: blue closed symbols fitted with blue continuous line to the Hill equation (1), with K_D = 2.77 µM ± 0.72 and n_H = 0.76 ± 0.16. Number of cells from left to right: 1 µM (n = 3), 3 µM (n = 3), 10 µM (n = 3), 30 µM (n = 3). FM1-43 treated basal OHCs: red closed symbols fitted with red continuous line to the Hill equation with K_D = 3.87 µM ± 1.85 and n_H = 0.51 ± 0.20. Number of cells from left to right: 1 µM (n = 6), 3 µM (n = 4), 10 µM (n = 5), 30 µM (n = 1).

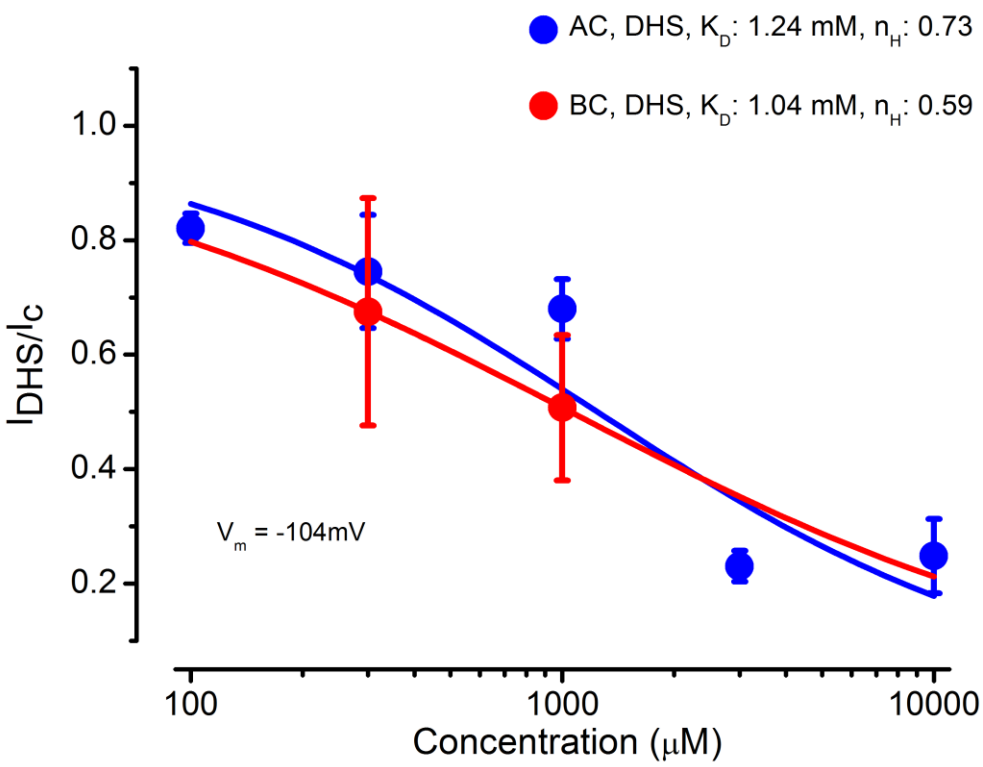

FIGURE 6-14 : **DHS dose response curves. DHS blocks anomalous currents in apical and basal OHCs to a similar degree.** Dose-response curves at -104 mV in BAPTA pre-treated CD-1 OHCs. DHS treated apical OHCs: blue closed symbols fitted with blue continuous line to the Hill equation (1), with K_D = 1.24 mM ± 0.385 and n_H = 0.73 ± 0.17. Number of cells from left to right: 100 µM (n = 4), 300 µM (n = 6), 1 mM (n = 2), 3 mM (n = 4), 10 mM (n = 2). DHS treated basal OHCs: red closed symbols fitted with red continuous line to the Hill equation with K_D = 1.04 mM ± 0.96 and n_H = 0.60 ± 0.71. Number of cells from left to right: 300 µM (n = 4), 1 mM (n = 4).

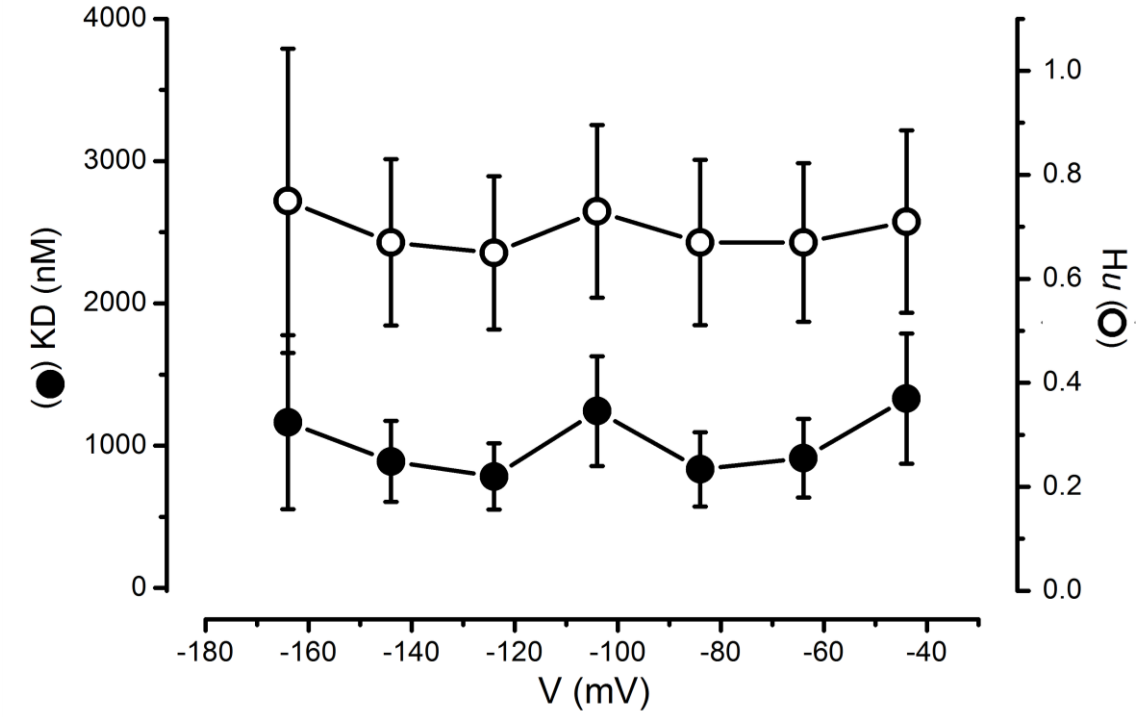

FIGURE 6-15 : Average K_D and n_H of anomalous currents from DHS treated apical OHCs plotted as a function of the membrane potential, from -164 mV to -64, including those shown in FIGURE 6-14. *Number of cells included in each dose-response curve used for obtaining the* **K_Ds and n_Hs**: 100 µM (n = 4), 300 µM (n = 6), 1 mM (n = 2), 3 mM (n = 4), 10 mM (n = 2).

6.4.6 The anomalous current can be elicited in normal OHCs

The anomalous current and MET current can sometimes be elicited and recorded at the same time (Marcotti et al., 2014). The MET and anomalous currents can be concurrently elicited during different phases of the same sine wave stimulus in the same cell and both currents simultaneously blocked by FM1-43 (FIGURE 6-16). In agreement with previous data obtained by Kim et al. (2013) and the other data presented here, FM1-43 blocks both to a similar degree, with 0.45 of the anomalous current remaining at -104 mV and 0.2 of the MET current remaining at -24 mV (the nearest potential to -4 mV (Gale et al., 2001) that it was possible to measure in my experiments due to noise) (n = 1, FIGURE 6-8), although, as previously mentioned, maximum block was at different membrane potentials for the two currents (FIGURE 6-10). It is also possible to elicit only the anomalous current without intending to in normal cells which have not been pre-treated with BAPTA (FIGURE 6-17), although this is anecdotal evidence from a single cell.

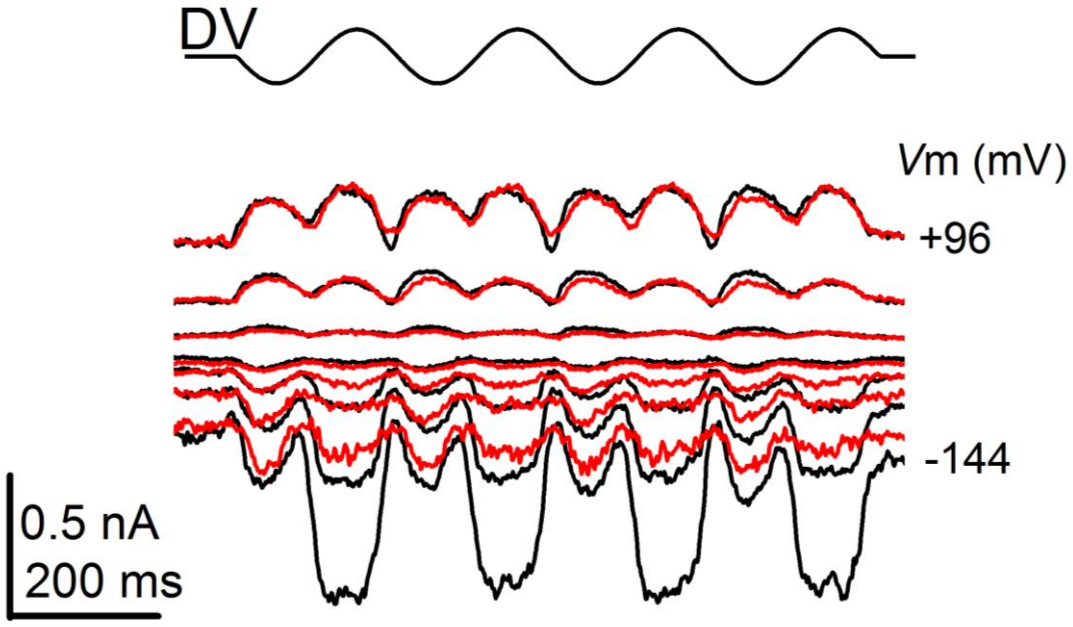

FIGURE 6-16 : **The Anomalous current and MET current in same trace blocked by FM1-43. The MET and anomalous currents can be concurrently elicited during different phases of the same sine wave stimulus in the same cell.** The MET current and the anomalous current being alternatingly elicited by a 45 Hz sinusoidal force stimulus, before (black trace) and during (red trace) the superfusion of 10 µM FM1-43.

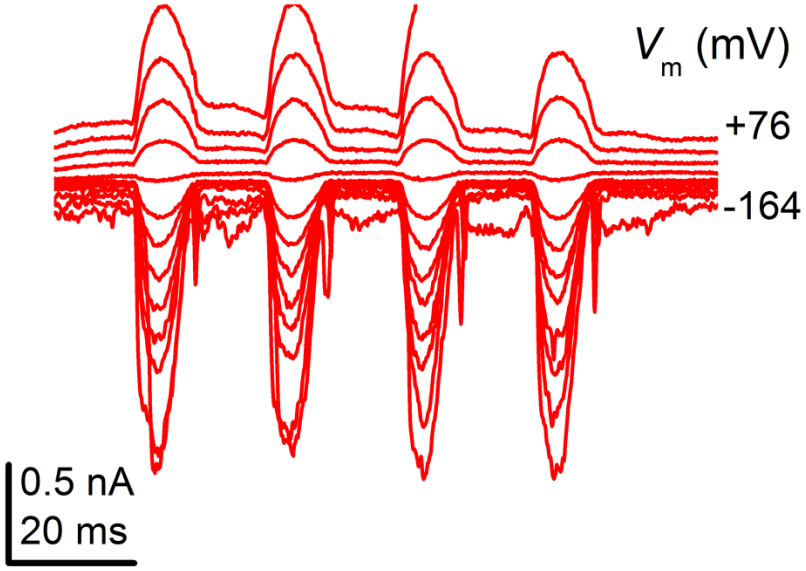

FIGURE 6-17 : The anomalous in normal OHCs. The anomalous current alone was elicited in untreated, undamaged TRPC 1/3/6 triple knockout mouse OHC, without explicitly intending to. The OHCs otherwise had normal MET currents. This recording provides anecdotal evidence. Note the seal was lost during the voltage step to +76 mV.

6.5 Discussion

6.5.1 Does eliciting the anomalous mechanosensitive current require a different kind of stimulation?

It is apparent from my experience in conducting these experiments that after BAPTA pretreatment, in order to elicit the maximal anomalous current, it is necessary to put the fluid jet nearer to the bundle than normal, getting closer to the apical surface. Using a larger fluid jet with a larger diameter (~14 μm) also aids in this. Eliciting anomalous currents in homozygous myo7a^{6J} mutants requires stimulation such as this, which is so great that it is beyond the normal MET operating range (Kros et al., 2002). However, these observations are somewhat incongruent with the fact that in untreated CD-1 mice the anomalous current can sometimes appear as if without specific experimental intention, so that it is possible to elicit the normal MET current and the anomalous current with alternating phases of the same sine wave stimulus. It is also, more rarely possible to elicit the anomalous current alone, without intending to (FIGURE 6-17).

6.5.2 FM1-43 and DHS block the anomalous current differently to the MET current

There are several distinctions between FM1-43 and DHS block of the anomalous current when compared with the MET current. Firstly, no apical to basal gradient in anomalous current block is evident for DHS, where DHS blocks the MET current of apical OHCs more strongly than basal OHCs. Whilst the K_D for FM1-43 is similar in both the anomalous and the normal MET current, the block has altered voltage dependence, with maximum block at -104 mV instead of -4 mV as reported by Gale et al., (2001). DHS blocks the anomalous current two orders of magnitude

less strongly than the MET current. Its voltages dependence is also shifted, such that the block is not released at extreme negative potentials, indicating that DHS is unable to permeate the protochannel. Additionally, there is evident negative cooperativity of DHS that differs from the neutral cooperativity ($n_H = 1$) that it has with its MET channel binding site(s). Whilst that Hill coefficient of 1 may indicate one binding site as previously mentioned, this does not negate the possibility of more than one binding site. The negative cooperativity may indicate that DHS has more than one available binding site in the protochannel, with both binding sites either having different DHS affinities or the binding of one molecule of DHS impeding the binding of additional molecules of DHS. FM1-43 is also negatively cooperative with its binding site, very different from its normal profile of positive cooperativity at intermediate potentials ($n_H = 2$) and neutral cooperativity at extreme positive and negative potentials ($n_H = 1$) (Gale et al., 2001).

Of additional interest is the fact that the control experiments on MET currents revealed that DHS appears to block currents in apical OHCs more strongly than in basal OHCs. As DHS appears to bind deep inside the vestibule, near the narrow part of the channel pore (Marcotti et al., 2005), this may represent some degree of difference in the pores of apical and basal MET channels, in addition to differences in the size of the inside of the channel and any difference in vestibule isoforms. With the other compounds I have tested, where there has been a gradient in channel block, the strongest block has always been in basal OHCs. DHS block however is stronger in apical OHC MET channels. Results have previously been obtained showing the same pattern of stronger block in apical OHCs treated with the water-soluble peptide toxin GsMTx-4 (Beurg et al., 2014b).

6.5.3 Potential theories about the nature of the anomalous current and the associated channel

A study which may offer an example of an analogous channel construction to that responsible for the anomalous current, but in a different system, was conducted on BK K+ channels by Zhang et al. (2006). The BK channel is formed of a transmembrane domain, four voltage sensing subunits, a pore domain which conducts K^+ ions and a gating ring at the entrance of the inner vestibule, formed of eight negatively charged residues (FIGURE 6-18). The gating ring appears akin to MET channel vestibule. The removal of this gating ring decreases block by Mg^{2+} and the polyamine spermine and decreased inward rectification (Zhang et al., 2006). This is similar to the concept of removal of the vestibule resulting in a protochannel with altered DHS affinity and no apparent rectification of the anomalous current.

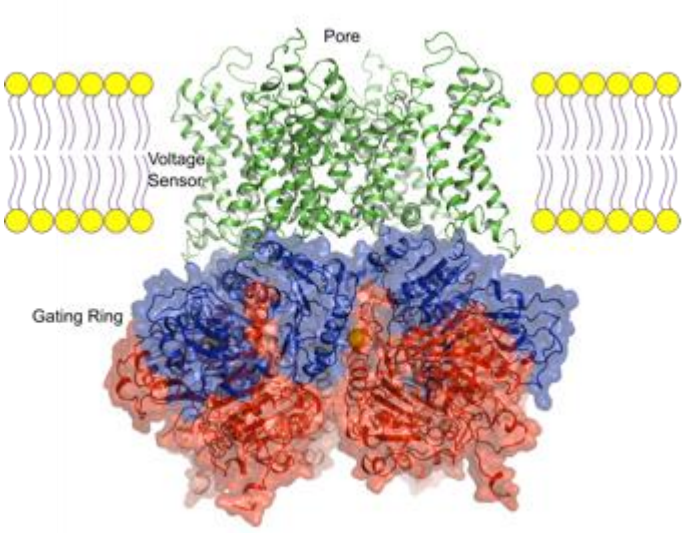

Yuan, P. & Mackinnon, R. The Rockefeller University.

from http://lab.rockefeller.edu/mackinnon/members/PengYuan (retrieved 05/06/15)

FIGURE 6-18 Model of the BK channel

More recently Budelli et al. (2013) also studied the the Slo1 (BK) channel, using different Slo1 channel constructs to attempt to see how the channel would function with and without the gating ring. Budelli et al. (2013) found that removing the 827 amino acid gating ring from the BK channel and replacing it with a short 11 amino acid tail resulted in decrease in single channel conductance of about 30% and although the channel was still voltage activated, the Ca^{2+} and Mg^{2+}-dependent gating was gone. They noted that BK channels without a gating ring have a right shifted voltage conductance relationship, indicating that more voltage is required to open the channel in the absence of the gating ring, presumably to replace the passive opening force that was applied by the gating ring before it was removed. This is again akin to the altered voltage dependence of the FM1-43 block of the protochannel.

Interestingly, as the channel model by Yuan, P. illustrates (FIGURE 6-18), the gating ring of the BK channel is a cytoplasmic domain, which is not embedded in the phospholipid bilayer which may be a good basis for envisaging a MET channel which resides, at least partially, in the extracellular space. As has been represented in diagrams of models presented previously, the narrow pore region is embedded in the phospholipid bilayer whilst the vestibule containing region may not be (Beurg et al., 2014b).

In my anecdotal experience, having attempted to elicit anomalous currents in untreated CD1 mice, pressing down with the fluid jet on the apical surface of the hair cell does not actually appear to work. Nor does more forceful stimulation generated by placing the fluid jet closer to the hair bundle. However, the anomalous current does appear to be evident in some recordings where there is no intention to elicit it.

In the vast majority of instances of anomalous current occurrence, there is no evidence of normal MET current and the tip links are almost entirely obliterated. For LHFPL5 -/- around 65% of tip links are absent and as a result one can elicit the anomalous current with inverse polarity stimuli. Interestingly the normal MET current can also be elicited, with the normal sine

wave stimulus pattern (Marcotti et al., 2014; Beurg et al., 2014). One would infer potential correlation between tip link damage and anomalous current appearance, however, what seems somewhat incongruent is the fact that TMC1 and TMC2 double mutant mice have intact tip links, yet only possess the anomalous current. Only normal MET currents could be recorded in the TMC1 -/-, TMC2 +/- and TMC1 +/-, TMC2 -/- mice (Kim et al., 2013), the currents in the latter potentially being somewhat smaller than normal.

Knocking out any part of the MET machinery components that are known of and have subsequently been tested results in hair bundle stimulation which generates anomalous currents, therefore it seems likely that the other instances of anomalous current occurrence arise because the elements removed are part of the MET complex. TMC1 and TMC2 may indeed form some part of the channel, whether that is the vestibule or the narrow part of the channel pore, although the latter seems less likely. The anomalous current could either be the result of relocation and reorganisation of the proteins to a location where they are opened by inverse stimuli or the unmasking of a distinct population of mechanosensitive protochannels.

DHS may be less attracted into the channel, when the highly electronegative vestibule is not present, as has been suggested (Beurg et al., 2014b). They postulate that the nature of the DHS molecule is the reason that they find DHS blocks the TMC double knockout channel less well, stating that it may lack an external vestibule which would draw the polycationic DHS into the channel.

6.6 Conclusions

The anomalous current has clearly distinct features from the MET current. The anomalous current is elicited by stimuli of inverse polarity in the majority of recordings. There is little or no resting current evident in any traces at any membrane potentials. Although strong "adaptation" of the current is evident (FIGURE 6-1, 6-2, 6-3, 6-4), unlike for the MET current, this does not appear to depend upon Ca^{2+} as Marcotti et al. (2014) illustrated as they were able to elicit the strongly adapting anomalous current whilst the hair cells were bathing in a solution containing BAPTA, meaning there was no Ca^{2+} block. As Marcotti et al. (2014) also found there the anomalous current lacks the double rectification of the MET current.

Both the FM1-43 and DHS data suggest a distinct lack of the normal apical to basal channel property gradient for the protochannel. DHS additionally illustrates the difference in characteristics between the MET and the anomalous channel, blocking the latter 100x less well.

As previously mentioned, Kurima et al. (2015) have found that TMC1-mCherry and TMC2-AcGFP puncta remain localised, albeit very sparsely, along the length of mature stereocilia, which they suggest may represent a reserve pool of channels. Where tip links are missing or broken, this reserve pool of protochannels may be mobilised, re-locating to the previous MET channel location or near it, thus also being activated by stereociliary motion. Without the tip links to create cohesive motion, however, greater force is required in order to open the channels and the activation kinetics are slower. This may also explain the erratic nature of the currents in terms of their appearance and size. Whilst perhaps this seems at odds with the fact that the anomalous current can be elicited in double mutant TMC1 and TMC2 mice, it may be the case that since all MET channel components seem to be required for normal MET, where TMC1 and TMC2 are absent a protochannel composed of the other

remaining components is formed at or near the correct MET channel position. Furthermore, although tip links are still intact the protochannel would in that scenario not be tethered or otherwise gated by them, therefore their ablation would have no effect (Kim et al., 2013).

Alternatively, the observation that stronger stimulation is needed to activate the anomalous current could indicate that the channel is located on the apical surface of the hair cells and thus exerting pressure on the apical surface elicits it. However, in my experience, having attempted to elicit anomalous currents in normal untreated OHCs this method does not.

The control data presented for DHS in itself interesting, as it is the first compound we have found that appears to block apical MET channels with a higher binding affinity than basal cells, although further experimentation is required to confirm this finding.

6.7 Future experiments

As presented in Chapter 4, the peptide data lead us to the conclusion that D-TAT binds further into the channel's electrical field near the narrow part of the channel pore. Whereas, the data which illustrates the apparent apical to basal gradient in D-JNKi1 binding combined with the distinct energy profiles for apical and basal D-JNKi1, leads us to the conclusion that D-JNKi1 binds in the highly electronegative vestibule nearer the extracellular side of the channel. This may indicate that this MET channel component may be one which varies from the apex to the base of the cochlea in either its size or the quantity of negatively charged residues within it.

If we take the view that the anomalous current represents a reserve pool of protochannels which are lacking the highly negatively charged vestibule, then we would expect D-JNKi1 to block the anomalous current less effectively than D-TAT. This is because, whilst they both bind in the vestibule, the binding of D-JNKi1 appears more reliant on the concentrated negatively

charged residues in the centre of the vestibule, whereas D-TAT binds nearer the narrow region of the channel pore which may still form part of the protochannel. Therefore, testing the blocking potential of these compounds on the anomalous current may be useful, as the removal of the vestibule may have a greater influence on the binding affinity of D-TAT compared with D-JNKi1. However, the lack of the vestibule may still reduce the affinity of D-TAT block at least somewhat. The DHS data lends weight to this idea, as it is suggested that in the normal MET channel, DHS binds in the vestibule but nearer the narrow part of the channel pore (Marcotti et al., 2014) and additionally has a less great affinity for the protochannel. When binding in the protochannel, where the vestibule is absent, binding may effectively occur in the only remaining part of the channel, the narrow part of the channel pore, as this may be all that the protochannel is comprised from. This is near to where binding in the normal MET channel occurs, but yet further towards the intracellular side of the channel. Affinity would thus be reduced due to the presence of only a small number of positively charged residues residing in the narrow part of the channel pore, which may form the protochannel. This would explain why DHS block of the anomalous current is less great but the affinity for the smaller FM1-43 molecule is relatively unaffected.

It would be interesting to see if Texas Red conjugated compounds, which are very large yet permeate through the MET channel pore, are also able to permeate through the anomalous channel pore.

7 MECHANO-ELECTRICAL TRANSDUCTION IN TRPC 3/6, 1/3/6 AND 1/3/5/6 KNOCKOUT MICE IS NORMAL

7.1 TRP channels

Transient receptor potential (TRP) channels are tetrameric channels formed of six transmembrane domain proteins. The majority of TRP superfamily channel types are either characterised as calcium selective (O'Neil and Heller, 2005) or nonselective cation channels, permeable to Ca^{2+}, K^{+} and Na^{+}, with some types being having permeability to other ions such as Mg^{2+} (Nadler et al., 2001; Monteilh-Zoller et al., 2003), TRPM4 whilst activated by Ca^{2+}, is impermeable to it (Launay et al., 2002). There are many categories of TRP proteins based on the alignments of their amino acid sequences which include TRPV, TRPM, TRPP and TRPC (Bon and Beech, 2013). Many TRP members have been hypothesised to be MET channel candidates due to some members being mechanically activated (Venkatachalam and Montell, 2007).

TRP channels have been of interest in terms of their role in MET. TRPA1 channels are activated by pungent compounds such as AITC and facilitate mechanosensation in Drosophila (Walker et al., 2000) and zebrafish (Sidi et al., 2003). They were previously thought to be a candidate channel in the search for the MET channel as inhibiting TRPA1 protein expression in mice appeared to affect MET (Corey et al., 2004). In spite of this they have now been eliminated as TRPA1 knock-out mice show normal MET and hearing (Kwan et al., 2006). Additionally, application of TRPA1 activating pungent compounds does not alter MET (Kwan et al., 2006).

7.1.1 TRPC channels

TRPC1, TRPC2, TRPC3, TRPC4, TRPC5, TRPC6 and TRPC7 are all expressed in the mammalian genome, however in humans TRPC2 is not expressed as the human form of this protein is a pseudogene (Wes et al., 1995; Venkatachalam and Montell, 2007). TRPC1 and TRPC5 are expressed in sensory ganglia (Elg et al., 2007), as are TRPC3 and TRPC6 which are also expressed in cochlear hair cells (Quick et al., 2012). There are two subgroups; the first is

formed of TRPC1, TRPC4 and TRPC5. The second is formed of TRPC3, TRPC6 and TRPC7 (Bon and Beech, 2013). Ca^2+ is a common modulator of both these subgroups (Hui et al., 2006).

As with other TRPC channels, the difficulty with identifying the TRPC channels that may potentially form part of the MET complex is that there are multiple TRPC isoforms. These multiple monomers, in a multitude of possible combinations, form heteromers to create ion channels. TRPC channels are particularly prolific forming heteromers with other TRPC channels as well as TRPV2, TRPV4 and Orai1 Ca^2+ channels (Ma et al., 2010, Beech, 2012). This introduces a level of redundancy where knocking out one or more TRPC channels can be compensated for by replacement with other TRPC monomers to form heteromers.

7.1.2 TRPC 3 and 6 channels

Having found expression of TRPC3 and TRPC6 in cochlear hair cells, a recent publication (Quick et al., 2012) suggested that knocking out TRPC3 and TRPC6 channels had a detrimental effect on hearing in mice. TRPC DKO mice appeared to have a degree of hearing loss, assessed by exposure to high-intensity (around 20 kHz at 90 dB) sound and subsequent Preyer reflex response. Whilst single knockouts showed a normal Preyer reflex (startle response in to auditory stimuli), the DKOs did not. Vestibular deficits were also apparent from trunk curl and swim test data. Moreover, they showed that the basal OHC MET channels of double knock-out TRPC3/TRPC6 mice exhibited MET currents of drastically reduced magnitude compared with wild-type controls. The results reported suggested that whilst MET currents in apical OHCs remained intact in terms of their size, those in basal OHCs only reached 20-25% of control mice (Quick et al., 2012). It was postulated that they may have a role in the control of intracellular levels of Ca^{2+} in OHCs. Single knock-outs of either of these channels did not result any alteration in behavioural phenotype, however knocking out both of these channels caused hearing deficits. Auditory brain stem responses were utilised, which are measurements of auditory evoked potentials in the brain taken using electrodes attached, in this case, to the

vertex between the ears and the mastoid behind the ears of the mice. The ABRs were recorded from 4 – 12 week old mice. The required threshold (in dB) to elicit a response at a given frequency was determined by auditory tone pip stimuli and recordings were made at 8, 24, 32 and 45 kHz. The results showed elevated response thresholds in DKO animals compared to wild-types (Quick et al., 2012) and later unpublished data shows significantly higher response thresholds in quadruple TRPC 1/3/5/6 knockout mice, when compared with WT and double TRPC 3/6 knockout animals.

The data published by Sexton et al. (2016) on TRPC quadruple TRPC 1/3/5/6 knockout mice showed deficits in light touch sensitivity in both TRPC 3/6 DKO and 1/3/5/6 QKO animals, when withdrawal reaction was tested with von Frey hairs and dynamic cotton swab application. Whilst deficits in the former tests were of equal magnitude for both DKO and QKO animals, an additional deficiency was noted for QKO relative to DKO animals were the latter stimuli was concerned. They also investigated the potential for involvement of TRPC channels in transduction of noxious heat, based on responses to noxious heat stimuli, however no evident impairment was found. Behavioural tests have unveiled some level of impairment in the auditory and vestibular function of TRPC DKO and QKO knockout mice. The trunk curl test, a rudimentary measure of vestibular function, demonstrated some potential deficits in vestibular function in QKO mice.

7.2 Results

Following from the tests on double knock-out (TRPC3, TRPC6, DKO) mice conducted by Quick et al. (2012) triple knock-out (TRPC1, TRPC3, TRPC6, TKO) and quadruple knock-out (TRPC1, TRPC3, TRPC5, TRPC6, QKO) mice were created and tested. I conducted the same set of whole-cell patch clamp electrophysiology experiments on DKO, TKO and QKO mice. Interestingly, unlike previous findings Quick et al. (2012) suggest, basal OHCs in TRPC DKO (FIGURE 7-1 C)

mice produce MET currents within the range seen in WT mice (FIGURE 7-1 A, B). There is in fact no deficit in MET in these mice. The basal (FIGURE 7-2 B) OHCs of TRPC TKO mice also exhibit MET currents of comparable size to those witnessed in wild-type mice (FIGURE 7-2 A). Furthermore, one would expect a difference in size between MET currents exhibited by apical and basal OHCs to be apparent (FIGURE 3-2; Kim and Fettiplace, 2013). The MET currents of apical (FIGURE 7-3 C) and basal (FIGURE 7-3 D) OHCs in the QKO mice are within the range of WT MET current (FIGURE 7-3 A, B), however, unlike in the WT controls, the currents in apical and basal OHCs are the same size (FIGURE 7-3 E). Recordings should be made from apical TRPC DKO and TKO OHCs in order to see if there is also a lack of gradient in these mice. Moreover, a greater number of recordings from TRPC QKO apical and basal OHCs will also be necessary to establish if this is in fact a robust trend.

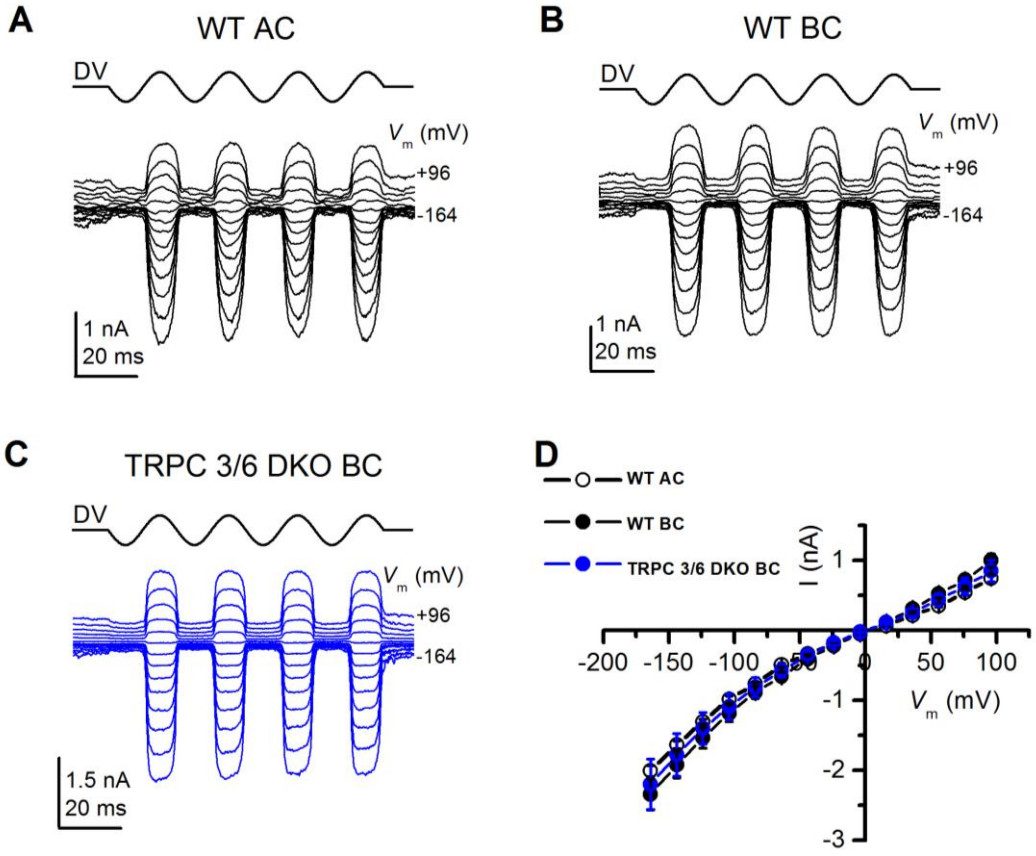

FIGURE 7-1 : TRPC 3/6 DKO. MET in WT (C57/SV129) and TRPC3/TRPC6 double knockout (DKO) OHCs. A, B, C, MET currents in response to 45 Hz sinusoidal force stimuli from a fluid jet in C57/SV129 control (A, B) and TRPC3/TRPC6 (C) OHCs. The holding potential was -84 mV and the membrane potential was stepped in 20 mV increments from -164 mV to +96 mV. Driver voltage (DV, amplitude 40 V) waveform to the fluid jet is shown above the current traces. Positive DV moves the hair bundles in the excitatory direction towards the kinocilium. C57/SV129 control OHC, mid-apical coil, P2 + 1 (A). C57/SV129 WT OHC, mid-basal coil, P2 + 2 (B). TRPC3/TRPC6 DKO OHC, mid-basal coil, P2 + 2 (C). **D**, Current-voltage curves averaged from 5 C57/SV129 WT OHCs from the mid-apical coil (black open circles), 4 C57/SV129 WT OHCs from the mid-basal coil (black closed circles), 3 mid-basal coil TRPC3/TRPC6 DKO OHCs (blue circles).

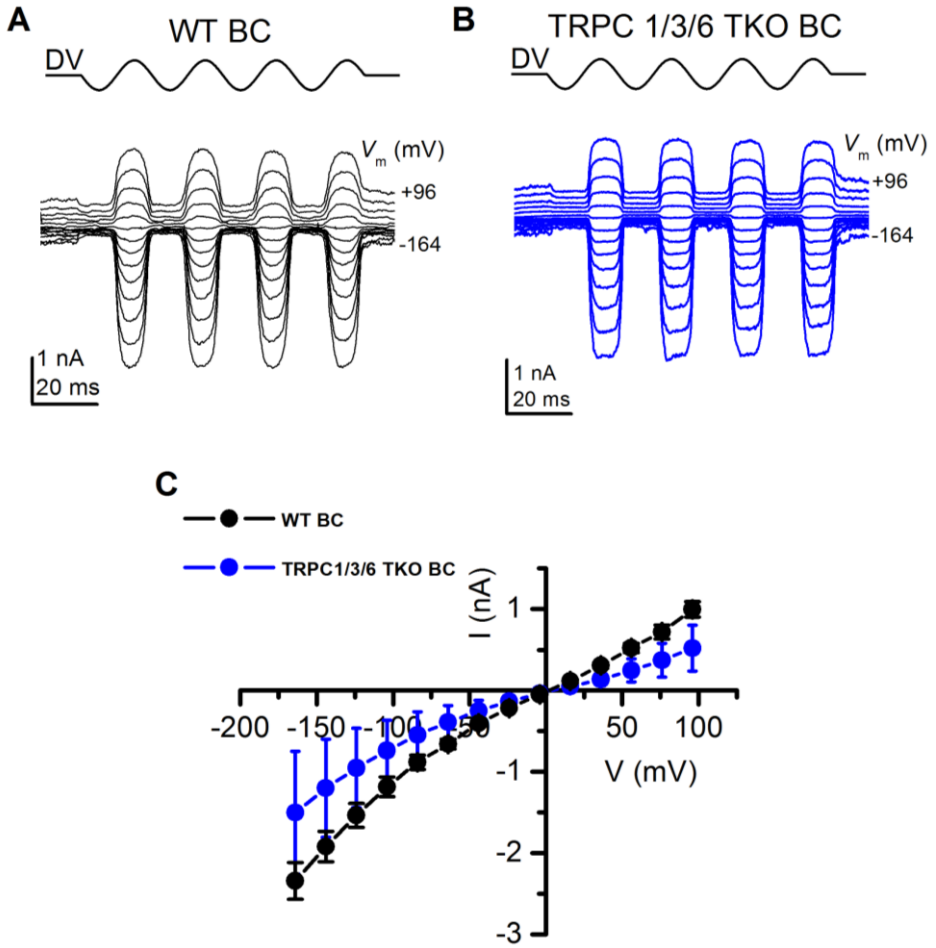

FIGURE 7-2 : TRPC 1/3/6 TKO. MET in WT (C57/SV129) OHCs and TRPC1/TRPC3/TRPC6 triple knockout (TKO) OHCs. A, B, MET currents induced by a 45 Hz sinusoidal force stimuli from a fluid jet in C57/SV129 WT (A) and TRPC1/TRPC3/TRPC6 OHCs (B). The holding potential was -84 mV and the membrane potential was stepped in 20 mV increments from -164 mV to +96 mV. Driver voltage (DV, amplitude 40 V) waveform to the fluid jet is shown above the current traces. Positive DV moves the hair bundles towards the kinocilium. C57/SV129 WT OHC, mid-basal coil, P2 + 2 (A). TRPC3/TRPC6 TKO OHC, mid-basal coil P2 + 2 (B). **C**, Current-voltage curves averaged from 4 C57/SV129 WT OHCs from the basal coil (black circles), 4 TRPC1/TRPC3/TRPC6 OHCs from the basal coil (blue circles).

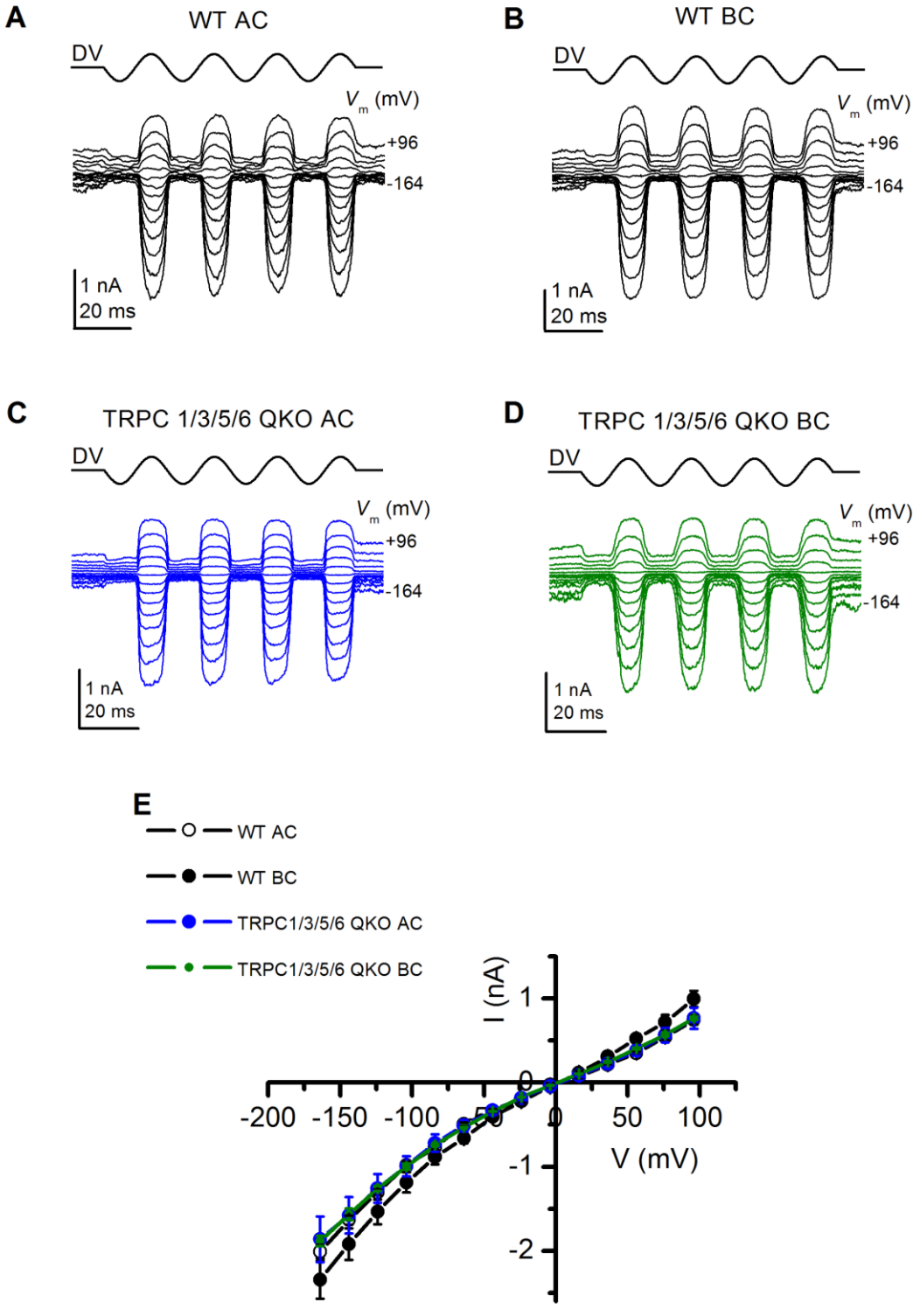
A
WT AC
DV
V_m (mV)
+96
-164
1 nA
20 ms
B
WT BC
DV
V_m (mV)
+96
-164
1 nA
20 ms
C
TRPC 1/3/5/6 QKO AC
DV
V_m (mV)
+96
-164
1 nA
20 ms
D
TRPC 1/3/5/6 QKO BC
DV
V_m (mV)
+96
-164
1 nA
20 ms
E
WT AC
WT BC
TRPC1/3/5/6 QKO AC
TRPC1/3/5/6 QKO BC
I (nA)
1
0
-1
-2
-200
-150
-100
-50
0
50
100
V (mV)

FIGURE 7-3 : TRPC 1/3/5/6 QKO. MET in C57/SV129 WT and TRPC1/TRPC3/TRPC5/TRPC6 quadruple knock-out (QKO) OHCs. A, B, C, D, MET currents in response to 45 Hz sinusoidal force stimuli from a fluid jet in CD-1 (A, B) and TRPC1/3/5/6 (C, D) OHCs. The holding potential was -84 mV and the membrane potential was stepped in 20 mV increments from -164 mV to +96 mV. Driver voltage (DV, amplitude 40 V) waveform to the fluid jet is shown above the current traces. Positive DV moves the hair bundles in the excitatory direction towards the kinocilium. C57/SV129 WT OHC, mid-apical coil, P2 + 1 (A). C57/SV129 WT OHC, mid-basal coil, P2 + 2 (B). TRPC3/TRPC6/TRPC5/TRPC6 QKO OHC, mid-apical coil, P2 + 1 (C), TRPC1/TRPC3/TRPC5/TRPC6 QKO OHC, mid-basal coil, P2 + 2 (D). **E**, Current-voltage curves averaged from 5 C57/SV129 OHCs from the apical coil (black open circles), 4 C57/SV129 OHCs from the basal coil (black closed circles), 2 apical-coil TRPC1/3/5/6 QKO OHCs (blue open circles), 3 basal-coil TRPC1/3/5/6 QKO OHCs (small blue circles).

	Average apical current size (pA)	Average basal current size (pA)
WT control (C57/SV129)	-983 ± 47	-1185 ± 121
DKO	N/A	-1091 ± 187
TKO	N/A	-738 ± 373
QKO	-994 ± 120	-997 ± 37

TABLE 5 - TRPC 3/6 DKO, TRPC 1/3/6 and TRPC 1/3/5/6 knockout mice MET currents

A comparison of currents in control, double knockout (DKO) TRPC 3/6, triple knockout (TKO) TRPC 1/3/6 and quadruple knockout (QKO) TRPC 1/3/5/6 mice. Mean MET current sizes averaged ± S.E.M. from C57/SV129 apical OHCs (n = 5), C57/SV129 basal OHCs (n = 4), TRPC 3/6 DKO basal OHCs (n = 3), 4 TRPC1/TRPC3/TRPC6 TKO basal OHCs (n = 4), TRPC 1/3/5/6 QKO apical OHCs (n = 2) and TRPC 1/3/5/6 QKO basal OHCs (n = 3).

7.3 Discussion and conclusions

Unlike previous data suggested, it does not appear that TRPC channels form part of the MET complex. MET current recordings from DKO, TKO and QKO basal OHCs were of comparable size to WT OHCs. This supersedes the previous finding that MET currents recorded from basal DKO OHCs were around 75% smaller than those in WT OHCs (Quick et al., 2012). The likelihood is that the previously published result was obtained due to some unidentified issue with the state of the cells. Whilst it appears that TRPC1, TRPC3, TRPC5 and TRPC6 do not form part of MET channel or the MET complex itself, it is possible that they contributed to the viability of the cells in some way. It was noted by several people in the lab including myself that the basal cells from all the knockout mice did seem quite fragile.

As mentioned, the only apparent difference in MET current characteristics was the lack of difference in the size of the currents between apical and basal QKO OHCs, but, given the small number of cells recorded from, further investigation would be necessary to determine whether or not this result is robust.

Knocking out TRPC channels seems to have a combined effect, such that deficits in some areas are increased after knocking out additional TRPC channels, which makes sense as fewer TRPC monomer candidates are available to form compensatory heteromers. These defects, while they do not pertain to the MET complex itself, appear to indirectly play a role in cutaneous reception and some aspect of vestibular and hearing related mechanosensory reception.

Incongruent with the aforementioned results, but nonetheless indicative of TRPC3s role in hair cell MET Wong *et al*. (2013) found that TRPC3 -/- mice have hyperacusis at 8-16 kHz, which corresponds to somewhere in the region of 4mm to 6mm in FIGURE 3-1. As previously mentioned, DPOAE are a measure of resultant distortion products emanating from the cochlea, after two simultaneous pure tone stimuli are presented. Where a mean primary 8 kHz

tone was used at 20 – 50 dB SPL, stronger DPOAE gain was witnessed, suggesting that basilar membrane motion was enhanced in TRPC 3/6 knockout mice.

They also found a 40% reduction in re-entry of Ca^{2+} following depletion of intracellular calcium in TRPC 3/6 knockout mice. Together they interpret these data to suggest that TRPC3 is at least partially responsible for the cytosolic Ca^{2+} negative feedback system in hair cells. When TRPC3 absent Ca^{2+} homeostasis is disrupted, resulting in enhancement of OHC electromotility, causing hyperacusis. The MET complex and the motor protein prestin are regulated by Ca^{2+} and thus if homeostasis is disrupted, this will have effects OHC motility (Housley and Ashmore, 1992; Zheng et al., 2000).

The great number of interactions between TRPC monomers and with other TRP channel types makes pinning down which interaction is of mechanistic significance difficult. Withal, it does seem that TRPC channels are indeed involved in mechanosensation in some capacity. Further investigation on mature TRPC knockout mice, would help to ascertain what hearing deficits these mice exhibit, how these develop and the cause of any hearing defects witnessed. Further investigation of knocking out TRPC channels in conjunction with other channels which they form heteromers with may also be of use.

8 FINAL CONCLUSIONS AND SUGGESTIONS FOR FUTURE EXPERIMENTS

Further evidence of the apical to basal gradient in macroscopic MET current size is presented here, where currents increase in size along the length of the cochlea (FIGURE 3-1), allowing for calculations of number of the number of MET channels for OHCs in each region to be made (TABLE 1). The finding that there is a gradient in D-JNKi1 block of IHCs is intriguing, as it provides the first published evidence of any kind of gradient in the properties of IHC MET. The difference in IHC MET channel isoforms between apex and base must be one that does not affect single channel conductance, as this known to be uniform between the two regions in IHCs (Beurg et al., 2006). Additional recordings in the presence of the concentrations of compounds already tested are necessary as well as testing other concentrations in order to develop a comprehensive view of the gradient in IHCs. Using a protocol which applies square mechanical steps to look at the kinetics of the block of IHCs would be useful. First an inhibitory mechanical step is applied and then a excitatory step, before and during the application of the drug, whilst the cell is being held at -84 mV (see Marcotti et al., 2005). A curve can then be fitted to the current in the presence of the drug, which yields information about the kinetics of the block**.** Additionally such data would allow for creation of energy profiles for the binding of the compounds and allow us to see the entry rates of the compounds into IHCs which would yield more information about the differences between the apical and basal IHC isoforms. To create an even more comprehensive picture, other known channel blockers could be utilised to see if there are other gradients of channel block in IHCs.

There is no doubt the molecular identity of the MET channel is a highly significant mystery to solve as its discovery will allow for further elucidation of the complexities of MET in the cochlea. A great deal of searching and repeating measures is necessary. The complexities that may arise are evident for the TMC knockouts, where even after apparently establishing an abolishment of MET currents in TMC1 TMC2 double knockout mice (Kawashima et al., 2011), the use of stronger stimuli unveiled that the anomalous current was present in these mice (Kim et al., 2013). Establishing how a deficit manifests at the cellular level is challenging and

the TRPC knockout mice provide further illustration of this, where a previously identified deficit was not in fact the result of a problem with MET. To establish exactly what it is that is causing a particular deficit may require many experiments.

TRPC clearly is not part of the MET channel or the MET complex itself, however, if TRPC3 does have a role in cystolic Ca^{2+} homeostasis (Wong et al., 2013), this may have developmental impact upon the hair cells which results in hearing defects in mature TRPC knockout mice. Perhaps OHCs in TRPC knockout mice are more fragile than those in WT mice and thus their viability is affected. I would also be intrigued to see if indeed the apical and basal OHC MET currents are the same size, as they appeared in the modest number of recordings I have conducted, in QKO mice and what implications this may have.

What we can do to attempt to elucidate further information about the structure of the MET channel is to piece together the data that has been already collected. Experiments over many years have contributed to the finding that the MET channel is a non-specific cation channel (Corey and Hudspeth, 1979), Ca^{2+} having high permeability and being able to occlude the channel pore (Ricci et al., 2005). As well as this the MET channel can be blocked and permeated by a myriad of channel blockers (Gale et al., 2001; Farris et al., 2004; Marcotti et al., 2005). The MET channel has been localised to the tip links of the two shortest rows of stereocilia (Beurg et al., 2009). Moreover, some of the properties of the MET channel are still debated such as the double-rectification (Kros et al., 1992; Pan et al., 2012) of the MET current and the origination and Ca^{2+} dependence of fast and slow adaptation (Peng et al., 2013; Corns et al., 2014).

The binding profiles of D-TAT and D-JNKi1, with their concentration and voltage dependence have distinctive energy profiles, when fitted with the two-barrier one binding site model. The binding sites for the two peptides are at different electrical distances form the extracellular face of the MET channel, indicating that they bind in different regions of the channel pore. The

conclusion is that there are a minimum of two binding sites in the MET channel pore: one in the centre of the vestibule and another which is also in the vestibule but nearer the narrow pore region. We think that D-TAT binds nearer the narrow pore region due to the distance from the extracellular face of the channel being substantially further towards the intracellular side than that of D-JNKi1. Whereas the shorter distance from the extracellular side of the channel of D-JNKi1, leads us to the conclusion that D-JNKi1 binds in the middle of the highly electronegative channel vestibule as this is thought to reside there. The fact that there is a variation in the energy profiles of D-JNKi1 binding in the apical and basal OHCs provides further evidence for the notion that the vestibule is the MET channel component which varies from the apex to the base of the cochlea, in either its size or the quantity of negatively charged residues within it. Because of the positioning of its binding site(s), D-JNKi1 is affected by the difference in vestibule isoform, whereas D-TAT is not. Binding and thus channel block of D-JNKi1 may be stronger in the basal MET channel isoform because of its more negatively charged vestibule, indicated by the slightly deeper energy well of the D-JNKi1 binding site in the basal OHC MET channel. D-TAT, because of its smaller dimensions and the positioning of its binding site is not affected by the size of the channel or the amount of positively charged residues in the vestibule. Additionally, it may be the vestibule which is the MET channel component which is lacking in the anomalous current protochannel, like the BK channel without a gating ring (Budelli et al., 2013).

The size of the narrow part of the MET channel pore must clearly be re-estimated, in light of the finding that D-TAT and D-JNKi1 are able to permeate the channel. Both have an end on diameter of 1.5 nM, and if we assume that the compounds have the unfolded structure presented in FIGURE 4-2, then the narrow pore region of both MET channel isoforms must be at least this wide. Additionally, if we assume, based on the lower free energies of the extracellular and intracellular barriers for D-JNKi1, that the basal MET channel isoform is larger than the apical isoform then its dimensions will be even greater than this.

It seems that the most likely form of channel conducting the anomalous current is some form of protochannel, perhaps mobilised from a reserve pool as is indicated by the work of Kurima et al. (2015). The many instances in which the anomalous current can be recorded suggest that it originates from a protochannel formed of different subunits to the normal MET channel. Knocking out, point mutating, or ablating any MET channel subunit or part of the MET channel machinery has an effect on the operation of the channel, affecting the onset kinetics, "adaptation", shape and rectification of the currents which flow through it. The notion of the vestibule being what is lacking has been previously postulated (Marcotti et al., 2014; Beurg et al., 2014b). Different subunits may then form distinct channel isoforms, through which mechanosensitive currents of different magnitudes flow. These protochannel isoform(s) have been shown to be differentially susceptible to the channel block and entry into the hair cells by DHS and lack the apical to basal gradient in channel block which is evident for MET channels. Using D-JNKi1 to block the anomalous current, with its defined apical to basal gradient of the MET current, would provide further proof of the lack of gradient.

If we take the view that the anomalous current represents a reserve pool of protochannels which are lacking the highly negatively charged vestibule, then we would expect D-JNKi1 to block the anomalous current less effectively than D-TAT. Therefore, to further test the theory that it is the electronegative vestibule which the protochannel is lacking, testing the blocking potential of D-TAT and D-JNKi1 may be illuminating. The hypothesis is that as D-JNKi1 binds in the middle of the vestibule, its K_D for the protochannel will be much reduced compared to that for the MET channel. As D-TAT binds near the narrow part of the channel pore, its binding in the protochannel may be less reduced. If results supported this prediction it would support the anomalous current arises from a protochannel which is missing the subunit(s) which comprise the vestibule.

The information I have obtained taken together has allowed me to develop an idea of the structural architecture of the MET channel (FIGURE 8-1). It seems clear that it is formed of multiple subunits but as to how many there are remains to be unveiled. I have represented the distinct subunits which form the vestibule, of which there may be many isoforms of different sizes with different numbers of positively charged residues within them. Sitting nearer the intracellular face of the channel are the narrow pore region subunits. I have represented two binding sites, as characterised by the blocking and energy profiles of D-TAT and D-JNKi1. There is one in the centre of the vestibule and one nearer the narrow part of the channel pore. Whilst most of the residues which form the latter binding site are in the vestibule forming subunit, I have drawn some in the narrow pore region itself. I feel that this is necessary to account for the assumption that the protochannel lacks the vestibule forming subunit(s) yet FM1-43 blocks the channel to a comparable degree with the MET channel, albeit with altered voltage dependence and DHS does still block the channel to some degree in spite of its reduced affinity. Additionally there are two barriers, represented by the negative charges, at the extracellular and intracellular faces of the channel. The MET channel pore length is 3.1 nm and as suggested by Farris et al. (2004) the plasma membrane in which the MET channel is embedded is in the region of 2.4 nm in width, a third of 7.2 nm (7.2nm / 3) (Farris et al., 2004). I have thus illustrated the MET channel as protruding slightly at its extracellular face of the phospholipid bilayer.

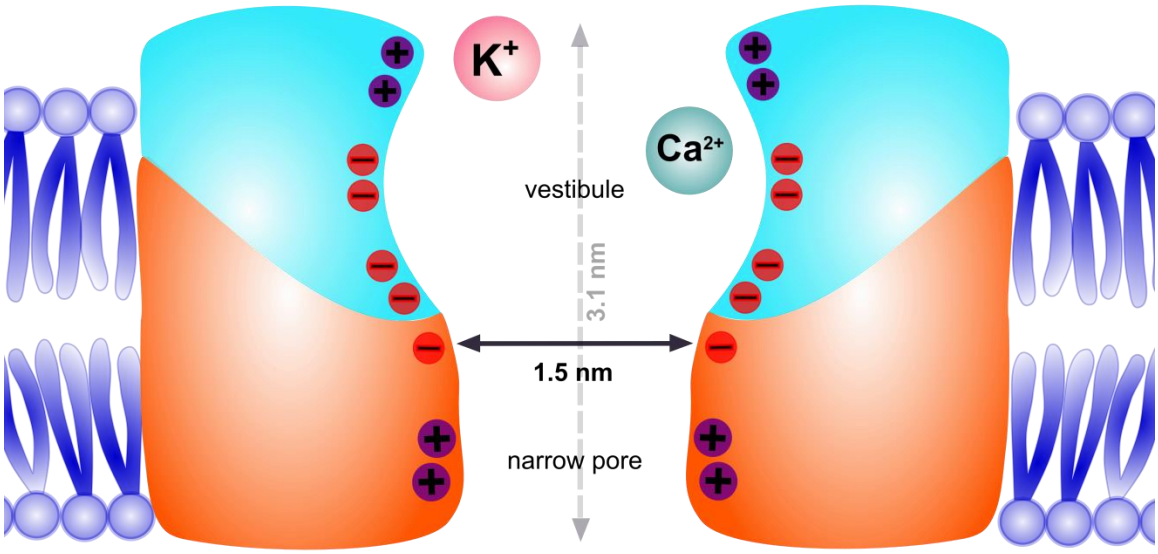

FIGURE 8-1 : MET channel model, based on the findings presented in this thesis and the data obtained by others discussed within.

REFERENCES

Abi-Hachem, R. N., Zine, A., and R. Van De Water, T. (2010). The Injured Cochlea as a Target for Inflammatory Processes, Initiation of Cell Death Pathways and Application of Related Otoprotective Strategies. Recent Patents on CNS Drug Discovery *5*, 147–163.

Alagramam, K.N., Goodyear, R.J., Geng, R., Furness, D.N., van Aken, A.F.J., Marcotti, W., Kros, C.J., and Richardson, G.P. (2011). Mutations in Protocadherin 15 and Cadherin 23 Affect Tip Links and Mechanotransduction in Mammalian Sensory Hair Cells. PLoS ONE *6*, e19183.

Alharazneh, A., Luk, L., Huth, M., Monfared, A., Steyger, P.S., Cheng, A.G., and Ricci, A.J. (2011). Functional Hair Cell Mechanotransducer Channels Are Required for Aminoglycoside Ototoxicity. PLoS ONE *6*, e22347.

Assad, J.A., and Corey, D.P. (1992). An active motor model for adaptation by vertebrate hair cells. J. Neurosci. *12*, 3291–3309.

Assad, J.A., Shepherd, G.M.G., and Corey, D.P. (1991). Tip-link integrity and mechanical transduction in vertebrate hair cells. Neuron *7*, 985–994.

Avraham, K.B. (2003). Mouse models for deafness: lessons for the human inner ear and hearing loss. Ear Hear *24*, 332–341.

Beech, D.J. (2012). Orai1 calcium channels in the vasculature. Pflugers Arch - Eur J Physiol *463*, 635–647.

Beurg, M., Evans, M.G., Hackney, C.M., and Fettiplace, R. (2006). A Large-Conductance Calcium-Selective Mechanotransducer Channel in Mammalian Cochlear Hair Cells. J. Neurosci. *26*, 10992–11000.

Beurg, M., Fettiplace, R., Nam, J.-H., and Ricci, A.J. (2009). Localization of inner hair cell mechanotransducer channels using high-speed calcium imaging. Nature Neuroscience *12*, 553–558.

Beurg, M., Nam, J.-H., Chen, Q., and Fettiplace, R. (2010). Calcium Balance and Mechanotransduction in Rat Cochlear Hair Cells. J Neurophysiol *104*, 18–34.

Beurg, M., Xiong, W., Zhao, B., Müller, U., and Fettiplace, R. (2014a). Subunit determination of the conductance of hair-cell mechanotransducer channels. PNAS 201420906.

Beurg, M., Kim, K.X., and Fettiplace, R. (2014b). Conductance and block of hair-cell mechanotransducer channels in transmembrane channel–like protein mutants. J Gen Physiol *144*, 55–69.

Bon, R.S., and Beech, D.J. (2013). In pursuit of small molecule chemistry for calcium-permeable non-selective TRPC channels – mirage or pot of gold? Br J Pharmacol *170*, 459–474.

Bonny, C. (2003). Cell-permeable peptide inhibitors of the JNK signal transduction pathway.

Bonny, C., Oberson, A., Negri, S., Sauser, C., and Schorderet, D.F. (2001). Cell-Permeable Peptide Inhibitors of JNK Novel Blockers of B-Cell Death. Diabetes *50*, 77–82.

Böttger, E.C., Springer, B., Prammananan, T., Kidan, Y., and Sander, P. (2001). Structural basis for selectivity and toxicity of ribosomal antibiotics. EMBO Rep. *2*, 318–323.

Brelidze, T.I., Niu, X., and Magleby, K.L. (2003). A ring of eight conserved negatively charged amino acids doubles the conductance of BK channels and prevents inward rectification. PNAS *100*, 9017–9022.

Brown, R.D., and Feldman, A.M. (1978). Pharmacology of Hearing and Ototoxicity. Annual Review of Pharmacology and Toxicology *18*, 233–252.

Brummett, R., Himes, D., Saine, B., and Vernon, V. (1972). A comparative study of the ototoxicity of tobramycin and gentamicin. Arch Otolaryngol *96*, 505–512.

Budelli, G., Geng, Y., Butler, A., Magleby, K.L., and Salkoff, L. (2013). Properties of Slo1 K+ channels with and without the gating ring. PNAS *110*, 16657–16662.

Burke, J.F., and Mogg, A.E. (1985). Suppression of a nonsense mutation in mammalian cells in vivo by the aminoglycoside antibiotics G-418 and paromomycin. Nucleic Acids Research *13*, 6265–6272.

Cheng, A.G., Cunningham, L.L., and Rubel, E.W. (2005). Mechanisms of hair cell death and protection. Curr Opin Otolaryngol Head Neck Surg *13*, 343–348.

Corey, D.P., and Hudspeth, A.J. (1979). Ionic basis of the receptor potential in a vertebrate hair cell. Nature *281*, 675–677.

Corey, D.P., and Hudspeth, A.J. (1983). Kinetics of the receptor current in bullfrog saccular hair cells. J. Neurosci. *3*, 962–976.

Corey, D.P., Garc|[iacute]|a-A|[ntilde]|overos, J., Holt, J.R., Kwan, K.Y., Lin, S.-Y., Vollrath, M.A., Amalfitano, A., Cheung, E.L.-M., Derfler, B.H., Duggan, A., et al. (2004). TRPA1 is a candidate for the mechanosensitive transduction channel of vertebrate hair cells. Nature *432*, 723–730.

Corns, L.F., Johnson, S.L., Kros, C.J., and Marcotti, W. (2014). Calcium entry into stereocilia drives adaptation of the mechanoelectrical transducer current of mammalian cochlear hair cells. PNAS *111*, 14918–14923.

Corns, L.F., Johnson, S.L., Kros, C.J., and Marcotti, W. (2016). Tmc1 Point Mutation Affects Ca2+ Sensitivity and Block by Dihydrostreptomycin of the Mechanoelectrical Transducer Current of Mouse Outer Hair Cells. J. Neurosci. *36*, 336–349.

Cunningham, L.L., Cheng, A.G., and Rubel, E.W. (2002). Caspase Activation in Hair Cells of the Mouse Utricle Exposed to Neomycin. J. Neurosci. *22*, 8532–8540.

Dallos, P., Santos-Sacchi, J., and Flock, A. (1982). Intracellular recordings from cochlear outer hair cells. Science *218*, 582–584.

Davis, H., Deatherage, B.H., Rosenblut, B., Fernandez, C., Kimura, R., and Smith, C.A. (1958). Modification of cochlear potentials produced by streptomycin poisoning and by extensive venous obstruction. The Laryngoscope *68*, 596–627.

Deloche, C., Lopez-Lazaro, L., Mouz, S., Perino, J., Abadie, C., and Combette, J.-M. (2014). XG-102 administered to healthy male volunteers as a single intravenous infusion: a randomized, double-blind, placebo-controlled, dose-escalating study. Pharmacol Res Perspect *2*, n/a – n/a.

Delprat, B., Michel, V., Goodyear, R., Yamasaki, Y., Michalski, N., El-Amraoui, A., Perfettini, I., Legrain, P., Richardson, G., Hardelin, J.-P., et al. (2005). Myosin XVa and whirlin, two deafness gene products required for hair bundle growth, are located at the stereocilia tips and interact directly. Hum. Mol. Genet. *14*, 401–410.

Duscha, S., Boukari, H., Shcherbakov, D., Salian, S., Silva, S., Kendall, A., Kato, T., Akbergenov, R., Perez-Fernandez, D., Bernet, B., et al. (2014). Identification and Evaluation of Improved 4'-O-(Alkyl) 4,5-Disubstituted 2-Deoxystreptamines as Next-Generation Aminoglycoside Antibiotics. mBio *5*, e01827–14.

Effertz, T., Nadrowski, B., Piepenbrock, D., Albert, J.T., and Göpfert, M.C. (2012). Direct gating and mechanical integrity of Drosophila auditory transducers require TRPN1. Nat Neurosci *15*, 1198–1200.

Ehret, G., and Frankenreiter, M. (1977). Quantitative analysis of cochlear structures in the house mouse in relation to mechanisms of acoustical information processing. J. Comp. Physiol. *122*, 65–85.

Elg, S., Marmigere, F., Mattsson, J.P., and Ernfors, P. (2007). Cellular subtype distribution and developmental regulation of TRPC channel members in the mouse dorsal root ganglion. J. Comp. Neurol. *503*, 35–46.

Encyclopedia Britannica: Ockham's razor. Encyclopedia Britannica (retrieved June 24, 2010)

Eshraghi, A.A., He, J., Mou, C.H., Polak, M., Zine, A., Bonny, C., Balkany, T.J., and Van De Water, T.R. (2006). D-JNKI-1 Treatment Prevents the Progression of Hearing Loss in a Model of Cochlear Implantation Trauma: Otology & Neurotology *27*, 504–511.

Eyring, H. and Eyring, E.M (1963). Modern Chemical Kinetics. Reinhold Publishing Corporation, New York, London

Farris, H.E., LeBlanc, C.L., Goswami, J., and Ricci, A.J. (2004). Probing the pore of the auditory hair cell mechanotransducer channel in turtle. The Journal of Physiology *558*, 769–792.

Farris, H.E., Wells, G.B., and Ricci, A.J. (2006). Steady-state adaptation of mechanotransduction modulates the resting potential of auditory hair cells, providing an assay for endolymph [Ca2+]. The Journal of Neuroscience *26*, 12526–12536.

Ferguson, R.N., Edelhoch, H., Saroff, H.A., Robbins, J., and Cahnmann, H.J. (1975). Negative cooperativity in the binding of thyroxine to human serum prealbumin. Biochemistry *14*, 282–289.

Fettiplace, R., and Kim, K.X. (2014). The Physiology of Mechanoelectrical Transduction Channels in Hearing. Physiological Reviews *94*, 951–986.

Fischel-Ghodsian, N. (2005). Genetic factors in aminoglycoside toxicity. Pharmacogenomics *6*, 27–36.

Fujioka, M., Okano, H., and Edge, A.S.B. (2015). Manipulating cell fate in the cochlea: a feasible therapy for hearing loss. Trends in Neurosciences *38*, 139–144.

Gale, J.E., Marcotti, W., Kennedy, H.J., Kros, C.J., and Richardson, G.P. (2001a). FM1-43 Dye Behaves as a Permeant Blocker of the Hair-Cell Mechanotransducer Channel. The Journal of Neuroscience *21*, 7013–7025.

Gale, J.E., Marcotti, W., Kennedy, H.J., Kros, C.J., and Richardson, G.P. (2001b). FM1-43 Dye Behaves as a Permeant Blocker of the Hair-Cell Mechanotransducer Channel. J. Neurosci. *21*, 7013–7025.

Garetz, S.L., Altschuler, R.A., and Schacht, J. (1994). Attenuation of gentamicin ototoxicity by glutathione in the guinea pig in vivo. Hearing Research *77*, 81–87.

Gillespie, P.G., and Cyr, J.L. (2004). Myosin-1c, the Hair Cell's Adaptation Motor. Annual Review of Physiology *66*, 521–545.

Gonzalo, X., Hutchison, D.C.S., Drobniewski, F.A., Pimkina, E., and Davidaviciene, E. (2014). Multidrug-resistant tuberculosis in the United Kingdom and Lithuania. The International Journal of Tuberculosis and Lung Disease *18*, 663–665.

Goodyear, R.J., Gale, J.E., Ranatunga, K.M., Kros, C.J., and Richardson, G.P. (2008a). Aminoglycoside-Induced Phosphatidylserine Externalization in Sensory Hair Cells Is Regionally Restricted, Rapid, and Reversible. The Journal of Neuroscience *28*, 9939–9952.

Goodyear, R.J., Gale, J.E., Ranatunga, K.M., Kros, C.J., and Richardson, G.P. (2008b). Aminoglycoside-Induced Phosphatidylserine Externalization in Sensory Hair Cells Is Regionally Restricted, Rapid, and Reversible. J. Neurosci. *28*, 9939–9952.

Grati, M., and Kachar, B. (2011). Myosin VIIa and sans localization at stereocilia upper tip-link density implicates these Usher syndrome proteins in mechanotransduction. PNAS *108*, 11476–11481.

Gross, A., Jockel, J., Wei, M.C., and Korsmeyer, S.J. (1998). Enforced dimerization of BAX results in its translocation, mitochondrial dysfunction and apoptosis. EMBO J. *17*, 3878–3885.

Hashino, E., and Shero, M. (1995). Endocytosis of aminoglycoside antibiotics in sensory hair cells. Brain Research *704*, 135–140.

Heffner, H.E., and Heffner, R.S. (2007). Hearing ranges of laboratory animals. J. Am. Assoc. Lab. Anim. Sci. *46*, 20–22.

Herce, H.D., and Garcia, A.E. (2007). Molecular dynamics simulations suggest a mechanism for translocation of the HIV-1 TAT peptide across lipid membranes. PNAS *104*, 20805–20810.

Hille, B. (2001). Ion Channels of Excitable Membranes (Mass.).

Hirose, K., Westrum, L.E., Stone, J.S., Zirpel, L., and Rubel, E.W. (1999). Dynamic studies of ototoxicity in mature avian auditory epithelium. Ann. N. Y. Acad. Sci. *884*, 389–409.

Hirt, L., Badaut, J., Thevenet, J., Granziera, C., Regli, L., Maurer, F., Bonny, C., and Bogousslavsky, J. (2004). D-JNKI1, a cell-penetrating C-Jun-N-terminal kinase inhibitor, protects against cell death in severe cerebral ischemia. Stroke *35*, 1738–1743.

Holm, T., Räägel, H., Andaloussi, S.E., Hein, M., Mäe, M., Pooga, M., and Langel, Ü. (2011). Retro-inversion of certain cell-penetrating peptides causes severe cellular toxicity. Biochimica et Biophysica Acta (BBA) - Biomembranes *1808*, 1544–1551.

Holt, J.R., Gillespie, S.K.H., Provance Jr., D.W., Shah, K., Shokat, K.M., Corey, D.P., Mercer, J.A., and Gillespie, P.G. (2002). A Chemical-Genetic Strategy Implicates Myosin-1c in Adaptation by Hair Cells. Cell *108*, 371–381.

Housley, G.D., and Ashmore, J.F. (1992). Ionic currents of outer hair cells isolated from the guinea-pig cochlea. The Journal of Physiology *448*, 73–98.

Howard, J., and Hudspeth, A.J. (1988). Compliance of the hair bundle associated with gating of mechanoelectrical transduction channels in the Bullfrog's saccular hair cell. Neuron *1*, 189–199.

Hu, Z., and Ulfendahl, M. (2013). The potential of stem cells for the restoration of auditory function in humans. Regenerative Medicine *8*, 309–318.

Hu, D.N., Qui, W.Q., Wu, B.T., Fang, L.Z., Zhou, F., Gu, Y.P., Zhang, Q.H., Yan, J.H., Ding, Y.Q., and Wong, H. (1991). Genetic aspects of antibiotic induced deafness: mitochondrial inheritance. J Med Genet *28*, 79–83.

Hudspeth, A.J. (2008). Making an Effort to Listen: Mechanical Amplification in the Ear. Neuron *59*, 530–545.

Hui, H., McHugh, D., Hannan, M., Zeng, F., Xu, S.-Z., Khan, S.-H., Levenson, R., Beech, D.J., and Weiss, J.L. (2006). Calcium-sensing mechanism in TRPC5 channels contributing to retardation of neurite outgrowth. The Journal of Physiology *572*, 165–172.

Huizing, E.H., and Groot, J.C.M.J. de (1987). Human Cochlear Pathology in Aminoglycoside Ototoxicity—A Review. Acta Oto-Laryngologica *104*, 117–125.

Huth, M.E., Ricci, A.J., and Cheng, A.G. (2011a). Mechanisms of Aminoglycoside Ototoxicity and Targets of Hair Cell Protection. International Journal of Otolaryngology *2011*, 1–19.

Huth, M.E., Ricci, A.J., and Cheng, A.G. (2011b). Mechanisms of Aminoglycoside Ototoxicity and Targets of Hair Cell Protection. International Journal of Otolaryngology *2011*, 1–19.

Huth, M.E., Han, K.-H., Sotoudeh, K., Hsieh, Y.-J., Effertz, T., Vu, A.A., Verhoeven, S., Hsieh, M.H., Greenhouse, R., Cheng, A.G., et al. (2015). Designer aminoglycosides prevent cochlear hair cell loss and hearing loss. Journal of Clinical Investigation *125*, 583–592.

Indzhykulian, A.A., Stepanyan, R., Nelina, A., Spinelli, K.J., Ahmed, Z.M., Belyantseva, I.A., Friedman, T.B., Barr-Gillespie, P.G., and Frolenkov, G.I. (2013). Molecular Remodeling of Tip Links Underlies Mechanosensory Regeneration in Auditory Hair Cells. PLoS Biol *11*, e1001583.

Ishibashi, T., Takumida, M., Akagi, N., Hirakawa, K., and Anniko, M. (2008). Expression of transient receptor potential vanilloid (TRPV) 1, 2, 3, and 4 in mouse inner ear. Acta Otolaryngol *128*, 1286–1293.

J, Y. (1973). Correlative studies on the cochlear pathology and hearing loss in guinea-pigs after intoxication with ototoxic antibiotics. Acta Otolaryngol Suppl *326*, 1–62.

Jackson, M.B. (2002). Allosteric Mechanisms in the Activation of Ligand-Gated Channels.

Johnson, S.L., Beurg, M., Marcotti, W., and Fettiplace, R. (2011). Prestin-Driven Cochlear Amplification Is Not Limited by the Outer Hair Cell Membrane Time Constant. Neuron *70*, 1143–1154.

Johnson, M.L., Holt, J.M., and Ackers, G.K. (2011). Biothermodynamics (Academic Press).

Kachar, B., Parakkal, M., Kurc, M., Zhao, Y., and Gillespie, P.G. (2000). High-resolution structure of hair-cell tip links. PNAS *97*, 13336–13341.

Kamimura, T., Whitworth, C.A., and Rybak, L.P. (1999). Effect of 4-methylthiobenzoic acid on cisplatin-induced ototoxicity in the rat. Hear. Res. *131*, 117–127.

Kant, I (1929). Immanuel Kant's Critique of Pure Reason, translated by Smith, N.K. (Macmillan).

Karashima, Y., Prenen, J., Talavera, K., Janssens, A., Voets, T., and Nilius, B. (2010). Agonist-Induced Changes in Ca2+ Permeation through the Nociceptor Cation Channel TRPA1. Biophysical Journal *98*, 773–783.

Kawashima, Y., Geleoc, G.S.G., Kurima, K., Labay, V., Lelli, A., Asai, Y., Makishima, T., Wu, D.K., Della Santina, C.C., Holt, J.R., et al. (2011). Mechanotransduction in mouse inner ear hair cells requires transmembrane channel-like genes. J Clin Invest *121*, 4796–4809.

Kawashima, Y., Kurima, K., Pan, B., Griffith, A.J., and Holt, J.R. (2014). Transmembrane channel-like (TMC) genes are required for auditory and vestibular mechanosensation. Pflugers Arch - Eur J Physiol 1–10.

Kazmierczak, P., Sakaguchi, H., Tokita, J., Wilson-Kubalek, E.M., Milligan, R.A., Müller, U., and Kachar, B. (2007). Cadherin 23 and protocadherin 15 interact to form tip-link filaments in sensory hair cells. Nature *449*, 87–91.

Keeling, K.M., Wang, D., Conard, S.E., and Bedwell, D.M. (2012). Suppression of premature termination codons as a therapeutic approach. Critical Reviews in Biochemistry and Molecular Biology *47*, 444–463.

Kennedy, H.J., Evans, M.G., Crawford, A.C., and Fettiplace, R. (2006). Depolarization of Cochlear Outer Hair Cells Evokes Active Hair Bundle Motion by Two Mechanisms. J. Neurosci. *26*, 2757–2766.

Kim, K.X., and Fettiplace, R. (2013a). Developmental changes in the cochlear hair cell mechanotransducer channel and their regulation by transmembrane channel–like proteins. J Gen Physiol *141*, 141–148.

Kim, K.X., and Fettiplace, R. (2013b). Developmental changes in the cochlear hair cell mechanotransducer channel and their regulation by transmembrane channel–like proteins. J Gen Physiol *141*, 141–148.

Kim, J., Chung, Y.D., Park, D., Choi, S., Shin, D.W., Soh, H., Lee, H.W., Son, W., Yim, J., Park, C.-S., et al. (2003). A TRPV family ion channel required for hearing in Drosophila. Nature *424*, 81–84.

Kim, K.X., Beurg, M., Hackney, C.M., Furness, D.N., Mahendrasingam, S., and Fettiplace, R. (2013). The role of transmembrane channel–like proteins in the operation of hair cell mechanotransducer channels. J Gen Physiol *142*, 493–505.

Koo, J.-W., Quintanilla-Dieck, L., Jiang, M., Liu, J., Urdang, Z.D., Allensworth, J.J., Cross, C.P., Li, H., and Steyger, P.S. (2015). Endotoxemia-mediated inflammation potentiates aminoglycoside induced ototoxicity.

Kopke, R.D., Liu, W., Gabaizadeh, R., Jacono, A., Feghali, J., Spray, D., Garcia, P., Steinman, H., Malgrange, B., Ruben, R.J., et al. (1997). Use of organotypic cultures of Corti's organ to study the protective effects of antioxidant molecules on cisplatin-induced damage of auditory hair cells. Am J Otol *18*, 559–571.

Kroese, A.B.A., Das, A., and Hudspeth, A.J. (1989). Blockage of the transduction channels of hair cells in the bullfrog's sacculus by aminoglycoside antibiotics. Hearing Research *37*, 203–217.

Kros, C.J., Rusch, A., and Richardson, G.P. (1992). Mechano-Electrical Transducer Currents in Hair Cells of the Cultured Neonatal Mouse Cochlea. Proc. R. Soc. Lond. B *249*, 185–193.

Kros CJ (1996). Physiology of mammalian cochlear hair cells.In *The Cochlea*, ed. Dallos P, Popper AN & Fay RR, pp. 318–385. Springer-Verlag, New York.

Kros, C.J., Marcotti, W., van Netten, S.M., Self, T.J., Libby, R.T., Brown, S.D.M., Richardson, G.P., and Steel, K.P. (2002). Reduced climbing and increased slipping adaptation in cochlear hair cells of mice with Myo7a mutations. Nat Neurosci *5*, 41–47.

Kros, C.J., and Desmonds, T. (2015). Drug-induced hearing loss: Infection raises the odds. Science Translational Medicine *7*, 298fs31–fs298fs31.

Krusek, J. (2004). Allostery and cooperativity in the interaction of drugs with ionic channel receptors. Physiological Research *53*, 569–579.

Kumana, C.R., and Yuen, K.Y. (1994). Parenteral aminoglycoside therapy. Selection, administration and monitoring. Drugs *47*, 902–913.

Kurima, K., Peters, L.M., Yang, Y., Riazuddin, S., Ahmed, Z.M., Naz, S., Arnaud, D., Drury, S., Mo, J., Makishima, T., et al. (2002). Dominant and recessive deafness caused by mutations of a novel gene, TMC1, required for cochlear hair-cell function. Nat Genet *30*, 277–284.

Kurima, K., Ebrahim, S., Pan, B., Sedlacek, M., Sengupta, P., Millis, B.A., Cui, R., Nakanishi, H., Fujikawa, T., Kawashima, Y., et al. (2015). TMC1 and TMC2 Localize at the Site of Mechanotransduction in Mammalian Inner Ear Hair Cell Stereocilia. Cell Rep.

Kwan, K.Y., Allchorne, A.J., Vollrath, M.A., Christensen, A.P., Zhang, D.-S., Woolf, C.J., and Corey, D.P. (2006). TRPA1 Contributes to Cold, Mechanical, and Chemical Nociception but Is Not Essential for Hair-Cell Transduction. Neuron *50*, 277–289.

Launay, P., Fleig, A., Perraud, A.-L., Scharenberg, A.M., Penner, R., and Kinet, J.-P. (2002). TRPM4 Is a Ca2+-Activated Nonselective Cation Channel Mediating Cell Membrane Depolarization. Cell *109*, 397–407.

Lelli, A., Asai, Y., Forge, A., Holt, J.R., and Géléoc, G.S.G. (2009). Tonotopic Gradient in the Developmental Acquisition of Sensory Transduction in Outer Hair Cells of the Mouse Cochlea. Journal of Neurophysiology *101*, 2961–2973.

Lelli, A., Kazmierczak, P., Kawashima, Y., Müller, U., and Holt, J.R. (2010). Development and Regeneration of Sensory Transduction in Auditory Hair Cells Requires Functional Interaction Between Cadherin-23 and Protocadherin-15. J. Neurosci. *30*, 11259–11269.

Li, W., Wu, J., Yang, J., Sun, S., Chai, R., Chen, Z.-Y., and Li, H. (2015). Notch inhibition induces mitotically generated hair cells in mammalian cochleae via activating the Wnt pathway. PNAS *112*, 166–171.

Lim, D.J. (1986). Effects of noise and ototoxic drugs at the cellular level in the cochlea: A review. American Journal of Otolaryngology *7*, 73–99.

Lombarte, A., Yan, H.Y., Popper, A.N., Chang, J.S., and Platt, C. (1993). Damage and regeneration of hair cell ciliary bundles in a fish ear following treatment with gentamicin. Hearing Research *64*, 166–174.

Ma, X., Cao, J., Luo, J., Nilius, B., Huang, Y., Ambudkar, I.S., and Yao, X. (2010). Depletion of Intracellular Ca2+ Stores Stimulates the Translocation of Vanilloid Transient Receptor Potential 4-C1 Heteromeric Channels to the Plasma Membrane. Arterioscler Thromb Vasc Biol *30*, 2249–2255.

Manor, U., Disanza, A., Grati, M., Andrade, L., Lin, H., Di Fiore, P.P., Scita, G., and Kachar, B. (2011). Regulation of Stereocilia Length by Myosin XVa and Whirlin Depends on the Actin-Regulatory Protein Eps8. Current Biology *21*, 167–172.

Marcotti, W., van Netten, S.M., and Kros, C.J. (2005a). The aminoglycoside antibiotic dihydrostreptomycin rapidly enters mouse outer hair cells through the mechano-electrical transducer channels. J. Physiol. (Lond.) *567*, 505–521.

Marcotti, W., van Netten, S.M., and Kros, C.J. (2005b). The aminoglycoside antibiotic dihydrostreptomycin rapidly enters mouse outer hair cells through the mechano -electrical transducer channels. J Physiol *567*, 505–521.

Marcotti, W., Corns, L.F., Desmonds, T., Kirkwood, N.K., Richardson, G.P., and Kros, C.J. (2014a). Transduction without Tip Links in Cochlear Hair Cells Is Mediated by Ion Channels with Permeation Properties Distinct from Those of the Mechano-Electrical Transducer Channel. J. Neurosci. *34*, 5505–5514.

Marcotti, W., Corns, L.F., Desmonds, T., Kirkwood, N.K., Richardson, G.P., and Kros, C.J. (2014b). Transduction without Tip Links in Cochlear Hair Cells Is Mediated by Ion Channels with Permeation Properties Distinct from Those of the Mechano-Electrical Transducer Channel. J. Neurosci. *34*, 5505–5514.

Marcus, D.C., Wu, T., Wangemann, P., and Kofuji, P. (2002). KCNJ10 (Kir4.1) potassium channel knockout abolishes endocochlear potential. American Journal of Physiology - Cell Physiology *282*, C403–C407.

Matsui, J.I., Haque, A., Huss, D., Messana, E.P., Alosi, J.A., Roberson, D.W., Cotanche, D.A., Dickman, J.D., and Warchol, M.E. (2003). Caspase inhibitors promote vestibular hair cell survival and function after aminoglycoside treatment in vivo. J. Neurosci. *23*, 6111–6122.

Matsui, J.I., Gale, J.E., and Warchol, M.E. (2004). Critical signaling events during the aminoglycoside-induced death of sensory hair cells in vitro. J. Neurobiol. *61*, 250–266.

Meyers, J.R., MacDonald, R.B., Duggan, A., Lenzi, D., Standaert, D.G., Corwin, J.T., and Corey, D.P. (2003). Lighting up the Senses: FM1-43 Loading of Sensory Cells Through Nonselective Ion Channels. J. Neurosci. *23*, 4054–4065.

Monod, J., Wyman, J., and Changeux, J. (1965). On the nature of allosteric transitions: A plausible model. Journal of Molecular Biology *12*, 88–118.

Monteilh-Zoller, M.K., Hermosura, M.C., Nadler, M.J.S., Scharenberg, A.M., Penner, R., and Fleig, A. (2003). TRPM7 Provides an Ion Channel Mechanism for Cellular Entry of Trace Metal Ions. J Gen Physiol *121*, 49–60.

Müller, M., Hünerbein, K. von, Hoidis, S., and Smolders, J.W.T. (2005). A physiological place–frequency map of the cochlea in the CBA/J mouse. Hearing Research *202*, 63–73.

Nadler, M.J.S., Hermosura, M.C., Inabe, K., Perraud, A.-L., Zhu, Q., Stokes, A.J., Kurosaki, T., Kinet, J.-P., Penner, R., Scharenberg, A.M., et al. (2001). LTRPC7 is a Mg·ATP-regulated divalent cation channel required for cell viability. Nature *411*, 590–595.

Nam, J.-H., Peng, A.W., and Ricci, A.J. (2015). Underestimated Sensitivity of Mammalian Cochlear Hair Cells Due to Splay between Stereociliary Columns. Biophysical Journal *108*, 2633–2647.

van Netten, S.M., Kros, C.J., and Hamill, O.P. (2007). Insights into the Pore of the Hair Cell Transducer Channel from Experiments with Permeant Blockers. In Mechanosensitive Ion Channels, Part B, (Academic Press), pp. 375–398.

Nilius, B., Prenen, J., and Owsianik, G. (2011). Irritating channels: the case of TRPA1. The Journal of Physiology *589*, 1543–1549.

Ohlemiller, K.K., Wright, J.S., and Dugan, L.L. (1999). Early elevation of cochlear reactive oxygen species following noise exposure. Audiol. Neurootol. *4*, 229–236.

Omotehara, Y., Hakuba, N., Hato, N., Okada, M., and Gyo, K. (2011). Protection Against Ischemic Cochlear Damage by Intratympanic Administration of AM-111: Otology & Neurotology *32*, 1422–1427.

O'Neil, R.G., and Heller, S. (2005). The mechanosensitive nature of TRPV channels. Pflugers Arch - Eur J Physiol *451*, 193–203.

Owens, K.N., Santos, F., Roberts, B., Linbo, T., Coffin, A.B., Knisely, A.J., Simon, J.A., Rubel, E.W., and Raible, D.W. (2008). Identification of Genetic and Chemical Modulators of Zebrafish Mechanosensory Hair Cell Death. PLoS Genet *4*, e1000020.

Palma, F.D., Belyantseva, I.A., Kim, H.J., Vogt, T.F., Kachar, B., and Noben-Trauth, K. (2002). Mutations in Mcoln3 associated with deafness and pigmentation defects in varitint-waddler (Va) mice. PNAS *99*, 14994–14999.

Pan, B., and Holt, J.R. (2015). The molecules that mediate sensory transduction in the mammalian inner ear. Current Opinion in Neurobiology *34*, 165–171.

Pan, B., Waguespack, J., Schnee, M.E., LeBlanc, C., and Ricci, A.J. (2012). Permeation Properties of the Hair Cell Mechanotransducer Channel Provide Insight into Its Molecular Structure. J Neurophysiol *107*, 2408–2420.

Pan, B., Géléoc, G.S., Asai, Y., Horwitz, G.C., Kurima, K., Ishikawa, K., Kawashima, Y., Griffith, A.J., and Holt, J.R. (2013). TMC1 and TMC2 Are Components of the Mechanotransduction Channel in Hair Cells of the Mammalian Inner Ear. Neuron *79*, 504–515.

Peng, A.W., Salles, F.T., Pan, B., and Ricci, A.J. (2011). Integrating the biophysical and molecular mechanisms of auditory hair cell mechanotransduction. Nature Communications *2*, 523.

Peng, A.W., Effertz, T., and Ricci, A.J. (2013). Adaptation of Mammalian Auditory Hair Cell Mechanotransduction Is Independent of Calcium Entry. Neuron *80*, 960–972.

Petersen, L., and Rogers, C. (2015). Aminoglycoside-induced hearing deficits – a review of cochlear ototoxicity. South African Family Practice *0*, 1–6.

Picard, W., Bazin, F., Clouzeau, B., Bui, H.-N., Soulat, M., Guilhon, E., Vargas, F., Hilbert, G., Bouchet, S., Gruson, D., et al. (2014). Propensity-Based Study of Aminoglycoside Nephrotoxicity in Patients with Severe Sepsis or Septic Shock. Antimicrob. Agents Chemother. *58*, 7468–7474.

Pickles, J.O. (2008a). An Introduction to the Physiology of Hearing (Emerald).

Pickles, J.O. (2008b). An Introduction to the Physiology of Hearing (Emerald).

Pirvola, U., Xing-Qun, L., Virkkala, J., Saarma, M., Murakata, C., Camoratto, A.M., Walton, K.M., and Ylikoski, J. (2000). Rescue of Hearing, Auditory Hair Cells, and Neurons by CEP-1347/KT7515, an Inhibitor of c-Jun N-Terminal Kinase Activation. J. Neurosci. *20*, 43–50.

Powers, R.J., Roy, S., Atilgan, E., Brownell, W.E., Sun, S.X., Gillespie, P.G., and Spector, A.A. (2012). Stereocilia Membrane Deformation: Implications for the Gating Spring and Mechanotransduction Channel. Biophysical Journal *102*, 201–210.

Prezant, T.R., Agapian, J.V., Bohlman, M.C., Bu, X., Öztas, S., Qiu, W.-Q., Arnos, K.S., Cortopassi, G.A., Jaber, L., Rotter, J.I., et al. (1993). Mitochondrial ribosomal RNA mutation associated with both antibiotic–induced and non–syndromic deafness. Nat Genet *4*, 289–294.

Pujol, R., Lavigne-Rebillard, M., and Lenoir, M. (1998). Development of Sensory and Neural Structures in the Mammalian Cochlea. In Development of the Auditory System, E.W. Rubel, A.N. Popper, and R.R. Fay, eds. (Springer New York), pp. 146–192.

Quick, K., Zhao, J., Eijkelkamp, N., Linley, J.E., Rugiero, F., Cox, J.J., Raouf, R., Gringhuis, M., Sexton, J.E., Abramowitz, J., et al. (2012). TRPC3 and TRPC6 Are Essential for Normal Mechanotransduction in Subsets of Sensory Neurons and Cochlear Hair Cells. Open Biol *2*.

Reichenbach, T., and Hudspeth, A.J. (2014). The physics of hearing: fluid mechanics and the active process of the inner ear. Rep. Prog. Phys. *77*, 076601.

Reinecke, K., Eminel, S., Dierck, F., Roessner, W., Kersting, S., Chromik, A.M., Gavrilova, O., Laukevicience, A., Leuschner, I., Waetzig, V., et al. (2012). The JNK Inhibitor XG-102 Protects against TNBS-Induced Colitis. PLoS ONE *7*, e30985.

Ren, T. (2002). Longitudinal pattern of basilar membrane vibration in the sensitive cochlea. Proc Natl Acad Sci U S A *99*, 17101–17106.

Ricci, A.J., Crawford, A.C., and Fettiplace, R. (2003). Tonotopic Variation in the Conductance of the Hair Cell Mechanotransducer Channel. Neuron *40*, 983–990.

Ricci, A.J., Kennedy, H.J., Crawford, A.C., and Fettiplace, R. (2005). The Transduction Channel Filter in Auditory Hair Cells. J. Neurosci. *25*, 7831–7839.

Richard, J.P., Melikov, K., Brooks, H., Prevot, P., Lebleu, B., and Chernomordik, L.V. (2005). Cellular Uptake of Unconjugated TAT Peptide Involves Clathrin-dependent Endocytosis and Heparan Sulfate Receptors. J. Biol. Chem. *280*, 15300–15306.

Richardson, G.P., and Russell, I.J. (1991). Cochlear cultures as a model system for studying aminoglycoside induced ototoxicity. Hearing Research *53*, 293–311.

Roth, B., and Bruns, V. (1992). Postnatal development of the rat organ of Corti. Anat Embryol *185*, 571–581.

Rüsch, A., Kros, C.J., and Richardson, G.P. (1994). Block by amiloride and its derivatives of mechano-electrical transduction in outer hair cells of mouse cochlear cultures. J Physiol *474*, 75–86.

Rybak, L.P., and Whitworth, C.A. (2005). Ototoxicity: therapeutic opportunities. Drug Discovery Today *10*, 1313–1321.

Rybak, L.P., Whitworth, C., and Scott, V. (1992). Development of endocochlear potential and compound action potential in the rat. Hearing Research *59*, 189–194.

Saar, K., Lindgren, M., Hansen, M., Eiríksdóttir, E., Jiang, Y., Rosenthal-Aizman, K., Sassian, M., and Langel, Ü. (2005). Cell-penetrating peptides: A comparative membrane toxicity study. Analytical Biochemistry *345*, 55–65.

Santos-Sacchi, J., and Dilger, J.P. (1988). Whole cell currents and mechanical responses of isolated outer hair cells. Hearing Research *35*, 143–150.

Sanz, L., Murillo-Cuesta, S., Cobo, P., Cediel, R., Contreras, J., Rivera, T., Varela-Nieto, I., and Avendaño, C. (2015). Swept-sine noise-induced damage as a hearing loss model for preclinical assays. Front. Aging Neurosci. *7*, 7.

Schacht, J., Talaska, A.E., and Rybak, L.P. (2012). Cisplatin and Aminoglycoside Antibiotics: Hearing Loss and Its Prevention. Anat Rec *295*, 1837–1850.

Sexton, J.E., Desmonds, T., Quick, K., Taylor, R., Abramowitz, J., Forge, A., Kros, C.J., Birnbaumer, L., and Wood, J.N. (2016). The contribution of TRPC1, TRPC3, TRPC5 and TRPC6 to touch and hearing. Neuroscience Letters *610*, 36–42.

Sha, S.-H., Taylor, R., Forge, A., and Schacht, J. (2001). Differential vulnerability of basal and apical hair cells is based on intrinsic susceptibility to free radicals. Hearing Research *155*, 1–8.

Shehata, W.E., Brownell, W.E., and Dieler, R. (1991). Effects of Salicylate on Shape, Electromotility and Membrane Characteristics of Isolated Outer Hair Cells from Guinea Pig Cochlea. Acta Oto-Laryngologica *111*, 707–718.

Shulman, E., Belakhov, V., Wei, G., Kendall, A., Meyron-Holtz, E.G., Ben-Shachar, D., Schacht, J., and Baasov, T. (2014). Designer Aminoglycosides That Selectively Inhibit Cytoplasmic Rather than Mitochondrial Ribosomes Show Decreased Ototoxicity A STRATEGY FOR THE TREATMENT OF GENETIC DISEASES. J. Biol. Chem. *289*, 2318–2330.

Sidi, S., Friedrich, R.W., and Nicolson, T. (2003). NompC TRP Channel Required for Vertebrate Sensory Hair Cell Mechanotransduction. Science *301*, 96–99.

Silhol, M., Tyagi, M., Giacca, M., Lebleu, B., and Vivès, E. (2002). Different mechanisms for cellular internalization of the HIV-1 Tat-derived cell penetrating peptide and recombinant proteins fused to Tat. European Journal of Biochemistry *269*, 494–501.

Spoendlin, H. (1972). Innervation Densities of the Cochlea. Acta Oto-Laryngologica *73*, 235–248.

Stepanyan, R.S., Indzhykulian, A.A., Vélez-Ortega, A.C., Boger, E.T., Steyger, P.S., Friedman, T.B., and Frolenkov, G.I. (2011). TRPA1-mediated accumulation of aminoglycosides in mouse cochlear outer hair cells. Journal of the Association for Research in Otolaryngology: JARO *12*, 729–740.

Strasser, A., O'Connor, L., and Dixit, V.M. (2000). Apoptosis signaling. Annu. Rev. Biochem. *69*, 217–245.

Suckfuell, >m., Canis, M., Strieth, S., Scherer, H., and Haisch, A. (2007). Intratympanic treatment of acute acoustic trauma with a cell-permeable JNK ligand: a prospective randomized phase I/II study. Acta Otolaryngol *127*, 938–942.

Suckfuell, M., Lisowska, G., Domka, W., Kabacinska, A., Morawski, K., Bodlaj, R., Klimak, P., Kostrica, R., and Meyer, T. (2014). Efficacy and Safety of AM-111 in the Treatment of Acute Sensorineural Hearing Loss: A Double-Blind, Randomized, Placebo-Controlled Phase II Study. Otology & Neurotology *35*, 1317–1326.

Tabuchi, K., Suzuki, M., Mizuno, A., and Hara, A. (2005). Hearing impairment in TRPV4 knockout mice. Neuroscience Letters *382*, 304–308.

Tan, K.H.-V., Mulheran, M., Knox, A.J., and Smyth, A.R. (2003). Aminoglycoside Prescribing and Surveillance in Cystic Fibrosis. Am J Respir Crit Care Med *167*, 819–823.

Tasaki, I., and Spyropoulos, C.S. (1959). Stria Vascularis as Source of Endocochlear Potential. Journal of Neurophysiology *22*, 149–155.

Tono, T., Kiyomizu, K., Matsuda, K., Komune, S., Usami, S., Abe, S., and Shinkawa, H. (2001). Different Clinical Characteristics of Aminoglycoside-Induced Profound Deafness with and without the 1555 A→G Mitochondrial Mutation. ORL *63*, 25–30.

Van Aken, A.F.J., Atiba-Davies, M., Marcotti, W., Goodyear, R.J., Bryant, J.E., Richardson, G.P., Noben-Trauth, K., and Kros, C.J. (2008). TRPML3 mutations cause impaired mechano-electrical transduction and depolarization by an inward-rectifier cation current in auditory hair cells of varitint-waddler mice. The Journal of Physiology *586*, 5403–5418.

Venkatachalam, K., and Montell, C. (2007). TRP Channels. Annual Review of Biochemistry *76*, 387–417.

Vermes, I., Haanen, C., Steffens-Nakken, H., and Reutellingsperger, C. (1995). A novel assay for apoptosis Flow cytometric detection of phosphatidylserine expression on early apoptotic cells using fluorescein labelled Annexin V. Journal of Immunological Methods *184*, 39–51.

Viberg, A., and Canlon, B. (2004). The guide to plotting a cochleogram. Hearing Research *197*, 1–10.

Vivès, E., Brodin, P., and Lebleu, B. (1997). A Truncated HIV-1 Tat Protein Basic Domain Rapidly Translocates Through the Plasma Membrane and Accumulates in the Cell Nucleus. J. Biol. Chem. *272*, 16010–16017.

Vollrath, M.A., and Eatock, R.A. (2003). Time Course and Extent of Mechanotransducer Adaptation in Mouse Utricular Hair Cells: Comparison With Frog Saccular Hair Cells. Journal of Neurophysiology *90*, 2676–2689.

Vu, A.A., Nadaraja, G.S., Huth, M.E., Luk, L., Kim, J., Chai, R., Ricci, A.J., and Cheng, A.G. (2013). Integrity and Regeneration of Mechanotransduction Machinery Regulate Aminoglycoside Entry and Sensory Cell Death. PLoS ONE *8*, e54794.

Waguespack, J., Salles, F.T., Kachar, B., and Ricci, A.J. (2007). Stepwise Morphological and Functional Maturation of Mechanotransduction in Rat Outer Hair Cells. J. Neurosci. *27*, 13890–13902.

Walker, R.G., Willingham, A.T., and Zuker, C.S. (2000). A Drosophila Mechanosensory Transduction Channel. Science *287*, 2229–2234.

Wang, J., Water, T.R.V.D., Bonny, C., Ribaupierre, F. de, Puel, J.L., and Zine, A. (2003). A Peptide Inhibitor of c-Jun N-Terminal Kinase Protects against Both Aminoglycoside and Acoustic Trauma-Induced Auditory Hair Cell Death and Hearing Loss. J. Neurosci. *23*, 8596–8607.

Wangemann, P. (2006). Supporting sensory transduction: cochlear fluid homeostasis and the endocochlear potential. J Physiol *576*, 11–21.

Ward, P.H., and Fernandez, C. (1961). The ototoxicity of kanamycin in guinea pigs. Ann. Otol. Rhinol. Laryngol. *70*, 132–142.

Weber, G. (1992). Protein Interactions. Chapman and Hall, New York. Chapter XVI, Biological Specificity and Ligand Binding

Weisleder, P., and Rubel, E.W. (1993). Hair cell regeneration after streptomycin toxicity in the avian vestibular epithelium. J. Comp. Neurol. *331*, 97–110.

Wes, P.D., Chevesich, J., Jeromin, A., Rosenberg, C., Stetten, G., and Montell, C. (1995). TRPC1, a human homolog of a Drosophila store-operated channel. PNAS *92*, 9652–9656.

Wong, A.C.Y., Birnbaumer, L., and Housley, G.D. (2013). Canonical transient receptor potential channel subtype 3-mediated hair cell Ca2+ entry regulates sound transduction and auditory neurotransmission. Eur J Neurosci *37*, 1478–1486.

Woodbury, J.W. (1971). Eyring Rate Theory Model of the Current-Voltage Relationships of Ion Channels in Excitable Membranes. In Advances in Chemical Physics, J.O. Hirschfelder, and D. Henderson, eds. (John Wiley & Sons, Inc.), pp. 601–617.

Woodhull, A.M. (1973). Ionic Blockage of Sodium Channels in Nerve. J Gen Physiol *61*, 687–708.

Wu, Y.-C., Ricci, A.J., and Fettiplace, R. (1999). Two Components of Transducer Adaptation in Auditory Hair Cells. Journal of Neurophysiology *82*, 2171–2181.

Wyman, J. (1990). Binding and Linkage: Functional Chemistry of Biological Macromolecules (University Science Books).

Yamashita, D., Jiang, H.-Y., Schacht, J., and Miller, J.M. (2004). Delayed production of free radicals following noise exposure. Brain Research *1019*, 201–209.

Ylikoski, J., Xing-Qun, L., Virkkala, J., and Pirvola, U. (2002). Blockade of c-Jun N-terminal kinase pathway attenuates gentamicin-induced cochlear and vestibular hair cell death. Hear. Res. *163*, 71–81.

Zhang, X., Zhang, X., and Wang, F. (2012). Intracellular transduction and potential of Tat PTD and its analogs: from basic drug delivery mechanism to application. Expert Opin. Drug Deliv. *9*, 457–472.

Zhang, Y., Niu, X., Brelidze, T.I., and Magleby, K.L. (2006). Ring of Negative Charge in BK Channels Facilitates Block by Intracellular Mg2+ and Polyamines through Electrostatics. J Gen Physiol *128*, 185–202.

Zhao, B., Wu, Z., Grillet, N., Yan, L., Xiong, W., Harkins-Perry, S., and Müller, U. (2014). TMIE Is an Essential Component of the Mechanotransduction Machinery of Cochlear Hair Cells. Neuron *84*, 954–967.

Zhao, H., Li, R., Wang, Q., Yan, Q., Deng, J.-H., Han, D., Bai, Y., Young, W.-Y., and Guan, M.-X. (2004). Maternally Inherited Aminoglycoside-Induced and Nonsyndromic Deafness Is Associated with the Novel C1494T Mutation in the Mitochondrial 12S rRNA Gene in a Large Chinese Family. The American Journal of Human Genetics *74*, 139–152.

Zhao, Y., Yamoah, E.N., and Gillespie, P.G. (1996). Regeneration of broken tip links and restoration of mechanical transduction in hair cells. PNAS *93*, 15469–15474.

Zheng, J., Shen, W., He, D.Z.Z., Long, K.B., Madison, L.D., and Dallos, P. (2000). Prestin is the motor protein of cochlear outer hair cells. Nature *405*, 149–155.

Ziegler, A. (2008). Thermodynamic studies and binding mechanisms of cell-penetrating peptides with lipids and glycosaminoglycans. Advanced Drug Delivery Reviews *60*, 580–597.